

Fission Rates Measured Using High-Energy Gamma-Rays from Short Half-Life Fission Products in Fresh and Spent Nuclear Fuel

THÈSE N° 4934 (2011)

PRÉSENTÉE LE 24 FÉVRIER 2011

À LA FACULTÉ SCIENCES DE BASE

LABORATOIRE DE PHYSIQUE DES RÉACTEURS ET DE COMPORTEMENT DES SYSTÈMES

PROGRAMME DOCTORAL EN ENERGIE

ÉCOLE POLYTECHNIQUE FÉDÉRALE DE LAUSANNE

POUR L'OBTENTION DU GRADE DE DOCTEUR ÈS SCIENCES

PAR

Hanna KRÖHNERT

acceptée sur proposition du jury:

Prof. A. Bay, président du jury
Prof. R. Chawla, directeur de thèse
Prof. H.-D. Berger, rapporteur
Dr P. D'hondt, rapporteur
Dr G. Perret, rapporteur



ÉCOLE POLYTECHNIQUE
FÉDÉRALE DE LAUSANNE

Suisse
2011

Abstract

In recent years, higher discharge burn-ups and initial fuel enrichments have led to more and more heterogeneous core configurations in light water reactors (LWRs), especially at the beginning of cycle when fresh fuel assemblies are loaded next to highly burnt ones. As this trend is expected to continue in the future, the Paul Scherrer Institute has, in collaboration with the Swiss Association of Nuclear Utilities, *swissnuclear*, launched the experimental programme LIFE@PROTEUS.

The LIFE@PROTEUS programme aims to better characterise interfaces between burnt and fresh UO_2 fuel assemblies in modern LWRs. Thereby, a novel experimental database is to be made available for enabling the validation of neutronics calculations of strongly heterogeneous LWR core configurations. During the programme, mixed fresh and highly burnt UO_2 fuel lattices will be investigated in the zero-power research reactor PROTEUS. One of the main types of investigations will be to irradiate the fuel in PROTEUS and measure the resulting fission rate distributions across the interface between fresh and burnt fuel zones.

The measurement of fission rates in burnt fuel re-irradiated in a zero-power reactor requires, however, the development of new experimental techniques which are able to discriminate against the high intrinsic activity of the fuel. The principal goal of the present research work has been to develop such a new measurement technique.

The selected approach is based on the detection of high-energy gamma-ray lines above the intrinsic background (i.e. above 2200 keV), which are emitted by short-lived fission products freshly created in the fuel. The fission products ^{88}Kr , ^{142}La , ^{138}Cs , ^{84}Br , ^{89}Rb , ^{95}Y , ^{90m}Rb and ^{90}Rb , with half-lives between 2.6 min and 2.8 h, have been identified as potential candidates.

During the present research work, the gamma-ray activity of short-lived fission products has, for the first time, been measured and quantitatively evaluated for re-irradiated burnt UO_2 fuel samples with burn-ups of about 36 and 46 GWd/t. Based on experiments carried out with these fuel samples in a reference test lattice of the PROTEUS reactor, fresh-to-burnt-fuel fission rate ratios could be determined. The 1σ uncertainties on the derived fission rate ratios are 1.7 to 3.4% and are mainly due to the statistical uncertainties. Calculated values of the fission rate ratios, as obtained using the Monte Carlo code MCNPX, have been shown to agree with the experimental results within these uncertainties.

In deriving fresh-to-burnt-fuel fission rate ratios, ^{142}La and ^{138}Cs have emerged as the preferred fission products. Their fission yields for the main fissile isotopes (^{235}U , ^{239}Pu and ^{241}Pu) are similar, which makes them relatively insensitive to the exact composition of the burnt fuel.

Finally, a measurement station for the future LIFE@PROTEUS experiments has been proposed and evaluated, along with a detailed formulation of recommendations for optimised irradiation and measurement strategies. The estimated accuracy for the foreseen measurements of fission

rate ratios between fresh and highly burnt fuel pins is 1 to 2%. The contribution of nuclear-data related uncertainties have been pointed out as possibly representing the main constraint on the achievable accuracy in future experiments.

In brief, the present research work has established a novel experimental technique for measuring and comparing fission rates in fresh and highly burnt fuels in a zero-power research reactor such as PROTEUS. Moreover, possibilities have been presented for the further optimisation needed for a future, routine application of the technique.

Keywords: Light water reactors (LWRs), burnt fuel, power distributions, fission rates, zero-power research reactors, LIFE@PROTEUS, gamma-ray spectrometry, high-energy gamma-rays, short-lived fission products.

Zusammenfassung

Höhere Entladeabbrände und Anfangsanreicherungen in modernen Leichtwasserreaktoren (LWR) haben in den letzten Jahren zu immer heterogeneren Kernkonfigurationen geführt, besonders zu Beginn des Zyklus, wenn frische Brennelemente neben stark abgebrannte Brennelemente geladen werden. Da sich in Zukunft dieser Trend voraussichtlich fortsetzen wird, hat das Paul Scherrer Institut in Zusammenarbeit mit der Fachgruppe Kernenergie der schweizerischen Stromverbundunternehmen *swissnuclear* das Versuchsprogramm LIFE@PROTEUS lanciert.

Das Programm LIFE@PROTEUS zielt darauf ab, die Übergänge zwischen abgebrannten und frischen UO_2 Brennelementen in modernen LWRs besser zu charakterisieren. Damit soll eine neue experimentelle Datenbasis zur Verfügung gestellt werden, die die Validierung neutronenphysikalischer Berechnungen von stark heterogenen LWR-Kernkonfigurationen ermöglicht. Im Rahmen des Programms werden im Nulleistungs-Forschungsreaktor PROTEUS gemischte Gitter aus abgebranntem und frischem UO_2 Brennstoff untersucht werden. Die geplanten Untersuchungen umschliessen unter anderem die Bestrahlungen des Brennstoffes und die Messung der resultierenden Spaltratenverteilungen an den Übergängen zwischen den Bereichen mit frischem und abgebranntem Brennstoff.

Die Bestimmung von Spaltraten in abgebranntem Brennstoff in einem Nulleistungsreaktor erfordert die Entwicklung neuer Messmethoden, die gegen die hohe spezifische Hintergrundstrahlung des Brennstoffes bestehen können. Die Entwicklung einer solchen Messmethode ist das Hauptziel der hier vorgestellten Forschungsarbeit.

Die entwickelte Messmethode beruht auf der Messung von Gammastrahlung, die durch Zerfall der im Brennstoff gebildeten, kurzlebigen Spaltprodukte entsteht und die im hohen Energiebereich über der spezifischen Gamma-Hintergrundstrahlung (d.h. über 2200 keV) liegt. Hierfür haben sich folgende Spaltprodukte, die Halbwertszeiten von 2.6 min bis 2.8 h aufweisen, als potenzielle Kandidaten herausgestellt: ^{88}Kr , ^{142}La , ^{138}Cs , ^{84}Br , ^{89}Rb , ^{95}Y , ^{90m}Rb und ^{90}Rb .

Im Rahmen der vorgestellten Forschungsarbeit wurde erstmalig die Gammastrahlung von kurzlebigen Spaltprodukten in wiederbestrahlten abgebrannten UO_2 Brennstabproben mit Abbränden von ca. 36 und 46 GWd/t gemessen und quantitativ ausgewertet. Basierend auf Experimenten mit diesen Brennstabproben, die in einem Referenztestgitter des PROTEUS Reaktors durchgeführt wurden, konnten Spaltratenverhältnisse zwischen frischen und abgebrannten Brennstabproben hergeleitet werden. Die Standardunsicherheiten der gemessenen Spaltratenverhältnisse liegen bei 1.7 bis 3.4% und sind hauptsächlich durch die statistische Messunsicherheit bedingt. Es wurde gezeigt, dass die mit dem Monte Carlo Code MCNPX berechneten Werte der Spaltratenverhältnisse mit den experimentellen Resultaten innerhalb dieser Standardunsicherheiten überstimmen.

Bei der Herleitung von gemessenen Spaltratenverhältnissen zwischen frischem und abgebranntem Brennstoff haben sich ^{142}La und ^{138}Cs als die zu bevorzugenden Spaltprodukte herauskristallisiert.

Beide weisen ähnliche Spaltausbeuten für die wichtigsten spaltbaren Isotope (^{235}U , ^{239}Pu und ^{241}Pu) auf, was sie relativ unempfindlich in Bezug auf die exakte Zusammensetzung des abgebrannten Brennstoffs macht.

In Hinblick auf das zukünftige LIFE@PROTEUS Programm wurde ein erster Vorschlag für eine Messstation präsentiert und evaluiert, wobei auch auf optimierte Bestrahlungs- und Messstrategien detailliert eingegangen wurde. Die erreichbare Genauigkeit für die vorgesehenen Messungen von Spaltratenverhältnissen zwischen frischen und hochabgebrannten Brennstäben wurde auf 1 bis 2% geschätzt. Dabei wurde hervorgehoben, dass in zukünftigen Messungen die Unsicherheiten der verwendeten nuklearen Datenbibliothek der begrenzende Faktor bezüglich der erreichbaren Messgenauigkeit darstellen könnte.

Abschliessend lässt sich sagen, dass im Rahmen der vorgestellten Forschungsarbeit eine neuartige Messtechnik etabliert wurde, die es ermöglicht, Spaltraten in frischen und hochabgebrannten Brennstoffen in Nullleistungs-Forschungsreaktoren wie PROTEUS zu messen und zu vergleichen. Ausserdem wurden Möglichkeiten zur weiteren Optimierung der Messmethode vorgestellt, die für eine zukünftige routinemässige Anwendung nötig sind.

Schlagwörter: Leichtwasserreaktoren (LWR), abgebrannter Brennstoff, Leistungsverteilungen, Spaltraten, Nullleistungs-Forschungsreaktoren, LIFE@PROTEUS, Gammaskpektrometrie, hochenergetische Gammastrahlen, kurzlebige Spaltprodukte.

Contents

1	Introduction	1
1.1	Status of nuclear power generation	1
1.2	Reactor types and evolution	2
1.3	Trends in LWR fuel technology	4
1.4	High burn-up neutronics issues	6
1.5	Scope and outline of the thesis	7
2	Background	11
2.1	Status of fission rate measurement techniques and short-lived fission product measurements	11
2.2	PROTEUS zero-power research reactor	13
2.3	LWR-PROTEUS Phase II spent fuel and transport flask	16
2.4	The LIFE@PROTEUS programme	18
2.5	Computational tools	20
2.5.1	MCNPX code system	21
2.5.2	HELIOS code system and used pincell model	22
3	Preliminary measurements on fresh and burnt fuel	29
3.1	High-resolution gamma-ray spectrometry system	29
3.2	Experimental campaign at the BR1 reactor	31
3.2.1	Experimental set-up and measurements	31
3.2.2	Gamma-ray spectra and observed gamma-ray lines	33
3.2.3	Results of the experimental campaign at BR1	36
3.3	Measurements on fresh fuel at PROTEUS	37
3.3.1	Experimental set-up and measurements	37
3.3.2	Gamma-ray spectra and observed gamma-ray lines	39
3.3.3	Results of measurements on top of PROTEUS	42
3.4	WOLF-A experimental campaign on fresh and burnt fuel	42
3.4.1	Experimental set-up and measurements	43
3.4.2	Gamma-ray spectra and observed gamma-ray lines	45
3.5	Conclusions from preliminary experiments	46
4	Measurements of high-energy gamma-rays emitted by short-lived fission products in burnt fuel	51
4.1	High-resolution gamma-ray spectrometry system	52
4.2	Experimental set-up	53
4.2.1	Modified sample changer	53
4.2.2	Specifications of fresh and burnt fuel samples	55
4.3	Test phase	56
4.3.1	Gamma-ray background	56
4.3.2	Neutron background from the reactor	58

4.3.3	Degradation of detector resolution due to fast neutron damage	59
4.3.4	Measurement position of irradiated samples	60
4.3.5	Irradiation times and power levels	61
4.4	Final measurements	62
4.4.1	List of experiments	62
4.4.2	Measured gamma-ray lines emitted by short-lived fission products in burnt fuel	63
4.5	Chapter summary	66
5	Derivation of measured fission rates in fresh and burnt fuel	69
5.1	Methodology to derive fission rate ratios	69
5.1.1	Fission rates	70
5.1.2	Inter-position fission rate ratios	71
5.1.3	Inter-sample fission rate ratios	71
5.2	Determination of net-count areas	72
5.2.1	Peak fitting with HyperLab software	72
5.2.2	Choice of analysed acquisition time	74
5.2.3	Dead-time correction and related uncertainty	75
5.2.4	Typical results for net-count areas	76
5.2.5	Reproducibility of the results	76
5.3	Saturation and decay corrections	78
5.3.1	Effective fission yields	80
5.3.2	Error propagation	82
5.3.3	Typical results	83
5.3.4	Sensitivity study regarding the parameters a_{U5} , a_{U8} , a_{P9} and a_{P1}	84
5.3.5	Sensitivity study regarding the cooling time	85
5.4	Solid angle and attenuation corrections	86
5.4.1	MCNPX model of the measurement set-up	86
5.4.2	Typical results	88
5.4.3	Sensitivity studies	89
5.5	Results for fission rate ratios	91
5.5.1	Inter-position fission rate ratios	92
5.5.2	Inter-sample fission rate ratios	93
5.6	Chapter summary	94
6	Comparison of calculated and measured fission rate ratios	97
6.1	MCNPX modelling	97
6.1.1	Whole-reactor model	97
6.1.2	Isotopic composition of fuel samples	99
6.2	Calculated fission rate ratios	101
6.2.1	Results	101
6.2.2	Sensitivity studies	103
6.3	Comparison of calculated and experimental fission rate ratios	105
6.3.1	Inter-position fission rate ratios	106
6.3.2	Inter-sample fission rate ratios	106
6.4	Chapter summary	108
7	Analysis and recommendations for the LIFE@PROTEUS measurement station	111
7.1	Reference test lattice and measurement station	112

7.1.1	Reference test lattice model	112
7.1.2	Measurement station model	113
7.2	Potential limitations of the measurement set-up	114
7.2.1	Neutron background from core during irradiation	114
7.2.2	Axial resolution of detection system	115
7.2.3	Intrinsic gamma-ray background from measured burnt fuel pin	117
7.3	Estimated counts from short-lived fission products	118
7.3.1	Methodology	119
7.3.2	Estimated net counts for the gamma-ray lines used in WOLF-B	123
7.3.3	Longer irradiation times	125
7.3.4	Additional gamma-ray lines	126
7.3.5	Conclusions with respect to achievable count rates	129
7.4	Expected uncertainties and sensitivities of fission rate ratios	130
7.4.1	Uncertainties on measured fission rate ratios	130
7.4.2	Sensitivities of measured and calculated fission rate ratios	132
7.4.3	Results for uncertainties and sensitivities	133
7.5	Further optimisation possibilities	134
7.6	Chapter summary	137
8	Summary and conclusions	141
8.1	Summary	141
8.2	Main achievements and findings	143
8.3	Recommendations for future work	147
8.4	Concluding remarks	150
A	Nuclear Data	153
	Acknowledgements	157
	CURRICULUM VITÆ	159

List of Figures

1.1	The Swiss nuclear power plant Leibstadt.	2
1.2	PWR plant layout.	3
1.3	Evolution of BWR SVEA fuel assemblies.	5
1.4	Evolution of average discharge burn-ups in LWRs.	6
2.1	Cutaway view of the PROTEUS reactor as used in the LWR-PROTEUS programme.	14
2.2	SCWR-like PROTEUS test lattice employed in the present research.	15
2.3	Combined transport flask and sample changer used to insert samples into the PROTEUS reactor.	17
2.4	Axial cross-section of the planned PROTEUS reactor block after refurbishment.	19
2.5	Proposed measurement station for LIFE@PROTEUS.	19
2.6	Example of mixed fresh and burnt fuel test lattice.	20
2.7	Layout of HELIOS pincell model.	23
3.1	Outside view and X-ray radiography of an ORTEC GEM HPGe detector.	30
3.2	View of the BR1 reactor.	32
3.3	General and schematic views of the experimental set-up at the BR1 reactor.	32
3.4	Gamma-ray spectrum of a fresh UO_2 pellet irradiated in the BR1 reactor.	34
3.5	PROTEUS test lattice and central irradiation position.	38
3.6	General and schematic views of the experimental set-up on top of the PROTEUS reactor.	38
3.7	Gamma-ray spectrum of a fresh UO_2 pin irradiated in the PROTEUS reactor.	40
3.8	Views of the experimental set-up during WOLF-A, without and with sample changer in position.	43
3.9	Example of detector position and filter used during the WOLF-A campaign.	44
3.10	Spectra of intrinsic gamma-ray activities of burnt fuel samples.	46
3.11	Comparison between gamma-ray spectrum of irradiated 36 GWd/t sample and background spectrum after irradiation without sample.	46
4.1	HPGe detector connected to the cooling unit X-Cooler II.	53
4.2	Views of the modified sample changer without and with additional neutron shielding.	54
4.3	Layout of the PROTEUS test lattice during the WOLF-B campaign.	54
4.4	Schematic cross-sections of the modified sample changer.	55
4.5	Background gamma-ray spectrum for WOLF-B set-up recorded from 5 min to 2.5 h after irradiation.	57
4.6	Evolution of the resolution of the detector model GEM-15180-P (4500 V).	59

4.7	Measurement positions of the fresh and burnt fuel samples during the WOLF-B campaign.	61
4.8	Example of gamma-ray spectra of re-irradiated burnt UO_2 fuel samples.	65
5.1	Example of fitted spectrum regions in HyperLab.	73
5.2	Reproducibility test of net-count areas obtained with HyperLab.	78
5.3	Schematic views of fresh and burnt fuel samples inside the sample changer. . . .	87
5.4	Cross-section of model of the germanium detector.	87
6.1	Axial and radial views of the MCNPX whole-reactor model of PROTEUS. . . .	98
6.2	Axial and radial views of the test lattice with the fresh fuel sample in position L11. .	99
6.3	Axial positions and axial dimensions of fresh and burnt fuel samples.	100
6.4	Within-sample isotopic densities and fission rates for the 36 GWd/t sample. . . .	105
7.1	Reference test lattice considered for the LIFE@PROTEUS campaign.	112
7.2	Preliminary design of the LIFE@PROTEUS measurement station.	113
7.3	Axial detection resolution of LIFE@PROTEUS measurement station for different gamma-ray sources (results for uncollided fluxes).	116
7.4	Saturation process during irradiation for the fission products ^{142}La , ^{89}Rb , ^{138}Cs and ^{95}Y	125
8.1	Gamma-ray spectra of the 36 GWd/t burnt sample before and after irradiation in PROTEUS.	144

List of Tables

3.1	HPGe detectors used in the preliminary experiments.	30
3.2	Irradiation and measurement conditions at the BR1 reactor.	33
3.3	Gamma-ray lines from a fresh UO_2 pellet irradiated in the BR1 reactor.	35
3.4	Measured net counts and signal-to-background ratios of high-energy peaks from a fresh UO_2 pellet irradiated in the BR1 reactor.	36
3.5	Irradiation and measurement conditions for measurements on top of the PROTEUS reactor.	39
3.6	Gamma-ray lines from fresh UO_2 fuel irradiated in the BR1 and PROTEUS reactors.	41
3.7	Measured net counts and signal-to-background ratios of high-energy peaks from a fresh UO_2 pin measured on top of PROTEUS.	42
3.8	Irradiation and measurement conditions for a set of WOLF-A experiments.	45
3.9	Gamma-ray line candidates for measuring fission rates in fresh and burnt fuel.	47
4.1	HPGe detectors used during the WOLF-B campaign	52
4.2	Characteristics of the fresh and burnt UO_2 samples used in the WOLF-B campaign.	56
4.3	Background gamma-ray lines for WOLF-B set-up after irradiation.	57
4.4	Measurement positions of fresh and burnt fuel samples and system dead times during the WOLF-B campaign.	60
4.5	Irradiations carried out during the WOLF-B campaign	63
4.6	Measured net counts and signal-to-background ratios of gamma-ray lines from short-lived fission products freshly induced in burnt fuel samples.	64
5.1	Characteristics of gamma-ray lines considered for the derivation of fission rate ratios in fresh and burnt fuel.	70
5.2	Additional fission products contributing to three of the investigated gamma-ray lines.	71
5.3	Timing and average dead-time corrections of series of gamma-ray spectra.	74
5.4	Net-count areas N_{net} derived with HyperLab.	77
5.5	List of considered parent isotopes and isomeric states for all fission products included in the analysis.	79
5.6	Contributions of fissioning isotopes to total fissions.	81
5.7	Cumulative fission yields and uncertainties of considered fission products.	82
5.8	Typical saturation and decay correction factors $(b_{\gamma,FP}C_{s,FP})_{eff}$	83
5.9	Ratios of correction factors $(b_{\gamma,FP}C_{s,FP})_{eff}$ as needed for inter-sample fission rate ratios.	84
5.10	Sensitivity of contributions to total number of fissions and of correction factors $(b_{\gamma,FP}C_{s,FP})_{eff}$ to different isotopic compositions of the 36 GWd/t sample modelled in MCNPX.	85
5.11	Sensitivities of correction factors $(b_{\gamma,FP}C_{FP})_{eff}$ to changes in cooling time t_c	85
5.12	Tallied uncollided fluxes in active germanium layer of the detector.	88
5.13	Ratios of solid angle and attenuation corrections factors $att(E_\gamma)$	89

5.14	Sensitivities of correction factors $att(E_\gamma)$ to changes of sample elevation in the MCNPX model of the sample changer.	89
5.15	Ratio of tallied uncollided fluxes ($E_\gamma = 2542$ keV) for different modelling of the germanium crystal of the detector.	90
5.16	Measured estimates for inter-position fission rate ratios.	92
5.17	Measured estimates for inter-sample fission rate ratios.	93
5.18	Contributions to the combined uncertainties of measured inter-sample fission rate ratios.*	94
6.1	Ratios of measured (Hotlab) and calculated (CASMO, HELIOS) isotopic densities of the main fissioning isotopes.	100
6.2	Calculated estimates for inter-position and inter-sample fission rate ratios. . . .	102
6.3	Sensitivities of isotopic densities, of contributions to total fissions and of calculated fission rates in the 36 GWd/t sample to increased burn-ups.	104
6.4	Comparison of calculated (C) and experimental (E) inter-position fission rate ratios, C/E values.	106
6.5	Comparison of calculated (C) and experimental (E) inter-sample fission rate ratios, C/E values.	107
6.6	Uncertainties and sensitivities of the C/E values for the fresh-to-36 GWd/t fission rate ratio.	108
7.1	Fractions of total detector responses for gamma-rays emitted in different sections of the measured fuel pin (uncollided fluxes).	116
7.2	Modelled gamma-ray source for the intrinsic activity of the burnt fuel.	118
7.3	Calculated fission densities and resulting fission rate ratios in LIFE@PROTEUS and WOLF-B.	120
7.4	Tallied uncollided fluxes for the LIFE@PROTEUS and WOLF-B measurement set-ups, and corresponding ratios of solid angle and attenuation correction factors.	121
7.5	Contributions to total number of fissions during the LIFE@PROTEUS and WOLF-B irradiations.	123
7.6	Ratios of saturation and decay correction factors between LIFE@PROTEUS and WOLF-B.	123
7.7	Characteristics of gamma-ray lines used in WOLF-B analysis.*	123
7.8	Estimated net counts in LIFE@PROTEUS (same irradiation time as for WOLF-B). . . .	124
7.9	Estimated net counts in LIFE@PROTEUS using longer irradiation times.	126
7.10	Characteristics of additional high-energy gamma-ray lines.*	126
7.11	Estimated net counts for additional gamma-ray lines in LIFE@PROTEUS.	128
7.12	Ratios of saturation and decay correction factors and their uncertainties as calculated for LIFE@PROTEUS.	131
7.13	Estimated net counts and uncertainties for LIFE@PROTEUS.	132
7.14	Estimated uncertainties and sensitivities for experimental fresh-to-60 GWd/t fission rate ratios in LIFE@PROTEUS.	134
8.1	Potential gamma-ray lines for the derivation of fission rates in fresh and burnt fuel. . . .	145
A.1	Nuclear data of short-lived fission products investigated in the present thesis. . . .	154
A.2	Nuclear data of considered precursors and isomeric states of fission products investigated in the present thesis.	155

Nomenclature

Abbreviations

BWR	Boiling Water Reactor
EPR	European Pressurised Reactor
FWHM	Full-Width-Half-Maximum
LWR	Light Water Reactor
MOX	Mixed Oxide Fuel
PIE	Post-Irradiation Examination
PSI	Paul Scherrer Institute
PWR	Pressurised Water Reactor
ROI	Region of Interest
SCWR	Supercritical-Water-Cooled Reactor
ZDT	Zero-Dead-Time

Parameters

λ	Decay constant	$[\text{s}^{-1}]$
σ	Standard deviation	[-]
$\varepsilon(E_\gamma)$	Detector efficiency	[-]
a	Contribution to total number of fissions	[-]
att_{sample}	Solid angle and attenuation correction factor	[-]
b_γ	Gamma-ray intensity	[-]
C_{FP}	Saturation and decay correction factor	[-]
E_γ	Gamma-ray energy	[keV]

F	Fission rate	$[s^{-1}]$
FRR	Fission Rate Ratio	$[-]$
i_{12}	Branching ratio of parent-to-fission-product decay	$[-]$
i_m	Branching ratio of isomeric-state-to-fission-product decay	$[-]$
N_{net}	Net-count area	$[-]$
$T_{1/2}$	Half-life	$[s]$
t_a	Acquisition time	$[s]$
t_c	Cooling time	$[s]$
t_i	Irradiation time	$[s]$
Y_{cum}	Cumulative fission yield	$[-]$
Y_{ind}	Independent fission yield	$[-]$
C	Calculational result	
dT	dead time	$[%]$
E	Experimental result	
N	Number of counts	$[-]$
S/Bg	Signal-to-Background ratio	$[-]$

Indices

1	Parent isotope
2	Considered fission product
eff	Effective
f	Fast
f	Fresh fuel
FP	Fission Product
m	Isomeric state
$P1$	^{241}Pu
$P9$	^{239}Pu
s	Spent fuel
th	Thermal
$U5$	^{235}U
$U8$	^{238}U

Chapter 1

Introduction

1.1 Status of nuclear power generation

As of January 2010, 437 nuclear power plants are in operation worldwide [IAE 09a]. Their electrical capacity is about 370 GW(e), which represents about 14% of the world's electricity generation. During 2009, only two new reactors were connected to the grid, which is low compared to previous years, and 3 reactors were shut down. Nonetheless, with 55 power plants under construction, which is the largest number since 1992, and with 17 member states of the IAEA actively preparing national nuclear power programmes, the interest in nuclear energy remains high and the worldwide nuclear production will increase in the near future.

Given the increasingly strong commitments by governments, utilities and fuel vendors to build new reactors, the IAEA recently revised its projections in nuclear power upwards by 8%. The updated high projection foresees 810 GW(e) installed global nuclear power capacity for 2030, well more than a doubling of the current capacity [IAE 09b]. The low projection for 2030 suggests 510 GW(e), which would be an increase of 38%. The expected increase can only be partly attributed to the construction of new power plants. Upgrades in already existing power plants are also responsible for the projected growth (see Section 1.3).

The centre of the growth in nuclear energy remains in Asia, where 36 of the 55 power plants under construction are located. Still, currently more than 45% of the world's capacity is installed in Europe (including the Russian Federation). At the beginning of 2010, 195 nuclear power plant units with an installed electric net capacity of 170 GW(e) were in operation in 16 European countries¹, supplying about a third of the total produced electricity [ENS 10]. Nineteen units were under construction in six European countries, namely in Bulgaria (2), Finland (1), France (1), the Russian Federation (9), Slovakia (2) and Ukraine (2). Several European countries have announced serious interest to start nuclear power production, e.g. Italy, Poland and Serbia. On the other hand, Germany continues to pursue its plans for the phase out of nuclear power.

In Switzerland, the new national policy includes renewable energies and gas fired power plants, but nuclear and hydro remain the two main pillars for electricity generation. Currently, five nuclear units are in operation at Beznau (2 units), Gösgen, Mühleberg and Leibstadt (shown in Fig. 1.1). Together, they supply about 40% of the consumed electricity of the country with a

¹These are Belgium, Bulgaria, Czech Republic, France, Germany, Hungary, the Netherlands, Romania, the Russian Federation, Slovakia, Slovenia, Spain, Sweden, Switzerland, Ukraine and the United Kingdom.

capacity of about 3.2 GW(e) [BFE 10]. The operation of the five power plants started between 1969 (Beznau I) and 1984 (Leibstadt), and is expected to end between 2019 and 2034, respectively [WNA 10].

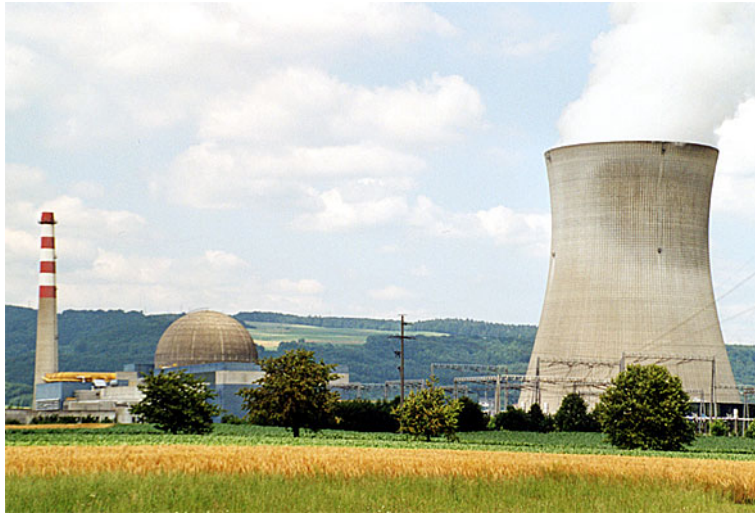


Figure 1.1: The Swiss nuclear power plant Leibstadt [VU 10].

In 2007, the Swiss government announced that the existing five nuclear power reactors should be replaced in due course with new units. In June 2008, ATEL's subsidiary, the Nuclear Power Plant Niederramt Ltd., applied to the Federal Office of Energy for the framework permit to build a new nuclear power plant in Niederramt near Gösigen, to replace the current Gösigen reactor. The envisaged reactor is to be an advanced 1100 to 1600 MW(e) reactor, with a hybrid cooling system to minimise the water use. Almost in parallel, in December 2008, the Axpo Group and BKW FMB Energie submitted framework permit applications for two new nuclear units at Beznau and Mühleberg, as replacement of the three smaller units Mühleberg, Beznau I and Beznau II. Two identical new reactors are envisaged. Also here, advanced 1100 to 1600 MW(e) reactors with hybrid cooling systems are planned [WNA 10].

The Federal Office of Energy is reported to favour construction of only two new reactors, not three. Decisions on the framework approvals are expected for mid 2012.

1.2 Reactor types and evolution

The most prevalent reactor type used for power production is the light water reactor (LWR). In fact, more than 85% of today's global nuclear capacity is generated by LWRs [IAE 09c]. The two major LWR categories are pressurised water reactors (PWRs) and boiling water reactors (BWRs).

In LWR cores, the water is used both to remove the heat produced and to slow down the fission neutrons so that a self-sustained chain reaction is possible. PWRs have two water loops which are connected via a heat exchanger (see Fig.1.2). The primary water loop, which removes the produced heat from the core, is kept under high pressure (~ 150 bar) to avoid the boiling of the water. In the secondary loop, steam is produced which is used to run the turbines connected to the generator. BWRs have only one water loop and work at a lower pressure (~ 70 bar) with

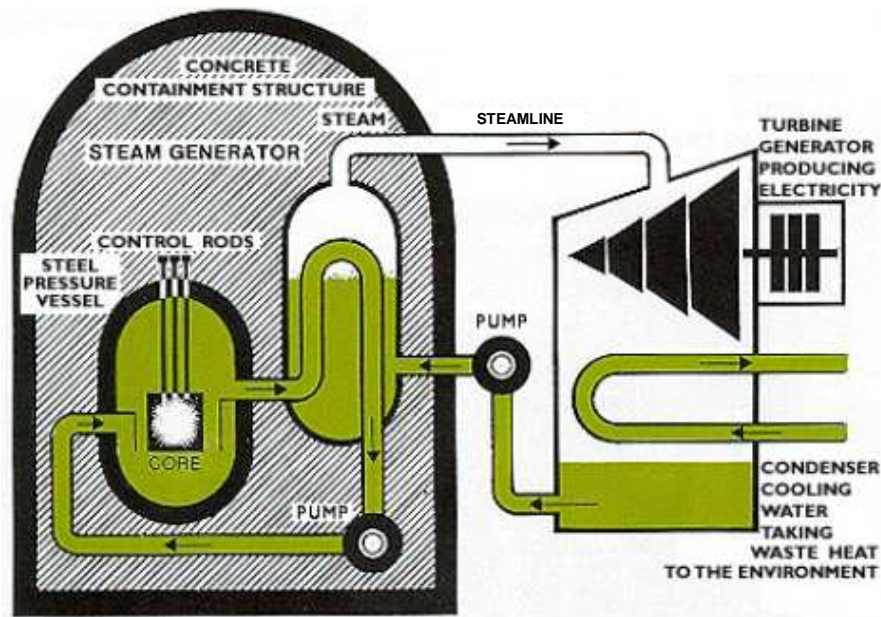


Figure 1.2: PWR plant layout [WNA 10].

water in two phases. Here, the steam is produced in the reactor core and is fed directly to the turbines.

The fuel used in LWRs is typically ^{235}U -enriched uranium oxide pellets (UO_2), stacked in Zircaloy tubes of about 4 m length and 12 mm diameter. Today, ^{235}U enrichments of 4.5 wt%² are standard. In some countries (e.g. Belgium, France, Germany, India and Switzerland), mixed oxide fuel (MOX), i.e. a mixture of UO_2 and PuO_2 , is also employed in order to re-use the plutonium from discharged UO_2 fuel. Depending on the reactor type (BWR/PWR), size and the design, 100 to 400 single fuel pins are combined to form fuel assemblies, and the reactor core contains 200 to 800 fuel assemblies.

Since they first began commercial operation in the late 1950s, LWRs have been continuously developed and improved. Today, they have reached a very high degree of maturity and have demonstrated a high level of safety and reliability, but still they continue to evolve. Given the deregulation of the power generation market in the 1990s, the driving force in the development of LWRs has been the reduction of the power generation cost in order to remain competitive with alternative technologies. Apart from economics, improved safety performance and operational flexibility are further incentives for the continuing evolution of LWR technology.

Most of the currently planned and being built LWRs belong to the advanced, so-called third generation (Generation III) of nuclear power plants, which has been developed with ambitious goals concerning safety and fuel economy. For example, the design of the European Pressurised Reactor (EPR), which has been developed by AREVA NP, and which is being built at Olkiluoto in Finland and at Flamanville in France, combines active and passive safety systems to increase safety. Furthermore, the EPRs will produce electricity about 10% cheaper than current plants and will produce at least 10% less long-lived radionuclides [EPR 10]. Another example of an advanced PWR type is the AP-1000 by Westinghouse, which emphasises passive safety systems even more.

²In the following, for the sake of convenience, the enrichment in ^{235}U , expressed in weight percent (wt%), is noted %.

To use uranium resources more effectively, both AP-1000 and EPR offer the possibility of 100% MOX core loadings. This allows a country or a utility to deploy MOX PWRs in conjunction with other PWRs fuelled with UO_2 . Recycling plutonium as LWR MOX can also be regarded as beneficial from the perspective of non-proliferation [NEA 03].

Besides national efforts, the two major international programmes Generation IV International Forum (GIF) and International Project on Innovative Reactors and Fuel Cycles (INPRO) have been set up to promote the development of an innovative fourth generation (Generation IV) of nuclear power systems. The main motivation for the fourth generation of reactors is to provide future nuclear energy systems with improved economic competitiveness while satisfactorily addressing concerns related to nuclear safety, fuel resources, proliferation, waste and public perception. In this context, six types of innovative advanced reactors have been selected by GIF for collaborative research and development. These are the gas-cooled fast reactor (GFR), the lead-cooled fast reactor (LFR), the molten salt reactor (MSR), the supercritical-water-cooled reactor (SCWR), the sodium-cooled fast reactor (SFR) and the very-high-temperature reactor (VHTR).

As the earliest estimated date for having Generation IV systems available for international deployment is about the year 2030, Generation III(+) LWRs will clearly continue to dominate the nuclear energy scene in the medium term.

1.3 Trends in LWR fuel technology

As mentioned above, the increase in nuclear power generation is partly due to power uprates of existing plants. In parallel, the fuel usage has been improved by extending the discharge burn-ups. With increased discharge burn-ups, less fresh fuel assemblies have to be loaded into the core per cycle and longer cycles can be run, so that the number of discharged assemblies is reduced. To reach the higher discharge burn-ups, the initial fuel enrichments have had to be increased significantly.

Considering the need to ensure that safety is not compromised, power up-rates and increased discharge burn-ups have only been possible thanks to the accumulation of experience, improvements of core design softwares, and advances in core layout and fuel assembly designs. Re-designed fuel assemblies have been necessary to effectively compensate for the various side-effects associated with increased power and increased assembly burn-ups.

In BWRs in particular, a trend to more and more heterogeneous fuel assembly layouts can be clearly observed. Modern BWR fuel assemblies feature, for instance, an increased number of burnable absorber rods to control the reactivity of the higher enriched fresh assemblies, additional by-pass channels to flatten the power distribution within the assemblies, part-length rods to improve the power distribution and the shutdown margins, and both radially and axially heterogeneous fuel enrichments.

The design of the ATRIUM 10 assembly by AREVA NP is one example of a modern BWR fuel assembly, with 7 different ^{235}U enrichments, an asymmetric central water canal, 10 gadolinia-poisoned fuel rods and 8 part-length rods. Another example is the SVEA-96 assembly by Westinghouse, which is subdivided into four sub-bundles and contains 16 burnable absorber rods, 7 different ^{235}U enrichments, a diamond shaped central water canal, internal water wings and

up to 12 part-length fuel rods. The evolution of Westinghouse BWR fuel assemblies, and the correspondingly achieved increased coolant flows and channel powers, are illustrated in Fig. 1.3. The typical time between successive assembly generations is about 5 years.

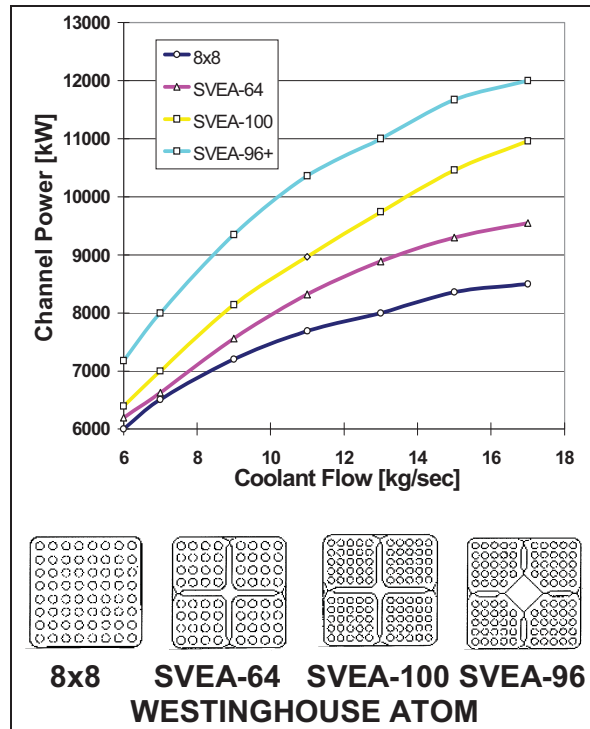


Figure 1.3: Evolution of BWR SVEA fuel assemblies [Perret 10b].

In PWRs, the evolution of fuel assemblies has been primarily focused on the development of cladding materials more resistant to corrosion and heat, which allow longer resident times in the core, power uprates and increased outlet water temperatures.

As already mentioned, both the initial enrichment and the average discharge burn-up have increased constantly in the past decades, with the primary aim of reducing the power generation cost and thus staying competitive in the deregulated energy market. Fig. 1.4 illustrates the evolution of average discharge burn-ups in BWRs and PWRs from 1970 to 2005. Currently, LWR fuel assemblies are irradiated for 4 to 5 years in the reactor and discharged with an average burn-up of typically 55 GWd/t. The average enrichment of the UO_2 fuel is around 4.5%, with a maximum at 4.95% since the highest licensed enrichment is 5 wt%. In comparison, twenty years ago, the average discharge fuel burn-up was only between 30 to 35 GWd/t and the average initial fuel enrichment was around 3-3.5% [Watteau 01]. The licensed maximum average discharge burn-up in Switzerland is currently 60 GWd/t.

The trend to increase burn-ups is expected to continue if the cladding integrity can be ensured and the fuel economics is improved. In this case, the maximum discharge burn-up may reach up to 80 GWd/t or even higher. To reach these very high burn-ups, initial fuel enrichments of up to 8% will be needed [NEA 06]. However, to ensure safe operation and thus to receive the necessary approval from the safety authority, several challenges entailed by higher burn-ups have to be mastered.

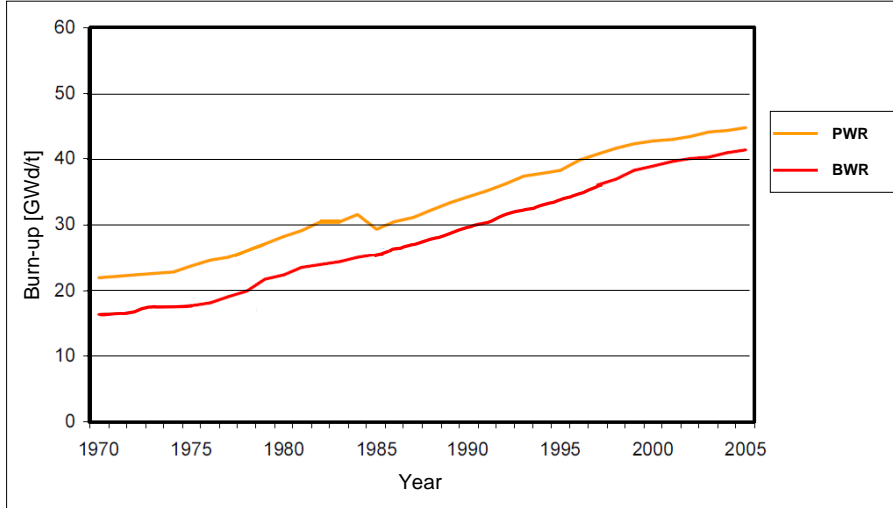


Figure 1.4: Evolution of average discharge burn-up in LWRs (based on [IAE 07]).

1.4 High burn-up neutronics issues

Higher initial enrichments and higher discharge burn-ups lead to several challenges with respect to reactor physics and criticality safety.

As an important out-of-pile challenge, the reactivity of fuel with enrichments above the currently licensed 5% will have to be re-assessed for transportation in appropriate transport casks, as well as for safe storage before loading into the reactor core. After discharge from the core, the decay heat of the highly burnt fuel assemblies and their maximum temperature have to be known to be within specified limits for their long-term dry storage.

In-pile challenges are especially related to the beginning-of-cycle, when fresh fuel assemblies might be loaded next to highly burnt ones. Such highly heterogeneous core configurations lead to very strong neutron flux gradients and neutron spectrum changes at the interfaces between the fresh and spent fuel assemblies.

In general, current neutronics codes will have to be validated for these high enrichment and burn-up conditions. Therefore, an urgent need for experimental data involving highly burnt fuel has been recognised (e.g. [NEA 06]).

To help meet these requirements, the experimental programme Large-scale Irradiated Fuel Experiments at PROTEUS (LIFE@PROTEUS) [Murphy 10] was initiated in 2006 at the Paul Scherrer Institute (PSI), as a joint programme between PSI and the Swiss nuclear utilities (*swissnuclear*). The experiments are to take place at the research reactor PROTEUS and will involve the investigation of mixed lattices containing fresh and burnt commercial fuel pins with burn-ups as high as 60 GWd/t. The investigations related to the accuracy of code predictions will include reactivity measurements, non-destructive characterisation of burnt fuel pins via passive gamma-ray and neutron emission measurements, and measurements of fission rate distributions in the mixed fuel lattice, especially at the interfaces between fresh and burnt fuel regions.

As regards the measurement of fission rates in the mixed fuel lattices, appropriate measurement techniques for fresh fuel experiments already exist. The investigation of burnt fuel, however, requires the development of new techniques which are able to discriminate against the intense

intrinsic gamma-ray and neutron activity of the burnt fuel. Two approaches are being investigated in PROTEUS. One involves the measurement of delayed neutrons emitted by the irradiated fuel pins. The other, which is the topic of the present doctoral research, is based on the detection of high-energy gamma-rays emitted by short-lived fission products. The aims and the outline of the thesis are summarised in the following section.

1.5 Scope and outline of the thesis

The principal goal of the present doctoral research is the development of a measurement technique which allows the determination of fission rates in fresh and spent fuel pins irradiated in a zero-power critical facility such as the PROTEUS reactor. The investigated approach is based on the detection of high energy (>2200 keV) gamma-rays from newly produced fission products in the burnt fuel. The gamma-ray technique as such is a standard technique to measure fissions in fresh fuel. However, gamma-ray lines used so far (e.g. ^{140}La (1596 keV) and ^{135}I (1260 keV)) have energies too low to be discriminated against the intrinsic background of the burnt fuel which reaches energies of up to 2200 keV. This intrinsic background is due to the activity of long-lived isotopes, mainly ^{137}Cs and ^{154}Eu .

The measurement of gamma-ray lines in the energy region above the intrinsic background is in itself a considerable challenge because of the decreased detection efficiency of the commonly used HPGe detectors at high energies and because of the short half-lives (minutes or hours) of the fission products emitting gamma-rays in this energy range. Furthermore, the high intrinsic gamma-ray background of burnt fuel requires the detector and the environment to be appropriately shielded during the measurements. In fact, because of these challenges, to the best of the author's knowledge, short-lived fission products have not been measured previously in burnt commercial nuclear fuel.

In the initial stage of the present research work, experiments have been conducted using fresh fuel irradiated in the Belgian research reactor BR1 and in PROTEUS. Access to the BR1 was facilitated thanks to the VENUS-EOLE-PROTEUS research reactors tripartite agreement between PSI, SCK-CEN (Belgium) and CEA (France). A first database of useful gamma-ray lines emitted by short-lived fission products was thus established. In the main experimental campaign, newly induced gamma-ray activity has been measured in fresh and, for the first time, also in burnt fuel samples, after their irradiation in PROTEUS. Based on the previously identified gamma-ray lines, fission rate ratios between fresh and burnt fuel samples have been derived. A systematic analysis has then been carried out for quantifying the experimental uncertainties and the sensitivities of the deduced fission rate ratios on various parameters. The measured fission rate ratios have also been compared to predictions obtained using the Monte Carlo code MC-NPX [Pelowitz 05]. Recommendations for further improvements of the experimental procedures have been elaborated. This has been done in the context of a preliminary design of the measurement station of the future LIFE@PROTEUS programme. Finally, measurement strategies and expected accuracies for the LIFE@PROTEUS experiments have been derived.

The thesis is organised in eight chapters.

Following this introduction, Chapter 2 covers three background topics. The first is the status of knowledge for fission rate measurements in fresh fuel and for the measurement of freshly induced short-lived fission products. The second topic consists of an overview describing the PROTEUS

reactor, the recent LWR-PROTEUS programme and the envisaged LIFE@PROTEUS experiments. The third topic is a short description of the main computer codes which have been employed in the present research work, namely MCNPX and HELIOS [Stu 05b].

Chapter 3 summarises the preliminary experiments conducted on fresh and burnt fuel, and presents a list of gamma-ray line candidates for the new measurement technique.

Chapter 4 describes the main measurement campaign (called WOLF-B) using fresh and burnt fuel samples irradiated in PROTEUS. In this campaign, the feasibility of measuring the newly induced gamma-ray activity in fresh and burnt UO_2 fuel samples has been demonstrated, with the acquisition of a suitable set of gamma-ray spectra for the derivation of fission rate ratios between the two fuel types.

Chapter 5 describes the measurement analysis procedure used during the WOLF-B campaign. The derivation of measured fission rate ratios based on high-energy gamma-rays and of their uncertainties and sensitivities are fully detailed.

In Chapter 6, the experimental (E) fission rate ratios are compared to calculational (C) results obtained using MCNPX. This is done mainly in the light of the uncertainties and sensitivities of both calculational and experimental results, the latter having been detailed in the preceding chapter.

In Chapter 7, a preliminary set-up for the LIFE@PROTEUS measurement station is presented and evaluated, based on the experience and findings gained in the frame of this research. The chapter also includes suggestions for potential improvements of the preliminary design and gives recommendations concerning the measurement procedure to follow during LIFE@PROTEUS.

Finally, Chapter 8 provides the main conclusions to be drawn from the thesis, effectively summarising the achievements and presenting recommendations for future development of the measurement technique.

Bibliography

- [BFE 10] <http://www.bfe.admin.ch/themen/00511/index.html?lang=de>. Bundesamt für Energie, 2010.
- [ENS 10] <http://www.euronuclear.org/info/energy-mixes.htm>. European Nuclear Society, 2010.
- [EPR 10] <http://www.areva.com/EN/global-offer-419/epr-reactor-one-of-the-most-powerful-in-the-world.html>. AREVA NP, 2010.
- [IAE 07] *Current Trends in Nuclear Fuel for Power Reactors*. 51st IAEA General Conference, Vienna, Austria, Information Document, 2007.
- [IAE 09a] IAEA. *Annual Report 2009*. www.iaea.org. 2009.
- [IAE 09b] IAEA. *Energy, Electricity and Nuclear Power Estimates for the Period up to 2030*. Reference Data Series No.1, 2009.
- [IAE 09c] *Status and Trends of Nuclear Technologies*. Report of the International Project on Innovative Nuclear Reactors and Fuel Cycles (INPRO), IAEA-TECDOC-1622, 2009.
- [Murphy 10] M.F. Murphy, G. Perret, O. Köberl, K.A. Jordan, P. Grimm, H. Kröhnert & M. Zimmermann. *Large-scale Irradiated Fuel Experiments at PROTEUS Research Program*. PHYSOR Conference 2010, Pittsburgh, Pennsylvania, USA, CD-ROM, ISBN 978-89448-079-9, 2010.
- [NEA 03] *Plutonium Management in the Medium Term*. NEA report No. 4451, ISBN 92-64-02151-5, 2003.
- [NEA 06] *Very High Burn-ups in Light Water Reactors*. NEA report No. 6224, ISBN 92-64-02303-8, 2006.
- [Pelowitz 05] D.B. Pelowitz. *MCNPX User's Manual Version 2.5.0*, 2005.
- [Perret 10b] G. Perret, F. Jatuff & M.F. Murphy. *Large-scale Irradiated Fuel Experiments at PROTEUS (LIFE@PROTEUS)*. Internal Report, AN-41-03-05, PSI, 2010.
- [Stu 05b] Studsvik Scandpower. *User's Manual HELIOS*, 2005.
- [VU 10] <http://www.virtualuniversity.ch/energie/kernenergie>, 2010.
- [Watteau 01] M. Watteau, B. Estève, R. Güldner & R. Hoffman. *Framatome ANP extended burnup experience and views on LWR fuels*. World Nuclear Association Annual Symposium, London, United Kingdom, 2001.
- [WNA 10] <http://www.world-nuclear.org/info/inf86.html>. World Nuclear Association, 2010.

Chapter 2

Background

This chapter provides general background information related to the present research work and can be divided into three parts. The first part gives, in Section 2.1, a brief literature survey on the status of fission rate measurement techniques using gamma-rays emitted by fission products and on the status of the usage of gamma-rays with energies above 2200 keV. The second part is devoted to the PROTEUS research reactor. The reactor and its past experimental programmes are described in Section 2.2. The LWR-PROTEUS Phase II programme, which provided the burnt fuel samples used in this research work, is described in Section 2.3. Section 2.4 describes the future experimental programme LIFE@PROTEUS, which has been the main motivation behind the present research work. In the third part (Section 2.5), the two reactor physics codes MCNPX and HELIOS are briefly described, as the two main computational tools used during this work.

2.1 Status of fission rate measurement techniques and short-lived fission product measurements

Using gamma-rays emitted by fission products is a standard technique to measure fission rates, both in nuclear power reactors and in research reactors. One of the fission products often used as a fission rate indicator is ^{140}La . Having reached secular equilibrium with its parent ^{140}Ba , ^{140}La decays with an effective half-life of 12.8 days. The most prominent gamma-ray line has an energy of 1596 keV.

For code validation in nuclear power reactors, ^{140}La has been applied as a monitor of the average thermal power distribution in the fuel, both on single fuel rods and on complete fuel assemblies. By measuring, in-pool, the activity of ^{140}La two to three weeks after reactor shut-down, the average thermal power distribution in the fuel during the last weeks of reactor operation can be derived. This technique has been applied to fuel assemblies with burn-ups ranging from 10 to 48 GWd/t at the Leibstadt nuclear power plant in Switzerland [Matsson 06].

Also at research reactors, ^{140}La is one of the standard fission products used to determine fission rates via neutron activation, e.g. at the two reactors EOLE (CEA Cadarache, France) and VENUS (SCK·CEN, Mol, Belgium) [Van der Meer 01]. The fuel samples (or fission foils) are typically irradiated at 50 W for about three hours, and the gamma-ray activity is measured after about three days of cooling time.

At the MINERVE reactor (CEA, Cadarache, France), the gamma-ray line at 293 keV emitted by the shorter-lived ^{143}Ce ($T_{1/2} = 33$ h) was measured during the OSMOSE programme to determine the fission rates in fresh UO_2 and MOX fuel pins [Klann 04]. The gamma-ray measurements were performed 2 to 4 days after irradiation at 240 Wh.

At PROTEUS, ^{143}Ce and other isotopes with shorter half-lives have been used as fission rate indicators in fresh fuel. The other fission products have been ^{135}Xe ($T_{1/2} = 9.14$ h), ^{133}I (20.8 h), ^{91}Sr (9.63 h), ^{135}I (6.6 h), and ^{92}Sr (2.7 h), with gamma-ray energies ranging from 250 to 1383 keV. As presented in [Bergmann 06], the irradiations were typically performed during 1 hour at about 30 W reactor power and the measurements were carried out after several hours of cooling time.

So far, fission rate measurements at low-power research reactors have been limited to fresh fuel. As indicated earlier, all of the above listed gamma-ray lines cannot be used for experiments on spent commercial nuclear fuel in a zero-power reactor, such as those which are planned in the LIFE@PROTEUS programme, because they would suffer serious interference from the intrinsic gamma-ray activity of long-lived fission products in the spent fuel. For a burnt fuel pin that has cooled down for several years, these are mainly ^{137}Cs with its 662 keV gamma-ray line, ^{134}Cs with its 569, 605, 796, 1039, 1168, and 1365 keV gamma-ray lines, and ^{154}Eu with its 723, 873, 996, 1005, 1275, 1494, and 1596 keV gamma-ray lines. If the cooling time is less than about five years, there will be some additional contribution from ^{144}Pr , which, in particular, emits a gamma-ray at 2182 keV.

As the gamma-rays emanating from reasonably cooled burnt fuel are thus seen to have energies below about 2200 keV, the measurement technique investigated in this work consists in observing fission product gamma-rays with energies above this value. Gamma-ray lines above 2200 keV are typically associated with very short-lived fission products with half-lives in the range of seconds, minutes and - at the maximum - hours.

There are no published results pertaining to the use of high-energy gamma-ray lines above 2200 keV for fission rate measurements in fresh fuel. This is due to the decreased efficiency of the commonly used HPGe detector at high energies and to the short half-lives which both would unnecessarily complicate the measurement process. As regards burnt commercial reactor fuel, to the best of the author's knowledge, freshly induced high-energy gamma-ray activity above 2200 keV has not been measured yet. Given the high intrinsic gamma-ray background, appropriate detector shielding and filter between the measured sample and detector are key issues to measure short-lived fission products in burnt fuel.

Some work has been done elsewhere to determine the fissile content and the burn-up of TRIGA type burnt fuel by re-irradiation using an iterative approach [Wang 00]. Here again, the ^{140}La activity was observed, and gamma-ray lines in the 700 keV region emitted by the shorter lived $^{97}\text{Zr}/^{97}\text{Nb}$ ($T_{1/2} = 16.6$ h/1.2 h) and ^{132}I (2.3 h) were measured. However, measurements were carried out after re-irradiation for four hours at 100 kW, which is much higher than the highest permissible power of 800 W in PROTEUS (neutron flux $\sim 4 \times 10^9 \text{ cm}^{-2} \text{ s}^{-1}$). Furthermore, the relatively low intrinsic gamma-ray activity of spent TRIGA fuel is not comparable to the very high activity of fuel rods which have been discharged from a 3000 MW(th) power reactor.

In the field of uranium assay, use has been made of high-energy fission product gamma-rays from fresh uranium samples [Firestone 05]. After neutron activation using cold and thermal neutron beams, the intensities of gamma-ray lines above 3000 keV from the very short-lived fission products ^{90}Rb (2.6 min), ^{90m}Rb (4.3 min) and ^{95}Y (10.3 min) have been measured to

accurately determine uranium depletion or analyse complex mixtures of fissile material. The fluxes used were rather modest, $<5 \times 10^7 \text{ cm}^{-2} \text{ s}^{-1}$ (cf. $4 \times 10^9 \text{ cm}^{-2} \text{ s}^{-1}$ in PROTEUS), but, of course, there was no background from burnt fuel long-lived fission products.

The use of high-energy fission product gamma-rays after neutron activation has also been suggested for safeguards and anti-smuggling applications [Norman 04, Slaughter 05]. To detect fissile material in cargo, the integrated gamma-ray activity above 3000 keV from short-lived fission products has been detected, taking advantage of the high penetration of the gamma-rays at these energies and of the fact that the detected gamma-rays at these energies are unique signatures of fissions in the cargo. A neutron generator was used and the suggested flux was low ($<10^6 \text{ cm}^{-2} \text{ s}^{-1}$), but, again, there was no competition from gamma-rays from burnt fuel.

In [Tobin 09, Tobin 08], the use of gamma-rays from very short-lived fission products after neutron activation has been recognised as one of the possible methods to determine the plutonium content in spent commercial fuel. However, the maturity of such a method has been rated very low because of the lack of experimental data.

In conclusion, one can say that there is no significant database, in the open literature, related to fission rate measurements in burnt fuel using low-power re-irradiation. Some work, however, has been done in reactors to detect newly induced fission products by re-irradiating fuel in a relatively high neutron flux. Furthermore, neutron activation techniques have been used for safeguard and anti-smuggling purposes, taking advantages of the high penetration of the high-energy gamma-rays emitted by short-lived fission products.

2.2 PROTEUS zero-power research reactor

The PROTEUS reactor at PSI is a zero-power research reactor, which has been in operation since 1968. The reactor is operated at room temperature and has a maximum power of 1 kW, corresponding to a neutron flux of $5 \times 10^9 \text{ cm}^{-2} \text{ s}^{-1}$. The maximum power at which experiments are allowed to be carried out is 800 W [Fassbind 09].

The facility is constructed as a multi-zone, driven system. The reactor basically consists of a graphite cylinder, 3.30 m in height and 3.26 m in diameter, containing a central cavity. The latter is of 1.25 m diameter and hosts the system under investigation. The graphite cylinder has remained almost unchanged since the first operation, whereas the configuration in the central cavity has been modified several times for the different experimental programmes.

Fig. 2.1 shows a cutaway view of the reactor. The central cavity currently contains three radial regions: the D₂O driver zone, the buffer zone and the test zone. The test zone itself is not critical, but is fed with neutrons by the surrounding driver zones for the reactor as a whole to reach criticality. The outer graphite block - in an annular region adjacent to the D₂O driver - contains driver rods of 5% enriched UO₂, 10 mm in diameter and 930 mm long, clad in 12.2 mm outer-diameter aluminium tubes. This annular region is the graphite driver zone (C-driver in Fig. 2.1). The graphite block, as a whole, also contains all the instrumentation, control and safety systems.

The D₂O driver zone contains further 5% enriched UO₂ rods immersed in a heavy-water moderator. This zone provides additional reactivity for the system and couples the inner part of

the reactor with the graphite zone. The buffer zone consists of tightly packed 22 mm diameter and about 1500 mm long natural uranium metal rods in air. It serves as a filter to minimise the thermal neutron flux coming from the driver regions and to harden the neutron spectrum in the test zone. The test zone contains the system under investigation. The test zone configuration shown in Fig. 2.1 is 45x45x430 cm³ in size and refers to the past experimental programme LWR-PROTEUS which is described below.

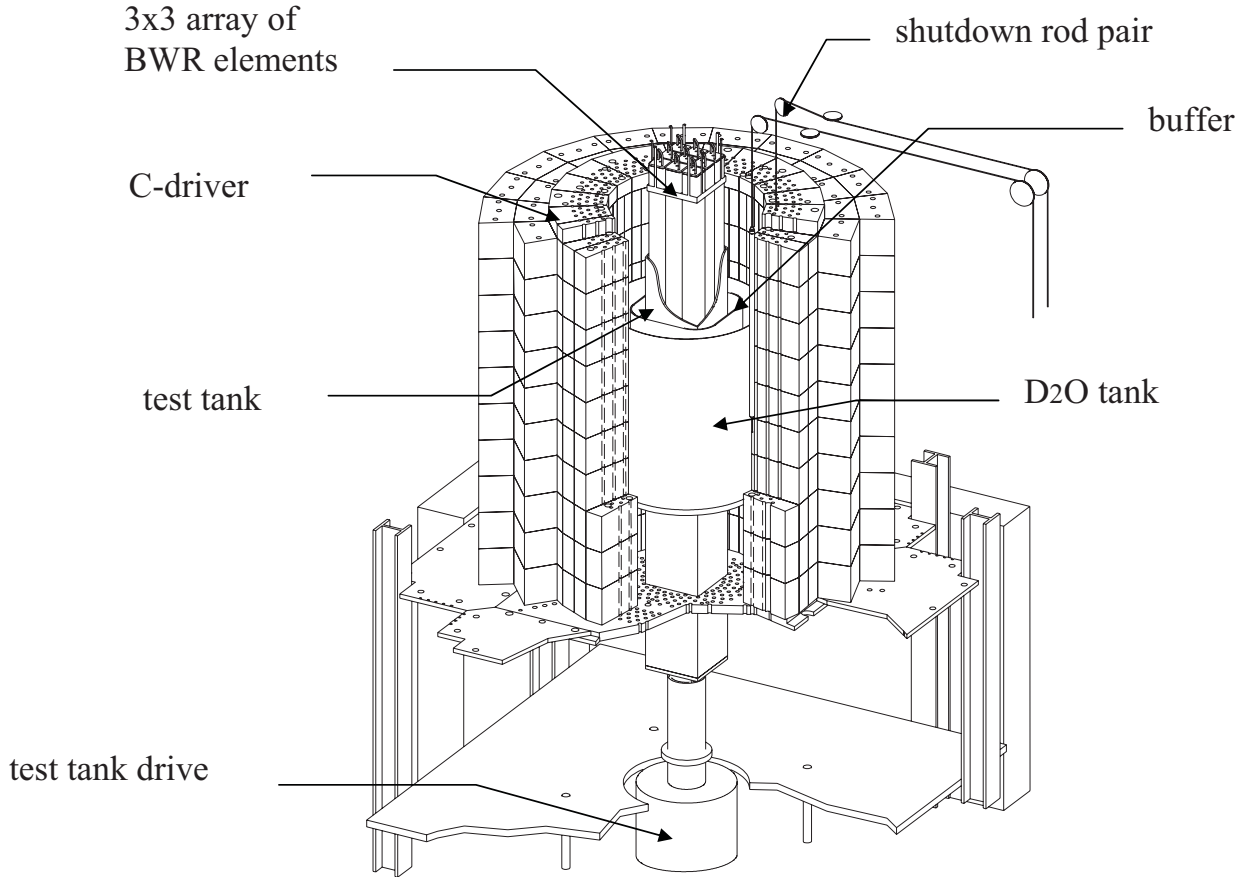


Figure 2.1: Cutaway view of the PROTEUS reactor as used in the LWR-PROTEUS programme.

In the past, a wide range of advanced reactor concepts were investigated at PROTEUS, e.g. the gas-cooled fast reactor (1970s), the high-conversion light water reactor (1980s) and the modular high temperature reactor (1990s). From 1997 to 2006, the Phases I, II and III of the LWR-PROTEUS programme were carried out. The primary goal of the LWR-PROTEUS programme was to provide an up-to-date database for the validation of LWR core analysis tools.

During Phase I (1997-2001) and Phase III (2003-2006), the central test zone of PROTEUS was composed of 3x3 fresh, 4 m long SVEA-96+ and SVEA-96 Optima2 BWR assemblies, respectively. They featured complex spacer and water canals, UO₂ pins with different ²³⁵U enrichments, UO₂-Gd₂O₃ gadolinium-poisoned pins, and part-length pins (in the case of the SVEA-96 Optima2 assemblies). The fuel assemblies were mainly investigated via measurements of detailed power and reaction rate distributions. The measurements were similar in the two phases, with Phase III focusing on regions near the end of part-length pins.

Phase II of the LWR-PROTEUS programme (2001-2003) was conducted with the aim of extending experimental databases to burnt LWR fuel. It will be detailed in the next section because it

provided the burnt fuel samples (and the hardware to handle them) used in this research work. Furthermore, depletion calculations using the deterministic code systems CASMO-4E and HELIOS had been carried out in the framework of the LWR-PROTEUS Phase II programme to estimate the composition of the burnt samples. These compositions have currently been used for cross-comparisons and for sensitivity studies.

During the experiments conducted in the context of this research work, the test zone of the PROTEUS reactor was equipped with an SCWR¹-like lattice. The lattice was constituted using the same type of fuel rods as employed in the PROTEUS driver zone, i.e. 5% enriched UO₂ rods of 930 mm length and 10 mm diameter, clad in 12.2 mm diameter aluminium tubes. The lattice is pictured in Fig.2.2 and is based on an SCWR assembly design, containing large moderator regions, which each replace a 4x4 fuel pin section [Yamaji 01]. The lattice pitch is 13.4 mm. The rods were held in place with the help of 5 polypropylene grid plates, plus an aluminium bottom plate. As moderator, a 1/3 - 2/3 heavy water/light water mixture was used in order to simulate hot pressurised feed-water.

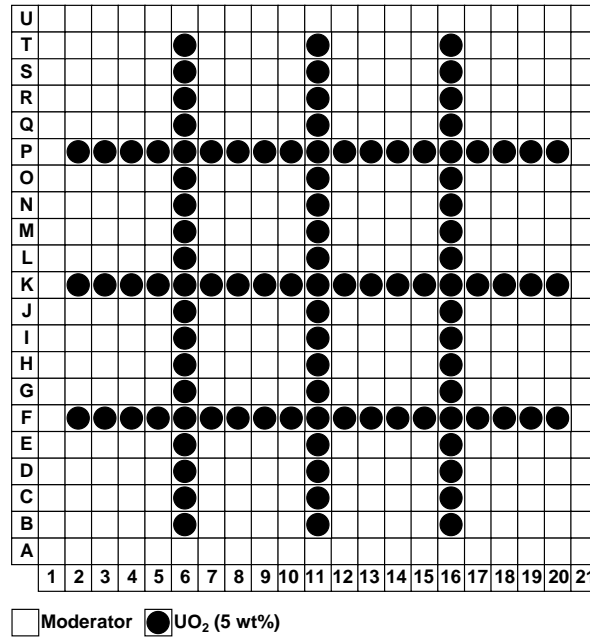


Figure 2.2: SCWR-like PROTEUS test lattice employed in the present research.

The lattice has been used as a test bed for the development of new techniques to measure fission rates in burnt fuel, which are the delayed neutron technique [Jordan 10b] and the high-energy gamma-ray technique, the latter being the topic of this research work. Furthermore, it has served for the validation of calculated reaction rate distributions in SCWR-like fuel lattices [Rätz 10].

For preliminary measurements (see Section 3.4), the central lattice pin (position K11) was removed to be able to insert samples for irradiation. For the main measurement campaign, the so-called WOLF-B campaign (see Chapter 4), further pins were removed so that samples could also be inserted into different lattice positions. In total, four lattice positions and two moderator positions were available for the WOLF-B campaign.

¹supercritical-water-cooled reactor

2.3 LWR-PROTEUS Phase II spent fuel and transport flask

The LWR-PROTEUS Phase II programme was conducted from 2001 to 2003 and had the goal of extending the experimental database related to reactivity and isotopic compositions to very high burn-up levels for both UO_2 and MOX fuel types. A total of 13 spent fuel samples were experimentally investigated during the programme.

The original fuel pins containing the samples had been irradiated in Swiss nuclear power plants between 1988 and 2001. Of the 13 samples, 11 samples (7 UO_2 , 4 MOX) originated from the Gösgen PWR and had nominal burn-ups ranging from about 36 to 120 GWd/t for UO_2 and from about 20 to 70 GWd/t for MOX. Two UO_2 samples originated from the Leibstadt BWR and had nominal burn-ups of 40 and 70 GWd/t. In order to achieve very high burn-up levels, the fuel pins containing the samples had to be moved from their initial assemblies to other, less irradiated assemblies, when the initial ones were discharged from the reactor. For instance, the 120 GWd/t sample was made from a fuel pin which had been relocated 4 times until it reached its final burn-up.

In the PSI Hot Laboratory, the 40 cm long samples had been cut from the original fuel pins and canned with a special Zircaloy overcladding, which was welded using a certified procedure to guarantee leak tightness and freedom from contamination [Murphy 06]. The samples used in this work are the 36, 46, 64 and 84 GWd/t PWR UO_2 samples.

The non-destructive experimental part of the LWR-PROTEUS Phase II programme consisted in axial gamma-ray scanning at the PSI Hot Laboratory and in neutron source and reactivity worth measurements in the PROTEUS reactor. A specially designed transport flask was used for the transfer of the fuel samples from the Hot Laboratory to the PROTEUS reactor (Fig. 2.3). The transport flask consisted of steel, and had a diameter of 710 mm and a weight of about 6 tons. The samples were loaded into a rotary revolver at the centre of the flask.

Placed on a special support structure, directly above the reactor inside the reactor shielding, the flask also served as a sample changer to lower the samples into the PROTEUS test lattice. For this purpose, the sample changer was equipped with a control unit to rotate the revolver inside the flask and to move the samples (one by one) in and out of the reactor. In its original version as used during the LWR-PROTEUS Phase II programme, the sample changer could be used to insert one sample in the central position of the test lattice in PROTEUS. This version of the sample changer (shown in Fig 2.3), loaded with the 36, 46, 64 and 84 GWd/t UO_2 samples and two fresh UO_2 samples, was used for the preliminary experiments of this research work (see Section 3.4). After this, the sample changer was modified to allow inserting samples into different lattice positions. Furthermore, a channel was manufactured into the side of the steel body, which allowed gamma-ray measurements to be carried out inside the flask. In this version, the sample changer was used for the main measurement campaign of the present research work. This was conducted on fresh UO_2 samples and on three of the burnt UO_2 samples (36, 46 and 64 GWd/t), and is described in Chapter 4.

The destructive experimental part of the LWR-PROTEUS Phase II programme consisted of precise radiochemical analysis of the sample composition at the PSI Hot Laboratory. Using adjacent segments of the original fuel pins from which the samples were cut, the analysis was carried out for more than 50 actinides and fission products. With this aim, the fuel was dissolved

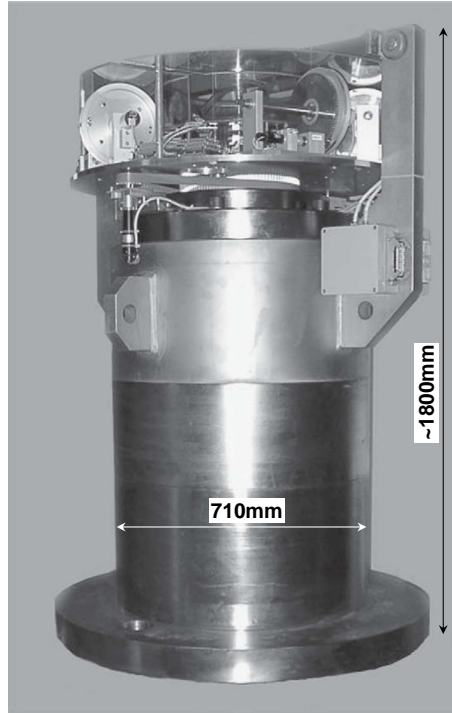


Figure 2.3: Combined transport flask and sample changer used to insert samples into the PRO-TEUS reactor.

and isotopic densities of the majority of the nuclides of interest were determined using an on-line combination of high performance liquid chromatography (HPLC) and a multicollector inductively coupled plasma mass spectrometer (MC-ICP-MS). The chromatographic system was used for the separation of chemical elements, and the mass spectrometry was used to determine the isotopic composition of the elements. The results of the radiochemical analysis are summarised in [Günther-Leopold 07].

Apart from the experimental characterisation of the samples, their isotopic compositions were calculated at PSI using the deterministic code systems CASMO-4E and HELIOS. Basic information with respect to the irradiation history of the fuel samples, i.e. nodal averaged values concerning parameters such as burn-up, power density, boron concentration, and moderator and fuel temperatures had been provided by the fuel vendor (AREVA NP GmbH, Erlangen, Germany) and are compiled in [Pralong Fauchère 04].

The depletion calculations of the PWR fuel samples using CASMO-4E are documented in [Grimm 07], the comparison of calculated and measured isotopic compositions being presented in [Grimm 10]. A reflected assembly model was used which fully took into account the actual surroundings of the investigated fuel pin, such as other fuel rods and guide tubes. The burn-up calculations were carried out using four time steps per cycle. In each time step, the specific power, the moderator temperature, the fuel temperature and the boron concentration were constant. The nuclear data library used for the calculation was based on ENDF/B-VI data [McLane 96].

The depletion calculations of the PWR fuel samples using HELIOS, along with the comparison of calculated and measured compositions, are documented in [Kröhnert 06]. A pincell model was used, i.e. only the fuel pin and the associated moderator zone were modelled, the assumption being that this pincell was surrounded by an infinite number of identical pincells. The HELIOS code and the pincell model are described in greater detail in Section 2.5.

2.4 The LIFE@PROTEUS programme

As described in Chapter 1, higher discharge burn-ups and higher initial fuel enrichments in modern PWRs and BWRs have led to more and more heterogeneous core configurations in recent years, especially at the beginning of the reactor cycle. This has resulted from the fact that fresh fuel assemblies are often loaded into core regions containing highly burnt assemblies, causing large energy-dependent neutron flux gradients to occur at the interfaces. Facing this trend of more heterogeneous core configurations, a general need for appropriate experimental data to validate the predictions of neutronics codes has been recognised.

In this context, the experimental programme LIFE@PROTEUS was launched jointly between PSI and the Swiss nuclear utilities (*swissnuclear*) in 2006 [Murphy 10]. The programme aims at better understanding the physics at the interfaces between fresh and burnt fuel assemblies in LWRs, by providing an appropriate experimental database for code validation. With this aim, it is planned to investigate, in the PROTEUS reactor, mixed zones of fresh and burnt fuel containing up to 100 full-length spent fuel pins with burn-ups up to 60 GWd/t.

Safely operating such lattices in the PROTEUS test zone and handling the large amount of spent fuel pins requires a major refurbishment of the facility. From the experimental point of view, the planned refurbishment mainly involves installing a new, large water tank and a measurement station inside this tank. An axial cross-section of the reactor block, as it would look after refurbishment, is shown in Fig. 2.4 (without measurement station). The water tank has a diameter of about 1.14 m and will fit inside the unchanged graphite block. It extends about 10 m, from the reactor basement nearly up to the reactor's top shielding doors. The lower part of the water tank will serve as wet storage for spent fuel pins. Above the wet storage region are the D₂O driver, buffer and test zones. The D₂O zone and the buffer zone are only slightly changed as compared to the current configuration. The dimensions of the test zone remain unchanged, with a cross-section of 45x45 cm² and a length of 4.3 m. It contains the fresh and spent fuel pins to be investigated, and can be moved up and down to study different fuel elevations.

The measurement station is planned to be attached to the top of the water tank above the test zone, inside the reactor shielding and within the water tank. As illustrated in Fig. 2.5, the gamma-ray detector will be installed in a large vertical tube at the top of the water tank. The measurement station will be movable to access each pin of the test zone. The pins will be brought into the measurement position through a stainless steel guide tube fixed next to the large tube containing the detector.

The first test zone in the LIFE@PROTEUS programme is foreseen to contain nine 10x10 fuel assemblies composed of fresh 5% enriched UO₂ pins moderated by light water. The next two phases will feature lattices with fresh fuel along with 40 and 60 GWd/t burnt fuel pins, respectively. An example of a test zone configuration containing burnt fuel pins is shown in Fig. 2.6. The majority of the fuel rods are fresh UO₂ fuel (green), and the central assembly contains a 6x6 bundle of 35 spent PWR fuel rods (red), one rod position being occupied by a stainless steel rod (orange) for structural reasons. In addition, absorber rods (blue) are inserted to control reactivity.

The envisaged investigations are the non-invasive characterisation of burnt fuel via neutron and gamma-ray emission measurements, the measurement of reactivity effects and the measurement of power distributions at the interfaces between fresh and burnt fuel regions in the test lattice. As

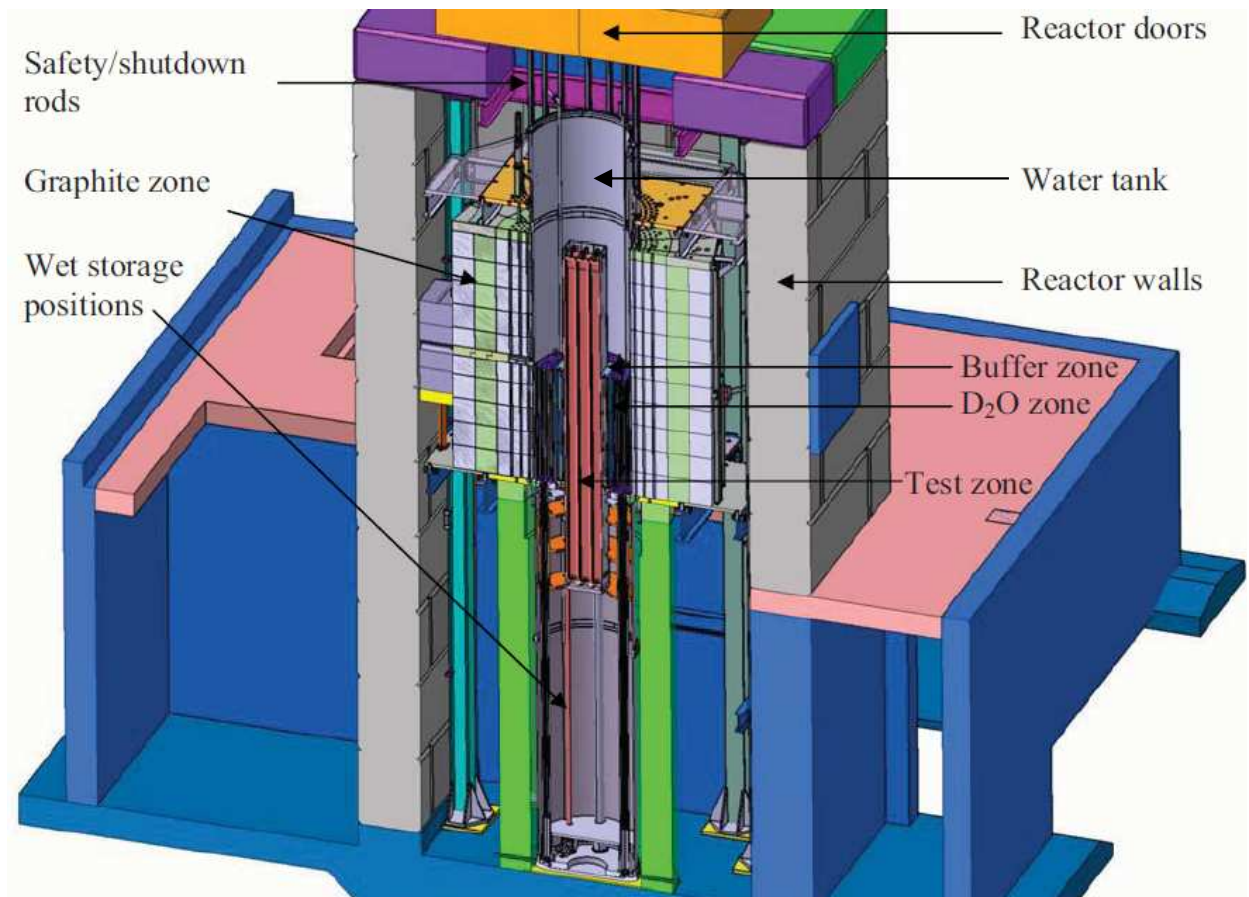


Figure 2.4: Axial cross-section of the planned PROTEUS reactor block after refurbishment.

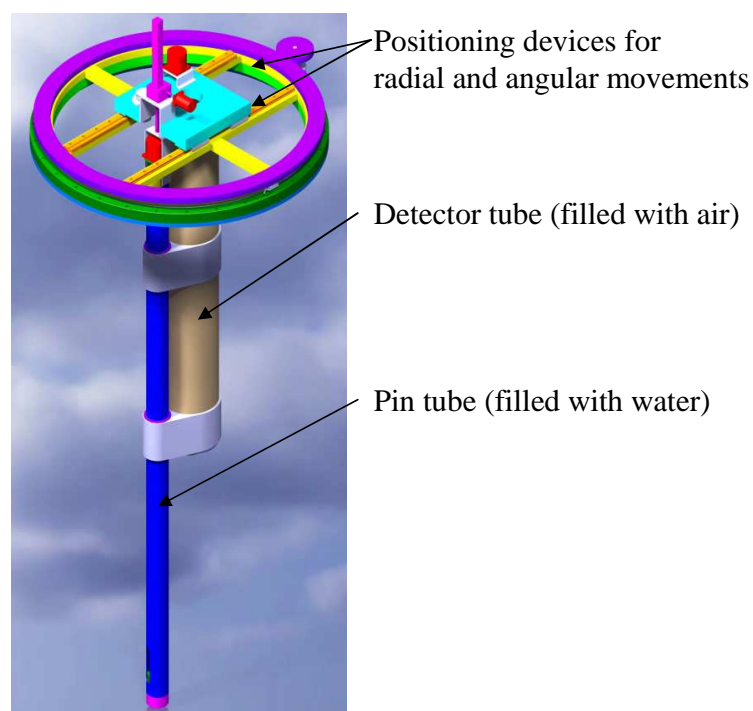


Figure 2.5: Proposed measurement station for LIFE@PROTEUS.

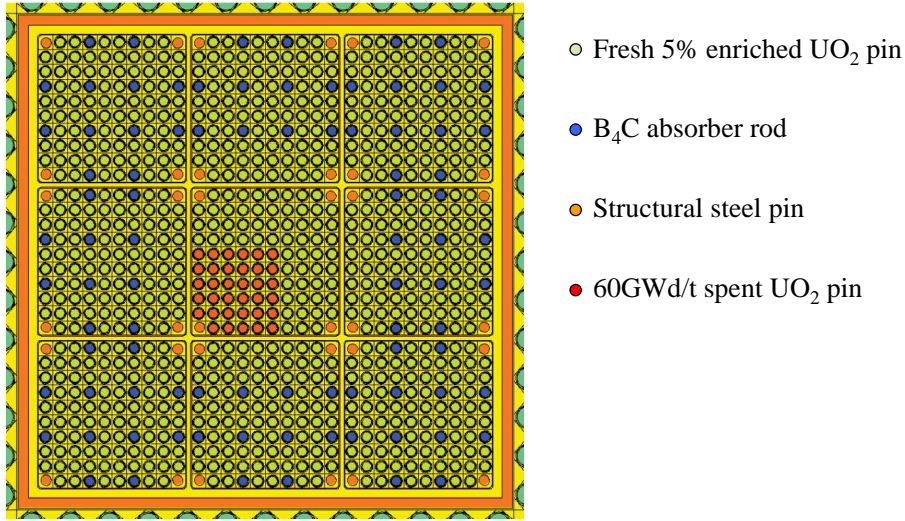


Figure 2.6: Example of mixed fresh and burnt fuel test lattice.

discussed earlier, the latter type of investigations is particularly challenging because it requires the development of new measurement techniques which are able to discriminate against the very high intrinsic activity of the burnt fuel.

Calculational support for the design and planning of the LIFE@PROTEUS programme is being provided at PSI via the use of the Monte Carlo code MCNPX and CASMO. For example, MCNPX models of the refurbished reactor have been used to assess various safety and operational parameters. Together with the results of the measurements conducted in the context of the present research work, the MCNPX models have been used to design the measurement station of LIFE@PROTEUS with respect to the planned gamma-ray measurements, to predict expected results and uncertainties, and to give recommendations to optimise the irradiation and measurement strategies. These aspects are presented and discussed in Chapter 7 of this thesis.

2.5 Computational tools

As indicated above, the Monte Carlo code MCNPX has been instrumental in extrapolating the currently developed experimental methodology to the future LIFE@PROTEUS configuration. Furthermore, most of the calculations necessary for the current experimental technique development have been carried out using MCNPX. MCNPX models were used to calculate the as-measured fission rate ratios in the PROTEUS test zone, to derive correction factors for solid angle and attenuation accounting for the measurement set-up, and to test the sensitivities of measured and calculated fission rate ratios to various parameters. Additional sensitivity studies, which were related to the isotopic composition of the burnt fuel samples, have been performed with the deterministic code HELIOS-1.9.

This section, accordingly, provides brief descriptions of these two currently employed computational tools - of MCNPX in Subsection 2.5.1 and of HELIOS in Subsection 2.5.2.

2.5.1 MCNPX code system

MCNPX is an extended version of the MCNP4C code, where MCNP stands for **M**onte **C**arlo **N**-**P**article code. The code is developed and maintained by Los Alamos National Laboratory, where it undergoes continuous development and has periodic new releases. The version used in this work is MCNPX-2.5.0 [McKinney 05, Pelowitz 05]. MCNPX is an internationally recognised, general purpose radiation transport code. It includes 3D geometries and continuous-energy data and allows transporting 34 different types of particles (e.g. neutrons, electrons, gamma-rays). The applications for the code are quite broad. Examples include the design and shielding of accelerators and reactors, medical therapies, space radiation applications, dosimetry and nuclear detector design.

At the PROTEUS reactor, MCNPX and its predecessor codes (e.g. MCNP4B) have been extensively used to model past and current experiments such as those related to the high-conversion light water reactor, the high temperature reactor and, more recently, the LWR-PROTEUS programme. The PROTEUS whole-reactor model used in this work is based on a generic model of the reactor which was specifically developed in 2001 [Jones 01].

The MCNPX code has the potential for very precise geometrical modelling. The user specifies the geometry of the problem by combining surfaces to form cells using Boolean operators. The surfaces can consist of first- and second-degree surfaces, of elliptical tori and of so-called macro-bodies such as spheres, boxes and cylinders. Materials are defined by their chemical compositions and the cross-section tables to be used. The materials are assigned to cells together with their atomic densities or weight densities.

Tallies are used to specify the physical quantity the user wants to predict with the calculation. The available tallies include currents and fluxes crossing a surface, fluxes at a point, average fluxes in a cell, energy deposition in a cell and pulse-height tallies. The results of a tally can be subdivided into bins such as energy bins, spatial bins, time bins and cosine bins. To obtain reaction rates, tally multipliers can be applied. In this work, the cell flux tally was mainly used, with the appropriate tally multiplier, to estimate the fission rates in the fuel samples, as also the solid angle and attenuation effects between the samples and the detector during measurement.

In comparison to deterministic codes, a Monte Carlo code statistically samples events, e.g. track length, surface crossing, collisions and next event. In MCNPX, the calculations are run either in the source calculation mode (SDEF) or in the critical calculation mode (KCODE). The KCODE mode is used in criticality calculations and runs inactive cycles followed by active cycles, with a given number of particle (neutron) histories per cycle. The purpose of the inactive cycles is to converge an initially guessed source distribution to the critical source distribution in the system. The inactive cycles are not included in the tally accumulation. The active cycles are the cycles over which the tally information is averaged. The fission rates in the fuel samples irradiated in PROTEUS were typically determined using 30 inactive cycles and 1000 active cycles of 500,000 neutrons each.

In the SDEF mode, the user defines a general source. The source can be assigned to cells or surfaces and is further specified with respect to its particle type, energy, direction, particle location, etc. In the SDEF mode, the total number of source particles is defined in the input file.

In the output file, the tally results are given with their statistical uncertainties, the latter depending on the number of calculated particle histories. To increase the computational efficiency

i.e. to converge faster to the solution, various variance reduction techniques can be applied. Variance reduction techniques are especially convenient for shielding problems, where only a small fraction of source particles contribute to the tallied quantity. The variance reduction techniques used in this work are mainly energy cut-offs, source biasing and weight-window generators.

2.5.2 HELIOS code system and used pincell model

The deterministic neutron and gamma-ray transport code HELIOS [Stu 05b] is used for lattice physics calculation of, in general, two-dimensional assembly geometries. The version currently used is HELIOS-1.10. The main HELIOS code is framed by the two separate codes AURORA [Stu 05a] and ZENITH [Stu 05c], which work as its input and output processors.

Within AURORA, the user defines the geometry of the system, the (initial) chemical compositions of the various materials, and one or more property sets which assign information such as temperatures, densities and materials to each region of the system. Combined with defined power densities, these property sets can be used in burn-up calculations to simulate a given irradiation history, i.e. a given fuel depletion.

As regards the energy discretisation for the transport calculation, the group structure of the cross-section library is used without any further collapsing within HELIOS. The cross-section library of HELIOS is based on ENDF/B-VI data. Three library versions exist: a master library with 190 neutron groups and two collapsed versions with 112 and 47 groups, the latter being the one normally used.

One remarkable characteristic of HELIOS is its geometrical flexibility. Almost any two-dimensional system can be calculated. The system is built up from so-called structures which can be subdivided into regions. The regions within a structure specify the spatial discretisation for solving the transport calculation. The material composition and properties are homogeneous for each region; fluxes are assumed to be flat, cross-sections to be constant. Currents between the regions of a structure, however, are not calculated. Instead, first-flight probabilities are used to assess in- and out-currents. In fact, HELIOS calculates interface currents only between two neighbouring structures and at the boundary of the entire system. The angular discretisation of the coupling currents between structures is assigned to each interface with the coupling order k . The factor k partitions the directional half-sphere into a number of polar and azimuthal sectors. The commonly used value for k is 4, which represents four polar sectors and one azimuthal sector.

For the boundary condition, an albedo reflection, a specular reflection, or a boundary coupling can be chosen. Boundary coupling is used to describe periodic or rotational symmetries (out-currents through one boundary segment are in-currents of another and vice versa). In the case of specular reflection, particles are simply reflected when they reach the specular boundary, keeping the same energy they had before crossing the boundary. An albedo matrix, for its part, explicitly defines the fraction of neutrons belonging to a certain energy group which is reflected into another energy group. Analogously to the case of current coupling between structures, a coupling order k has to be specified for the albedo matrix, in order to define the spatial discretisation of the boundary currents.

The results of a fuel depletion calculation essentially consist of fluxes, currents and material number densities for each burn-up step along the calculational path. However, no default data

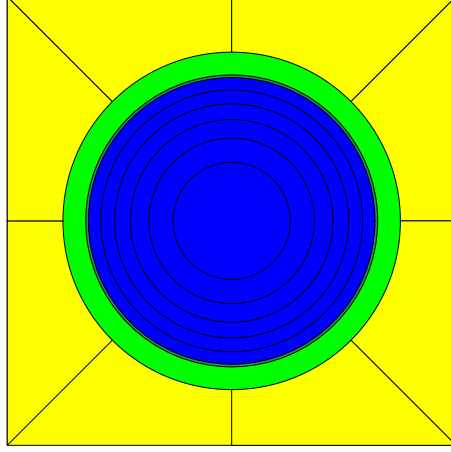


Figure 2.7: Layout of HELIOS pincell model.

are saved automatically for the output. The user has to define beforehand, in the input, all information that has to be saved by HELIOS during the calculation. This information can be, for example, fluxes or cross-sections condensed to a user-defined group structure and homogenised for a user-defined area of the system. These basic data generated by HELIOS can be later retrieved by the output processor ZENITH. The latter also allows the user to perform operations and calculations to obtain quantities such as reaction rates directly in the output file.

Fig. 2.7 shows the layout of the HELIOS pin cell model as used in the present research work. Four initial materials are modelled: the fuel zone (blue), an air gap, the Zircaloy cladding tube (green) and a square moderator zone (yellow). The size of the moderator zone corresponds to the lattice pitch of the fuel assembly hosting the sample. The moderator area is subdivided into 8 azimuthal regions. The fuel area consists of six concentric annular regions of equal areas and with outer radii of 0.186 cm, 0.264 cm, 0.323 cm, 0.373 cm, 0.417 cm, and 0.4565 cm.

All regions of the pin cell model are connected to a single structure. This means that interface currents are only calculated at the boundary of the system; inside the structure, first-flight probabilities are used. For the presented pin cell model, an albedo matrix which represents total reflection has been defined as the boundary condition. The coupling order k for the albedo reflection is set to 4, as recommended in the user's manual. As energetic discretisation for the transport calculation, the 47 neutron and 18 gamma-ray groups library is employed.

The irradiation histories, which have been used currently in HELIOS, differ slightly from those used in the CASMO-4E depletion calculation conducted during the LWR-PROTEUS Phase II. Thus, with HELIOS, the time steps employed are not those featured in the CASMO input. Instead, the time is calculated from the given burn-up steps and power densities. As documented in [Kröhnert 06], the irradiation histories consisted of about 11-12 burn-up steps per cycle, each burn-up step having a given power density. The fuel, cladding and moderator temperatures were specified as constant life-average values over all cycles. The same was done for boron concentration in the moderator.

To account for heterogeneities in the surroundings, such as guide tubes, water-density correction factors were used in order to adjust the pin cell calculations to the assembly conditions. The correction factors had been derived at AREVA NP GmbH by comparing CASMO-4 pincell and assembly calculations on the basis of the ^{235}U concentration [Attale 07]. Clearly, despite the use of water-density correction factors, pincell calculations are less accurate than assembly

calculations. Nonetheless, as they are much less time-consuming and less complex, they have formed a useful instrument for the sensitivity studies, which have currently been conducted with respect to the fuel compositions.

As output of the burn-up calculation, the average isotopic densities of all considered fission products and actinides in the fuel were saved, as well as the average isotopic densities in each of the six radial fuel regions.

Bibliography

- [Attale 07] F. Attale, H. Kröhnert & H.-D. Berger. *On the use of water density correction factors in pin cell calculations for the evaluation of isotope densities of irradiated samples*. Annual Meeting on Nuclear Technology (Jahrestagung Kerntechnik), Karlsruhe, Germany, 2007.
- [Bergmann 06] U. Bergmann, R. Chawla, F. Jatuff & M.F. Murphy. *Optimized non-invasive method to determine the ratio of ^{238}U -captures-to-total-fissions in reactor fuel*. Nuclear Instruments and Methods in Physics Research Section A, vol. 556, page 331-338, 2006.
- [Fassbind 09] M. Fassbind, O. Köberl & M. Murphy. *Betriebsvorschriften PROTEUS, Phase III der LWR-Experimente*. Internal Report AW-41-06-01, Rev. 3, PSI, 2009.
- [Firestone 05] R.B. Firestone & G.A. English. *Analysis of fissile materials by high-energy neutron-induced fission decay gamma-rays*. J. Radioanalytical and Nucl. Chemistry, vol. 265 No.2, page 241-245, 2005.
- [Günther-Leopold 07] I. Günther-Leopold. *LWR-PROTEUS programme, Phase II, Final Report*. Internal Report TM-43-06-05, PSI, 2007.
- [Grimm 07] P. Grimm. *CASMO-4E Calculations of the Isotopic Inventories of the LWR-PROTEUS Phase II Irradiated Fuel Samples from KKG*. Internal Report TM-41-07-07, PSI, 2007.
- [Grimm 10] P. Grimm. *Comparison of Calculated and Measured Isotopic inventories for the LWR-PROTEUS Phase II Irradiated Fuel Samples*. Internal Report TM-41-09-03, PSI, 2010.
- [Joneja 01] O.P. Joneja, F. Jatuff, P. Grimm, R. Seiler, R. Brogli, G. Meier, H.-D. Berger & R. Chawla. *Validation of an MCNP4B whole-reactor model for LWR-PROTEUS using ENDF/B-V, ENDF/B-VI and JEF-2.2 cross-section libraries*. Annals of Nuclear Energy, vol. 28, page 701-713, 2001.
- [Jordan 10b] K.A. Jordan, G. Perret & M.F. Murphy. *Delayed neutron measurements of induced fission rates in burnt LWR fuel samples at the PROTEUS zero-power reactor facility*. PHYSOR Conference 2010, Pittsburgh, Pennsylvania, USA, CD-ROM, ISBN 978-89448-079-9, 2010.
- [Klann 04] R. Klann, J.-P. Hudelot, M. Antony, B. Micklich, G. Perret, N. Thiollay, G. Imel, J.-M. Girard & V. Laval. *MINERVE reactor characterization in support of the OSMOSE program: Spectral indices*. PHYSOR Conference 2004, Chicago, Illinois, USA, CD-ROM, ISBN 0-89448-683-7, 2004.
- [Kröhnert 06] H. Kröhnert. *Analysis of the nuclide composition of highly-burnt PWR fuel examined in connection with the LWR PROTEUS Phase II project with the spectral code HELIOS*. Institut für Wärme- und Brennstofftechnik, Technische Universität Braunschweig, Diploma thesis, 2006.

- [Matsson 06] I. Matsson, B. Grapengiesser & B. Andersson. *LOKET - a gamma-ray spectroscopy system for in-pool measurements of thermal power distributions in irradiated nuclear fuel*. Nuclear Instruments and Methods in Physics Research Section A, vol. 569, page 872-882, 2006.
- [McKinney 05] G.W. McKinney, J.W. Durkee, J.S. Hendricks, M.R. James, D.B. Pelowitz, Waters L.S. & Gallmeier F.X. *MCNPX 2.5.0 - New Features Demonstrated*. The Monte Carlo Method: Versatility Unbounded in a Dynamic Computing World, Chattanooga, Tennessee, USA, CD-ROM, 2005.
- [McLane 96] V. McLane. *ENDF-201 - ENDF/B-VI summary documentation supplement 1 ENDF/HE-VI summary documentation - BNL-NCS-17541*, 1996.
- [Murphy 06] M.F. Murphy, F. Jatuff, P. Grimm, R. Seiler, R. Brogli, G. Meier, H-D. Berger & R. Chawla. *Reactivity and neutron emission measurements of highly burnt PWR fuel rod samples*. Annals of Nuclear Energy, vol. 33 (2006), page 760-765, 2006.
- [Murphy 10] M.F. Murphy, G. Perret, O. Köberl, K.A. Jordan, P. Grimm, H. Kröhnert & M. Zimmermann. *Large-scale Irradiated Fuel Experiments at PROTEUS Research Program*. PHYSOR Conference 2010, Pittsburgh, Pennsylvania, USA, CD-ROM, ISBN 978-89448-079-9, 2010.
- [Norman 04] E.N. Norman, S.G. Prussin & R-M. Larimer. *Signatures of fissile materials: high-energy gamma-rays following fission*. Nuclear Instruments and Methods in Physics Research Section A, vol. 521, page 608-610, 2004.
- [Pelowitz 05] D.B. Pelowitz. *MCNPX User's Manual Version 2.5.0*, 2005.
- [Pralong Fauchère 04] C. Pralong Fauchère. *Irradiation histories of LWR-PROTEUS Phase II Samples*. PSI report, 2004.
- [Rätz 10] D. Rätz, K.A. Jordan, M.F. Murphy, G. Perret & R. Chawla. *Experimental validation of reaction rate distributions in an SCWR-like fuel lattice at PROTEUS*. PHYSOR Conference 2010, Pittsburgh, Pennsylvania, USA, CD-ROM, ISBN 978-89448-079-9, 2010.
- [Slaughter 05] D.R. Slaughter, M.R. Accatino, A. Bernstein & J.A. Church. *Preliminary results utilizing high-energy fission product gamma-rays to detect fissionable material in cargo*. Nuclear Instruments and Methods in Physics Research Section B, vol. 241, page 777-781, 2005.
- [Stu 05a] Studsvik Scandpower. *User's Manual AURORA*, 2005.
- [Stu 05b] Studsvik Scandpower. *User's Manual HELIOS*, 2005.
- [Stu 05c] Studsvik Scandpower. *User's Manual ZENITH*, 2005.
- [Tobin 08] S.J. Tobin, S.F. Demuth, M.L. Fensin, J.S. Hendricks, H.O. Menlove & M.T. Swinhoe. *Determination of plutonium content in spent fuel with NDA - Why an integrated approach?* Annual Meeting of the Institute of Nuclear Material Management, Nashville, Tennessee, USA (LA-UR-08-03763), 2008.

- [Tobin 09] S.J. Tobin, M.L. Fensin, B.A. Ludewigt, H.O. Menlove, B.J. Quinter, N.P. Sandoval, M.T. Swinhoe & S.J. Thompson. *Determining plutonium mass in spent fuel with nondestructive assay techniques - Preliminary modeling results emphasizing intergration among techniques*. Proceedings of Global, Paris, France, Paper 9303, 2009.
- [Van der Meer 01] K. Van der Meer, P. D'Hondt & R. Vandebroek. *Qualifying C8/F9 Spectrum Index Measurements by Using Standard Neutron Fields*. In: *Reactor Dosimetry: Radiation Metrology and Assessment*, ASTM STP 1398, John G. Williams, page 753-760, American Society for Testing and Materials, West Conshohocken, Pennsylvania, USA, ISBN 0-8031-2884-3, 2001.
- [Wang 00] T-K. Wang & J-J. Peir. *An iterative approach for TRIGA fuel burn-up determination using non-destructive gamma-ray spectrometry*. Applied Radiation and Isotopes, vol. 52, page 105-118, 2000.
- [Yamaji 01] A. Yamaji, Y. Oka & S. Koshizuka. *Conceptual Core Design of a 1000MWe Supercritical Pressure Light Water Cooled and Moderated Reactor*. Proceedings of ANS/HPS Student Conference, Texas, USA, 2001.

Chapter 3

Preliminary measurements on fresh and burnt fuel

As described in the previous chapter, the gamma-ray lines generally measured to determine fission rates in fresh fuel have energies lower than 1600 keV and are emitted by fission products which have half-lives of several hours or longer. Relatively low energies and long half-lives have the advantage to enhance the detection efficiency and to ease the measurement procedure. Shorter-lived fission products have therefore not been routinely measured in low-power research reactors. Concerning burnt fuel, to the best of the author's knowledge, gamma-ray activity from short-lived fission products has not been previously investigated in a systematic manner.

For this reason, during the initial phase of the present work, several preliminary experimental campaigns were conducted on fresh and burnt fuel samples irradiated in different research reactors. The goals were to gain experience in the gamma-ray spectrometry of short-lived fission products induced in nuclear fuel, and to establish an extensive database of gamma-ray spectra. The campaigns were successful in helping to identify gamma-ray lines with energies above 2200 keV which could be used to demonstrate the feasibility of deriving fission rates in fresh and burnt fuel.

Three preliminary experimental campaigns and their outcomes are presented in this chapter. The gamma-ray spectrometry system used for all the measurements is specified in Section 3.1. Section 3.2 is devoted to the first experiments on fresh UO_2 pellets irradiated in the BR1 reactor at SCK-CEN in Mol, Belgium. A subsequent experimental campaign, where a fresh UO_2 pin was irradiated in PROTEUS, is described in Section 3.3, while Section 3.4 refers to the WOLF-A measurement campaign at PROTEUS, which was the first campaign using not only fresh, but also burnt UO_2 fuel samples. Conclusions drawn from these preliminary experiments are summarised in Section 3.5.

3.1 High-resolution gamma-ray spectrometry system

In the context of the present research work, gamma-ray spectrometry has been conducted with high-purity germanium (HPGe) detectors belonging to the ORTEC GEM series [ORT 03b]. GEM detectors are high-resolution p-type semiconductor detectors with a closed-end coaxial geometry. An outside view and a X-ray radiography of a GEM detector are shown in Fig. 3.1.

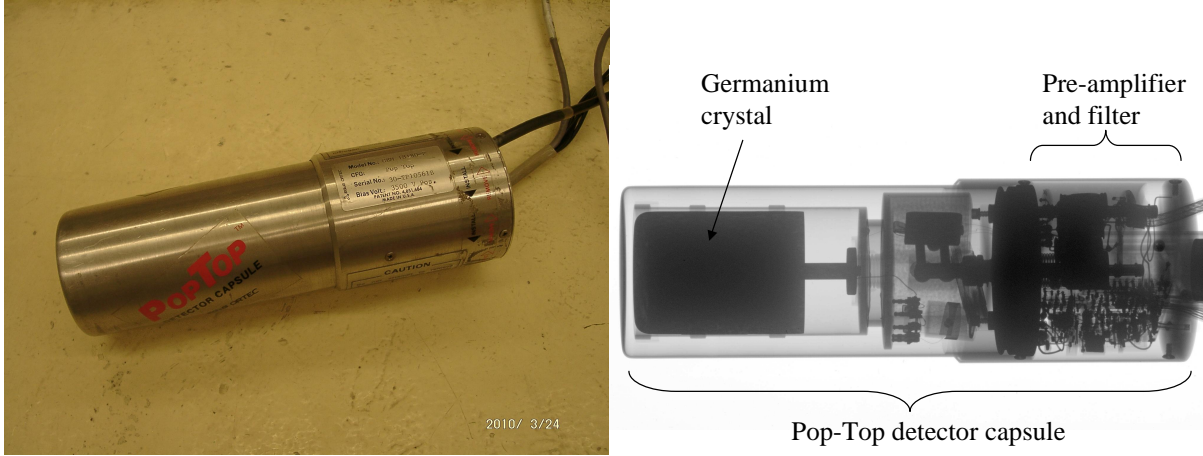


Figure 3.1: Outside view and X-ray radiography of an ORTEC GEM HPGe detector.

Two different detectors have been used for the preliminary measurements. Their dimensions and performance specifications are summarised in Table 3.1. Both detectors are so-called Pop-Top models in which the cryostat, the pre-amplifier and the high voltage filter are housed within a single detector capsule having its own vacuum [ORT 03b]. The advantage is that each detector is independent of the cooling system and can be mounted on any available cryostat and dewar combination, or be coupled to any mechanical cooling system. The disadvantage is that a Pop-Top detector is more susceptible to neutron damage as the detector is at a slightly higher temperature.

Table 3.1: HPGe detectors used in the preliminary experiments.

Model	GEM-15180-P	GEM-18180-P
Cryostat configuration	Pop-Top	Pop-Top
Crystal diameter	49.5 mm	47.0 mm
Crystal length	68.9 mm	61.0 mm
End cap to crystal	3 mm	3 mm
Absorbing Al layer	1.27 mm	1.27 mm
Absorbing inactive Ge layer	0.7 mm	0.7 mm
Recommended high voltage bias	4500 V	3500 V
Resolution* (FWHM) at 1.33 MeV, ^{60}Co	1.80 keV	1.80 keV
Relative efficiency** at 1.33 MeV, ^{60}Co	15%	18%

*The warranted values refer to a nominal count rate of 1000 cps and an amplifier time constant of $6\text{ }\mu\text{s}$.

**The efficiency of germanium detectors is commonly quoted relative to that of a standard 3 inch x 3 inch (7.62 cm x 7.62 cm) cylindrical NaI(Tl) scintillation crystal [Knoll 00].

For all measurements of the preliminary experimental campaigns, the germanium crystal of the detector was cooled with liquid nitrogen stored in a dewar. The aluminium cap of each detector was wrapped with a cadmium-and-copper shielding. This was used to stop the X-rays of energies between 10 and 90 keV, produced by fluorescence in the lead filter of the experimental set-ups.

The detector was connected to an EG&G ORTEC DSPEC Plus digital multi-channel analyser [DSP]. The DSPEC Plus is a comprehensive unit for powering the preamplifier, supplying high-voltage to the detector, and processing the signals generated by the detector. The data

were saved by the ORTEC software Gamma-Vision [ORT 03a] which also served to control the various parameters of the DSPEC Plus. The rise time was selected manually for each experimental campaign in order to optimise the peak resolution and the dead time level. For all other amplifier settings (e.g. pole zero, and flat top width and tilt), the automatic optimisation of the DSPEC Plus was used. During the preliminary measurement campaigns, the rise time was typically set to $1.6\ \mu\text{s}$ and the data were acquired using 16384 energy channels.

One feature of the DSPEC Plus is the so-called zero-dead-time counting mode [ORT a], in which two spectra are recorded in parallel. In this research work, the live-time spectrum, which is uncorrected for dead time, and the zero-dead-time spectrum (ZDT) were recorded. In the latter spectrum, additional counts are added on a channel-by-channel basis during the acquisition to produce an apparently dead-time free spectrum. The ZDT option is particularly suitable for measurements of rapidly changing count rates, as was the case for the conducted experiments on short-lived fission products. The reliability of the ZDT methodology has been proven for higher dead times (reaching levels up to 90%) than for the presented experiments and for more strongly varying count rates [Blaauw 03], ensuring its successful use in the current experiments.

During the measurement, the data were saved in a series of spectra. Typically, the first five minutes of the acquisition were saved in 10 spectra of 30 sec (real time), the next 55 min were saved in 11 spectra of 5 min, and the rest of the acquisition was saved in several spectra of 30 min. This allowed a highly flexible analysis of the spectra, which could be carried out on different sums of spectra depending on the half-lives of the fission products emitting the gamma-ray lines of interest. During the preliminary measurements, the analysis of the gamma-ray spectra was carried out using Gamma-Vision.

3.2 Experimental campaign at the BR1 reactor

Fresh UO_2 fuel pellets were irradiated at the BR1 research reactor at the SCK·CEN in Mol, Belgium, and spectra of their gamma-ray activity after irradiation were recorded. The measurements were carried out in the frame of the VENUS-EOLE-PROTEUS research reactors tripartite agreement between PSI, SCK·CEN and CEA (France).

Being the first campaign carried out in the context of this research work, the main goal of the experiments was to establish a database of gamma-ray lines emitted by short-lived fission products suitable to derive fission rates in the fuel. This experimental campaign focused on the detection of gamma-rays above 2200 keV, emitted by very short-lived fission products with half-lives of several minutes.

3.2.1 Experimental set-up and measurements

The BR1 reactor, which was made critical for the first time in 1956, was designed for research in reactor physics [Wagemans 08] [BR1]. It is moderated with graphite, cooled by air circulation, and fuelled with 25 tons of natural metallic uranium. A view of the reactor is shown in Fig. 3.2. The total volume of the reactor block is about $6.7 \times 6.8 \times 6.8\ \text{m}^3$. The fuel is loaded into horizontal channels (square section $\sim 5 \times 5\ \text{cm}^2$, lattice pitch 18 cm). The fuel channels are distributed such as to approximately form a cylinder with a diameter of 4.7 m and a length of 4.9 m. The nominal

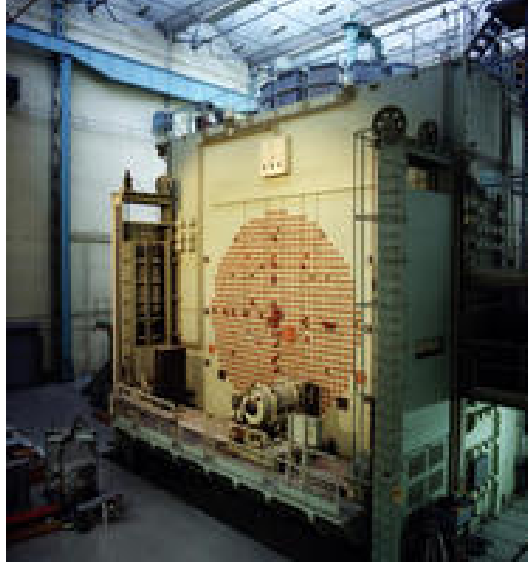


Figure 3.2: View of the BR1 reactor.

thermal power of the BR1 is 4 MW. Nowadays, it is operated on a daily basis on experimenters' request at a maximum power of 700 kW, or at 1 MW for short time periods of a few hours.

A particularity of the BR1 reactor is the high degree of thermalisation of the neutron spectrum, thanks to the large amount of graphite moderator. Examples of performed measurements are neutron activation analysis, neutron radiography, and calibration of neutron and gamma-ray detectors. The main irradiation facilities of the reactor consist of about 50 irradiation channels crossing the reactor core, both parallel and perpendicular to the fuel channels, a thermal column above the core with a fully thermalised neutron spectrum, and a pneumatic fast rabbit system. The fast rabbit system allows in-core irradiations in different core positions and is mainly used for neutron activation analyses. Thanks to very short transfer times between irradiation position and measurement position, it allows the detection of nuclides with half-lives down to a few seconds.

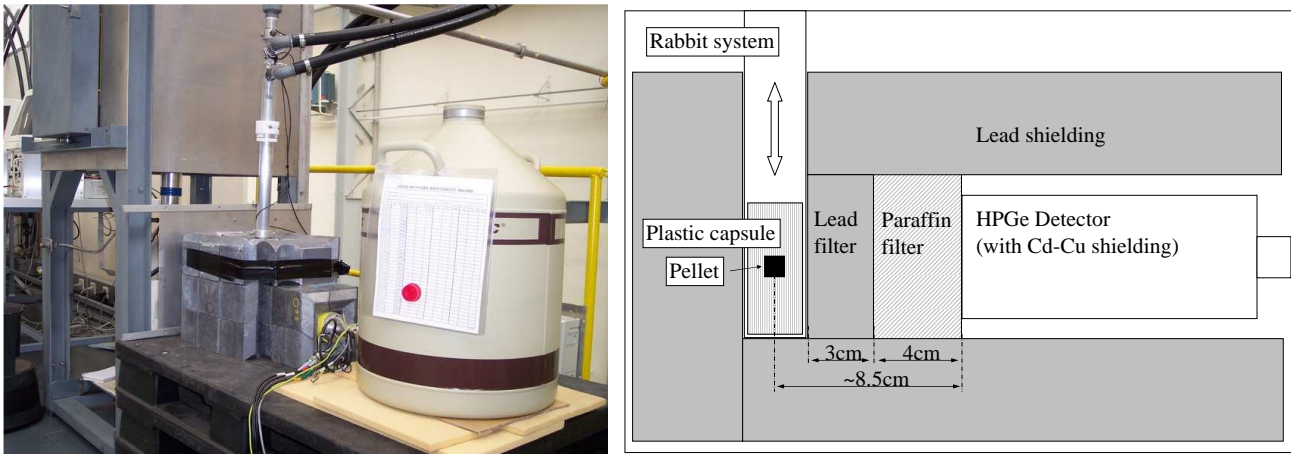


Figure 3.3: General and schematic views of the experimental set-up at the BR1 reactor.

During the described measurements, the HPGe detector (model GEM-18180-P) was placed on the top of the reactor, where the measurement station was connected to the end of the pneumatic rabbit system. The detection set-up with the lead shielding and the tube of the rabbit system is shown in Fig.3.3, together with a schematic sketch showing the sample in front of the detector.

Two fresh UO_2 fuel pellets were successively irradiated in the reactor core. The fuel pellets had a length of ~ 1 cm, a diameter of ~ 0.85 cm and had two different enrichments of 3.3% and 4%. For transfer within the rabbit system, the pellets were placed inside a cylindrical plastic capsule (diameter ~ 2.5 cm, length ~ 6 cm) and held in position with tissue. The fast rabbit system enabled the activated samples to be transported after irradiation to the measurement position within less than a second.

A series of irradiations was conducted for each pellet under various irradiation and measurement conditions. The irradiation times were varied from 2 to 30 min and the data acquisition was typically performed during 5 to 90 min, starting directly after irradiation. The reactor power was varied from 1 to 10 kW. The total neutron flux at the irradiation position is about $2.6 \cdot 10^8 \text{ cm}^{-2} \text{ s}^{-1} \text{ kW}^{-1}$. The ratio of the thermal flux (at 25.3 meV), measured with a Au dosimeter, and the fast flux (threshold 2.6 MeV), measured with a ^{58}Ni dosimeter, is about 20 [Wagemans 10].

The conditions for three irradiations, which have been included in the qualitative analysis described in Subsection 3.2.3, are given in Table 3.2. A complete list of all the irradiations carried out is provided in [Plaschy 07b].

Table 3.2: Irradiation and measurement conditions at the BR1 reactor.

		Irradiation		Measurement			
Index	Pellet enrichment	Reactor power	t_{irr}	Lead filter	Paraffin filter	Distance pellet-detector	t_a
A	4%	10 kW	2 min	3 cm	4 cm	8.5 cm	6 h
B	4%	1 kW	10 min	3 cm	4 cm	8.5 cm	15 min
C	4%	1 kW	30 min	3 cm	4 cm	8.5 cm	40 min

t_{irr} : irradiation time; t_a : acquisition time

3.2.2 Gamma-ray spectra and observed gamma-ray lines

As an example, the gamma-ray spectrum recorded after irradiating the 4% enriched pellet during 30 min at a reactor power of 1 kW is shown in Fig. 3.4 (irradiation C in Table 3.2). The counts were recorded during 40 min starting directly after irradiation. The lower parts of the figure focus on the energy regions 800-2100 keV, 2100-3400 keV and 3400-4700 keV, respectively.

The first step of the analysis consisted in the identification of the detected gamma-ray lines. The marked peaks in Fig. 3.4 are gamma-ray lines belonging to short-lived fission products (except for the 511 keV annihilation peak). The energies and the intensities of the identified lines, together with the related fission products and their half-lives, are listed in Table 3.3. The list emphasises the region of interest above 2200 keV, whereas with respect to lower energies, only the most prominent peaks are given. Note that some lines in Table 3.3 (e.g. No. 13) appear as blanks. This has been done for the sake of consistency with respect to results presented in Section 3.3.

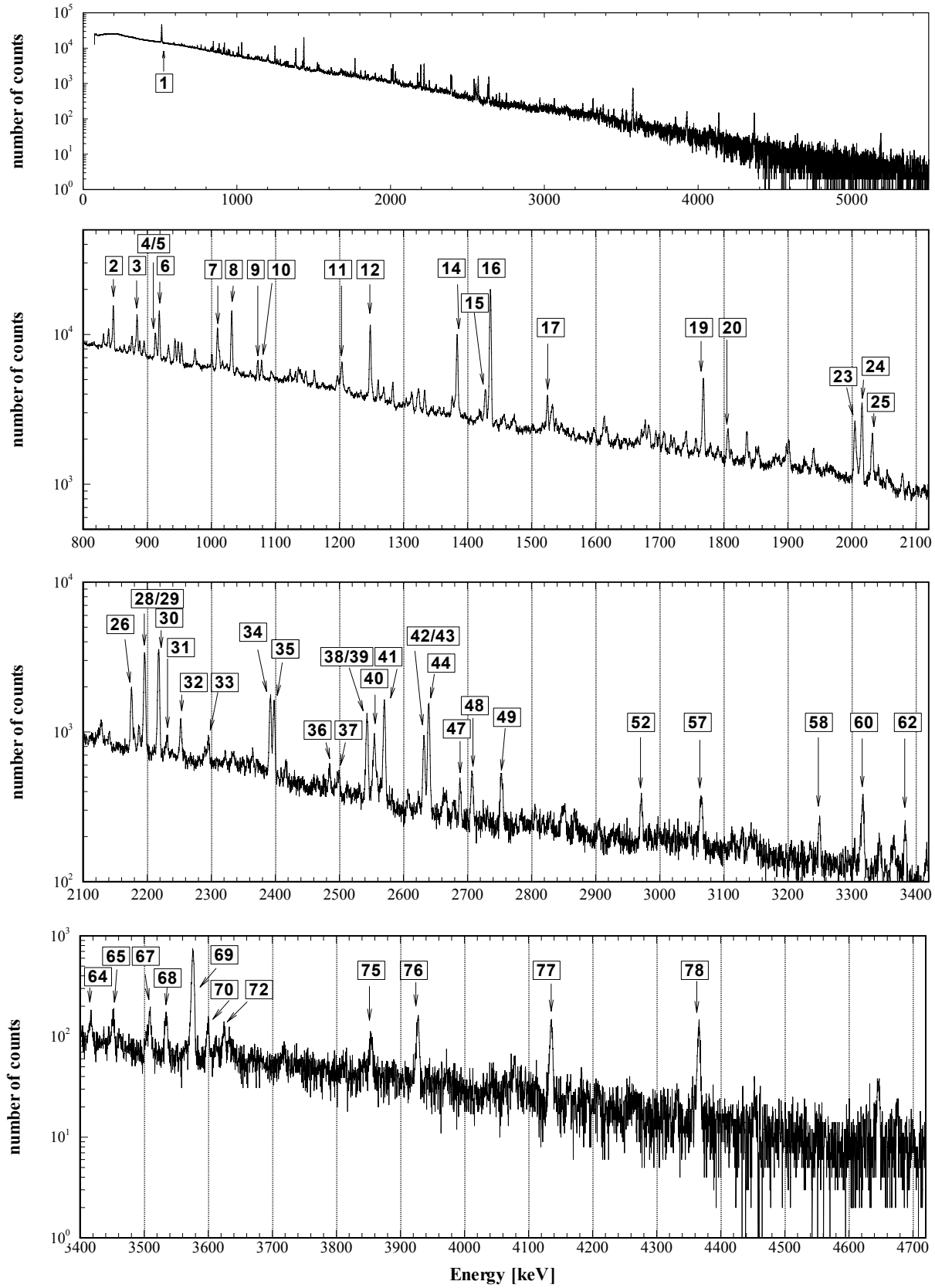


Figure 3.4: Gamma-ray spectrum of a fresh UO_2 pellet irradiated in the BR1 reactor (top), with focus on the 800-2100 keV, 2100-3400 keV and 3400-4700 keV regions.

Table 3.3: Gamma-ray lines from a fresh UO₂ pellet irradiated in the BR1 reactor. The listed lines correspond to the spectrum shown in Fig. 3.4.

No.	Energy	a	Origin	No.	Energy	a	Origin
1	511 keV	x	annihilation	41	2570 keV	x	⁸⁹ Rb (10.2%) 15.4 min
2	847 keV	x	¹³⁴ I (95.4%) 52.5 min	42	2632 keV	x	⁹⁵ Y (4.8%) 10.3 min
3	884 keV	x	¹³⁴ I (64.9%) 52.5 min	43	2634 keV	(x)	¹³⁶ I (6.7%) 1.4 min
4	913 keV	x	^{133m} Te (55.3%) 55.4 min	44	2640 keV	x	¹³⁸ Cs (7.6%) 33.4 min
5	915 keV	x	^{133m} Te (10.9%) 55.4 min	45			
6	919 keV	x	⁹⁴ Y (56%) 18.7 min	46			
7	1010 keV	x	¹³⁸ Cs (2.3%) 33.4 min	47	2688 keV	(x)	⁹³ Sr (2.1%) 7.4 min
8	1032 keV	x	⁸⁹ Rb (63.6%) 15.4 min	48	2707 keV	x	⁸⁹ Rb (2.1%) 15.4 min
9	1072 keV	(x)	¹³⁴ I (14.9%) 52.5 min	49	2753 keV	(x)	^{90m} Rb (11.5%) 4.3 min
10	1079 keV	(x)	¹⁴² Ba (11.5%) 10.6 min	50			
11	1204 keV	x	¹⁴² Ba (14.2%) 10.6 min	51			
12	1248 keV	x	⁸⁹ Rb (45.6%) 15.4 min	52	2971 keV	(x)	¹⁴² La (3.2%) 1.5 h
13				53			
14	1383 keV	x	⁹² Sr (93%) 2.7 h	54			
15	1428 keV	(x)		55			
16	1435 keV	x	¹³⁸ Cs (76.3%) 33.4 min	56			
17	1525 keV	x		57	3065 keV	x	
18				58	3249 keV	(x)	⁹⁵ Y (0.9%) 10.3 min
19	1768 keV	x	¹³⁸ Xe (16.7%) 14.1 min	59			
20	1807 keV	(x)		60	3317 keV	x	^{90m} Rb (14.3%) 4.3 min
21				61			
22				62	3383 keV	(x)	⁹⁰ Rb (6.7%) 2.6 min
23	2004 keV	x		63			
24	2016 keV	x		64	3416 keV	(x)	
25	2032 keV	(x)		65	3451 keV	(x)	⁹⁵ Y (0.7%) 10.3 min
26	2175 keV	x	⁹⁵ Y (7.0%) 10.3 min	66			
27				67	3509 keV	(x)	⁸⁹ Rb (1.3%) 15.4 min
28	2195 keV	(x)	⁸⁸ Kr (13.2%) 2.8 h	68	3534 keV	x	⁹⁰ Rb (4.0%) 2.6 min
29	2196 keV	x	⁸⁹ Rb (14.6%) 15.4 min	69	3576 keV	x	⁹⁵ Y (6.4%) 10.3 min
30	2218 keV	x	¹³⁸ Cs (15.2%) 33.4 min	70	3600 keV	(x)	
31	2232 keV	(x)	⁸⁸ Kr (3.4%) 2.8 h	71			
32	2252 keV	(x)	¹³⁸ Xe (2.3%) 14.1 min	72	3625 keV	(x)	
33	2295 keV	(x)	⁹⁵ Y (1.1%) 10.3 min	73			
34	2392 keV	x	⁸⁸ Kr (35%) 2.8 h	74			
35	2398 keV	x	¹⁴² La (13.3%) 1.5 h	75	3853 keV	(x)	
36	2484 keV	(x)	⁸⁴ Br (6.7%) 31.8 min	76	3928 keV	x	⁸⁴ Br (6.8%) 31.8 min
37	2500 keV	(x)		77	4135 keV	x	⁹⁰ Rb (6.7%) 2.6 min
38	2542 keV	x	¹⁴² La (10%) 1.5 h	78	4365 keV	x	⁹⁰ Rb (8.0%) 2.6 min
39	2544 keV	x	⁹³ Sr (3%) 7.4 min				
40	2555 keV	x	⁸⁷ Kr (9.2%) 1.3 h				

 a: peaks observed in spectrum in Fig. 3.4, $t_{irr} = 30$ min at 1 kW, $t_{cool} = 0$, $t_a = 40$ min

x: signal-to-background ratio > 0.4 or net-count area > 10000 counts

(x): signal-to-background ratio < 0.4 and net-count area < 10000 counts

3.2.3 Results of the experimental campaign at BR1

From the identified gamma-ray lines listed in the previous subsection, potential candidates for the measurement of fission rates in fresh and burnt fuel were selected. The selection of appropriate gamma-ray lines was guided by several criteria. First of all, keeping in mind the envisaged investigation on burnt fuel, the gamma-ray energy had to be above 2200 keV. Appropriate peaks should ideally show good counting statistics due to high gamma-ray intensities and equally high cumulative fission yields of the fission product both for ^{235}U and ^{239}Pu fissions. With regard to the determination of net-count areas, the gamma-ray lines should preferably not interfere with other lines.

The fission products ^{90}Rb ($T_{1/2} = 2.6$ min), ^{90m}Rb (4.3 min), ^{95}Y (10.3 min), ^{89}Rb (15.4 min), ^{84}Br (31.8 min), ^{138}Cs (33.4 min), ^{142}La (1.5 h) and ^{88}Kr (2.8 h) have several gamma-ray lines fulfilling (at least partly) these criteria.

Table 3.4: Measured net counts and signal-to-background ratios (S/Bg) of high-energy peaks from a fresh UO_2 pellet irradiated in the BR1 reactor.

Energy	Fission product	Net counts*	S/Bg*
1435 keV	^{138}Cs	149132 (1.0%)	0.79
2218 keV	^{138}Cs	25208 (1.3%)	1.21
2392 keV	^{88}Kr	10951 (1.8%)	0.75
2398 keV	^{142}La	9803 (2.1%)	0.60
2542 keV	^{142}La	8880 (2.7%)	0.76
2570 keV	^{89}Rb	11226 (2.2%)	0.92
2632 keV	^{95}Y	5829 (2.6%)	0.66
2640 keV	^{138}Cs	11930 (1.4%)	1.45
2753 keV	^{90m}Rb	3636 (6.6%)	0.39
2971 keV	^{142}La	1634 (11.8%)	0.23
3317 keV	^{90}Rb	2884 (6.2%)	0.56
3383 keV	^{90}Rb	916 (8.6%)	0.36
3576 keV	^{95}Y	7432 (1.9%)	2.81
3928 keV	^{84}Br	1540 (7.3%)	0.92
4135 keV	^{90}Rb	1384 (8.5%)	0.93
4365 keV	^{90}Rb	1283 (5.7%)	1.69

*The quoted values refer to the gamma-ray spectrum shown in Fig. 3.4.

Based on the spectrum shown in Fig. 3.4, the observed net-count areas, their statistical uncertainties and the signal-to-background ratios of the selected gamma-ray lines above 2200 keV are listed in Table 3.4. The 1435 keV line from ^{138}Cs is given as well because, due to its high net-count area and low counting uncertainty, it was included in the analysis for cross-comparison purposes with the high-energy lines. The quoted net-count areas and signal-to-background ratios have been obtained with the region-of-interest (ROI) method within Gamma-Vision [ORT 03a].

In most of the spectra, the gamma-ray lines given in Table 3.4 were clearly apparent. Still, not all of them could be included in a suitable quantitative analysis due to too small net-count areas. In addition, the peak fitting, which was carried out with the Gamma-Vision software, was complicated because of the complex spectra with slightly non-Gaussian peak shapes and because of the lack of appropriate calibration spectra for covering energies up to 4000 keV. In particular, the deconvolution of the two peaks ^{88}Kr (2392 keV) and ^{142}La (2398 keV) was found to be very difficult using Gamma-Vision.

Finally, the quantitative analysis was carried out based on the five gamma-ray lines ^{138}Cs (2218 keV), ^{89}Rb (2570 keV), ^{138}Cs (2640 keV), ^{95}Y (2632 keV) and - as reference - ^{138}Cs (1435 keV). Based on these peaks, relative fission rates comparing the three irradiations listed in Table 3.2 were derived, and thus the feasibility of determining relative fission rates using the short-lived fission product activity could be demonstrated. The uncertainties (1σ) of the derived fission rate ratios were about 2% to up to 6% and mainly consisted of statistical uncertainties of the net-count areas. Taking the result obtained based on the ^{138}Cs (1435 keV) peak as reference (which had a 1σ uncertainty of 0.7 to 2%), the derived fission rate ratios agreed within 1 standard deviation [Kröhnert 08].

In general, the low count rates in the high-energy region were found to be a challenge for future experiments. Furthermore, it was noted that the Gamma-Vision software might not be appropriate for the analysis of complex spectra with non-Gaussian peak shapes.

3.3 Measurements on fresh fuel at PROTEUS

Following irradiations of fresh fuel pellets in the BR1 reactor, a fresh fuel pin was irradiated in the PROTEUS reactor. During this campaign, the measurements of the induced gamma-ray activities were conducted on top of the reactor shielding. This measurement position had the advantage to be well shielded against the gamma-ray and neutron background from the core, because of the ~ 80 cm thick concrete doors of the reactor.

The main goals of this campaign were to reproduce the gamma-ray lines previously identified in the frame of the BR1 campaign, to extend the database from the BR1 campaign to fission products with longer half-lives (30 min to several hours), and to better estimate the power levels, the irradiation and measurement times, as also the filter needed, to obtain sufficient counts in the identified gamma-ray lines for the future experiments on burnt fuel.

3.3.1 Experimental set-up and measurements

The fresh fuel pin was irradiated in the central position of the current test lattice of the PROTEUS reactor. To allow the insertion of this experimental fuel pin, the central lattice pin had been removed, as illustrated in Fig. 3.5.

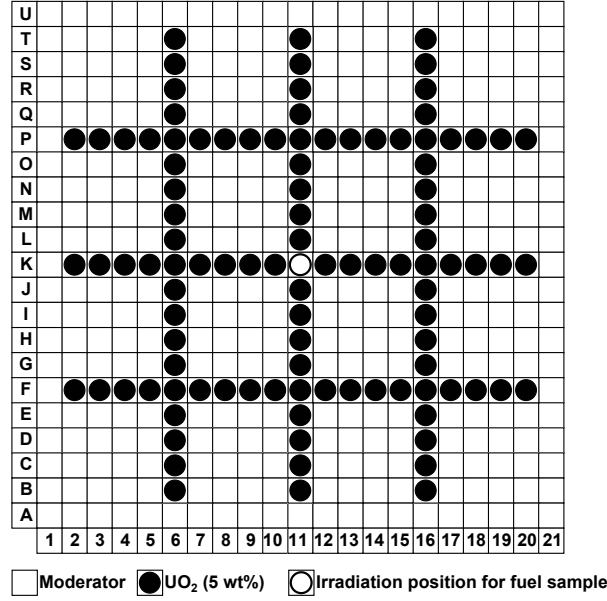


Figure 3.5: PROTEUS test lattice and central irradiation position.

After irradiation, the pin was withdrawn manually from the core with the help of a wire attached to its top. The pin was taken out of the reactor through a 20 mm diameter penetration in the reactor top shielding and was brought into the measurement position in front of the detector. As shown in Fig.3.6, the HPGe detector (model GEM-15180-P, 4500V) was mounted on top of the reactor shielding. The distance between the detector and the centre of the sample was about 18 cm. The filter between the detector and the pin consisted of 10 cm of lead. This amount of lead was chosen as a good compromise to shield against the low-energy gamma-rays without attenuating the high-energy gamma-rays too much. With linear attenuation coefficients μ of 1.832 cm^{-1} for 500 keV photons and 0.481 cm^{-1} for 3000 keV photons [Hubbel 95], it can be estimated that 10 cm of lead reduce the intensity of a 500 keV photon flux by more than 99.9%, whereas the intensity of a 3000 keV photon flux is reduced by 99.2%.

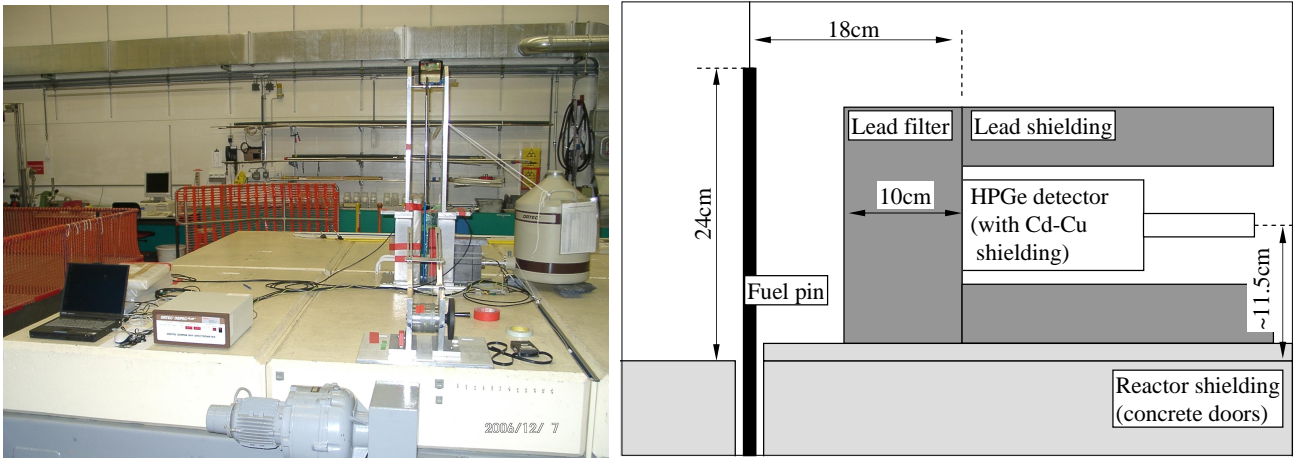


Figure 3.6: General and schematic views of the experimental set-up on top of the PROTEUS reactor.

The fresh fuel pin used was an experimental UO₂ pin with an enrichment of 4.74%. It had an active length of about 90 cm and a fuel pellet diameter of 8.19 mm. In order to minimise the

gamma-ray dose received by the operator while handling the pin, only the upper 24 cm of the irradiated pin were drawn out of the reactor doors. To account for the fact that only the upper part of the pin was measured, the vertical position of the pin in the core during irradiation was chosen in a way that the maximum induced fission rate was to be expected in the upper part of the pin.

In Table 3.5, the conditions for the main irradiations carried out in the context of the described campaign are summarised. The irradiations were performed at reactor powers varying from 120 to 400 W. The irradiation times were typically between 10 and 45 min. After irradiation, the gamma-ray activity of the pin was measured for up to about 12 h, starting 5 min after the reactor shutdown. The time needed to withdraw the pin from the core to the measurement position was about 1 min. However, the pin was not withdrawn from the core earlier than 4 min after shutdown, in order to reduce the radiation dose received by the operator handling the pin.

Table 3.5: Irradiation and measurement conditions for measurements on top of the PROTEUS reactor.

		Irradiation		Measurement			
Index	Pin enrichment	Reactor power	t_{irr}	Lead filter	Distance pin-detector	t_a	dT_{max}
A	4.74%	400 W	10 min	10 cm	18 cm	~ 1.5 h	26%
B	4.74%	200 W	30 min	10 cm	18 cm	~ 12 h	23%
C	4.74%	120 W	45 min	10 cm	18 cm	~ 12 h	17%
D	4.74%	160 W	45 min	10 cm	18 cm	~ 12 h	22%

t_{irr} : irradiation time; t_a : acquisition time; dT_{max} : maximum system dead time at the beginning of data acquisition (5 min after irradiation)

3.3.2 Gamma-ray spectra and observed gamma-ray lines

An example of the acquired gamma-ray spectra is shown in Fig. 3.7. This spectrum was obtained after irradiating the pin for 45 min at a reactor power of 160 W (irradiation D in Table 3.5). The counts were acquired for about 6.5 h starting 5 minutes after shutdown. The peaks marked are listed in Table 3.6. To ease the comparison, the peaks marked in the spectrum obtained at BR1 (Fig. 3.4) are also included in the table. Several gamma-ray lines from ^{142}La ($T_{1/2} = 1.5$ h), which were barely visible in the spectra obtained at the BR1 reactor, can be clearly seen due to the longer irradiation and measurement times.

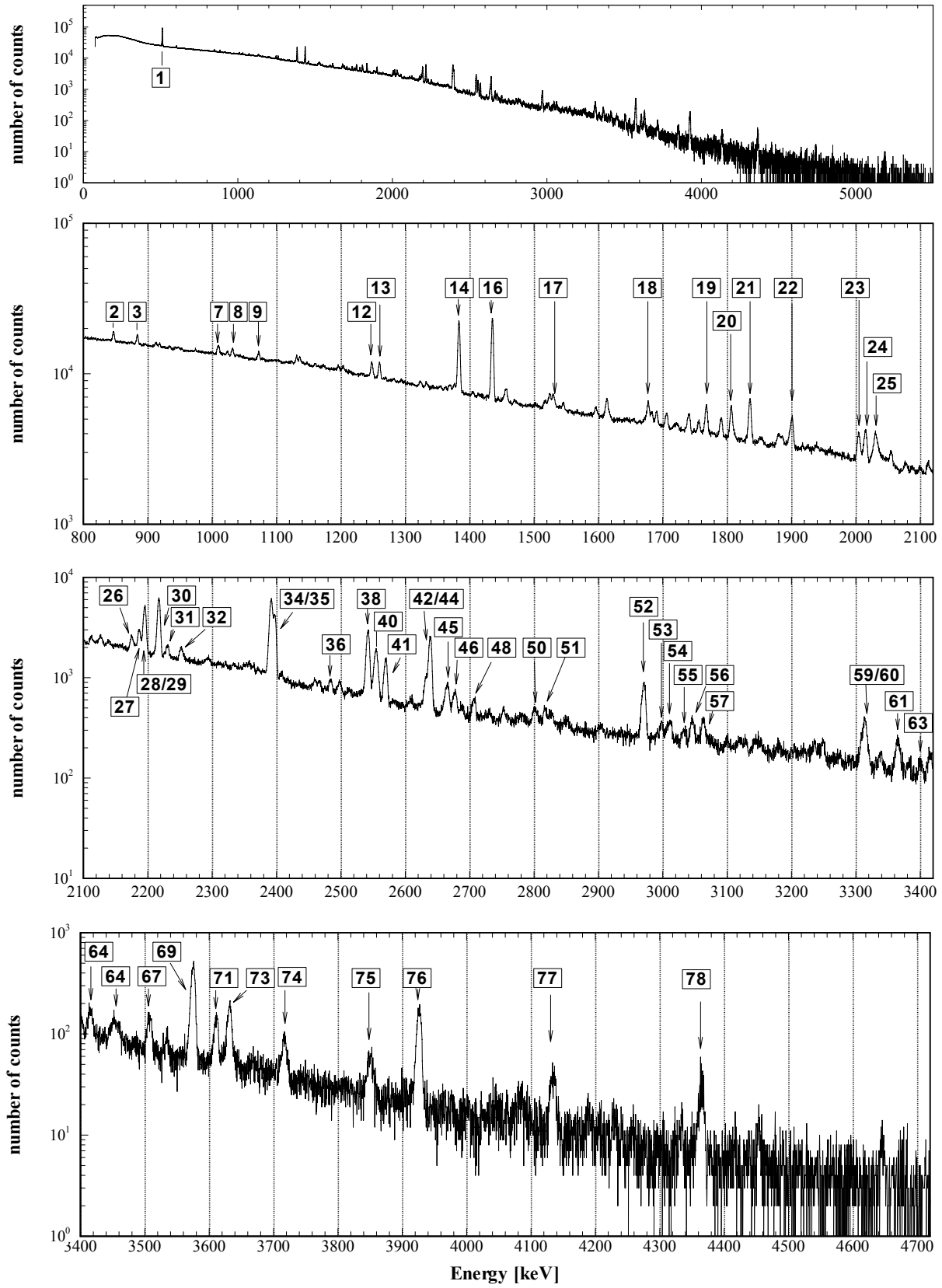


Figure 3.7: Gamma-ray spectrum of a fresh UO_2 pin irradiated in the PROTEUS reactor (top), with focus on the 800-2100 keV, 2100-3400 keV and 3400-4700 keV regions.

Table 3.6: Gamma-ray lines from fresh UO₂ fuel irradiated in the BR1 and PROTEUS reactors. The listed lines correspond to the spectra shown in Fig. 3.4 and Fig. 3.7.

No.	Energy	a	b	Origin	No.	Energy	a	b	Origin
1	511 keV	x	x	annihilation	41	2570 keV	x	x	⁸⁹ Rb (10.2%) 15.4 min
2	847 keV	x	x	¹³⁴ I (95.4%) 52.5 min	42	2632 keV	x	(x)	⁹⁵ Y (4.8%) 10.3 min
3	884 keV	x	x	¹³⁴ I (64.9%) 52.5 min	43	2634 keV	(x)		¹³⁶ I (6.7%) 1.4 min
4	913 keV	x		^{133m} Te (55.3%) 55.4 min	44	2640 keV	x	x	¹³⁸ Cs (7.6%) 33.4 min
5	915 keV	x		^{133m} Te (10.9%) 55.4 min	45	2666 keV		(x)	¹⁴² La (1.8%) 1.5 h
6	919 keV	x		⁹⁴ Y (56%) 18.7 min	46	2678 keV		(x)	⁸⁸ Rb (2.1%) 18.3 min
7	1010 keV	x	x	¹³⁸ Cs (2.3%) 33.4 min	47	2688 keV	(x)	(x)	⁹³ Sr (2.1%) 7.4 min
8	1032 keV	x	(x)	⁸⁹ Rb (63.6%) 15.4 min	48	2707 keV	x	(x)	⁸⁹ Rb (2.1%) 15.4 min
9	1072 keV	(x)	x	¹³⁴ I (14.9%) 52.5 min	49	2753 keV	(x)		^{90m} Rb (11.5%) 4.3 min
10	1079 keV	(x)		¹⁴² Ba (11.5%) 10.6 min	50	2801 keV		(x)	¹⁴² La (0.8%) 1.5 h
11	1204 keV	x		¹⁴² Ba (14.2%) 10.6 min	51	2818 keV		(x)	¹⁴² La (0.8%) 1.5 h
12	1248 keV	x	x	⁸⁹ Rb (45.6%) 15.4 min	52	2971 keV	(x)	x	¹⁴² La (3.2%) 1.5 h
13	1260 keV		x	¹³⁵ I (28.7%) 6.6 h	53	3000 keV		(x)	
14	1383 keV	x	x	⁹² Sr (93%) 2.7 h	54	3012 keV		(x)	
15	1428 keV	(x)			55	3034 keV		(x)	
16	1435 keV	x	x	¹³⁸ Cs (76.3%) 33.4 min	56	3045 keV		(x)	⁸⁴ Br (2.5%) 31.8 min
17	1525 keV	x	(x)		57	3065 keV	x		
18	1679 keV		(x)		58	3249 keV	(x)		⁹⁵ Y (0.9%) 10.3 min
19	1768 keV	x	x	¹³⁸ Xe (16.7%) 14.1 min	59	3313 keV		x	¹⁴² La (1.0%) 1.5 h
20	1807 keV	(x)	x		60	3317 keV	x	(x)	^{90m} Rb (14.3%) 4.3 min
21	1836 keV		x		61	3366 keV		(x)	⁸⁴ Br (2.9%) 31.8 min
22	1900 keV		x		62	3383 keV	x		⁹⁰ Rb (6.7%) 2.6 min
23	2004 keV	x	x		63	3401 keV		(x)	
24	2016 keV	x	x		64	3416 keV	(x)	(x)	
25	2032 keV	(x)	x		65	3451 keV	(x)		⁹⁵ Y (0.7%) 10.3 min
26	2175 keV	x	(x)	⁹⁵ Y (7.0%) 10.3 min	66				
27	2187 keV		(x)		67	3509 keV	(x)	(x)	⁸⁹ Rb (1.3%) 15.4 min
28	2195 keV	(x)	x	⁸⁸ Kr (13.2%) 2.8 h	68	3534 keV	x		⁹⁰ Rb (4.0%) 2.6 min
29	2196 keV	x	x	⁸⁹ Rb (14.6%) 15.4 min	69	3576 keV	x	x	⁹⁵ Y (6.4%) 10.3 min
30	2218 keV	x	x	¹³⁸ Cs (15.2%) 33.4 min	70	3600 keV	(x)		
31	2232 keV	(x)	(x)	⁸⁸ Kr (3.4%) 2.8 h	71	3612 keV		x	¹⁴² La (0.9%) 1.5 h
32	2252 keV	(x)	(x)	¹³⁸ Xe (2.3%) 14.1 min	72	3625 keV	(x)		
33	2295 keV	(x)		⁹⁵ Y (1.1%) 10.3 min	73	3632 keV		x	¹⁴² La (1.0%) 1.5 h
34	2392 keV	x	x	⁸⁸ Kr (35%) 2.8 h	74	3719 keV		(x)	
35	2398 keV	x	x	¹⁴² La (13.3%) 1.5 h	75	3853 keV	(x)	(x)	
36	2484 keV	(x)	(x)	⁸⁴ Br (6.7%) 31.8 min	76	3928 keV	x	x	⁸⁴ Br (6.8%) 31.8 min
37	2500 keV	(x)			77	4135 keV	x	(x)	⁹⁰ Rb (6.7%) 2.6 min
38	2542 keV	x	x	¹⁴² La (10%) 1.5 h	78	4365 keV	x	(x)	⁹⁰ Rb (8.0%) 2.6 min
39	2544 keV	x		⁹³ Sr (3%) 7.4 min					
40	2555 keV	x	x	⁸⁷ Kr (9.2%) 1.3 h					

a: peaks observed in spectrum in Fig. 3.4, $t_{irr} = 30$ min at 1 kW, $t_{cool} = 0$, $t_a = 40$ minb: peaks observed in spectrum in Fig. 3.7, $t_{irr} = 45$ min at 1 kW, $t_{cool} = 5$ min, $t_a = 6.5$ hx: signal-to-background ratio > 0.4 or net-count area > 10000 counts(x): signal-to-background ratio < 0.4 and net-count area < 10000 counts

3.3.3 Results of measurements on top of PROTEUS

As the gamma-ray measurements were not started earlier than 5 min after shut-down, the very short-lived fission products (e.g. ^{90}Rb and ^{90m}Rb) which had been detected at the BR1 were hardly visible in this campaign at PROTEUS. All other gamma-ray lines from short-lived fission products, previously detected at the BR1 reactor, could be identified.

Thanks to longer irradiation and measurement times, better counting statistics were achieved for the relatively long-lived fission products such as ^{138}Cs and ^{142}La . The net-count areas and signal-to-background ratios, as obtained with Gamma-Vision, of the most promising peaks shown in Fig. 3.7 are listed in Table 3.7. It should be mentioned that the 10 cm lead filter between the fuel pin and the detector was found to be appropriate for limiting the maximum system dead time at the beginning of data acquisition to below 30%.

Table 3.7: Measured net counts and signal-to-background ratios (S/Bg) of high-energy peaks from a fresh UO_2 pin measured on top of PROTEUS.

Energy	Fission product	Net counts*	S/Bg*
2218 keV	^{138}Cs	60065 (1.3%)	0.77
2392 keV	^{88}Kr	72197 (0.7%)	0.85
2398 keV	^{142}La	45895 (1.1%)	0.44
2542 keV	^{142}La	31969 (1.4%)	1.03
2570 keV	^{89}Rb	14193 (2.4%)	0.67
2632 keV	^{95}Y	7867 (4.0%)	0.17
2640 keV	^{138}Cs	33752 (0.9%)	1.30
2971 keV	^{142}La	10946 (2.5%)	1.00
3313 keV	^{142}La	5588 (5.2%)	0.64
3576 keV	^{95}Y	8489 (2.3%)	2.57
3612 keV	^{142}La	1701 (6.9%)	0.77
3632 keV	^{142}La	2170 (6.1%)	0.78
3928 keV	^{84}Br	3110 (3.6%)	2.36

*The quoted values refer to the gamma-ray spectrum shown in Fig. 3.7.

3.4 WOLF-A experimental campaign on fresh and burnt fuel

In the previous sections, the first experiments with fresh fuel have been described. During these experiments, carried out at the BR1 and PROTEUS reactors, the gamma-ray measurements themselves could be conducted outside of the reactor blocks, where the detectors could be easily shielded in an adequate manner.

The final measurements on burnt fuel samples have been conducted during the so-called WOLF-B campaign (WOLF = **W**echsselflasche **O**ptimisation for **L**IFE@**P**ROTEUS), described in the following chapter. The goal set for the WOLF-B campaign has been to use the combined transport and sample changer flask described in Section 2.3 for introducing the burnt fuel samples into the reactor, and to measure their gamma-ray activity after irradiation. For this purpose, the sample changer flask needed to be located on top of the reactor inside the reactor shielding, and consequently, the measurements had to take place within the reactor shielding. The WOLF-A campaign, described in this section, was performed to carry out a first assessment of this environment for measuring freshly induced, fission product gamma-ray activity in burnt fuel. During WOLF-A, both fresh and burnt fuel samples were irradiated in PROTEUS, and the gamma-ray measurements were conducted within the reactor shielding.

3.4.1 Experimental set-up and measurements

During the WOLF-A campaign, the sample changer was loaded with two fresh and four burnt fuel samples with nominal burn-ups of 0 (fresh), 36, 46, 64 and 84 GWd/t. The samples had an active length of about 40 cm and a fuel diameter of about 0.91 cm. The characteristics of the samples will be described in further detail in Chapter 4. At this point, only the experimental set-up and the main outcome of the campaign are reported.

The sample changer was positioned on a special support structure directly above the reactor, inside the reactor shielding. The support structure and the sample changer in position are shown in Fig. 3.8. The fuel samples inside the sample changer were arranged in a revolver. By rotating this revolver, single samples could be inserted into the central position of the test lattice via a guiding tube, the test lattice being the same as described in the previous section (see Fig. 3.5).

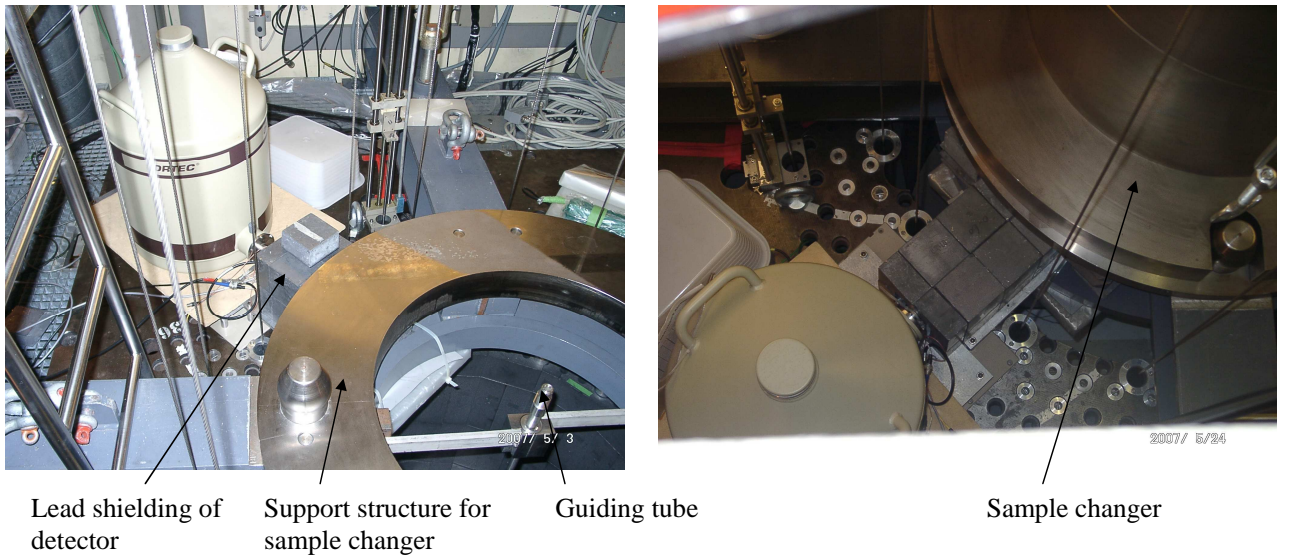


Figure 3.8: Views of the experimental set-up during WOLF-A, without (left) and with (right) sample changer in position.

As illustrated in Fig. 3.9, the HPGe detector (model GEM-15180-P, 4500 V) was mounted between the two rings of the support structure below the sample changer. During the WOLF-A campaign, various detector positions and filter conditions have been tested. The measurements presented in this thesis refer to the set-up shown in Fig. 3.9, where the distance between detector

and the centre of the guiding tube was approximately 52 cm. The filter in front of the detector consisted of 5 cm of paraffin and of 11 cm of lead; 6 cm of the lead contained a horizontal collimator slit with a width of 1.6 cm. The detector was surrounded by 5 cm wide lead bricks to mitigate the gamma-ray background from the reactor core, while polyethylene was placed around and below the detector to moderate the fast neutrons from the reactor core.

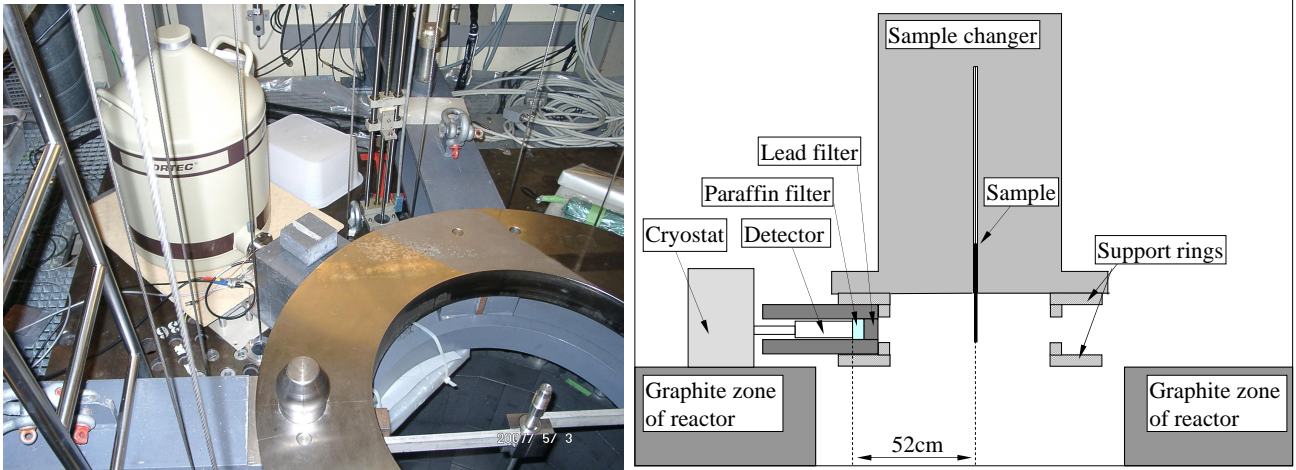


Figure 3.9: Example of detector position and filter used during the WOLF-A campaign.

The set of WOLF-A experiments described here in greater detail is given in Table 3.8. The first four measurements (A - D) are background measurements of the intrinsic gamma-ray activities of the burnt fuel samples without irradiation. To this end, the burnt fuel samples were moved one at a time into the measurement position below the sample changer, while the other burnt samples remained inside the sample changer. In the measurement position, the sample was placed such that only about 21 cm of the fuel were protruding out from the shielding steel body of the sample changer (see Fig. 3.9). This measurement position was chosen to achieve acceptable dead time levels of the detection system. The average dead times due to the intrinsic background activities of the 36, 46, 64 and 84 GWd/t burnt samples in this measurement position were 49%, 63%, 73% and 80%, respectively¹.

Using the same measurement position, measurements were conducted on both fresh and burnt fuel samples after irradiation in PROTEUS (measurements E and F in Table 3.8). For these measurements, the samples were irradiated in the test lattice for 5 min at a reactor power of 100 W.

In addition, to measure the background due to the reactor, the same irradiation was carried out leaving all samples in the sample changer and measuring gamma-ray spectra during the same time after reactor shutdown (measurement G in Table 3.8).

One essential aspect to be considered during the WOLF-A campaign was the high fast neutron flux reaching the detector crystal during the irradiations. The resulting damage of the germanium crystal led to a continuous worsening of the detector resolution, which limited the number of possible irradiations and the reactor power. In fact, after having reached a very poor resolution of ~ 5.9 keV at 1293 keV², the detector had to be replaced by another one (model GEM-18180-P,

¹The very high dead times of more than 70% were accepted in this case since the measurements were reference measurements of the burnt fuel samples with constant count rates.

²The gamma-line at 1293 keV is emitted by ^{116m}In , which is an activation product in the detector mount ($T_{1/2} = 54$ min). The resolution was determined for a total input count rate of 5200 cps and a rise time of 1.6 μs .

3500 V) in the middle of the campaign. The damaged detector was later repaired via annealing and was used again for measurements in the following experimental campaigns.

Several sets of measurements similar to that shown in Table 3.8 were conducted to test different distances between sample and detector (41 cm to 52 cm) and different filter configurations (5 to 11 cm of lead, with and without collimator). In addition, different shielding strategies to protect the detector from the neutron background from the reactor core were tested. For example, additional polyethylene blocks were placed below and next to the detector. For all measurement sets, however, the results were very similar.

Table 3.8: Irradiation and measurement conditions for a set of WOLF-A experiments.

		Irradiation		Measurement			
Index	Sample burn-up	Reactor power	t_{irr}	Distance sample-detector	Lead filter*	t_a	dT_{max}
A	36 GWd/t	-	-	52 cm	11 cm	30 min	49%
B	46 GWd/t	-	-	52 cm	11 cm	30 min	63%
C	64 GWd/t	-	-	52 cm	11 cm	30 min	73%
D	84 GWd/t	-	-	52 cm	11 cm	30 min	80%
E	fresh	100 W	5 min	52 cm	11 cm	~5 h	37%
F	36 GWd/t	100 W	5 min	52 cm	11 cm	~5 h	70%
G	-	100 W	5 min	-	-	~5 h	37%

t_{irr} : irradiation time; t_a : acquisition time; dT_{max} : maximum dead time (for E, F, and G: 5 min after irradiation)

*6 cm of the lead filter contained a collimator slit ($1.6 \times 6 \text{ cm}^2$)

3.4.2 Gamma-ray spectra and observed gamma-ray lines

Reference spectra of the intrinsic gamma-ray activities of the four burnt fuel samples were recorded, and these are compared in Fig. 3.10 in the form of dead-time corrected (ZDT) spectra. The most prominent peaks from long-lived fission products are marked.

In Fig. 3.11, the gamma-ray spectrum after irradiating the 36 GWd/t burnt sample (5 min at 100 W) is compared with that due to the reactor background after irradiation. The burnt fuel spectrum illustrates the possibility to detect, even in the presence of the intrinsic activity of the burnt fuel sample, gamma-ray peaks from short-lived fission products above 2200 keV. However, the comparison with the reactor background spectrum clearly shows that the major part of the detected activity in the high-energy region resulted from fission products freshly produced in the reactor fuel, rather than in the measured burnt fuel sample.

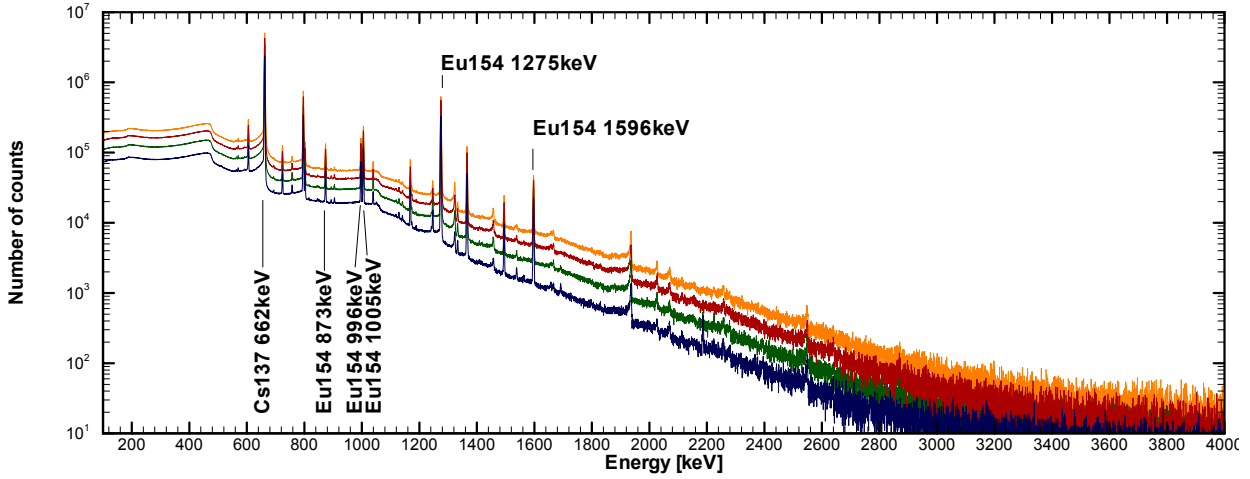


Figure 3.10: Spectra of intrinsic gamma-ray activities of burnt fuel samples with nominal burn-ups of 36 GWd/t (blue), 46 GWd/t (green), 64 GWd/t (red), and 84 GWd/t (orange).

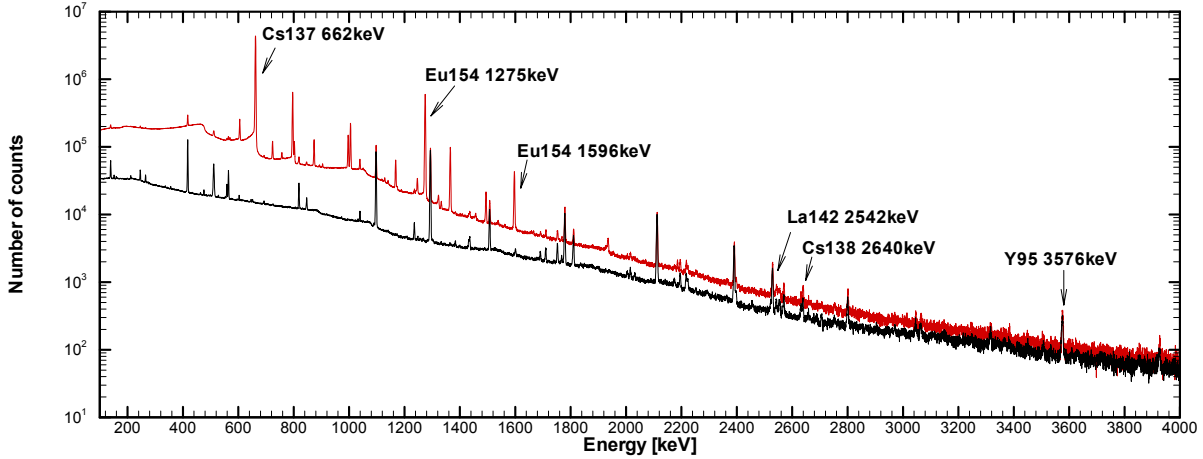


Figure 3.11: Comparison between gamma-ray spectrum of irradiated 36 GWd/t sample (red) and background spectrum after irradiation without sample (black).

3.5 Conclusions from preliminary experiments

The goals of the described preliminary experimental campaigns were to build up an extensive database of gamma-ray lines emitted by short-lived fission products in nuclear fuel and to identify suitable gamma-ray lines, which could be used for the new measurement technique to determine fission rates in fresh and burnt fuel.

An experimental campaign on irradiated fresh UO_2 fuel pellets was conducted at the BR1 reactor focusing on very short-lived fission products. The irradiation and measurement times were typically between 2-30 min and 5-90 min, respectively. In the analysis of the measurements, ^{138}Cs ($T_{1/2} = 33.4$ min), ^{89}Rb (15.4 min) and ^{95}Y (10.3 min) were identified as promising fission products from which relative fission rates could be derived. ^{142}La , with a half-life of 1.5h, was identified as an additional candidate for future experiments, but could not be included in the quantitative analysis because of poor statistics in most of its gamma-ray lines. ^{88}Kr has a

very prominent gamma-ray line at 2392 keV which overlaps partly the ^{142}La (2398 keV) peak. Although both peaks had sufficient counts, neither of them was included in the analysis because of peak fitting difficulties within the Gamma-Vision software, which was used for the determination of the peak net-count areas. Finally, the feasibility to derive experimental fission rate ratios was demonstrated on the basis of the four high-energy gamma-ray lines ^{138}Cs (2218 keV), ^{89}Rb (2570 keV), ^{95}Y (2632 keV) and ^{138}Cs (2640 keV).

An campaign on a fresh UO_2 experimental pin was carried out at PROTEUS and aimed at improving the irradiation and data acquisition strategies. The irradiation and measurement times were extended to up to 45 min and 6 h, respectively. Thus, better counting statistics were obtained for the ^{142}La peaks.

^{90}Rb and ^{90m}Rb are two further fission products which have gamma-ray lines in the high-energy region. However, they do not have as high fission yields as the other identified isotopes. Because of their very short half-lives, they will most likely not be suitable for the LIFE@PROTEUS experiments, where the transfer time to bring the irradiated fuel pins to the measurement position will probably be in the range of several minutes.

Another fission product which could be theoretically used as a fission rate indicator is ^{84}Br , which has a gamma-ray line at 3928 keV. However, its fission yields for both ^{235}U and ^{239}Pu fissions are very low. Furthermore, ^{90}Rb and ^{84}Br have gamma-ray lines in the very high energy region (about 4000 keV). This is a disadvantage compared to the other identified peaks because, due the rapidly decreasing efficiency of the HPGe detectors with higher energy, it is very difficult to obtain sufficiently high count rates in these peaks.

In Table 3.9, the characteristics of all identified fission products which could serve as fission rate indicators in fresh and burnt fuel are summarised. The most prominent gamma-ray lines above 2200 keV are listed as well. All nuclear data are extracted from JEFF-3.1 [Koning 06].

Table 3.9: Gamma-ray line candidates for measuring fission rates in fresh and burnt fuel.

Fission product	Half-life	Cumulative th. fission yields [%]		Gamma-ray lines (intensity)
		^{235}U	^{239}Pu	
^{88}Kr	2.84 h	3.54 (1.8%)	1.25 (2.8%)	2392 keV (35%)
^{142}La	1.52 h	5.86 (1.7%)	4.97 (1.1%)	2398 keV (13.3%), 2542 keV (10%), 2971 keV (3.2%)
^{138}Cs	33.4 min	6.69 (1.7%)	5.94 (2.7%)	2218 keV (15.2%), 2640 keV (7.6%)
^{89}Rb	15.4 min	4.69 (1.2%)	1.68 (1.9%)	2570 keV (10.2%)
^{95}Y	10.3 min	6.47 (1.1%)	4.82 (2.0%)	2632 keV (4.8%), 3576 keV (6.4%)
^{84}Br	31.8 min	1.01 (1.9%)	0.45 (4.3%)	3928 keV (6.8%)
^{90m}Rb	4.3 min	1.36 (14.1%)	0.71 (14.0%)	2753 keV (11.5%), 3317 keV (14.3%)
^{90}Rb	2.6 min	4.37 (3.0%)	1.27 (5.4%)	3383 keV (6.7%) , 4135 keV (6.7%), 4365 keV (8%)

In the frame of the WOLF-A experimental campaign, during which measurements were conducted inside the reactor shielding, the possibility to detect high-energy gamma-ray activity

from short-lived fission products next to the high intrinsic gamma-ray background of a 36 GWd/t burnt fuel sample was demonstrated, albeit the detected short-lived activity was mainly coming from the reactor fuel. The observed high gamma-ray background from the reactor, together with the observed degradation in the detector resolution due to neutron damage, emphasised the need for an appropriate gamma-ray and neutron shielding of the detector during and after irradiation.

The next chapter describes the WOLF-B experimental campaign, during which both gamma-ray and neutron backgrounds were mitigated by placing the gamma-ray detector inside the sample changer.

Bibliography

- [Blaauw 03] M. Blaauw. *Experimental tests of zero dead time gamma-ray spectrometry of rapidly decaying sources with the DSPECPLUS*. J. Radioanalytical and Nucl. Chemistry, vol. 257, No.3, page 457-462, 2003.
- [BR1] <http://www.sckcen.be/en/Our-Research/Research-facilities/BR1-Belgium-Reactor-1>. SCK·CEN, Mol, Belgium.
- [DSP] *DSPECPLUSTM, Digital Gamma-Ray Spectrometer*. EG&G ORTEC Catalog, Oak Ridge.
- [Hubbel 95] J.H. Hubbel & S.M. Seltzer. *Tables of X-Ray Mass Attenuation Coefficients and Mass Energy-Absorption Coefficients from 1keV to 20MeV for Elements $Z = 1$ to 92 and 48 Additional Substances of Dosimetric Interest*. National Institute of Standards and Technology, Gaithersburg, Maryland, USA, NISTIR 5632, 1995.
- [Knoll 00] G.F. Knoll. *Radiation Detection and Measurements*. Third edition, page 450, ISBN 0-471-07338-5, 2000.
- [Koning 06] A. Koning. *The JEFF-3.1 Nuclear Data Library*, 2006.
- [Kröhnert 08] H. Kröhnert, M.F. Murphy, G. Perret, M. Plaschy, J. Wagemans & R. Chawla. *Measurement of fission rate ratios in fresh UO_2 fuel utilising short-lived high-energy gamma activity*. PHYSOR Conference 2008, Interlaken, Switzerland, CD-ROM, ISBN 978-3-9521409-5-6, 2008.
- [ORT a] ORTEC. *Loss-Free Counting with Uncertainty Analysis*. Application note AN56.
- [ORT 03a] ORTEC. *GammaVision-32, Gamma-ray Spectrum Analysis and MCA Emulator*, A66-B32 User's Manual, 2003.
- [ORT 03b] ORTEC. *GEM Series Coaxial HPGE Detector*, Product Configuration Guide, 2003.
- [Plaschy 07b] M. Plaschy, G. Perret & M.F. Murphy. *Trip report (PA-1): Physical data corresponding to the measurements achieved in SCK·CEN*. Internal Report AN-41-07-01, PSI, 2007.
- [Wagemans 08] J. Wagemans. *The BR1 Reactor: A Versatile Tool For Fission Experiments*. PHYSOR Conference 2008, Interlaken, Switzerland, CD-ROM, ISBN 978-3-9521409-5-6, 2008.
- [Wagemans 10] J. Wagemans. *personal communication*. SCK·CEN, Mol, Belgium, 2010.

Chapter 4

Measurements of high-energy gamma-rays emitted by short-lived fission products in burnt fuel

This chapter is devoted to the WOLF-B experimental campaign, which was conducted at the PROTEUS reactor. The goals of the WOLF-B campaign were to measure freshly induced gamma-ray activities in burnt UO_2 fuel samples irradiated in PROTEUS and to establish a suitable set of gamma-ray spectra for the derivation of fission rate ratios between fresh and burnt fuels.

The WOLF-B campaign followed the WOLF-A campaign (see Section 3.4), which was part of the preliminary measurements described in the previous chapter. For both the WOLF-A and WOLF-B campaigns, fresh and burnt fuel samples were irradiated in the PROTEUS core using a specially designed sample changer.

During the preliminary measurements on fresh fuel at the BR1 and PROTEUS reactors, various high-energy gamma-ray lines emitted by short-lived fission products (e.g. ^{142}La , ^{138}Cs , ^{89}Rb and ^{95}Y) were identified as suitable for the determination of fission rates in fresh and burnt fuel. During the WOLF-A campaign, gamma-ray spectrometry was conducted for the first time on irradiated burnt fuel samples. However, because the detector was located too close to the reactor core and could not be adequately shielded, the measured gamma-rays lines of interest were mainly emitted by short-lived fission products created in the PROTEUS driver fuel rather than in the measured burnt fuel sample. In addition, the damage in the detector crystal caused by fast neutrons emitted from the reactor core during the irradiation was also found to be problematic. To meet these issues, the WOLF-B campaign used a modified sample changer which allowed the gamma-ray measurements to be carried out inside the sample changer to mitigate the crystal damage during the irradiation and to enhance the signal-to-noise ratio of the measurement.

The WOLF-B campaign comprised two phases. In the first phase, test measurements were conducted to estimate the neutron and gamma-ray background in the new measurement position, and to optimise irradiation and measurement strategies. The second phase consisted of the final measurements, during which fresh and burnt fuel samples were irradiated in different lattice positions of the PROTEUS test zone. These final measurements were later used for the derivation of first fission rate ratios between fresh and burnt fuel. The quantitative analysis will be presented in the next chapter.

The gamma-ray spectrometry system used for the WOLF-B campaign is presented in Section 4.1. A description of the experimental set-up, which includes the modified sample changer and the fresh and burnt fuel samples, is given in Section 4.2. The test phase and the final measurements of the WOLF-B campaign are described in Sections 4.3 and 4.4. The presentation of typical spectra, as also of net-count areas of gamma-ray lines of interest and their uncertainties, is included in these two sections. A summary of the chapter is given in Section 4.5.

4.1 High-resolution gamma-ray spectrometry system

During the WOLF-B experimental campaign, gamma-ray spectrometry was conducted with two HPGe detectors manufactured by ORTEC. The specifications of the detectors are given in Table 4.1. One of the detectors (model GEM-15180-P, 4500 V) had already been employed during the WOLF-A campaign and had been damaged because of the high fluence of fast neutrons (see Section 3.4). It was recovered via annealing of the crystal and was used again during the WOLF-B campaign.

Table 4.1: HPGe detectors used during the WOLF-B campaign

Model	GEM-15180-P	GEM-15180-P
Cryostat configuration	Pop-Top	Pop-Top
Crystal diameter	49.5 mm	50.0 mm
Crystal length	68.9 mm	57.2 mm
End cap to crystal	3 mm	3 mm
Absorbing Al layer	1.27 mm	1.27 mm
Absorbing inactive Ge layer	0.7 mm	0.7 mm
Recommended high voltage bias	4500 V	3600 V
Resolution* (FWHM) at 1.33 MeV, ^{60}Co	1.80 keV	1.80 keV
Relative efficiency** at 1.33 MeV, ^{60}Co	15%	15%

*The warranted values refer to a nominal count rate of 1000 cps and an amplifier time constant of $6\text{ }\mu\text{s}$.

**The efficiency of germanium detectors is commonly quoted relative to that of a standard 3 inch x 3 inch (7.62 cm x 7.62 cm) cylindrical NaI(Tl) scintillation crystal [Knoll 00].

In general, the gamma-ray spectrometry was carried out as described for the preliminary measurements in Section 3.1. The data were processed by the ORTEC DSPEC Plus multi-channel analyser [DSP], and the spectra were saved with the Gamma-Vision software [ORT 03a]. The automatic optimisation of the DSPEC Plus was used for most amplifier settings (e.g. pole zero, and flat top width and tilt). The rise time and the number of channels in the spectrum were set manually to $1.2\text{ }\mu\text{s}$ and 8192 channels (instead of $1.6\text{ }\mu\text{s}$ and 16384 channels during the previous measurement campaigns) to mitigate the loss of resolution during the campaign due to neutron damage (see Subsection 4.3.2).

Another new feature compared to the preliminary measurements was the cooling of the detector. The new detector position inside the sample changer (see Section 4.2) required a flexible cooling solution and precluded the use of liquid nitrogen in a dewar which would be rigidly coupled to the detector. Instead of liquid nitrogen, the mechanical cooling unit X-Cooler II by ORTEC

[ORT 06], which is shown in Figure 4.1, was used. The X-Cooler II is an electric-powered cooling system containing a cold head, a transfer hose and a compressor. The cold head comprises the gas expansion and the heat exchanger, and is attached to the Pop-Top detector. The cold head and the compressor are connected via the 3 m long flexible and insulated transfer hose containing the gas pressure and return lines. According to the product specifications [ORT c], no degradation of the detector resolution is to be observed for energies above 500 keV.

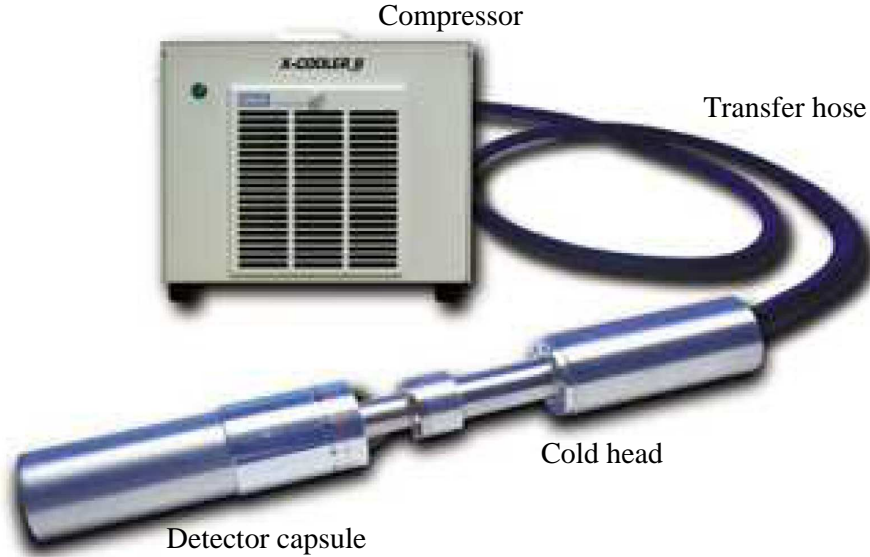


Figure 4.1: HPGe detector connected to the cooling unit X-Cooler II [ORT c].

4.2 Experimental set-up

4.2.1 Modified sample changer

As for the WOLF-A experiments, the fuel samples were loaded into the sample changer (see Section 2.3), which was placed above the reactor and allowed the insertion of the samples into the test lattice. For the WOLF-B campaign, however, the sample changer was modified. A view of the modified sample changer is shown in Fig. 4.2. A horizontal cavity was drilled into the steel body of the sample changer to accommodate the HPGe detector, which was mounted on a movable shield plug. Furthermore, the modified sample changer allowed the samples to be introduced into six different positions of the test lattice. To this aim, the guiding tube below the sample changer was replaced by a guide block which featured six channels guiding the samples into the different test lattice positions.

The layout of the PROTEUS test lattice as employed for the WOLF-B campaign, with indications of the positions into which the fuel samples could be inserted, is shown in Fig. 4.3. During the WOLF-A campaign, the samples could only be lowered into the central position of the test lattice. After the modification of the sample changer and after removing three additional test lattice pins, each sample could be lowered into six different irradiation positions. Four of the irradiation positions were located in the lattice (L11, K7, K11, and I11) and two were located in the moderator regions (M8, and I8).

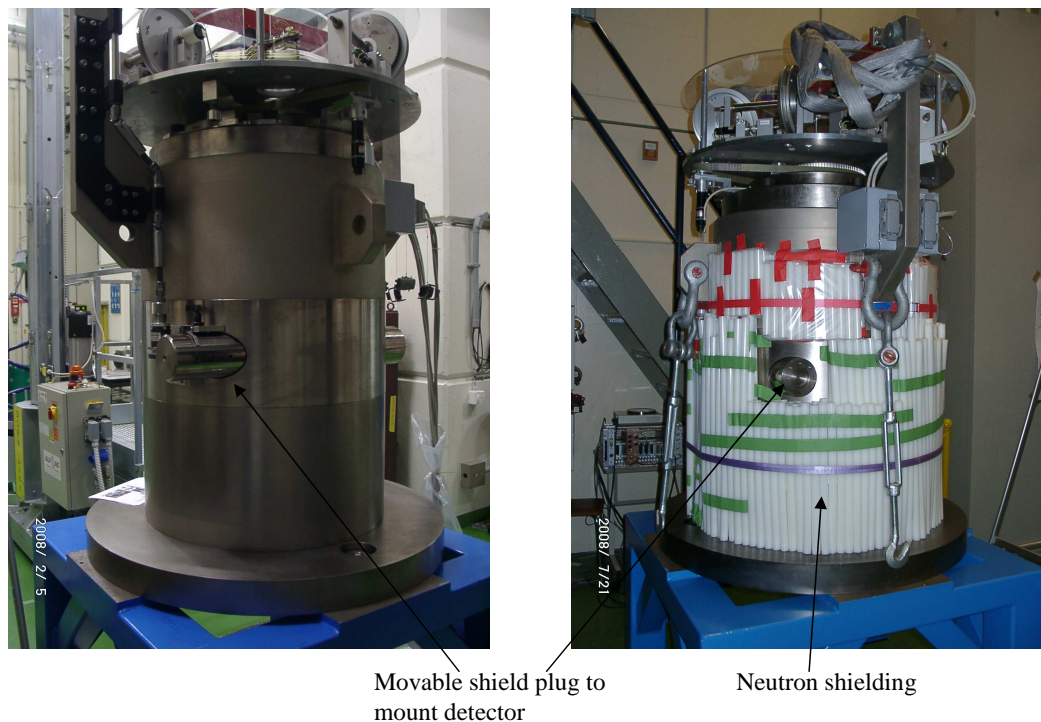


Figure 4.2: Views of the modified sample changer without (left) and with (right) additional neutron shielding.

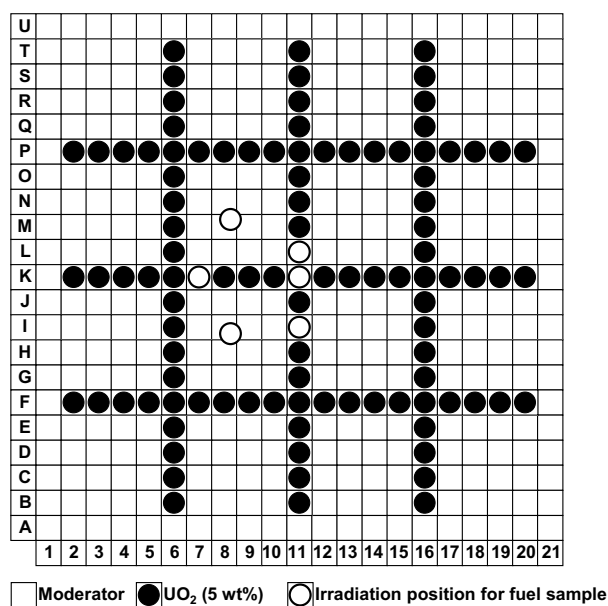


Figure 4.3: Layout of the PROTEUS test lattice during the WOLF-B campaign.

During the WOLF-B campaign, the detector was placed inside the sample changer, ready to measure the gamma-rays emitted by an irradiated sample once it had been withdrawn from the core into the steel body of the flask. Schematic vertical and radial cross-sections of the sample changer are shown in Fig.4.4. In the radial cross-section, the rotary revolver at the centre of the sample changer loaded with the six fuel samples is visible as well. For the measurements, there was at least 14 cm of steel between the sample and the detector. Compared with the 10 cm of lead that was previously used as a filter during the measurements carried out on top of the reactor shielding (see Section 3.3), the attenuation of gamma-rays above 2000 keV was slightly

reduced (e.g. 98.1% instead of 99.2% at 3000 keV), whereas the attenuation of gamma-rays below 2000 keV remained greater than 99%.

Fig. 4.4 also shows the neutron shielding set-up that was used for the final measurements, which are described in Section 4.4. To better shield the detector against fast neutrons emitted by the reactor core, the cylindrical body of the sample changer was first wrapped with a 1 mm thick sheet of cadmium (enclosed in a 0.5 cm thick sheet of polyethylene) and with three layers of polyethylene rods, which had a diameter of 2.55 cm (see 1 in Fig. 4.4). In the frame of the test phase of the WOLF-B campaign, the neutron shielding was further improved by placing polyethylene and paraffin wax plates below the sample changer and in between the support structure rings (see 2 in Fig. 4.4). Their minimum thickness was 6 cm. Furthermore, the detector itself was surrounded by 5wt% borated (natural boron) polyethylene rings which had a thickness of 1.4 cm (see 3 in Fig. 4.4).

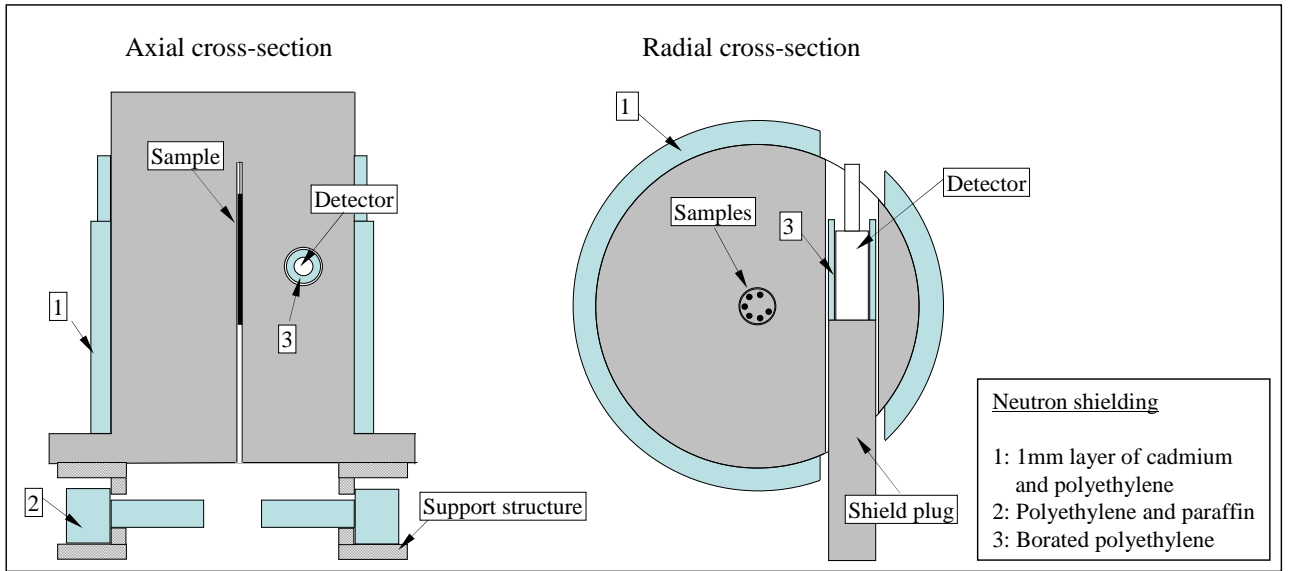


Figure 4.4: Schematic cross-sections of the modified sample changer.

4.2.2 Specifications of fresh and burnt fuel samples

Three fresh and three burnt UO_2 fuel samples were loaded into the modified sample changer. One of the fresh fuel samples and the three burnt ones were measured in the context of the present research work. The general specifications of the three burnt samples and of the measured fresh sample are summarised in Table 4.2.

The measured fresh fuel sample had an enrichment of 3.5% and a length of 38.9 cm. The burnt fuel samples had initial enrichments of either 3.5% or 4.1%, and nominal burn-ups of 36, 46 and 64 GWd/t. They were part of one of the sets of burnt fuel samples which had been prepared for Phase II of the LWR-PROTEUS programme (see Section 2.3). In the PSI Hot Laboratory, 40 cm long segments had been cut from PWR fuel rods used in a Swiss nuclear power plant and had been over-clad with Zircaloy.

As mentioned earlier, the isotopic compositions and burn-ups of the burnt fuel samples had been well characterised for the LWR-PROTEUS programme. The composition of the samples

Table 4.2: Characteristics of the fresh and burnt UO_2 samples used in the WOLF-B campaign.

No.	Nominal burn-up	Initial enrichment	Reactor cycles	Cooling time	Fuel length	Fuel diameter
1	Fresh	3.5%	-	-	389 mm	9.16 mm
2	36 GWd/t	4.1%	2	~ 12.5 years	400 mm	9.13 mm
3	46 GWd/t	3.5%	3	~ 12.5 years	400 mm	9.13 mm
4	64 GWd/t	3.5%	4	~ 12.5 years	400 mm	9.13 mm

had been estimated by measuring adjacent segments of the original fuel pin at the PSI Hot Laboratory [Günther-Leopold 07]. The measured isotopic compositions were used in this work for modelling the fuel samples in Monte Carlo simulations (see Section 6.1).

In addition to the results of the chemical analysis, the isotopic compositions had been calculated with the CASMO-4E [Rhodes 04] and HELIOS [Stu 05b] burn-up codes. Both CASMO-4E and HELIOS results were employed in the context of this work for sensitivity studies described in Subsections 5.3.4 and 6.2.2.

4.3 Test phase

The test phase of the WOLF-B campaign aimed at deciding on appropriate irradiation and measurement strategies for the final measurements. Several irradiations with and without samples were conducted to investigate the gamma-ray and fast neutron backgrounds at the new detector position, to monitor the detector loss of resolution with the repeated irradiations, to optimise the position of the samples during the measurement with respect to the detector dead time and count rates, and to optimise the power and time of irradiation for the different samples.

4.3.1 Gamma-ray background

The high gamma-ray background from the reactor fuel was a major problem during the WOLF-A campaign. Placing the detector inside the sample changer during the WOLF-B campaign solved this problem, thanks to the lower solid angle seen from the reactor and to the large amount of attenuating steel surrounding the detector.

During the test phase of WOLF-B, the gamma-ray background was measured after operating the reactor for 20 min at a power of 800 W. For this measurement, the detector was positioned inside the sample changer and all burnt fuel samples were moved 70 cm down, where their intrinsic gamma-ray activities would not interfere with the measurement. The spectrum was recorded during 2.5 h, starting 5 min after reactor shutdown, and is shown in Fig. 4.5.

A detailed list of the various observed background lines after irradiation is given in Table 4.3, focusing on the high-energy region above 2200 keV. No full-energy peaks characteristic of short-lived fission products are apparent, which proves the shielding to be adequate against the gamma-ray background coming from the reactor core.

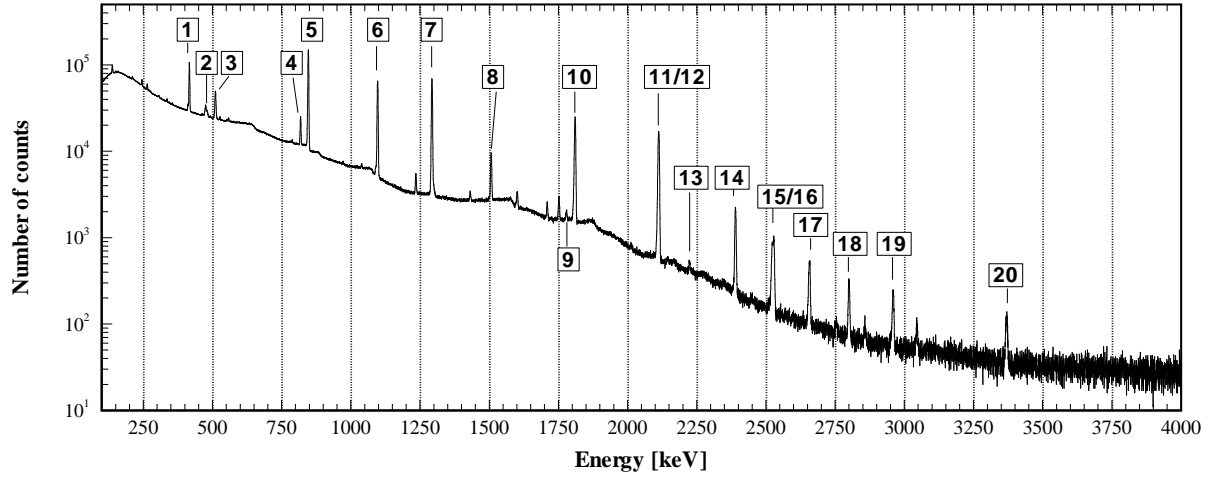


Figure 4.5: Background gamma-ray spectrum for WOLF-B set-up recorded from 5 min to 2.5 h after irradiation.

Table 4.3: Background gamma-ray lines for the WOLF-B set-up after irradiation (spectrum shown in Fig. 4.5).

Index	Energy	Origin (isotope, gamma-ray intensity, half-life)	Net counts*
1	417 keV	^{116m}In 27.9% $T_{1/2} = 54$ min	524752 (0.28%)
2	478 keV	^{10}B Prompt neutron capture gamma-ray	124791 (2.04%)
3	511 keV	Annihilation	295170 (0.67%)
4	819 keV	^{116m}In 11.6% $T_{1/2} = 54$ min	88152 (0.91%)
5	847 keV	^{56}Mn 98.8% $T_{1/2} = 2.6$ h	1294506 (0.13%)
6	1097 keV	^{116m}In 57.6% $T_{1/2} = 54$ min	584233 (0.21%)
7	1293 keV	^{116m}In 84.7% $T_{1/2} = 54$ min	707346 (0.17%)
8	1508 keV	^{116m}In 10.42% $T_{1/2} = 54$ min	78378 (1.11%)
9	1779 keV	^{28}Al 100% $T_{1/2} = 2.2$ min	3965 (15.1%)
10	1811 keV	^{56}Mn 27.6% $T_{1/2} = 2.6$ h	314446 (0.31%)
11	2112 keV	^{116m}In 15.3% $T_{1/2} = 54$ min	246379** (0.19%)
12	2113 keV	^{56}Mn 14.8% $T_{1/2} = 2.6$ h	
13	2223 keV	^1H Prompt neutron capture gamma-ray	1163 (16.0%)
14	2391 keV	^{116m}In Coincidence summing 1097 keV + 1293 keV	27040 (1.25%)
15	2523 keV	^{56}Mn 1.03% $T_{1/2} = 2.6$ h	22784*** (1.54%)
16	2530 keV	^{116m}In Coincidence summing 417 keV + 2113 keV	
17	2658 keV	^{56}Mn 0.66% $T_{1/2} = 2.6$ h	7081 (2.56%)
18	2800 keV	^{116m}In Coincidence summing 1293 keV + 1508 keV	3398 (3.88%)
19	2960 keV	^{56}Mn 0.31% $T_{1/2} = 2.6$ h	2589 (4.94%)
20	3369 keV	^{56}Mn 0.17% $T_{1/2} = 2.6$ h	1254 (8.05%)

* The quoted net counts refer to the spectrum shown in Fig. 4.5 and were acquired during 2.5 h after a reactor operation of 20 min at 800 W, starting 5 min after shutdown.

** summed net counts of lines 11 and 12

*** summed net counts of lines 15 and 16

Most of the observed peaks are related to activation of the materials composing the sample changer and the detector mount. The most prominent neutron activation products are ^{56}Mn ($T_{1/2} = 2.6\text{ h}$), which is formed by the (n,γ) reaction on the ^{55}Mn of the steel of the sample changer, and ^{116m}In ($T_{1/2} = 54\text{ min}$) due to the (n,γ) reaction on ^{115}In in the detector mount¹. Two peaks at 478 keV and 2223 keV, corresponding to prompt gamma-rays from neutron captures in ^{10}B and ^1H , could be observed. Both isotopes are part of the borated polyethylene rings surrounding the detector for neutron shielding. These prompt gamma-rays are most probably due to the intrinsic neutron background of the burnt fuel samples located 70 cm further down.

With respect to the measurement of the high-energy gamma-ray lines emitted by short-lived fission products, the ^1H (2223 keV) and ^{116m}In (2391 keV) peaks are of importance as they can interfere with the ^{138}Cs (2218 keV) peak on the one hand, and with the ^{88}Kr (2392 keV) and ^{142}La (2398 keV) peaks on the other hand. The ^1H (2223 keV) and ^{116m}In (2391 keV) peaks could not be avoided in the current experimental set-up as ^1H was present in the borated polyethylene around the detector, which represented an important part of the neutron shielding, and ^{115}In was present in the detector mount.

Since no gamma-ray background from the reactor fuel could be observed, no further measures with respect to the gamma-ray shielding were necessary.

4.3.2 Neutron background from the reactor

The neutron damage of the detector crystal during the WOLF-A campaign was - in addition to the high gamma-ray background from the reactor - a major problem and provided another reason to perform the WOLF-B measurements with the detector placed inside the sample changer.

In order to quantify the improved neutron shielding in the new detector position, two Monte Carlo models using MCNPX-2.5 [Pelowitz 05] were employed: a whole-reactor model and a model of the sample changer. These models are described in greater detail in the following chapters, in Subsections 5.4.1 and 6.1.1. The whole-reactor model was used to create an artificial neutron source representing the neutron background of the reactor during operation. To this end, the neutrons emitted by the reactor in the direction of the sample changer were recorded using a surface source write (ssw) card, which creates a source file containing the neutron tracks crossing an artificial surface above the reactor. Using a surface source read (ssr) card, the neutron source file was later read into the model of the sample changer. In the latter, the detector positions during the WOLF-A and WOLF-B measurements were modelled and, for each position, the fast neutron flux (0.1 keV - 12 MeV) was tallied in the germanium crystal of the detector.

Compared to the position of the detector below the sample changer during the WOLF-A campaign, the new location inside the sample changer led to a smaller solid angle seen from the reactor, as also to more attenuating material between detector and reactor. The MCNPX simulations of the two detector positions showed that the fast neutron flux during reactor operation in the new detector position was reduced to $\sim 16\%$ of the WOLF-A value.

With the help of additional MCNPX simulations, an optimised neutron shielding was designed. As described in Subsection 4.2.1, the final neutron shielding consisted of polyethylene rods and a

¹The two most prominent gamma-ray lines of ^{116m}In are at 1097 keV and 1293 keV. Theoretically, the two observed peaks at these energies could also be related to ^{59}Fe ($T_{1/2} = 44\text{ d}$), which could be formed by (n,γ) reactions on ^{58}Fe in the steel body of the sample changer. Measurements of the amplitude in the two peaks at different times confirmed, however, that the related half-life was that of ^{116m}In (i.e. 54 min) and not of ^{59}Fe .

cadmium sheet placed around the body of the sample changer, and of paraffin and polyethylene blocks placed below the sample changer. Furthermore, rings of a borated polyethylene were placed directly around the detector. All in all, the optimised neutron shielding led to a final fast neutron flux in the germanium crystal which was as little as about 2% of the WOLF-A value.

Despite the reduced fast neutron flux, the damage to the detector could not be completely eliminated. An average fast neutron flux (0.1 keV - 12 MeV) of about $1 \cdot 10^3 \text{ cm}^{-2} \text{ s}^{-1} \text{ W}^{-1}$ still reached the detector during reactor operation. The resulting neutron damage represented a limiting factor with respect to the number of possible irradiations, as also to the power levels and irradiation times.

4.3.3 Degradation of detector resolution due to fast neutron damage

For the test phase of the WOLF-B campaign, the detector model GEM-15180-P (4500 V) was used. As mentioned above, in spite of an optimised neutron shielding, the detector crystal was damaged by the fast neutron flux during reactor operation. This led to a continuous worsening of the detector resolution with each irradiation.

The degradation of detector resolution with irradiation during the test phase is illustrated in Fig. 4.6. The figure shows the evolution of the Full-Width-Half-Maximum (FWHM)² for two peaks of ⁵⁶Mn (1811 keV and 2113 keV) with respect to the integrated reactor power, i.e. the product of reactor power and irradiation time expressed in Wh. For example, the two first irradiations indicated in Fig. 4.6 lasted 30 min at a reactor power of 200 W, and thus corresponded each to an integrated power of 100 Wh.

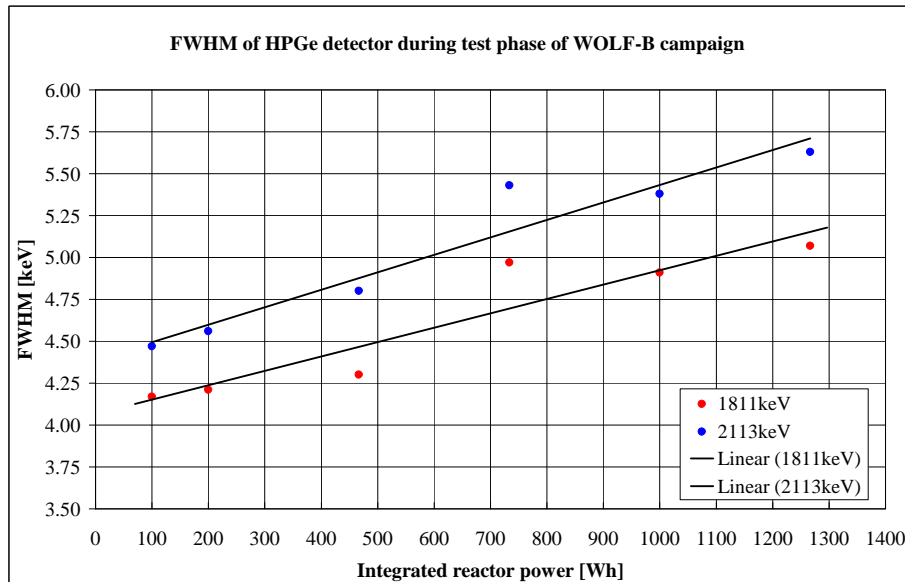


Figure 4.6: Evolution of the resolution of the detector model GEM-15180-P (4500 V).

After exposure to an integrated power of about 1300 Wh, the detector resolution for the 2113 keV peak reached a FWHM value of about 5.6 keV, compared to about 4.5 keV at the beginning of the

²The FWHM values were determined with Gamma-Vision for background spectra recorded after irradiation, with average input rates varying from 10000 to 20000 cps (corresponding to average dead times of about 6 to 12%).

test phase. It was found that this FWHM represented approximately the worst usable detector resolution, above which the peak fitting process was not possible any more in a reliable manner.

For the final measurements, the damaged detector was replaced by the newer model GEM-15180-P (3600 V), which showed a similar initial resolution. Consequently, it could be estimated that, during the final measurements, it would be possible to carry out irradiations equivalent to 1300 Wh before the worsened detector resolution prevented further usable measurements.

4.3.4 Measurement position of irradiated samples

The fuel samples were housed inside the sample changer in a rotary revolver which served to place the samples into different positions in the test lattice. By rotating the irradiated sample inside the sample changer and adjusting its elevation, the amount of attenuating steel between sample and detector could be modified.

The irradiated fresh fuel sample, having a negligibly low intrinsic activity, could be measured as close as possible to the detector. The distance between detector and sample centre was about 20 cm, with about 12 cm steel as filter, as shown schematically in Fig. 4.7.

The irradiated burnt fuel samples, however, had very high intrinsic gamma-ray activities, and therefore had to be moved further away from the detector to maintain reasonable system dead times. As indicated in Fig. 4.7, a more distant radial position was used and the samples were placed 30 cm further down. As a consequence, the detected counts in the freshly-induced gamma-ray lines were also reduced. To compensate for this effect, the burnt fuel samples needed to be irradiated at higher power levels than the fresh fuel sample.

The system dead times, before and after irradiation of each sample in the moderator positions M8 and I8, are summarised in Table 4.4. While the gamma-ray spectrometry of a particular sample was being performed, all the other burnt fuel samples were moved below the steel flask, so that their intrinsic gamma-ray activities did not interfere with the measurements. All the other fresh fuel samples, having no intrinsic activity, remained in the sample changer, as indicated in Fig. 4.7.

Table 4.4: Measurement positions of fresh and burnt fuel samples and system dead times during the WOLF-B campaign.

Sample	Measurement position*		System dead time	
	Radial distance	Vertical displacement	Before irradiation	After irradiation**
fresh	20 cm	-	0.6%	57%
36 GWd/t	25 cm	30 cm	33%	47%
46 GWd/t	25 cm	30 cm	62%	68%
64 GWd/t	25 cm	30 cm	68%	74%

* see Fig. 4.7

** The values are given for irradiation in the moderator positions M8 and I8. The fresh sample was irradiated for 30 min at a power of 100 W; the burnt samples were irradiated for 15 min at a power of 800 W.

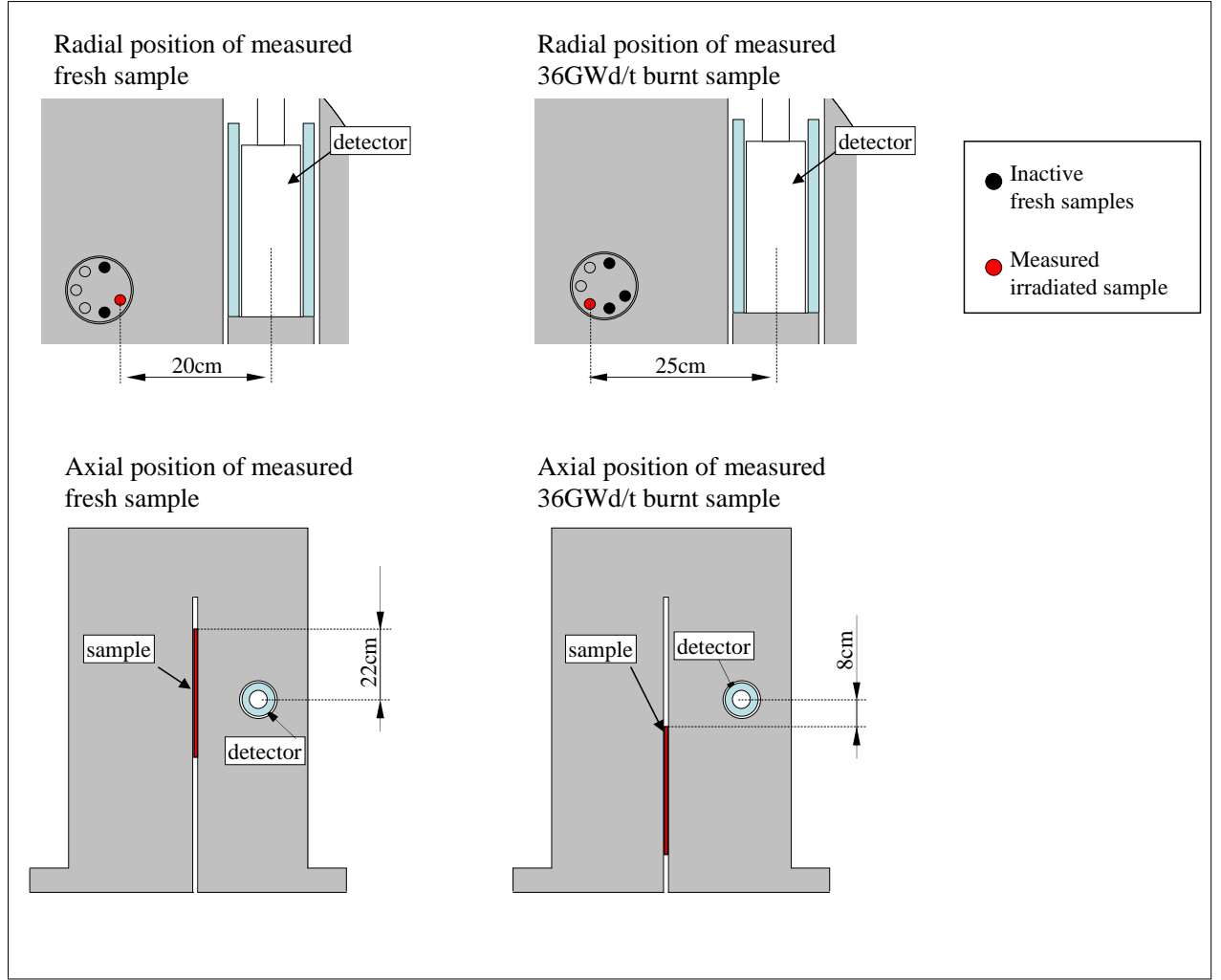


Figure 4.7: Measurement positions of the fresh and burnt fuel samples during the WOLF-B campaign.

4.3.5 Irradiation times and power levels

The principal goal of the WOLF-B measurements was to measure the short-lived fission products with half-lives from 10.3 min (^{95}Y) to 1.5 h (^{142}La). Consequently, the ideal irradiation times to obtain high count rates in the gamma-ray lines of interest should have been at least 30 min, and in the case of ^{142}La , preferably more than an hour. However, the irradiation times and the power levels for the final measurements had to be carefully chosen as a compromise between desired high count rates in the investigated gamma-ray lines and undesired neutron damage of the detector.

Test measurements showed that irradiating the fresh fuel sample in position M8 for 30 min at a power level of 100 W would be sufficient to reach net-count areas of about 69,000 counts in the ^{142}La (2542 keV) peak and 24,000 counts in the ^{95}Y (3576 keV) peak.

As indicated in the previous subsection, the burnt fuel samples needed to be measured further away from the detector, because of their high intrinsic gamma-ray activities. In order to compensate for the resulting lower count rates, the burnt samples were irradiated at the higher power level of 800 W. To minimise the neutron fluence in the detector, the irradiation times were reduced to 15 min, putting more emphasis on the shorter-lived fission products ^{89}Rb and ^{95}Y . The

obtained net-count areas for the 36 GWd/t sample, after an irradiation in the lattice position M8, were about 4,200 counts in the ^{142}La (2542 keV) peak and 4,150 counts in the ^{95}Y (3576 keV) peak.

To establish a good database for the analysis and the derivation of fission rate ratios, the priority during the final measurement campaign was set on the irradiation of the fresh and the 36 GWd/t burnt samples in at least three different lattice positions, with the burnt sample to be irradiated twice in each position to obtain better counting statistics and to demonstrate the reproducibility of the measurements. Speaking in terms of integrated reactor power, each irradiation of the fresh fuel sample represented an integrated power of 50 Wh, whereas each irradiation of the burnt samples represented an integrated power of 200 Wh. In total, the envisaged irradiations summed to an integrated power of 1350 Wh ($3 \times 50 \text{ Wh} + 6 \times 200 \text{ Wh}$), which was in the range of the estimated feasible integrated power of 1300 Wh before a too high degradation of the detector resolution would be reached (see Subsection 4.3.3).

4.4 Final measurements

As mentioned earlier, the test phase of the WOLF-B campaign served for defining the irradiation and acquisition strategies to be applied in the final measurements, during which quantitative gamma-ray spectrometry was carried out on appropriately irradiated fresh and burnt fuel samples.

For the final measurements, the first detector, which had been damaged by fast neutrons during the test phase, was replaced by the model GEM-15180-P (3600 V).

4.4.1 List of experiments

In total, 14 irradiations were conducted for the final measurements (see Table 4.5). As indicated earlier, the fresh sample was irradiated at a reactor power of 100 W, whereas the burnt samples were irradiated at 800 W. The average neutron flux in the fresh fuel sample was about $1.5 \cdot 10^7 \text{ cm}^{-2} \text{ s}^{-1} \text{ W}^{-1}$ in the lattice position L11 and about $1.6 \cdot 10^7 \text{ cm}^{-2} \text{ s}^{-1} \text{ W}^{-1}$ in the moderator positions M8. The values of the fast-to-thermal flux ratio were 0.27 and 0.36, respectively (energy boundary 0.625 eV). The time needed to bring the sample to the measurement position after reactor shutdown was 1 to 5 min, depending on the sample and irradiation positions. The maximum dead times quoted in Table 4.5 refer to the average dead times 5 min after irradiation.

The final measurements can be considered in terms of three sets of irradiations. The first set consisted of irradiations of the 36 GWd/t burnt sample in the three different lattice positions M8, K7 and L11. Each irradiation was carried out twice to improve the counting statistics and to demonstrate the reproducibility of the experiments. In the second set, the fresh fuel sample was irradiated in the same three lattice positions. After the two first sets, the detector resolution was found to be still in the usable range (FWHM of about 5.1 keV at 2113 keV) so that further irradiations using the higher-burnt sample were conducted. This third set comprised irradiations of the three burnt samples in the lattice position I8.

The irradiation number 14 in Table 4.5 is a measurement of the pure reactor background after operation without any sample inserted into the lattice. In this case, all burnt samples were placed below the sample changer during data acquisition.

Before each irradiation, a 30 min background spectrum was recorded with the soon-to-be-irradiated sample in the measurement position. During the gamma-ray measurement of a given sample, all remaining burnt samples were lowered below the sample changer. For safety reasons, all samples were retracted into the sample changer after the end of the data acquisition. To limit the damage of the detector due to the neutrons emitted by the burnt fuel samples, the detector was moved outside of the sample changer into a “parking position” when no measurement was being carried out.

Table 4.5: List of irradiations carried out during the final measurement phase of the WOLF-B campaign.

		Irradiation			Measurement		
No.	Sample	Lattice position	Reactor power	t_{irr}	t_{cool}	t_a	dT_{5min}
1	36 GWd/t	M8	800 W	15 min	~8.5 min	7 h	
2	36 GWd/t	K7	800 W	15 min	4.5 min	7 h	~43.3%
3	36 GWd/t	L11	800 W	15 min	2 min	7.5 h	~45.7%
4	36 GWd/t	K7	800 W	15 min	3 min	7 h	~44.7%
5	36 GWd/t	L11	800 W	15 min	2 min	7 h	~45.3%
6	36 GWd/t	M8	800 W	15 min	3 min	7 h	~46.7%
7	fresh	K7	100 W	30 min	2 min	8 h	~42.6%
8	fresh	M8	100 W	30 min	4 min	8 h	~57.4%
9	fresh	L11	100 W	30 min	4.5 min	8 h	~48.4%
10	46 GWd/t	I8	800 W	15 min	3.5 min	7.5 h	~67.8%
11	46 GWd/t	I8	800 W	15 min	4 min	6.5 h	~68.1%
12	64 GWd/t	I8	800 W	15 min	4 min	5 h	~73.8%
13	36 GWd/t	I8	800 W	15 min	3.5 min	7 h	~47.2%
14	-	-	800 W	15 min	2 min	7 h	~7.4%

t_{irr} : irradiation time; t_{cool} : cooling time; t_a : acquisition time; dT_{5min} : system dead time 5 min after irradiation

4.4.2 Measured gamma-ray lines emitted by short-lived fission products in burnt fuel

During the final measurements on fresh and burnt fuel samples, it was possible to quantitatively assess the freshly induced gamma-ray activity, not only in the fresh, but also in the burnt fuel samples with burn-up values of 36, 46 and 64 GWd/t. The most prominent peaks from the freshly-induced fission products were ^{142}La (2542 keV), ^{89}Rb (2570 keV), ^{95}Y (2632 keV), ^{138}Cs (2640 keV) and ^{95}Y (3576 keV). Based on these peaks, the final quantitative analysis of the spectra was carried out, as is described in the following chapter. The three peaks ^{138}Cs (2218 keV), ^{88}Kr (2392 keV) and ^{142}La (2398 keV) were not considered because of their interference with the background peaks ^1H (2223 keV) and ^{116m}In (2391 keV). All other observed peaks from short-lived fission products, which had previously been identified as potential fission rate indicators (see Table 3.9), had too poor counting statistics to be included in the quantitative analysis.

The recorded activities from the three burnt samples after irradiation in the moderator positions (irradiations 6, 10 and 12 in Table 4.5) are shown in the top part of Fig. 4.8. Apart from the long-lived fission products ^{137}Cs and ^{154}Eu present in the burnt fuel, the background peaks from the two activation products ^{116m}In and ^{56}Mn are marked. Fig. 4.8 also provides two sets of focused views on the energy regions 2500-2700 keV and 3500-3675 keV, containing the observed short-lived fission product gamma-ray lines ^{142}La (2542 keV), ^{89}Rb (2570 keV), ^{95}Y (2632 keV), ^{138}Cs (2640 keV) and ^{95}Y (3576 keV). The first set (shown in the middle of the figure) contains the counts acquired during 1 h starting 3.5 min after irradiation, to emphasise the very short-lived fission products ^{95}Y and ^{89}Rb . The second set (shown at the bottom) contains the counts acquired during 4 h starting 3.5 min after irradiation, putting the emphasis on the gamma-ray lines emitted by the somewhat longer-lived fission products ^{138}Cs and ^{142}La .

The marked peaks from the short-lived fission products are clearly apparent for the 36 GWd/t sample. For the higher burnt samples, the peaks are less pronounced. The reasons for this are, on the one hand, the lower fission rates in the higher burnt samples due to the lower amount of fissionable material, and on the other hand, the already advanced degradation of detector resolution. In fact, for these reasons, the 64 GWd/t sample was not considered for the quantitative analysis.

The obtained net-count areas of the marked short-lived fission product peaks, as obtained with the region-of-interest (ROI) method within Gamma-Vision, and the related signal-to-background ratios are listed in Table 4.6.

Table 4.6: Measured net counts and signal-to-background ratios (S/Bg) of most prominent gamma-ray lines from short-lived fission products freshly induced in burnt fuel samples.

Gamma-ray line	36 GWd/t		46 GWd/t		64 GWd/t	
	Net counts	S/Bg	Net counts	S/Bg	Net counts	S/Bg
^{142}La (2542 keV)	4244 (4.3%)	0.22	2710 (9.5%)	0.09	2130 (14.4%)	0.05
^{89}Rb (2570 keV)	2788 (5.7%)	0.23	1340 (12.8%)	0.10	-	
^{138}Cs (2640 keV)*	8583 (3.4%)	0.35	6598 (5.4%)	0.20	4539 (9.0%)	0.10
^{95}Y (3576 keV)	4150 (2.6%)	1.16	2719 (5.3%)	0.57	1922 (8.2%)	0.32

* The counts given for the ^{138}Cs (2640 keV) peak also contain the counts of the adjacent ^{95}Y (2632 keV) peak.

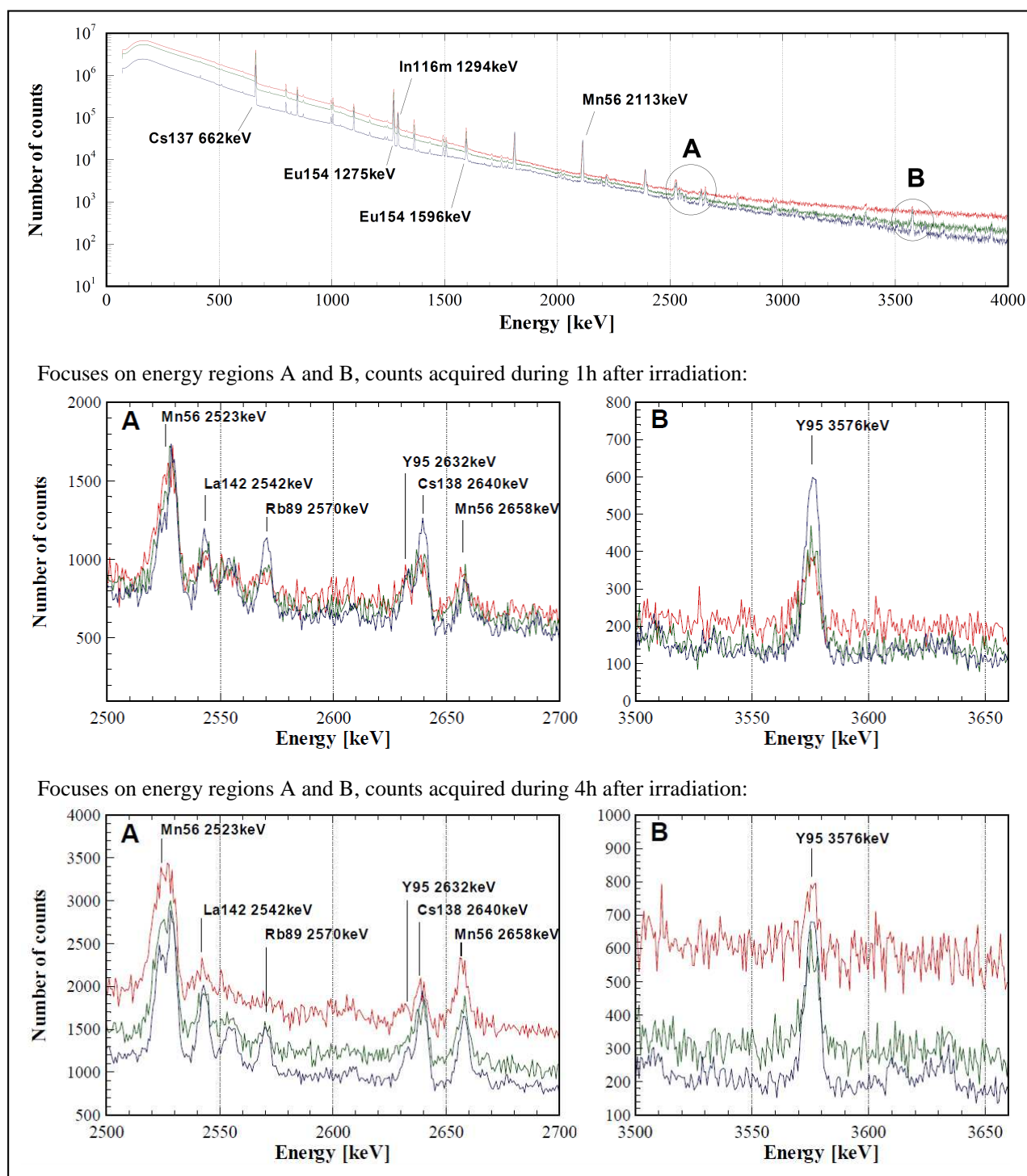


Figure 4.8: Top: gamma-ray spectra of re-irradiated burnt UO_2 fuel samples with burn-up values 36 GWd/t (blue), 46 GWd/t (green), 64 GWd/t (red), recorded during 4 h after irradiation. Middle and bottom: focuses on the energy regions 2500-2700 keV (A) and 3500-3675 keV (B) for different acquisition times.

4.5 Chapter summary

During the WOLF-B campaign, gamma-ray spectrometry was performed on fresh and burnt fuel samples (with nominal burn-ups of 36, 46 and 64 GWd/t), irradiated in different positions of the PROTEUS test lattice. The gamma-ray spectrometry took place inside the sample changer, which had been modified for this purpose. This new measurement position proved to offer adequate gamma-ray and neutron shielding against the reactor background after reactor operation. During reactor operation, the fast neutron flux in the detector position could, however, not be eliminated completely and caused a continuous worsening of the detector resolution. Therefore, the total possible number of irradiations, the reactor power levels and the irradiation times were limited.

For the final measurements, 14 irradiations were carried out. The emphasis was put on irradiating a fresh and a 36 GWd/t burnt fuel sample in different lattice positions. After these measurements, the three burnt samples were irradiated using a single lattice position.

It was demonstrated that - for the first time in a zero-power reactor - it was possible to detect gamma-rays emitted by short-lived fission products freshly produced in burnt nuclear fuel. Concerning the fresh sample, and the 36 and 46 GWd/t burnt samples, various gamma-ray peaks from short-lived fission products showed sufficiently high count rates for a quantitative analysis. The measurements of the 64 GWd/t burnt samples, however, had lower statistics, and the acquired gamma-ray spectra were found harder to analyse due to the already advanced neutron damage of the detector crystal when these measurements were conducted.

Five high-energy gamma-ray lines were considered for the analysis of the measurements of the fresh, the 36 and the 46 GWd/t burnt samples. These are ^{142}La (2542 keV), ^{89}Rb (2570 keV), ^{95}Y (2632 keV), ^{138}Cs (2640 keV) and ^{95}Y (3576 keV). All the other gamma-ray lines, which had been previously identified as potential fission rate indicators, showed too low counting statistics or suffered interference with background peaks.

The analysis of the WOLF-B experiments, i.e. the methodology to derive fission rate ratios from the short-lived fission product peaks, is presented in the following chapter, together with the experimental results for inter-position and inter-sample fission rate ratios.

Bibliography

- [DSP] *DSPECPLUSTM, Digital Gamma-Ray Spectrometer.* EG&G ORTEC Catalog, Oak Ridge.
- [Günther-Leopold 07] I. Günther-Leopold. *LWR-PROTEUS programme, Phase II, Final Report.* Internal Report TM-43-06-05, PSI, 2007.
- [Knoll 00] G.F. Knoll. *Radiation Detection and Measurements.* Third edition, page 450, ISBN 0-471-07338-5, 2000.
- [ORT c] ORTEC. *X-Cooler II, The Next Generation in HPGe Detector Technology.* Product Configuration Guide.
- [ORT 03a] ORTEC. *GammaVision-32, Gamma-ray Spectrum Analysis and MCA Emulator,* A66-B32 User's Manual, 2003.
- [ORT 06] ORTEC. *X-Cooler II, Mechanical Cooler for HPGe Detectors,* User's Manual, 2006.
- [Pelowitz 05] D.B. Pelowitz. *MCNPX User's Manual Version 2.5.0,* 2005.
- [Rhodes 04] J. Rhodes, Smith K. & Edenius M. *CASMO-4E, Extended Capability CASMO-4: User Manual.* Studsvik Scandpower, SSP-01/401 Rev. 2, Inc., 2004.
- [Stu 05b] Studsvik Scandpower. *User's Manual HELIOS,* 2005.

Chapter 5

Derivation of measured fission rates in fresh and burnt fuel

This chapter is dedicated to the derivation of fission rate ratios using gamma-ray lines from short-lived fission products, based on the irradiations conducted during the WOLF-B campaign which is described in the previous chapter. Ratios of fission rates have been derived for the same sample irradiated in different lattice positions (inter-position fission rate ratios), and for different samples irradiated in the same position (inter-sample fission rate ratios).

In total, 15 gamma-ray lines above 2200 keV from the short-lived fission products ^{88}Kr , ^{142}La , ^{138}Cs , ^{89}Rb , ^{95}Y , ^{84}Br , ^{90}Rb and ^{90m}Rb were initially identified as potential fission rate indicators in fresh and spent fuel; these are listed in Table 3.9 of Chapter 3. In the framework of the WOLF-B campaign, most of these gamma-ray lines could be detected in fresh and in spent fuel samples having burn-up values up to 64 GWd/t. However, for the quantitative analysis described in this chapter, some gamma-ray lines were rejected because of their low statistics or interference with background peaks. The 64 GWd/t sample was entirely excluded from the quantitative analysis.

As mentioned at the end of the previous chapter, it is the five gamma-ray lines ^{142}La (2542 keV), ^{89}Rb (2570 keV), ^{95}Y (2632 keV), ^{138}Cs (2640 keV) and ^{95}Y (3576 keV) which have been retained for the derivation of measured fission rate ratios for the fresh, and the 36 and 46 GWd/t burnt samples. For the fresh fuel sample, three additional prominent lines in the lower-energy region have been included for cross-comparison purposes. These are ^{138}Cs (1435 keV), ^{135}I (1260 keV) and ^{92}Sr (1383 keV). The last two belong to the lower-energy gamma-ray lines routinely used in PROTEUS as fission rate indicators in fresh fuel (see Section 2.1).

The methodology to derive fission rate ratios is described in Section 5.1. The following three sections deal with the three main factors needed for the derivation of fission rate ratios, which are the net-count area of the selected gamma-ray peaks (Section 5.2), the corrections for activity saturation and decay (Section 5.3), and the corrections for solid angle and attenuation of gamma-rays between sample and detector (Section 5.4). The derived measured inter-position and inter-sample fission rate ratios are presented in Section 5.5. A chapter summary is given in Section 5.6.

5.1 Methodology to derive fission rate ratios

The various gamma-ray lines considered for the presented analysis of the WOLF-B campaign are summarised in Table 5.1. The general methodology for deriving fission rates, inter-sample fission

rate ratios and inter-position fission rate ratios from the measured activity in these gamma-ray lines is described in the following.

Table 5.1: Characteristics of gamma-ray lines considered for the derivation of fission rate ratios in fresh and burnt fuel.

Energy	Fission product	Half-life	Gamma-ray intensity
2542 keV	¹⁴² La	1.52 h	10.0%
2570 keV	⁸⁹ Rb	15.4 min	10.2%
2632 keV*	⁹⁵ Y	10.3 min	4.8%
2640 keV*	¹³⁸ Cs	33.4 min	7.6%
3576 keV	⁹⁵ Y	10.3 min	6.4%
1260 keV**	¹³⁵ I	6.57 h	28.7%
1383 keV**	⁹² Sr	2.71 h	93.0%
1435 keV**	¹³⁸ Cs	33.4 min	76.3%

*These two gamma-ray lines had to be evaluated together (see text below).

**Used for fresh fuel only.

5.1.1 Fission rates

In general, the fission rate F in a sample during an irradiation in PROTEUS can be derived by correcting the measured activity of a freshly built-up fission product FP as follows:

$$F(E_\gamma) = \frac{N_{net}}{\varepsilon(E_\gamma) \cdot att_{sample}(E_\gamma) \cdot b_{\gamma,FP} \cdot C_{FP}} \quad (5.1)$$

where N_{net} is the measured net-count area of the gamma-ray line of energy E_γ in the ZDT spectrum; $\varepsilon(E_\gamma)$ is the detection efficiency of the germanium detector at this energy; the correction factor $att_{sample}(E_\gamma)$ accounts for the solid angle and the attenuation of the gamma-rays between sample and detector; C_{FP} denotes a correction factor taking into account the build-up of the considered fission product during irradiation and its decay after irradiation, and $b_{\gamma,FP}$ is the intensity of the considered gamma-ray line.

Since two of the main peaks - ⁹⁵Y (2632 keV) and ¹³⁸Cs (2640 keV) - are closely overlapping (see Fig. 5.1), only one fission rate was determined on the basis of the sum of these two peaks to avoid high uncertainties due to the spectrum deconvolution in this multiplet area. Consequently, Eq. 5.1 has to be modified to account for both contributing isotopes by introducing an effective saturation and decay correction factor $(b_{\gamma,FP}C_{FP})_{eff}$, as given by Eq. 5.2.

$$F(2640keV) = \frac{N_{net}}{\varepsilon_{det}(2640keV) \cdot att_{sample}(2640keV) \cdot (b_{\gamma,FP}C_{FP})_{eff}} \quad (5.2)$$

with $(b_{\gamma,FP}C_{FP})_{eff} = (b_{2632keV,^{95}Y} \cdot C_{^{95}Y}) + (b_{2640keV,^{138}Cs} \cdot C_{^{138}Cs})$

In this case, N_{net} denotes the sum of the two net-count areas of ^{95}Y (2632 keV) and ^{138}Cs (2640 keV). Both $\varepsilon(E_\gamma)$ and $att_{sample}(E_\gamma)$ are assumed to be the same for the two peaks, since their energies are just 8 keV apart from each other. In the following, for simplicity's sake, a value of $E_\gamma = 2640 \text{ keV}$ is used to characterise parameters related to the joint counting of the two gamma-ray lines.

Several additional minor gamma-ray lines contribute to the gamma-ray lines ^{142}La (2542 keV), ^{92}Sr (1383 keV) and ^{138}Cs (1435 keV). These additional gamma-ray lines, which are listed in Table 5.2, cannot be separated from the main gamma-ray lines. Although they had only minor contributions to the net-count areas, they have been systematically taken into account in the analysis. Thus, the net-count areas of ^{142}La (2542 keV), ^{92}Sr (1383 keV) and ^{138}Cs (1435 keV) have been corrected for minor contributions from ^{133}Te , ^{93}Sr , ^{99m}Nb and ^{101}Mo , in an analogous manner to Eq. 5.2.

Table 5.2: Additional fission products contributing to three of the investigated gamma-ray lines.

Energy	Fission product	Fission products contributing to same energy
2542 keV	^{142}La	^{133}Te (2542 keV), ^{93}Sr (2544 keV), ^{99m}Nb (2544 keV)
1383 keV	^{92}Sr	^{101}Mo (1382 keV)
1435 keV	^{138}Cs	^{93}Sr (1434 keV)

5.1.2 Inter-position fission rate ratios

Estimates of the inter-position fission rate ratio FRR_{A-B} , comparing irradiations of the same sample in different lattice positions A and B , are obtained according to Eq. 5.3.

$$FRR_{A-B}(E_\gamma) = \frac{F_A(E_\gamma)}{F_B(E_\gamma)} = \frac{N_{net,A}}{N_{net,B}} \cdot \frac{(b_{\gamma,FP}C_{FP})_{eff,B}}{(b_{\gamma,FP}C_{FP})_{eff,A}} \quad (5.3)$$

Since only fission rates based on the same gamma-ray lines are compared, the energy dependent detector efficiencies $\varepsilon(E_\gamma)$ cancel out when calculating these fission rate ratios. As the counting of the each particular sample was always carried out in the same measurement position, independently of the irradiation position, the correction factors $att_{sample}(E_\gamma)$ are also the same for the two measurements and cancel out as well. For the three fission rate ratio estimates based on the ^{89}Rb (2570 keV), ^{95}Y (3576 keV) and ^{135}I (1260 keV) gamma-ray lines, the respective gamma-ray intensities $b_{\gamma,FP}$ also cancel out. For the fission rate ratio estimated with the joint counting of the ^{95}Y (2632 keV) and ^{138}Cs (2640 keV) gamma-ray lines, however, the gamma-ray intensities are part of the sum which forms the effective saturation and decay correction factor, as given in Eq. 5.2, and therefore do not cancel out. The same is also valid for the fission rate ratios based on gamma-ray lines ^{142}La (2542 keV), ^{92}Sr (1383 keV) and ^{138}Cs (1435 keV), which contain small contributions from other fission product gamma-ray lines.

5.1.3 Inter-sample fission rate ratios

Eq. 5.4 gives the relation for estimating the inter-sample fission rate ratio FRR_{f-s} between a fresh (f) and a spent (s) fuel sample irradiated in the same lattice position. The solid angle and

attenuation correction factors $att_{sample}(E_\gamma)$ no longer cancel because the measurement positions of the fresh and the spent samples were different.

$$FRR_{f-s}(E_\gamma) = \frac{F_f(E_\gamma)}{F_s(E_\gamma)} = \frac{N_{net,f}}{N_{net,s}} \cdot \frac{att_s(E_\gamma) \cdot (b_{\gamma,FP}C_{FP})_{eff,s}}{att_f(E_\gamma) \cdot (b_{\gamma,FP}C_{FP})_{eff,f}} \quad (5.4)$$

As shown in Eq. 5.3 and 5.4, the energy dependent detector efficiency $\varepsilon_{det}(E_\gamma)$ is not required because only ratios of fission rates are considered. The determination of the quantities N_{net} , $(b_{\gamma,FP}C_{FP})_{eff}$ and $att_{sample}(E_\gamma)$ are discussed in the following three sections.

5.2 Determination of net-count areas

5.2.1 Peak fitting with HyperLab software

During the WOLF-B campaign, the recorded data were saved with the ORTEC software Gamma-Vision. Using the NORM_CORR mode [ORT 03a], two spectra were recorded in parallel: the live-time spectrum (LTC) containing dead-time losses and the zero-dead-time spectrum (ZDT) corrected for dead-time losses (see Section 3.1). For the determination of the net-peak areas, the ZDT spectra were used. In general, the analysis of the spectra was very challenging. The main difficulty was the peak shape distortion which increased with the number of irradiations because of the fast neutron damage in the detector crystal. In contrast to the preliminary measurement campaigns, where the spectra analysis was carried out using Gamma-Vision, a new deconvolution software was required. Additional aspects were the high number of multiplet areas and the lack of calibration spectra covering the energy range above 2200 keV.

Meeting these challenges, the net-count area of each gamma-ray line was determined using the gamma-ray spectrum analysis code HyperLab [Hyp 05], which proved to be quite suitable for the analysis of the obtained gamma-ray spectra. One characteristic of the HyperLab code is that the non-linear spectrum deconvolution does not require an a priori peak shape calibration, since the FWHM calibration process is highly automated. The spectrum deconvolution is performed as described in [Hyp 05] and [Simonis 03] on a region-by-region basis using a semi-empirical fit function. Examples of the spectrum fits for the two energy regions containing the analysed high-energy gamma-ray lines are shown in Fig. 5.1.

The spectrum peak evaluation within HyperLab consists of several steps [Hyp 05]. First, a database is created by reading the spectrum files. As a next step, the FWHM calibration can be checked in the FWHM calibration editor where the used FWHM calibration curve is displayed together with the width of suspected peaks identified by HyperLab. Although no exact calibration is needed for the spectrum deconvolution, a manual modification of the used calibration curve is recommended if large deviations are found between the current calibration curve and the suspected peaks' FWHMs. In this work, the FWHM calibration was, in general, slightly adjusted to fit the suspected peaks' FWHMs before performing the automatic fit.

The fit function used for the automatic fitting in HyperLab is a sum of six terms, which are related to the Gaussian peak function (one term), the left and right skew peak functions (two terms), the background functions (two terms) and a low-energy tail function (one term). The

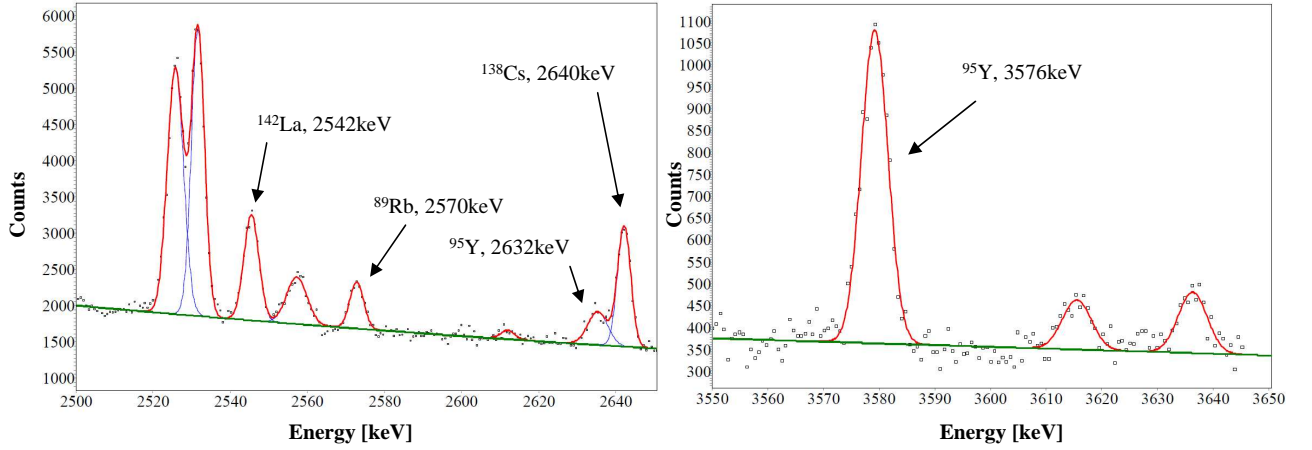


Figure 5.1: Example of fitted spectrum regions in HyperLab.

various parameters of the function are fitted in order to find the best match between the model function and the measured counts. In the default peak evaluation setting for moderate count rates and regular peaks, the low energy tail function is disabled. For this work, however, the optional setting for high count rates and slightly distorted peaks was selected in order to enable the low energy tailing.

After performing the automatic fitting, the user can check and, if necessary, fine-tune the results. As shown in Fig. 5.1, the original counts of the spectrum can be displayed along with the fitted curve of the individual peaks (blue), the fitted curves of all singlet and multiplets (red), and the fitted curve of the background components (green). In the analysis of the spectra from the fresh and the 36 GWd/t samples, fine-tuning was used especially for the multiplet areas containing the peaks ^{142}La (2542 keV), ^{89}Rb (2570 keV), ^{95}Y (2632 keV) and ^{138}Cs (2640 keV). The typical reason for the fine-tuning was the non-realistic background estimated in the first automatic fit. The fine-tuning mainly consisted of merging the initial two or more regions into a single region covering the range from about 2500 to 2700 keV and adjusting the region boundaries, until the background curve appeared realistic. Normally, the number of fitted peaks and their shapes were not affected. Nonetheless, the net-count areas of the peaks could change depending on the fine-tuning. This aspect is further discussed in the frame of the reproducibility study with respect to the fitted net-count areas in Subsection 5.2.5.

The fitting of the spectra from the 46 GWd/t sample was more challenging because of the advanced neutron damage in the detector crystal. As the focus of the WOLF-B campaign was on the measurements of the fresh and the 36 GWd/t samples, the irradiations of the higher burnt samples took place at the end of the campaign, when the detector resolution was already very degraded. In order to obtain a realistic background fit in these spectra, fine-tuning was necessary not only for the energy region from 2500 to 2700 keV, but also for the ^{95}Y (3576 keV) peak. Furthermore, the ^{95}Y (2632 keV) peak had to be added manually, because the two neighbouring peaks ^{95}Y (2632 keV) and ^{138}Cs (2640 keV) were not recognized as separated in the automatic fit. Although the fitting of the two peaks after the manual fine-tuning appeared reasonable, the quoted uncertainties on their net-count areas were extremely high (about 30%).

After the spectrum fit, a report is created containing the net-count areas and estimated uncertainties of the single peaks. Typical results for net-count areas and corresponding uncertainties are given for the three samples in Subsection 5.2.4.

5.2.2 Choice of analysed acquisition time

During data acquisition, the counts were saved in series of spectra. Starting 2 minutes after irradiation, 6 spectra of 30 seconds each, followed by 11 spectra of 5 minutes and 11-14 spectra of 30 minutes, were recorded. This procedure allowed one to analyse different sums of spectra, depending on the chosen gamma-ray line and the half-life of the corresponding fission product. The typical starting times, duration and average dead-times of the spectra are given in Table 5.3 for irradiations of the fresh, the 36 GWd/t and the 46 GWd/t samples. The time delay in Gamma-Vision for storing one spectrum, before the subsequent spectrum could be recorded, was about 2-3 seconds.

Table 5.3: Timing and average dead-time corrections of series of gamma-ray spectra.

No.	Fresh, irr. position K7			36 GWd/t, irr. position K7			46 GWd/t, irr. position I8		
	t_c [sec]	t_a [sec]	av. dT [%]	t_c [sec]	t_a [sec]	av. dT [%]	t_c [sec]	t_a [sec]	av. dT [%]
1	120	30	64.33	120	30	-	120	30	-
2	153	30	60.33	152	30	-	152	30	-
3	185	30	57.00	184	30	52.00	185	30	-
4	217	30	54.33	216	30	50.33	216	30	73.33
5	249	30	52.00	248	30	49.33	250	30	70.00
6	281	30	50.00	281	30	48.33	282	30	70.00
7	314	300	42.63	313	300	45.67	314	300	68.00
8	616	300	34.27	615	300	43.30	617	300	66.67
9	918	300	29.00	917	300	42.13	919	300	66.00
10	1221	300	25.17	1220	300	41.33	1221	300	65.33
11	1523	300	22.23	1522	300	40.73	1524	300	65.00
12	1825	300	19.83	1825	300	40.27	1826	300	65.00
13	2127	300	17.87	2127	300	39.87	2129	300	64.67
14	2430	300	16.20	2429	300	39.53	2431	300	64.33
15	2732	300	14.80	2732	300	39.23	2734	300	64.33
16	3034	300	13.60	3034	300	38.97	3036	300	64.00
17	3336	300	12.60	3336	300	38.73	3338	300	64.00
18	3639	1800	10.01	3639	1800	38.16	3641	1800	63.56
19	5442	1800	7.19	5441	1800	37.44	5443	1800	63.11
20	7244	1800	5.53	7243	1800	36.96	7245	1800	62.89
21	9046	1800	4.40	9046	1800	36.60	9048	1800	62.67
22	10848	1800	3.65	10848	1800	36.34	10850	1800	62.50
23	12651	1800	3.09	12651	1800	36.11	12652	1800	62.39
24	14452	1800	2.66	14453	1800	35.96	14455	1800	62.28
25	16255	1800	2.34	16256	1800	35.82	16257	1800	62.22
26	18058	1800	2.08	18058	1800	35.71	18059	1800	62.17
27	19860	1800	1.86	19860	1800	35.63	19863	1800	62.11
28	21662	1800	1.71	21662	1800	35.55	21665	1800	62.06
29	23464	1800	1.57	23464	1800	35.48	23467	1800	62.00

t_c : cooling time, i.e. time between end of irradiation and start of data acquisition; t_a : acquisition time; av. dT: average dead time

In most cases, it took longer than 2 minutes to bring the samples into the measurement position after irradiation. Nonetheless, the data acquisition was always started 2 minutes after irradiation to keep the same timing for all measurements. The 6 spectra of 30 seconds were not included in the analysis.

In order to optimise the signal-to-background ratio of the investigated peaks and thus to minimise the statistical uncertainties on the net-count areas, different sums of spectra were used for the analysis of the peaks of the very short-lived fission products ^{89}Rb and ^{95}Y , on the one hand, and the longer-lived fission products ^{142}La , ^{138}Cs , ^{135}I and ^{92}Sr on the other hand. The ^{89}Rb and ^{95}Y peaks were normally fitted using the 11 spectra of 5 minutes starting 5 minutes after irradiation. Also for the ^{138}Cs (2640 keV) peak, which was fitted together with the neighbouring ^{95}Y (2632 keV) peak, the fitting in HyperLab proved to be easier for this relatively short acquisition time. The net-count areas of all other peaks were determined using the sum all 5-minutes spectra and all available spectra of 30 minutes, the total acquisition time being about 6.5 to 8 hours.

In order to increase the counting statistics, the 36 GWd/t and the 46 GWd/t spent fuel samples had been irradiated and measured twice in each lattice position, which are K7, L11 and M8 for the first, and I8 for the latter sample. Normally, the analysis was conducted on the summed spectra of the two measurements. An exception was the irradiation of the 36 GWd/t sample in position M8. The data acquisition after the first irradiation (irradiation 1 in Table 4.5) had to be restarted because of an initial incorrect positioning. This led to a certain doubt with respect to the accuracy of the time at which the acquisition was started¹. Consequently, only the measurements after the second irradiation in the M8 position (irradiation 6 in Table 4.5) was included in the final analysis.

5.2.3 Dead-time correction and related uncertainty

The zero-dead-time counting correction of the DSPEC Plus relies on adding more than one count at a time to a given channel, depending on the dead time in the spectrometer at the moment of the detection. As a consequence, simple Poisson statistics are no longer applicable to the ZDT spectrum, and the true uncertainties on the net-count areas are higher than what they would be in a Poisson-distributed spectrum. Gamma-Vision offers the possibility to record, instead of the LTC spectrum, the variance spectrum which would contain the variance of the ZDT spectrum on a channel-by-channel basis.

According to [Pommé 02], the variance spectrum is a good estimate of the true statistical variance of the counts accumulated in the ZDT spectrum as long as the region of interest (ROI) is a small portion of the total spectrum. The uncertainty $\sigma(ZDT)$ on the counts $N(ZDT)$ in the ROI of the ZDT spectrum can be written as:

$$\sigma^2(ZDT) = \langle n \rangle \cdot N(ZDT), \quad (5.5)$$

with $\langle n \rangle = \Sigma(n \cdot n)/N(ZDT)$ being the average dead-time correction on the ROI and n being the short-term dead-time correction (i.e. the correction applied to one single count). The value $\sqrt{\langle n \rangle}$ represents the deviation of the uncertainties from the Poisson distribution.

¹The acquisition times were recorded accurately within Gamma-Vision. However, as the clock of the laptop used for the data acquisition was not working correctly, it was necessary to note the time at which each data acquisition was started in order to know the exact cooling times.

In this work, however, it was decided to record both the LTC and ZDT spectra in order to have an estimate of the average dead times for the full spectrum expressed as the real-to-live time ratio. Not having the variance spectra, the true variance can be calculated by Eq. 5.5 using an average dead time correction $\langle n \rangle = \Sigma n / \Sigma 1 = N(ZDT)$, as in the dual loss-free counting spectrum technique. This approximation holds for a large range of conditions [Pommé 03]. In the current work, however, we chose to further approximate $\langle n \rangle$ by the real-to-live time ratio, as the approximation $\langle n \rangle = \Sigma n / \Sigma 1$ cannot readily be calculated on sums of spectra.

As illustrated in Table 5.3, the dead time decreased slowly during the measurements of the irradiated spent fuel samples. A good approximation of the dead time is thus given by the real-to-live time ratio of the first 5-minutes spectrum. Typically, for the 36 GWd/t and 46 GWd/t samples, the factor $\sqrt{\langle n \rangle}$ for the uncertainty, as compared to a Poisson distribution, is about 1.3 and 1.8, respectively.

During the measurements of the irradiated fresh fuel sample, the dead time strongly varied, decreasing from about 43% for the first 5-minutes spectrum to less than 2% in the last 30-minutes spectrum. As most counts of ^{138}Cs , ^{89}Rb and ^{95}Y are recorded in the first half hour of the measurements, the real-to-live time ratio of the first 5-minutes spectrum is used as an approximation for $\sqrt{\langle n \rangle}$, which is about 1.4. For the longer-lived fission products, i.e. ^{135}I , ^{92}Sr and ^{142}La , most of the recorded counts are recorded after the first hour, when the dead time is significantly lower. A fair approximation of the uncertainty factor $\sqrt{\langle n \rangle}$ can thus, in this case, be obtained from the first 30-minutes spectrum and is about 1.1.

Concluding, the current experience has shown that fractioning the measurement time with several spectra allows easier analysis of fission products with different half-lives but significantly complicates the uncertainty treatment related to the zero-dead-time corrections. In the future, for dead times larger than 20%, where $\sqrt{\langle n \rangle}$ is higher than 1.1, it is recommended that the zero-dead-time and variance spectra are recorded in a single run.

5.2.4 Typical results for net-count areas

As an example, the obtained net-count areas for the fresh, 36 GWd/t and 46 GWd/t samples are listed in Table 5.4, for the irradiation positions K7 and I8, where the quoted uncertainties include the dead-time related factors described in the previous subsection. Although the fresh fuel sample had been irradiated at lower power, the obtained net counts are much higher, mainly because the fresh sample was measured closer to the detector than the spent ones. To increase the statistics for the spent fuel measurements, the 36 GWd/t and the 46 GWd/t samples were irradiated and measured twice in each lattice position. In Table 5.4, the net-count areas are given for the sum of spectra from both irradiations in K7 and I8, respectively, these being the values used for the derivation of fission rate ratios.

5.2.5 Reproducibility of the results

Apart from the increase in counting statistics, the repeated irradiations of the 36 GWd/t sample and the 46 GWd/t sample in each lattice position also served to investigate the reproducibility of the measurements. Thus, the reproducibility of the determination of net-count areas using HyperLab could be tested by comparing the individual results from the two irradiations in the

Table 5.4: Net-count areas N_{net} derived with HyperLab.

Energy	Fresh sample, K7		36 GWd/t sample, K7*		46 GWd/t sample, I8*	
	t_a	N_{net}	t_a	N_{net}	t_a	N_{net}
2542 keV	~7.5 h	44234 (0.8%)	~6 h	10530 (2.7%)	~6 h	13114 (5.5%)
2570 keV	55 min	18723 (1.6%)	55 min	4190 (4.5%)	55 min	4217 (9.2%)
2640 keV	55 min	34503 (3.9%)	55 min	10095 (3.0%)	55 min	9881 (29.7%)
3576 keV	55 min	15740 (1.4%)	55 min	6008 (2.2%)	55 min	6671 (4.4%)
1260 keV	~7.5 h	32036 (2.1%)				
1383 keV	~7.5 h	171557 (0.7%)				
1435 keV	55 min	111964 (0.8%)				

t_a : acquisition time, starting in each case 5 min after irradiation.

*In each of these cases, the counts were obtained for the sum of the acquired spectra from the two irradiations at the same lattice position.

same lattice position. Provided that the reactor power during the two irradiations was the same and that the analysed spectra had the same cooling times and measurement times, the obtained net-count areas in the investigated gamma-ray peaks would also be expected to be the same.

The reactor power during irradiation was monitored by BF_3 detectors and fission chambers located near the inner periphery of the graphite driver region of the reactor. Comparing the monitor signals recorded during two irradiations conducted at the same nominal reactor power of 800 W, it was shown that the reactor power was well reproducible (less than 0.4% deviation), so that no corrections were necessary with respect to the power level.

Regarding the cooling and measurement times, all measurements were performed with the same timing (see Subsection 5.2.2), except for the first irradiation of the 36 GWd/t sample in position M8. Because of the 2 to 3 seconds needed in Gamma-Vision for saving one spectrum and initiating the next one, a slight shift in the timing of the measurements was possible. However, for the repeated irradiations in L11 and K7 (36 GWd/t sample) and I8 (46 GWd/t sample), the recorded measurement times deviate by a maximum of 1 second over the entire acquisition time.

The acquisition of the gamma-ray spectra was started manually as accurately as possible. It was shown, with the help of a sensitivity study, however, that a delay of 1 second in the starting time of the measurements would affect the recorded net-count areas of the gamma-ray lines from the two shorter-lived fission products ^{89}Rb and ^{95}Y quite significantly, i.e. by 1.7% and 0.5%, respectively. This relatively high sensitivity has to be taken into account when interpreting the conducted reproducibility test. It is also important for the derivation of the saturation and decay correction factors C_{FP} (see Subsection 5.3.5).

The ratios of the net-count areas obtained from the two repeated irradiations of the 36 GWd/t sample in the position K7 and in the position L11 are shown in Fig. 5.2 for equivalent sums of spectra. The ratios for the ^{142}La (2542 keV) peak are obtained from spectra measured from 5 min to 6.5 h after irradiation. The ratios for the other peaks are obtained from spectra measured from 5 min to 60 min after irradiation. The results are seen to agree within 1-2 standard deviations. This indicates a satisfactory reproducibility of the HyperLab fits for this sample, though the uncertainties on the ratios are relatively high (ranging from 4 to 9%).

During the spectrum analysis, the necessary fine-tuning done by the user on the background fit after the automatic HyperLab spectrum fitting affected the obtained net-count areas. A test

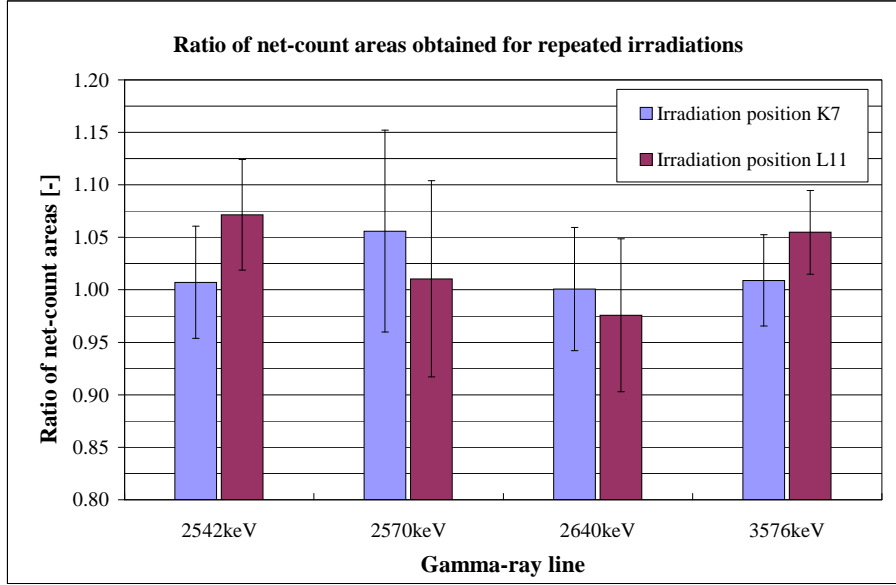


Figure 5.2: Reproducibility test of net-count areas obtained with HyperLab.

carried out on the spectra from the the 36 GWd/t sample irradiated in the position K7 showed that the ^{89}Rb (2570 keV) peak was especially sensitive to the chosen boundaries of the fitted region. Modifying the region boundaries by 10 to 80 channels (5 to 80 keV) resulted in changes of up to 5% on the net-count area, although the peak fit and the background fit appeared equally realistic and the quoted uncertainties on the net-count areas remained the same. For the ^{142}La (2542 keV) and ^{138}Cs (2640 keV) peaks, the maximum change in the net-count area was about 2%, whereas the net-count area of the ^{95}Y (3576 keV) peak, not being part of a multiplet area, was even less sensitive to fine-tuning by the user. Due to the high uncertainties, however, it is hardly possible to exactly quantify this user-dependency of the results.

The equivalent reproducibility test of the peak fitting for the 46 GWd/t sample showed that the net-count areas in the four peaks could be reproduced within 1-2 standard deviations. The uncertainties on the ratios of net-count areas were much higher in this case, varying from 8-20% to as high as 40% for the ^{138}Cs (2640 keV) peak. The main reason for the higher uncertainties was the more difficult spectrum fitting due to the highly distorted peaks as a consequence of the advanced neutron damage.

In general, if in future experiments it becomes possible to reduce the statistical uncertainty of the investigated peaks on the one hand, and to eliminate the neutron damage in the detector crystal on the other hand, the reproducibility of the peak fitting can be expected to improve correspondingly.

5.3 Saturation and decay corrections

The factor C_{FP} is fission-product dependent and accounts for the build-up (saturation) of the considered fission product during irradiation and its decay after irradiation. The gamma-ray intensity $b_{\gamma,FP}$ is the total fraction of the β^- -decays followed by the emission of a gamma-ray of energy E_γ . Consequently, the product $(b_{\gamma,FP}C_{FP})$ relates the number of gamma-rays of energy

E_γ emitted by the fission product to the number of fissions occurring in the sample during irradiation.

The analysed gamma-ray lines, together with the related fission products and their parent isotopes and isomeric states, are summarised in Table 5.5. Among the investigated fission products, only ^{138}Cs has an isomeric state with a non-negligible half-life. The parent isotope ^{138}Xe only decays into the ground state ^{138}Cs and not into the isomeric state ^{138m}Cs , which eases the saturation and decay corrections². An extensive list of the various nuclear data and their uncertainties used in this research work can be found in Appendix A.

Table 5.5: List of considered parent isotopes and isomeric states for all fission products included in the analysis.

Gamma-ray energy	Fission product ($T_{1/2}$)	Parent ($T_{1/2}$)	Isomeric state ($T_{1/2}$)
2542 keV	^{142}La (1.52 h)	^{142}Ba (10.6 min)	-
2570 keV	^{89}Rb (15.4 min)	^{89}Kr (3.2 min)	-
2632 keV	^{95}Y (10.3 min)	^{95}Sr (23.9 sec)	-
2640 keV	^{138}Cs (33.4 min)	^{138}Xe (14.1 min)	^{138m}Cs (2.9 min)
3576 keV	^{95}Y (10.3 min)	^{95}Sr (23.9 sec)	-
1260 keV	^{135}I (6.57 h)	^{135}Te (19 sec)	-
1383 keV	^{92}Sr (2.71 h)	-	-
1435 keV	^{138}Cs (33.4 min)	^{138}Xe (14.1 min)	^{138m}Cs (2.9 min)

Nuclear data are extracted from the JEFF-3.1 library.

The most general case in this work is the consideration of saturation and decay of ^{138}Cs . The corresponding correction factor C_{FP} is given by Eq. 5.6³:

$$\begin{aligned}
 C_{FP} = & \left(\frac{Y_{ind,2}}{\lambda_2} + \frac{i_{12} \cdot \lambda_1 \cdot Y_{cum,2}}{\lambda_2 \cdot (\lambda_1 - \lambda_2)} + \frac{i_m \cdot \lambda_m \cdot Y_{cum,m}}{\lambda_2 \cdot (\lambda_{m1} - \lambda_2)} \right) \cdot f(\lambda_2) \\
 & + \left(\frac{i_{12} \cdot \lambda_2 \cdot Y_{cum,1}}{\lambda_1 \cdot (\lambda_2 - \lambda_1)} \right) \cdot f(\lambda_1) \\
 & + \left(\frac{i_m \cdot \lambda_2 \cdot Y_{cum,m}}{\lambda_m \cdot (\lambda_2 - \lambda_m)} \right) \cdot f(\lambda_m) \\
 \text{with } f(\lambda_x) = & (1 - e^{-\lambda_x t_i}) \cdot e^{-\lambda_x t_c} \cdot (1 - e^{-\lambda_x t_a})
 \end{aligned} \tag{5.6}$$

where t_i is the irradiation time, t_c the cooling time between irradiation and measurement, and t_a the acquisition time. The index 1 refers to the parent of the detected fission product, the index 2 to the fission product itself and the index m to its isomeric state. Y_{cum} and Y_{ind} are the cumulative and independent effective fission yields, and λ_1 , λ_2 and λ_m are the decay constants. As mentioned, Eq. 5.6 describes the case of ^{138}Cs . Here, the parent of the fission product does not decay to the isomeric state but only to the ground state of the fission product, the corresponding

²Note that ^{133}Te , which has a minor contribution to the ^{142}La (2542 keV) peak, also has an isomeric state. In this case, the decay of the precursor ^{133}Sb to the isomeric state ^{133m}Te was neglected.

³During the irradiation of a spent fuel sample, a small amount of ^{138}Cs is produced by the ^{137}Cs (n, γ) reaction, ^{137}Cs being a long-lived fission product in the fuel. However, this contribution has been shown to be negligible and is therefore not considered in the saturation and decay correction.

branching ratio being i_{12} . The branching ratio for the decay of the isomeric state to the ground state is expressed with i_m .

All other fission products do not have isomeric states (or these isomeric states do not decay into the ground state), so that Eq. 5.6 reduces to:

$$C_{FP} = \left(\frac{Y_{ind,2}}{\lambda_2} + \frac{i_{12} \cdot \lambda_1 \cdot Y_{cum,2}}{\lambda_2 \cdot (\lambda_1 - \lambda_2)} \right) \cdot f(\lambda_2) + \left(\frac{i_{12} \cdot \lambda_2 \cdot Y_{cum,1}}{\lambda_1 \cdot (\lambda_2 - \lambda_1)} \right) \cdot f(\lambda_1) \quad (5.7)$$

As regards ^{92}Sr , the very short half-life of the parent isotope ^{92}Rb ($T_{1/2} = 4.5\text{ s}$) makes the corrections negligible and Eq. 5.6 simplifies even further to:

$$C_{^{92}\text{Sr}} = \frac{Y_{cum,2}}{\lambda_2} \cdot f(\lambda_2) \quad (5.8)$$

Equations 5.6 to 5.8 are derived for a single irradiation of the sample followed by a single measurement. During the data acquisition, the counts were saved in a series of spectra, as described in Subsection 5.2.2. Later, the analysis was carried out on appropriate sums of spectra. As mentioned earlier, the time delay in Gamma-Vision to store one spectrum and start the subsequent one was about 2 to 3 seconds. As the time was accurately recorded within Gamma-Vision, the “idle” time between the different spectra is accounted for by calculating the correction factor $C_{FP,spec}$ separately for each single spectrum *spec* (having a cooling time t_c and an acquisition times t_a) and then summing them.

During the WOLF-B campaign, only one irradiation was conducted per day such that most of the studied fission products produced during previous irradiations had completely decayed. However, for ^{135}I , which has a 6.6 hour half-life, previous irradiations have also to be taken into account. This is done by summing the correction terms $C_{FP,i}$ over all considered irradiations i , with the cooling time t_c updated to account for the time between each considered past irradiation and the current measurement.

Finally, the correction factor C_{FP} is formed as a sum over all considered irradiations i and all single spectra *spec* which are part of the analysed measurement:

$$C_{FP} = \sum_i \sum_{spec} C_{FP,i,spec} \quad (5.9)$$

In the special cases where the 36 GWd/t sample and the 46 GWd/t sample were irradiated twice in the same lattice position and the counts of the two measurements are summed for the analysis, the two correction terms C_{FP} were obtained separately and then summed.

5.3.1 Effective fission yields

As indicated in Eq. 5.6 and Eq. 5.7, the effective independent fission yield of a fission product has to be used if the half-life of its parent isotope is not negligible. Unfortunately, the independent fission yields of most of the investigated fission products have extremely high uncertainties (e.g.

30-36% on the thermal independent fission yields of ^{95}Y , ^{138}Cs , ^{89}Rb and ^{142}La). To avoid these high uncertainties, the effective independent fission yields have been derived as the difference between the effective cumulative fission yields of the fission product and the effective cumulative fission yields of the parent isotope (and of the isomeric state, in the case of ^{138}Cs) weighted by the branching ratios i_{12} (and i_m):

$$Y_{ind,2} = Y_{cum,2} - i_{12} \cdot Y_{cum,1} - i_m \cdot Y_{cum,m} \quad (5.10)$$

The effective cumulative fission yields Y_{cum} of the different isotopes are determined according to Eq. 5.11 as the sum of the cumulative fission yields for the main fissioning isotopes ^{235}U , ^{238}U , ^{239}Pu and ^{241}Pu , weighted by their contributions to the total number of fissions a_{U5} , a_{U8} , a_{P9} and a_{P1} . The latter four values have been obtained, for each sample in the different irradiation positions, on the basis of the whole-reactor Monte Carlo model which is described in detail in Subsection 6.1.1 of the next chapter. For fissions in ^{235}U , ^{239}Pu and ^{241}Pu , thermal fission yields Y_{th} are used, whereas for ^{238}U , the fast fission yield Y_f is applied. This assumption is valid because more than 99% of the fissions in ^{235}U , ^{239}Pu and ^{241}Pu occurred in the thermal energy group (0 - 9.1 keV), whereas more than 99% of the fissions in ^{238}U occurred in the fast energy group (9.1 keV - 10 MeV).

$$Y_{cum} = a_{U5} \cdot Y_{cum,th,U5} + a_{U8} \cdot Y_{cum,f,U8} + a_{P9} \cdot Y_{cum,th,P9} + a_{P1} \cdot Y_{cum,th,P1} \quad (5.11)$$

The contributions a_i to the total number of fissions are summarised for the different samples in Table 5.6.

Table 5.6: Contributions of fissioning isotopes to total fissions.

Sample	Lattice position	a_{U5}	a_{U8}	a_{P9}	a_{P1}
fresh	K7	96.4%	3.6%		
	L11	96.8%	3.2%		
	M8	97.7%	2.3%		
36 GWd/t	K7	50.7%	4.5%	38.8%	6.0%
	L11	51.4%	4.0%	38.6%	6.0%
	M8	53.1%	2.9%	38.0%	6.0%
46 GWd/t	I8	27.4%	3.7%	57.1%	11.8%

For the fresh and 36 GWd/t samples, the two positions K7 and L11 lead to similar distributions of fissions in ^{235}U , ^{238}U , ^{239}Pu and ^{241}Pu due to the similar neutron spectra in these positions. For the moderator position M8, which has a more thermal spectrum because of the higher amount of moderator, the contribution from ^{235}U is slightly higher and the contribution from ^{238}U accordingly lower. In general, however, the contributions a_i do not strongly vary for the different irradiation positions of the two samples. Generally speaking, the major part of fissions in the fresh sample occurred in ^{235}U . In the 36 GWd/t spent sample, ^{235}U and ^{239}Pu were the main fissioning isotopes, but with still more fissions in ^{235}U than in ^{239}Pu . In the 46 GWd/t sample, most fissions occurred in ^{239}Pu , and the relative contribution of ^{241}Pu doubled compared to the 36 GWd/t sample.

5.3.2 Error propagation

It is seen, from Eq. 5.6, that the correction-term product $(b_{\gamma,FP}C_{FP})_{eff}$ depends on a large number of variables x_i . Assuming that all these variables are independent, the combined standard uncertainty $\sigma_{(b_{\gamma,FP}C_{FP})_{eff}}$ is determined with the error propagation law:

$$\sigma_{(b_{\gamma,FP}C_{FP})_{eff}} = \sqrt{\sum_i \sigma_{x_i}^2 \left(\frac{\partial (b_{\gamma,FP}C_{FP})_{eff}}{\partial x_i} \right)^2} \quad (5.12)$$

Since times were carefully recorded during the measurements, the variables t_a and t_i can be considered as exact values. Also the cooling time t_c between irradiation and measurement can be considered exact for the error propagation; nevertheless, a sensitivity study was performed with respect to small shifts in t_c (see Subsection 5.3.5). Furthermore, the variables a_{U5} , a_{U8} , a_{P9} , a_{P1} , obtained on the basis of the Monte Carlo simulations, are not included in the current uncertainty analysis, as their Monte Carlo uncertainties were less than 0.2%. A sensitivity study on different parameter sets a_i is presented separately in Subsection 5.3.4.

Finally, the uncertainty analysis is carried out based on a set of 18 variables: $\mathbf{x} = \{b_{\gamma,FP}, Y_{cum,1,th,U5}, Y_{cum,1,f,U8}, Y_{cum,1,th,P9}, Y_{cum,1,th,P1}, Y_{cum,2,th,U5}, Y_{cum,2,f,U8}, Y_{cum,2,th,P9}, Y_{cum,2,th,P1}, Y_{cum,m,th,U5}, Y_{cum,m,f,U8}, Y_{cum,m,th,P9}, Y_{cum,m,th,P1}, \lambda_1, \lambda_2, \lambda_m, i_{12}, i_m\}$ for the correction regarding ^{138}Cs , and on a reduced set of 12 variables for the other fission products without isomeric states. Again, the indices 1, 2 and m refer to the parent isotope of the detected fission product, the fission product itself and its isomeric state, respectively; *th* and *f* indicate thermal and fast fission yields. If additional fission products contribute to a particular gamma-ray line (as is the case for ^{142}La (2542 keV) and ^{138}Cs (2640 keV), for example), the vector \mathbf{x} is extended by an equivalent set of variables for each additional fission product.

As in this study only ratios of fission rates are derived for the final results, the error propagation has ultimately to be conducted, according to Eq. 5.12, on the ratios of effective correction factors $(b_{\gamma,FP}C_{FP})_{eff,A}/(b_{\gamma,FP}C_{FP})_{eff,B}$ and $(b_{\gamma,FP}C_{FP})_{eff,f}/(b_{\gamma,FP}C_{FP})_{eff,s}$.

Table 5.7: Cumulative fission yields [%] and uncertainties of considered fission products (JEFF-3.1 data).

Energy	Fission product	$Y_{cum,th,U5}$	$Y_{cum,th,P9}$	Parent isotope	$Y_{cum,th,U5}$	$Y_{cum,th,P9}$
2542 keV	^{142}La	5.86 (1.7%)	4.97 (1.1%)	^{142}Ba	5.80 (1.7%)	4.68 (1.3%)
2570 keV	^{89}Rb	4.69 (1.2%)	1.68 (1.9%)	^{89}Kr	4.43 (1.4%)	1.42 (2.7%)
2640 keV	^{138}Cs	6.69 (1.7%)	5.94 (2.7%)	^{138}Xe	6.41 (1.8%)	5.02 (3.3%)
3576 keV	^{95}Y	6.47 (1.1%)	4.82 (2.0%)	^{95}Sr	5.28 (2.2%)	3.23 (5.2%)
1260 keV	^{135}I	6.39 (3.4%)	6.33 (3.7%)	^{135}Te	3.84 (7.1%)	2.14 (17.5%)
1383 keV	^{92}Sr	6.03 (1.1%)	3.00 (2.2%)			
1435 keV	^{138}Cs	6.69 (1.7%)	5.94 (2.7%)	^{138}Xe	6.41 (1.8%)	5.02 (3.3%)

Typical resulting uncertainties $\sigma_{(b_{\gamma,FP}C_{FP})_{eff}}$ on the different gamma-ray lines are indicated in Table 5.8 in the following subsection. Among the various nuclear data, the cumulative fission yields were found to have the main contribution to these uncertainties. The cumulative ^{235}U and

^{239}Pu fission yields of the fission products and their parent isotopes are given in Table 5.7 along with their uncertainties, which are in general between 1 and 5%. As mentioned, a complete list of nuclear data uncertainties is included in Appendix A.

5.3.3 Typical results

For the calculation of the saturation and decay correction factors $(b_{\gamma,FP}C_{FP})_{eff}$ and their combined uncertainties, a Matlab routine has been set up, which receives as input data the irradiation history of the sample, the starting time and the duration of the measurements and all required nuclear data. The results for the measurements of the fresh, 36 GWd/t and 46 GWd/t samples are given in Table 5.8 for the various investigated gamma-ray lines. The 1σ uncertainties strongly depend on the fission product. For the high-energy gamma-ray lines, they vary from about 3% for the ^{142}La (2542 keV) peak to 8.5% for the ^{95}Y (3576 keV) peak.

The results for the fresh and the 36 GWd/t samples shown in Table 5.8 have been obtained for irradiations in position K7. However, for a given sample, the irradiation, cooling and measurement times were kept the same and the effective fission yields were almost constant for the different irradiation positions. Consequently, the factors $(b_{\gamma,FP}C_{FP})_{eff}$ for the irradiation positions M8 and L11 are very similar to those listed in Table 5.8.

Table 5.8: Typical saturation and decay correction factors $(b_{\gamma,FP}C_{s,FP})_{eff}$

Gamma-ray line	Fresh $(b_{\gamma,FP}C_{f,FP})_{eff}$	36 GWd/t $(b_{\gamma,FP}C_{s,FP})_{eff}$	46 GWd/t $(b_{\gamma,FP}C_{s,FP})_{eff}$
^{142}La (2542 keV)	10.34 (2.8%)	9.95 (2.6%)	9.46 (2.5%)
^{89}Rb (2570 keV)	4.07 (6.3%)	3.07 (6.3%)	2.28 (6.3%)
^{138}Cs (2640 keV)	6.34 (3.4%)	6.82 (3.5%)	6.64 (3.5%)
^{95}Y (3576 keV)	2.24 (8.5%)	2.87 (8.5%)	2.61 (8.5%)
^{135}I (1260 keV)	18.02 (9.7%)		
^{92}Sr (1383 keV)	79.96 (1.2%)		
^{138}Cs (1435 keV)	46.73 (2.8%)		

The quoted values refer to irradiation in positions K7 (fresh and 36 GWd/t) and I8 (46 GWd/t).

As mentioned earlier, it is the ratios of the correction factors which are needed to derive fission rate ratios. For the inter-position fission rate ratios, which only compare the same fuel type in different irradiation positions, the individual correction factors are almost the same and the nuclear data uncertainties thus compensate almost entirely. The combined uncertainties on the ratios of correction factors are less than 0.03%.

The ratios of the correction factors for the inter-sample fission rate ratios are listed in Table 5.9. The combined 1σ uncertainties on the ratios $(b_{\gamma,FP}C_{FP})_{eff,f}/(b_{\gamma,FP}C_{FP})_{eff,s}$ for the fresh and the 36 GWd/t samples are 0.5-1%. The correction factors and their uncertainties do not compensate entirely because, as there is no plutonium in the fresh sample, the corresponding effective fission yields are not the same in the two samples. This effect is stronger for the comparison between the fresh and the 46 GWd/t sample. Since most of the fissions in the 46 GWd/t sample occur in plutonium, the uncertainties on the fission yields compensate less, and the combined uncertainties on the ratios $(b_{\gamma,FP}C_{FP})_{eff,f}/(b_{\gamma,FP}C_{FP})_{eff,s}$ are 1-1.4%.

Table 5.9: Ratios of correction factors $(b_{\gamma,FP}C_{s,FP})_{eff}$ as needed for inter-sample fission rate ratios.

Gamma-ray line	fresh 36GWd/t	fresh 46GWd/t
	$\frac{(b_{\gamma,FP}C_{FP})_{eff,f}}{(b_{\gamma,FP}C_{FP})_{eff,s}}$	$\frac{(b_{\gamma,FP}C_{FP})_{eff,f}}{(b_{\gamma,FP}C_{FP})_{eff,s}}$
^{142}La (2542 keV)	1.039 (0.8%)	1.093 (1.2%)
^{89}Rb (2570 keV)	1.096 (0.5%)	1.444 (1.0%)
^{138}Cs (2640 keV)	0.930 (1.0%)	0.970 (1.4%)
^{95}Y (3576 keV)	0.783 (0.9%)	0.854 (1.4%)

5.3.4 Sensitivity study regarding the parameters a_{U5} , a_{U8} , a_{P9} and a_{P1}

The contributions a_{U5} , a_{U8} , a_{P9} and a_{P1} of the fissioning isotopes ^{235}U , ^{238}U , ^{239}Pu and ^{241}Pu to the total number of fissions are needed for the determination of the effective fission yields. They were calculated with an MCNPX whole-reactor model and their purely statistical Monte Carlo uncertainties are less than 0.2%. They strongly depend, however, on the modelled composition of the fuel samples in the MCNPX calculations. Regarding the fresh fuel sample, the composition is well known and thus not affected by any such uncertainty. With respect to the spent fuel samples, the compositions are not known exactly and generally need to be measured.

For the present work, the isotopic compositions of the spent fuel samples had been determined by post-irradiation examination (PIE) measurements on an adjacent section of the fuel pin from which the sample had been cut. To study the sensitivity of the results to different isotopic compositions, the fuel composition of the 36 GWd/t sample was also modelled according to results of burn-up calculations using the deterministic code CASMO-4E [Rhodes 04] (see Section 2.3).

The sensitivities of the fission contributions a_{U5} , a_{U8} , a_{P9} and a_{P1} , and the resulting sensitivity of the saturation and decay correction $(b_{\gamma,FP}C_{FP})_{eff}$, to the measured and calculated isotopic compositions of the 36 GWd/t sample are listed in Table 5.10 for the irradiation position K7.

It is seen that the parameter a_{U8} is very similar for the two isotopic compositions, whereas a_{U5} , a_{P9} and a_{P1} change by -3.6%, +3.4% and +9.2%, respectively. This corresponds to the deviation in ^{235}U , ^{239}Pu and ^{241}Pu densities between the measured and the calculated compositions (see Subsection 6.1.2).

The correction factors for the ^{89}Rb (2570 keV) peak are most sensitive to the change in the parameter set a_{U5} , a_{U8} , a_{P9} and a_{P1} because of the very different fission yields for ^{235}U and ^{239}Pu fissions. In contrast to this, the results based on ^{142}La and ^{138}Cs are very insensitive to the exact knowledge of the individual contributions of the major fissioning isotopes.

Applying the calculated CASMO-4 isotopic composition to the 36 GWd/t sample irradiated in the other two positions L11 and M8 leads to very similar changes in the parameter sets a_i . Consequently, similar sensitivities of the correction factors are expected for these positions as well.

As mentioned earlier, the measured isotopic compositions of the spent fuel samples have been used for the derivation of fission rates in this work. Nonetheless, the sensitivities quoted in

Table 5.10: Sensitivity of contributions to total number of fissions and of correction factors $(b_{\gamma,FP}C_{s,FP})_{eff}$ to different isotopic compositions of the 36 GWd/t sample modelled in MCNPX.

	a_{U5}	a_{U8}	a_{P9}	a_{P1}
Meas. Composition	0.507	0.046	0.388	0.060
CASMO composition	0.489	0.045	0.401	0.065
Ratio CASMO/meas.	0.964	0.992	1.034	1.092
	^{142}La (2542 keV)	^{89}Rb (2570 keV)	^{138}Cs (2640 keV)	^{95}Y (3576 keV)
	$(b_{\gamma,FP}C_{s,FP})_{eff}$	$(b_{\gamma,FP}C_{s,FP})_{eff}$	$(b_{\gamma,FP}C_{s,FP})_{eff}$	$(b_{\gamma,FP}C_{s,FP})_{eff}$
Meas. composition	9.95	3.71	6.82	2.85
CASMO composition	9.94	3.65	6.81	2.84
Ratio CASMO/meas.	1.002	1.016	1.001	1.004

All quoted values refer to the irradiation position K7.

Table 5.10 should be considered for future applications of the developed measurement technique, since they show a clear disadvantage of ^{89}Rb (as compared to the other three fission products) in situations where measurements need to be carried out on fuels for which the composition is not exactly known.

5.3.5 Sensitivity study regarding the cooling time

During the gamma-ray measurements, the data acquisition was done automatically using a Gamma-Vision job-file. The job-file was started manually 2 minutes after irradiation of the sample. Although care was taken to guarantee a reproducible starting time of the job-file, a sensitivity study has been carried out in this context. This was done by deriving the saturation and decay correction factors $(b_{\gamma,FP}C_{FP})_{eff}$ of the four gamma-ray lines ^{142}La (2542 keV), ^{89}Rb (2570 keV), ^{138}Cs (2640 keV) and ^{95}Y (3576 keV), assuming that the job-file had been started with a delay of 1 or 3 seconds. For example, a delay of 1 second would increase the cooling time t_c of each spectrum by 1 second, whereas the acquisition time t_a would stay the same. The sensitivities of the correction factors are given in Table 5.11 for the irradiation of the 36 GWd/t sample.

 Table 5.11: Sensitivities of correction factors $(b_{\gamma,FP}C_{FP})_{eff}$ to changes in cooling time t_c

Gamma-ray line	[%/1sec]	[%/3sec]
^{142}La (2542 keV)	0.16	0.21
^{89}Rb (2570 keV)	1.67	1.80
^{138}Cs (2640 keV)	0.08	0.16
^{95}Y (3576 keV)	0.51	0.73

The results based on ^{142}La and ^{138}Cs are not very sensitive to the changes of 1 and 3 seconds in the cooling times because they and their parent isotopes have relatively long half-lives. The results based on ^{95}Y show a slightly higher sensitivity because it has a shorter half-life (10.2 min).

The results based on ^{89}Rb show an even higher sensitivity to the extension of the cooling time, mainly because of the half-life of the parent isotope ^{89}Kr , which is 189 seconds. On the one hand, this half-life is short enough so that a significant amount (0.35%) of ^{89}Kr decays within 1 second. On the other hand, it is long enough so that 5 minutes after irradiation, when the measurements of the analysed spectra have been started, there is still 33% of the initial amount of ^{89}Kr left in the fuel.

Extreme precaution in recording the measurement timing is thus necessary in order to guarantee the reproducibility of measurements. As an alternative solution, to reduce the sensitivity of the results, one could start the measurements later after the end of irradiation, but this would be at the expense of increasing the statistical uncertainty.

5.4 Solid angle and attenuation corrections

The ratio of solid angle and attenuation correction factors $att(E_\gamma)$, which is needed for the derivation of fission rate ratios between fresh and spent fuel samples, was determined using an MCNPX [Pelowitz 05] model of the measurement set-up. The MCNPX model, typical solid angle and attenuation correction factors and their sensitivities are detailed below.

5.4.1 MCNPX model of the measurement set-up

An already existing model of the sample changer [Plaschy 07a] was modified to represent the WOLF-B set-up with the detector positioned inside the body of the sample changer as shown in Fig. 5.3. Technical drawings were used to accurately model all steel parts of the sample changer with respect to their dimensions and materials; special care was taken for relevant parts located between the samples and the detector.

The HPGe detector was modelled according to the product data sheet which contains the dimensions of the active germanium crystal, the thickness of the absorbing inactive germanium layer (dead layer) and the position of the crystal inside the aluminium cap. The dimensions and the position of the cavity inside the germanium crystal are not specified in the data sheet, and were modelled according to measurements performed in the framework of a previous PhD thesis [Caruso 07]. A cross-section of the modelled detector is shown in Fig. 5.4.

The fresh and spent fuel samples were modelled in their measurement positions as illustrated in Fig. 5.3. Three different measurement set-ups were modelled, one for each sample. The composition of the fresh fuel sample was modelled according to its average nominal specifications. The isotopic composition of each burnt fuel sample was modelled, as mentioned earlier, according to the results of PIE measurements on an adjacent section of the fuel pin from which the sample had been cut. The models of the fresh and the spent fuel samples are described in more detail in the next chapter (see Subsection 6.1.2).

Gamma-ray sources with energies of 2542 keV, 2570 keV, 2640 keV and 3576 keV were distributed in the measured samples according to the axial fission profiles and transported to the detector. The axial total fission profiles in the samples were obtained with the whole-reactor model (see Subsection 6.1.1) and differed only marginally for the three different irradiation positions.

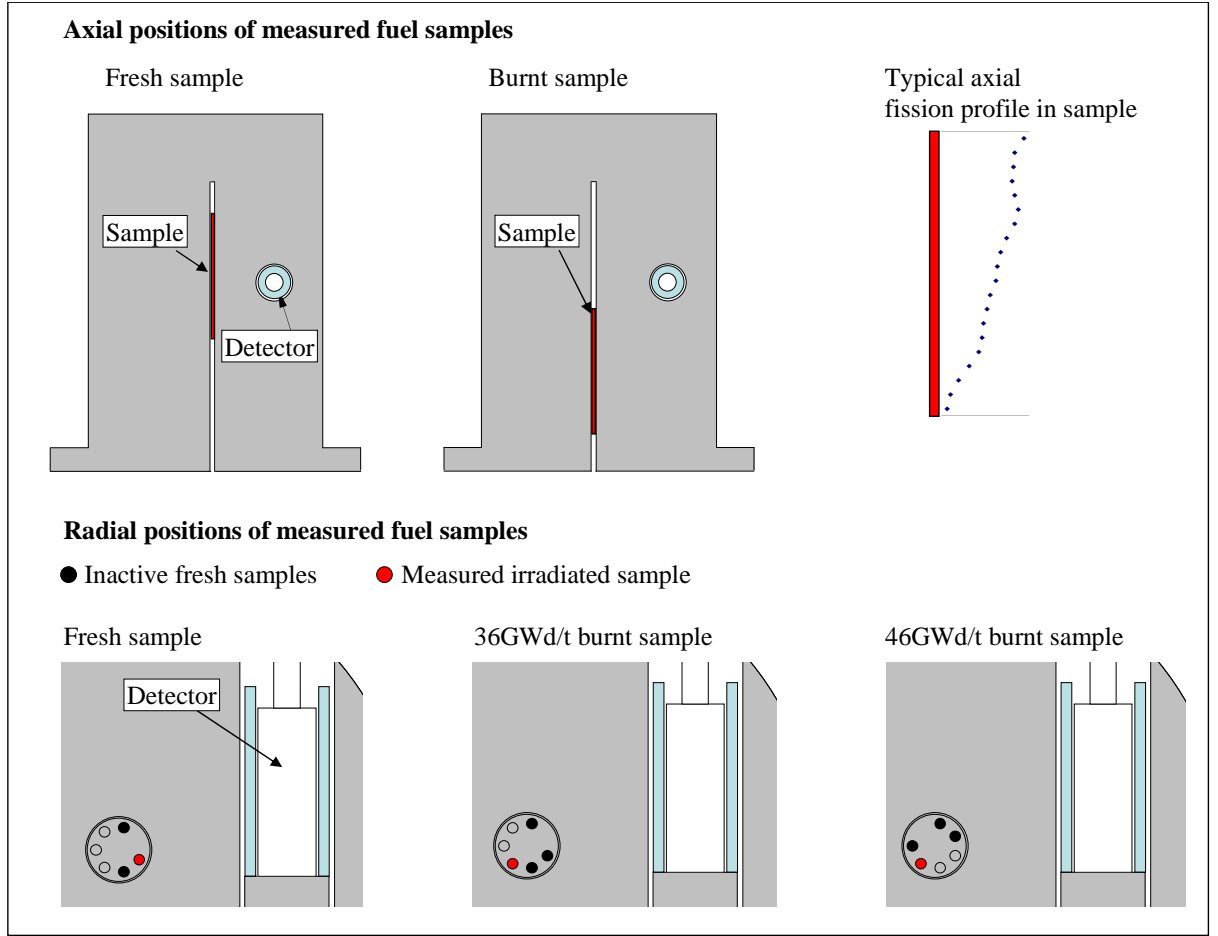


Figure 5.3: Schematic views of fresh and burnt fuel samples inside the sample changer.

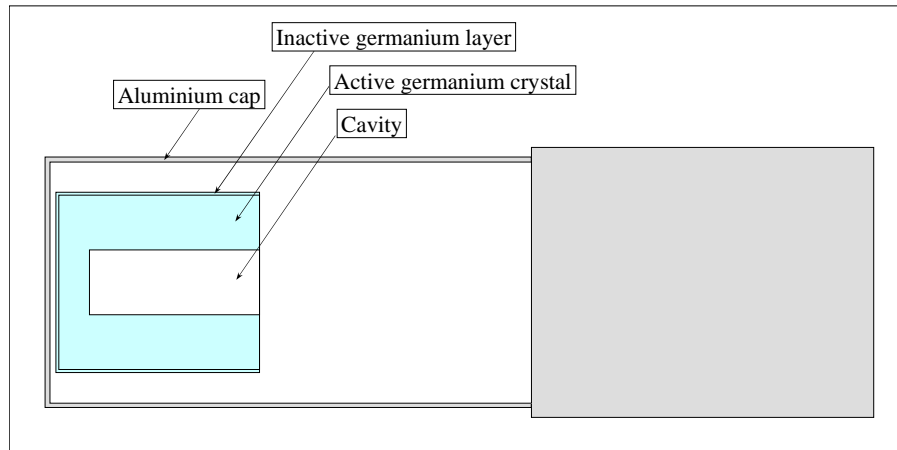


Figure 5.4: Cross-section of model of the germanium detector.

Nonetheless, the simulations were conducted for all investigated irradiation positions. The measurement set-up was the same for all irradiations of a given sample. Radially, the gamma-ray sources were assumed to be homogeneously distributed. Although the radial distribution of fissions (and thus that of gamma-ray emitting fission products) in a fuel sample is certainly not homogeneous, the corresponding sensitivity study presented in Subsection 5.4.3 has shown a limited impact on the detected response.

The solid angle and attenuation correction factors were obtained as the detector response per source gamma-ray in the sample. The detector response was tallied as the average uncollided gamma-ray flux in the active germanium crystal of the detector (see Fig 5.4).

5.4.2 Typical results

Results for the tallied average uncollided gamma-ray fluxes in the active germanium layer for the fresh, the 36 and the 46 GWd/t burnt samples are summarised in Table 5.12. The quoted values correspond to irradiations at the lattice positions K7 (fresh and 36 GWd/t samples) and I8 (46 GWd/t sample). Results for the fresh and 36 GWd/t samples irradiated in positions L11 and M8 do not differ significantly from those shown in Table 5.12 because of the similar axial fission profiles.

Table 5.12: Tallied uncollided fluxes in active germanium layer of the detector.

Gamma-ray line	Fresh [cm ⁻² sg ⁻¹]*	36 GWd/t [cm ⁻² sg ⁻¹]*	46 GWd/t [cm ⁻² sg ⁻¹]*
¹⁴² La (2542 keV)	1.02·10 ⁻⁶ (0.1%)	4.20·10 ⁻⁸ (0.3%)	5.15·10 ⁻⁸ (0.3%)
⁸⁹ Rb (2570 keV)	1.04·10 ⁻⁶ (0.1%)	4.32·10 ⁻⁸ (0.3%)	5.29·10 ⁻⁸ (0.3%)
¹³⁸ Cs (2640 keV)	1.09·10 ⁻⁶ (0.1%)	4.63·10 ⁻⁸ (0.3%)	5.66·10 ⁻⁸ (0.3%)
⁹⁵ Y (3576 keV)	1.74·10 ⁻⁶ (0.1%)	8.92·10 ⁻⁸ (0.3%)	1.08·10 ⁻⁷ (0.2%)

*sg = source gamma-ray

The 1 σ uncertainties on the tallied average gamma-ray fluxes are about 0.1% and 0.3% for source gamma-rays emitted in the measurement positions for the fresh and the spent fuel samples, respectively. The resulting Monte Carlo uncertainty on the ratio between fresh and spent fuel results is thus about 0.3%. Note that these uncertainties are only statistical Monte Carlo uncertainties (depending on the number of simulated source gamma-rays). The sensitivity of the detector response to other aspects of the modelling are presented in the following subsection.

The resulting ratios of solid angle and attenuation correction factors between the fresh and the 36 GWd/t sample and the fresh and the 46 GWd/t samples are summarised in Table 5.13. Depending on the gamma-ray energy, 15 to 25 times more gamma-rays reached the detector from the fresh-fuel measurement position than from the spent-fuel ones. Such large factors make the measured inter-sample fission rate ratios highly sensitive to the exact positioning of the spent fuel sample. This sensitivity is quantified in the following subsection.

The correction factors $att_s(E_\gamma)$ for the 36 GWd/t sample are about 20% higher than for the 46 GWd/t sample, although the two samples were measured in the same position. This is due to the additional presence of two fresh samples between the measured sample and the detector when measuring the 36 GWd/t sample (see Fig. 5.3). When the 46 GWd/t sample was measured, the two revolver channels between sample and detector were empty, because these were the channels containing the 36 GWd/t and the 64 GWd/t samples, which were moved below the sample changer to prevent any interference of their intrinsic activities during the measurement.

Table 5.13: Ratios of solid angle and attenuation corrections factors $att(E_\gamma)$.

Gamma-ray line	$\frac{\text{fresh}}{36\text{GWd/t}}$	$\frac{\text{fresh}}{46\text{GWd/t}}$
	$\frac{att_f(E_\gamma)}{att_s(E_\gamma)}$	$\frac{att_f(E_\gamma)}{att_s(E_\gamma)}$
^{142}La (2542 keV)	24.21 (0.3%)	19.65 (0.3%)
^{89}Rb (2570 keV)	24.04 (0.3%)	19.53 (0.3%)
^{138}Cs (2640 keV)	23.55 (0.3%)	18.16 (0.3%)
^{95}Y (3576 keV)	19.57 (0.3%)	16.14 (0.2%)

5.4.3 Sensitivity studies

Three aspects were investigated with respect to the sensitivities of the computed solid angle and attenuation correction factors: the z-position (elevation) of the samples inside the sample changer, the size of the modelled cavity in the germanium crystal of the detector, and the radial distribution of the gamma-ray sources in the fuel samples.

- **Elevation of the samples in the MCNPX model of the sample changer**

The position of the fuel pellets inside the cladding and the overcladding was modelled as exactly as possible following the available technical drawings. However, the fuel could be slightly displaced axially inside the cladding. In addition, the exact position of the sample inside the sample changer could slightly differ from the assumed one.

In this sensitivity study, the modelled positions of the fuel samples were shifted up by 1 and 5 mm in the z-direction, and the new solid angle and attenuation correction factors were calculated and compared to the original ones. The sensitivities for the 2542 keV and the 3576 keV gamma-ray sources are listed in Table 5.14 for the fresh ($att_f(E_\gamma)$) and the 36 GWd/t ($att_s(E_\gamma)$) fuel samples.

Table 5.14: Sensitivities of correction factors $att(E_\gamma)$ to changes of sample elevation in the MCNPX model of the sample changer.

		[%/1mm]	[%/5mm]
Fresh	$att_f(2542\text{keV})$	0.15	0.73
	$att_f(3576\text{keV})$	0.14	0.69
36 GWd/t	$att_s(2542\text{keV})$	1.50	8.60
	$att_s(3576\text{keV})$	1.44	7.86

The results for the 36 GWd/t sample are seen to be highly sensitive to the modelled sample elevation. In the employed measurement position, the top of the spent fuel sample was located approximately 7.5 cm below the detector (referring to the z-position). Therefore, the modelled elevation strongly influences the amount of attenuating material and the solid angle between sample and detector. In comparison, the fresh fuel was measured in front of the detector, and a change in its elevation affects the solid angle and attenuation correction factor only moderately.

The high sensitivity of the solid angle and attenuation correction factors for the spent fuel samples has to be taken into account when interpreting the comparison of measured and calculated inter-sample fission rate ratios, which will be presented in the next chapter (see Subsection 6.3.1).

- **Size of the modelled cavity in the germanium crystal of the detector**

The dimensions of the germanium crystal and its location inside the aluminium cap of the detector are well documented in the vendor’s data sheet. There is, however, no information concerning the axial cavity of the crystal, which was therefore assumed to have the same size as for the detector used in [Caruso 07]. A sensitivity study was carried out to test the impact of the modelling of the cavity on the results. Two extreme test cases were investigated. In a “no-cavity” case, the germanium crystal was modelled without any cavity, whereas in a “void” case, the germanium zone was modelled as void without any assigned material. The ratios of the tallied average uncollided gamma-ray fluxes in the germanium zone, relative to the original case, are listed for the 2542 keV gamma-ray sources in the fresh and 36 GWd/t samples in Table 5.15.

Table 5.15: Ratio of tallied uncollided fluxes ($E_\gamma = 2542 \text{ keV}$) for different modelling of the germanium crystal of the detector.

	$\frac{\text{no-cavity}}{\text{original}}$	$\frac{\text{void}}{\text{original}}$
Fresh sample	0.962 (0.1%)	1.389 (0.2%)
36 GWd/t sample	0.961 (0.4%)	1.393 (0.6%)
Ratio fresh/36 GWd/t	1.002 (0.5%)	0.997 (0.4%)

It is seen that the tallied flux depends quite significantly on the material assumed for the inside of the germanium crystal of the detector (see rows 2 and 3 in Table 5.15). However, the changes are the same for both fresh and spent fuel simulations and thus compensate for each other when taking the ratio (see row 4). Consequently, an exact modelling of the material inside the germanium crystal is not necessary for the derivation of inter-sample fission rate ratios.

- **Radial distribution of the gamma-ray sources in the fuel samples**

As mentioned earlier, the radial distribution of the gamma-ray sources within the fuel samples was assumed to be homogeneous, although in the actual fuel samples fissions (and therefore gamma-rays emitted by fission products) are not homogeneously distributed. To test this assumption, a radial profile was applied to the gamma-ray source in the spent fuel simulations for the two source energies 2542 keV and 3576 keV. The modelled radial profile was according to a MCNPX whole-reactor simulation, in which the 36 GWd/t sample was subdivided into 6 radial zones with equal areas (see Subsection 6.2.2). The isotopic compositions of the 6 zones were derived with a HELIOS depletion calculation (see Subsection 2.5.2) using a pincell model of the spent fuel sample with the same 6 radial fuel zones.

The radial profile obtained for each isotope was applied to the average measured isotopic composition used in the MCNPX whole-reactor model. Relative to the total number of fissions in the sample, the fractions of fissions obtained in the 6 zones for the irradiation position L11 were 0.223, 0.167, 0.157, 0.153, 0.151 and 0.149, with most fissions in the outer zone and a flattened

profile towards the centre of the sample. This profile was applied to the radial gamma-ray source of the spent fuel sample in the model of the sample changer, and the uncollided flux in the germanium crystal of the detector was tallied. In addition, the uncollided gamma-ray current leaving the sample was tallied using a surface tally. The latter served to estimate the self-attenuation of the gamma-rays within the fuel sample.

For both investigated energies, the self-attenuation was found to be the same (about 20%) with and without the radial source distribution in the sample. Furthermore, the tallied uncollided gamma-ray fluxes in the germanium crystal remained constant, justifying the use of flat radial source distributions in the MCNPX simulation to derive the solid angle and attenuation correction factors⁴.

5.5 Results for fission rate ratios

Measured fission rate ratios were derived, according to Eqs. 5.3 and 5.4, between different irradiation positions for the same fuel sample (inter-position fission rate ratios) and between different samples irradiated in the same lattice position (inter-sample fission rate ratios). The final results are presented in the following two subsections.

The quoted combined uncertainties for the fission rate ratios include the uncertainties on the net-count areas N_{net} and on the ratios of saturation and decay correction factors $(b_{\gamma,FP}C_{FP})_{eff}$. For the inter-sample fission rate ratios, they include also uncertainties on the applied correction factors $att(E_{\gamma})$ for the solid angle and attenuation between samples and detector. The uncertainty for each gamma-ray line was obtained using the error propagation law. Eq. 5.13 provides an example for the case of a fission rate ratio between the fresh (f) and a spent (s) fuel sample:

$$\sigma_{FRR(E_{\gamma})} = \sqrt{\sigma_{N_{net,f}}^2 + \sigma_{N_{net,s}}^2 + \sigma_{\frac{att_s(E_{\gamma})}{att_f(E_{\gamma})}}^2 + \sigma_{\frac{(b_{\gamma,FP}C_{FP})_{eff,s}}{(b_{\gamma,FP}C_{FP})_{eff,f}}}}^2} \quad (5.13)$$

It is important to note that the results of the sensitivity studies performed in connection with the calculation of $att_s(E_{\gamma})$ are not included in the combined uncertainties.

For each fission rate ratio, a set of four individual estimates was obtained corresponding to the four high-energy gamma-ray lines ^{142}La (2542 keV), ^{89}Rb (2570 keV), ^{138}Cs (2640 keV) and ^{95}Y (3576 keV). For the inter-position fission rate ratios of the fresh fuel sample, three additional estimates were obtained using the lower-energy gamma-ray lines ^{92}Sr (1260 keV), ^{135}I (1383 keV) and ^{138}Cs (1435 keV). As the individual estimates $FRR_i(E_{\gamma})$ are independent from each other, and provided that they are consistent within their uncertainties $\sigma_{FRR_i(E_{\gamma})}$, they can be combined into a single final estimate FRR by taking an appropriately weighted mean, according to Eq. 5.14.

$$FRR = \frac{\sum \frac{1}{\sigma_{FRR_i(E_{\gamma})}^2} \cdot FRR_i(E_{\gamma})}{\sum \frac{1}{\sigma_{FRR_i(E_{\gamma})}^2}}, \quad \sigma_{FRR}^2 = \frac{1}{\sum \frac{1}{\sigma_{FRR_i(E_{\gamma})}^2}} \quad (5.14)$$

⁴Note that, in this sensitivity study, a symmetric radial fission profile has been assumed as the realistic profile in the fuel samples. However, fuel pins which will be irradiated during the LIFE@PROTEUS campaign might show an asymmetric radial fission profile due to strong neutron-flux gradients between fresh and spent fuel zones. Therefore, the assumption of flat radial source distributions may thus need to be re-evaluated for LIFE@PROTEUS.

Strictly speaking, the two estimates $FRR(3576\text{ keV})$ and $FRR(2640\text{ keV})$ are not completely independent, the first being based on the gamma-ray line from ^{95}Y and the second including a small contribution from ^{95}Y . The two estimates are, however, only slightly correlated and can be considered as independent. The same is valid for the two estimates $FRR(1435\text{ keV})$ and $FRR(2542\text{ keV})$, which both contain minor contributions from ^{93}Sr (see Table 5.2). Furthermore, the two estimates $FRR(1435\text{ keV})$ and $FRR(2640\text{ keV})$ are strongly correlated since both gamma-ray lines are from ^{138}Cs . This correlation has been neglected in the current study, as it only affects the inter-position fission rate ratios of the fresh sample.

5.5.1 Inter-position fission rate ratios

Table 5.16 provides the results for the inter-position fission rate ratios for the fresh and the 36 GWd/t samples, taking the irradiation position L11 as reference position. For both samples, the irradiations in the positions M8 and K7 lead to about 1.27 and 0.82 times the number of fissions than in the reference position L11, respectively.

Table 5.16: Measured estimates for inter-position fission rate ratios.

Fresh sample		
	$\frac{\text{M8}}{\text{L11}}$	$\frac{\text{K7}}{\text{L11}}$
^{142}La (2542 keV)	1.269 ± 0.017 (1.4%)	0.813 ± 0.011 (1.3%)
^{89}Rb (2570 keV)	1.234 ± 0.028 (2.3%)	0.783 ± 0.014 (1.7%)
^{138}Cs (2640 keV)	1.313 ± 0.081 (6.2%)	0.831 ± 0.032 (3.8%)
^{95}Y (3576 keV)	1.266 ± 0.025 (2.0%)	0.842 ± 0.012 (1.4%)
^{135}I (1260 keV)	1.320 ± 0.031 (2.4%)	0.861 ± 0.025 (2.9%)
^{92}Sr (1383 keV)	1.297 ± 0.009 (0.7%)	0.829 ± 0.007 (0.9%)
^{138}Cs (1435 keV)	1.260 ± 0.015 (1.2%)	0.824 ± 0.010 (1.2%)
Weighted mean:	1.282 ± 0.006 (0.5%)	0.824 ± 0.005 (0.6%)
36 GWd/t sample		
	$\frac{\text{M8}}{\text{L11}}$	$\frac{\text{K7}}{\text{L11}}$
^{142}La (2542 keV)	1.291 ± 0.053 (4.1%)	0.843 ± 0.030 (3.6%)
^{89}Rb (2570 keV)	1.272 ± 0.087 (6.8%)	0.776 ± 0.050 (6.4%)
^{138}Cs (2640 keV)	1.187 ± 0.073 (6.2%)	0.844 ± 0.042 (4.9%)
^{95}Y (3576 keV)	1.273 ± 0.042 (3.3%)	0.811 ± 0.024 (3.0%)
Weighted mean:	1.265 ± 0.028 (2.2%)	0.821 ± 0.020 (2.4%)

The individual estimates in Table 5.16 are seen to have 1σ uncertainties of 1 to 6% for the fresh fuel results and 3 to 7% for the spent fuel results. The uncertainties on the weighted mean are about 0.5% (fresh fuel) and about 2.3% (spent fuel). The quoted uncertainties mainly consist of the uncertainties on the net-count areas. The nuclear data, being part of the saturation and decay corrections, do not contribute to the combined uncertainties because the corresponding correction factors basically cancel out in the ratio of fission rates.

5.5.2 Inter-sample fission rate ratios

The results for the measured inter-sample fission rate ratios between the fresh and the 36 GWd/t samples, and between the fresh and the 46 GWd/t samples are listed in Table 5.17.

Table 5.17: Measured estimates for inter-sample fission rate ratios.

Fresh-to-36 GWd/t			
	K7	M8	L11
^{142}La (2542 keV)	1.362 ± 0.039 (2.9%)	1.397 ± 0.049 (3.5%)	1.416 ± 0.040 (2.8%)
^{89}Rb (2570 keV)	1.382 ± 0.066 (4.8%)	1.337 ± 0.070 (5.2%)	1.373 ± 0.068 (5.0%)
^{138}Cs (2640 keV)	1.272 ± 0.064 (5.1%)	1.437 ± 0.103 (7.1%)	1.295 ± 0.068 (5.3%)
^{95}Y (3576 keV)	1.393 ± 0.038 (2.8%)	1.342 ± 0.041 (3.1%)	1.346 ± 0.035 (2.6%)
Weighted mean:	1.364 ± 0.024 (1.7%)	1.366 ± 0.028 (2.0%)	1.367 ± 0.023 (1.7%)
Fresh-to-46 GWd/t			
	M8 (I8)		
^{142}La (2542 keV)	2.003 ± 0.114 (5.7%)		
^{89}Rb (2570 keV)	2.026 ± 0.190 (9.4%)		
^{138}Cs (2640 keV)	2.428 ± 0.734 (30.2%)		
^{95}Y (3576 keV)	2.103 ± 0.101 (4.8%)		
Weighted mean:	2.057 ± 0.070 (3.4%)		

The fission rates in the different samples are normalised to the same reactor power of 100 W.

The fission rate ratios between the fresh and the 36 GWd/t samples were derived for the three irradiation positions K7, M8 and L11. The estimates based on ^{142}La and ^{95}Y have a 1σ uncertainty of 2 to 4%, whereas the estimates based on ^{89}Rb and ^{138}Cs have higher uncertainties, i.e. 4 to 7%. Within these uncertainties, the results agree with each other. Independent of the irradiation position, the weighted mean of the fission rate ratios is $\sim 1.37 \pm 0.02$ (1.7-2%).

The fission rate ratios comparing the fresh and the 46 GWd/t samples were derived for the equivalent irradiation positions M8 and I8. Again, the results based on the different gamma-ray lines agree within their respective uncertainties, these being generally between 5 and 9%. Only the result based on the ^{138}Cs (2640 keV) peak has an extremely high uncertainty (more than 30%), because of the large uncertainty on its net-count area for the 46 GWd/t sample. The weighted mean for the fresh-to-46 GWd/t fission rate ratio is $\sim 2.06 \pm 0.07$ (3.4%).

Table 5.18 gives the individual contributions to the combined uncertainties on the fresh-to-36 GWd/t fission rate ratio and for the fresh-to-46 GWd/t fission rate ratio.

As for the inter-position fission rate ratios, the uncertainties on the net-count areas represent the main contribution to the combined uncertainties. The nuclear data uncertainties do not compensate entirely any more and contribute to an uncertainty of 0.5-1% for the fresh-36 GWd/t results and of 1-1.4% for the fresh-to-46 GWd/t results. Compared to the net-count areas, these contributions from the nuclear data are relatively small. However, it should be noted that the nuclear-data related uncertainties may become more important in future experiments because

Table 5.18: Contributions to the combined uncertainties of measured inter-sample fission rate ratios.*

Fresh-to-36 GWd/t				
Gamma-ray line	Comb. uncert.	Statis.	Nucl. data	Monte Carlo
^{142}La (2542 keV)	2.90%	2.85%	0.74%	0.32%
^{89}Rb (2570 keV)	4.77%	4.73%	0.54%	0.32%
^{138}Cs (2640 keV)	5.06%	4.95%	0.97%	0.31%
^{95}Y (3576 keV)	2.76%	2.61%	0.83%	0.32%
Weighted mean	1.73%			
Fresh-to-46 GWd/t				
Gamma-ray line	Comb. uncert.	Statis.	Nucl. data	Monte Carlo
^{142}La (2542 keV)	5.67%	5.61%	1.18%	0.30%
^{89}Rb (2570 keV)	9.39%	9.32%	1.04%	0.30%
^{138}Cs (2640 keV)	30.2%	30.2%	1.41%	0.29%
^{95}Y (3576 keV)	4.78%	4.58%	1.35%	0.22%
Weighted mean	3.40%			

*The values for the fresh-to-36 GWd/t fission rate ratio refer to the irradiation position K7; those for the fresh-to-46 GWd/t fission rate ratio refer to the irradiation position M8 (I8).

they cannot be easily reduced. Generally speaking, the higher the burn-up difference between two compared samples, the higher is the uncertainty related to nuclear data, because of the differences in the effective fission yields caused by the different sample compositions (see Subsection 5.3.3).

The Monte Carlo uncertainties associated with the calculation of the solid angle and attenuation correction factors are only about 0.3% and hence have an almost negligible contribution to the total combined uncertainties.

5.6 Chapter summary

Based on the measurements of a fresh, a 36 GWd/t and a 46 GWd/t sample during the WOLF-B experimental campaign, a detailed description has been provided for the methodology to obtain experimental fission rate ratios using high-energy gamma-rays emitted by short-lived fission products. The analysis is based on the use of the four high-energy lines ^{142}La (2542 keV), ^{89}Rb (2570 keV), ^{138}Cs (2640 keV) and ^{95}Y (3576 keV) and, for the fresh fuel sample, the three additional lower-energy lines ^{138}Cs (1435 keV), ^{135}I (1260 keV) and ^{92}Sr (1383 keV).

Based on appropriately evaluated results for these gamma-ray lines, inter-position fission rate ratios have been derived for the fresh and the 36 GWd/t samples. Furthermore, inter-sample fission rate ratios are reported between the fresh and the 36 GWd/t samples on the one hand, and between the fresh and the 46 GWd/t samples on the other hand. It has been found that results obtained for different gamma-ray lines are quite consistent within the respective 1 σ uncertainties. For the inter-position fission rate ratios, these were 1-6% for the fresh fuel and 3-7% for the 36 GWd/t spent fuel results. The weighted means of the individual estimates had

uncertainties of about 0.5 and 2.3%, respectively. The uncertainties on the inter-sample fission rate ratios were in general 2-7% for the fresh-to-36 GWd/t comparison and 5-9% for the fresh-to-46 GWd/t comparison, the uncertainties on the weighted means being about 1.8% and 3.4%, respectively.

In all cases, the uncertainties on the net-count areas represent the main contribution to the combined uncertainties. It should be noted, however, that the contribution from the nuclear data uncertainties to the combined uncertainties reached more than 1% for the fresh-to-46 GWd/t comparison. This contribution mainly consisted of the uncertainties on the fission yields because of the very different sample compositions and the resulting difference in the relative number of fissions in ^{235}U , ^{238}U , ^{239}Pu and ^{241}Pu . This is important because, in contrast to the statistical uncertainties, the nuclear data uncertainties cannot be reduced in future experiments at PROTEUS.

The inter-sample fission rate ratios were found to be highly sensitive to slight axial displacements of the spent fuel samples in their measurement positions. Shifting the 36 GWd/t spent fuel sample by 1 mm led to a change of 1.5% in the solid angle and attenuation correction factor needed for the derivation of fission rate ratios between the fresh and spent fuel. With the fresh fuel sample having been measured directly next to the detector, the fission rates in this sample were only moderately sensitive to its modelled elevation.

The inter-sample fission rate ratios based on the ^{89}Rb peak show a high sensitivity to the assumed contributions of ^{235}U , ^{238}U , ^{239}Pu and ^{241}Pu to the total number of fissions, these being needed for the derivation of effective fission yields (used in the saturation and decay correction). The results based on ^{95}Y show a lower sensitivity, whereas the results based on ^{142}La and ^{138}Cs are quite insensitive to the exact knowledge of the individual fission contributions.

A sensitivity study with respect to the exact time at which the gamma-ray measurements were started has emphasised the importance of an accurate record of the cooling time between the end of irradiation and the start of measurement. This is particularly true in the current analysis, where the cooling time was 5 minutes, the results based on the ^{89}Rb peak being particularly sensitive to the exact knowledge of the cooling time.

In the following chapter, the currently measured fission rate ratios are compared to MCNPX predictions. The possible future reduction of the measurement uncertainties, as also of the sensitivities of the results to irradiation and measurement parameters, is addressed in Chapter 7. Recommendations are made in this context for an optimised measurement station, and for optimised irradiation and measurement strategies to be applied in the main LIFE@PROTEUS experimental campaign.

Bibliography

- [Caruso 07] S. Caruso. *Characterisation of high-burnup LWR fuel rods through gamma tomography*. PhD thesis, École Polytechnique Fédérale de Lausanne (EPFL), Switzerland, 2007.
- [Hyp 05] HyperLabs software. *HyperLab 2005 Gamma-Spectroscopy Software System*, Manuals, 2005.
- [ORT 03a] ORTEC. *GammaVision-32, Gamma-ray Spectrum Analysis and MCA Emulator*, A66-B32 User's Manual, 2003.
- [Pelowitz 05] D.B. Pelowitz. *MCNPX User's Manual Version 2.5.0*, 2005.
- [Plaschy 07a] M. Plaschy. *Reference MCNPX model of the "Wechselflasche" shielding and corresponding dose rate calculations*. Internal Report AN-41-07-01, PSI, 2007.
- [Pommé 02] S. Pommé. *A plausible mathematical interpretation of the variance spectra obtained with the DSPECPlusTM digital spectrometer*. Nuclear Instruments and Methods in Physics Research Section A, vol. 482, page 565-566, 2002.
- [Pommé 03] S. Pommé. *On the statistical control of loss-free counting and zero dead time spectrometry*. J. Radioanalytical and Nucl. Chemistry, vol. 257 No.3, page 463-466, 2003.
- [Rhodes 04] J. Rhodes, Smith K. & Edenius M. *CASMO-4E, Extended Capability CASMO-4: User Manual*. Studsvik Scandpower, SSP-01/401 Rev. 2, Inc., 2004.
- [Simonis 03] A. Simonis, J. Östör, S. Kálvin & B. Fazekas. *HyperLab: A new concept in gamma-ray spectrum analysis*. J. Radioanalytical and Nucl. Chemistry, vol. 257 No.3, page 589-595, 2003.

Chapter 6

Comparison of calculated and measured fission rate ratios

In the previous chapter, the derivation of experimental results for inter-position and inter-sample fission rate ratios, based on the use of high-energy gamma-ray lines emitted by short-lived fission products, was presented in detail. In this chapter, the measured fission rate ratios are compared to calculated results obtained using an MCNPX whole-reactor model of the multi-zone PROTEUS facility.

The employed MCNPX model is described in Section 6.1. Section 6.2 gives the results for the calculated fission rate ratios and contains sensitivity studies with respect to the modelled spent fuel compositions and the positioning of the fuel samples in the model. The comparison of the measured and calculated fission rate ratios are presented in Section 6.3, and the chapter is summarised in Section 6.4.

6.1 MCNPX modelling

The Monte Carlo simulations in the current research have been conducted using the MCNPX code version 2.5.0 [Pelowitz 05], together with the JEFF-3.1 nuclear data library [Koning 06]. The whole-reactor model was primarily set up to obtain calculated predictions for fission rates in the fresh and spent fuel samples that were irradiated in the PROTEUS test zone during the WOLF-B campaign. In addition to the total fission rates, the axial profiles of fissions in the samples and the contributions a_i of the major fissioning isotopes (^{235}U , ^{238}U , ^{239}Pu and ^{241}Pu) to the total number of fissions were also calculated. These results were needed for the analysis of the measured gamma-ray spectra, as described in Chapter 5.

6.1.1 Whole-reactor model

A detailed 3-D MCNPX model of the multi-zone PROTEUS reactor was already available at PSI [Joneja 01]. This model was modified to match the WOLF-B experiments with respect to the critical loading and the test tank configuration. Axial and radial cuts of the model are shown in Fig. 6.1.

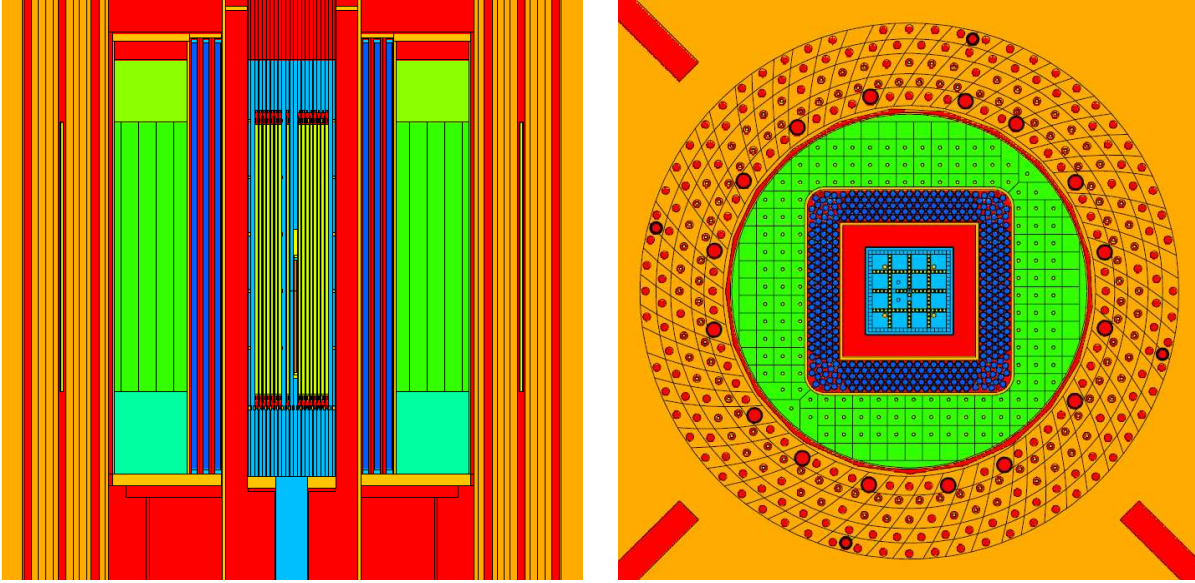


Figure 6.1: Axial and radial views of the MCNPX whole-reactor model of PROTEUS.

Axial and radial cuts focussing on the test lattice are shown in Fig. 6.2. The lattice pins were held in position with polypropylene grid plates. The two radial cuts correspond to elevations without grid plate (top) and with grid plate (bottom). As an example, the fresh fuel sample in the irradiation position L11 is shown. In the radial cuts, the other possible irradiation positions M8, I8, K7, K11 and I11 are also visible, the latter two not having been used in the WOLF-B campaign. The axial elevation during irradiation, which is indicated in the axial cut in the left part of Fig. 6.2, was the same for all samples and was chosen such that the maximum number of fissions occurred in the top part of the samples (because of the axial buckling in the test zone). This was done to increase the statistics of the burnt fuel measurements, since the measurement position below the detector favoured the detection of gamma-rays emitted in the upper part of the samples. As described earlier, the measurement position below the detector had been chosen to limit the system dead time due to the intrinsic gamma-ray activity of the burnt samples (see Subsection 4.3.4).

The materials and the dimensions of the cladding and the overcladding of the samples were modelled accurately according to the technical drawings and [Perret 07]. As regards the fresh fuel sample, the dimensions of the cladding, end plugs and fuel pellets were measured.

The cladding of the spent fuel samples was the original cladding of the fuel pin from which the burnt samples had been cut. The 40.0 cm long samples had been encapsulated in Zircaloy overcladding. In total, the overcladding of the spent fuel samples had a length of about 50.9 cm, including the end plugs at both ends.

Regarding the fresh fuel sample, a stack of fresh fuel pellets (of 38.9 cm length) had been loaded into a specially designed cladding tube which was closed at its bottom. This tube was placed into an overlaid similar to those of the spent fuel samples. The total length of the fresh fuel overcladding including end plugs was about 51.4 cm.

To determine the axial position of the samples inside the test lattice, the lowest possible elevation in the test lattice, i.e. when the samples touched the bottom plate, was taken as reference. Although the nominal axial position during irradiation was the same for all samples, the effective elevation of the fuel pellets differed slightly between the fresh and the spent samples, because

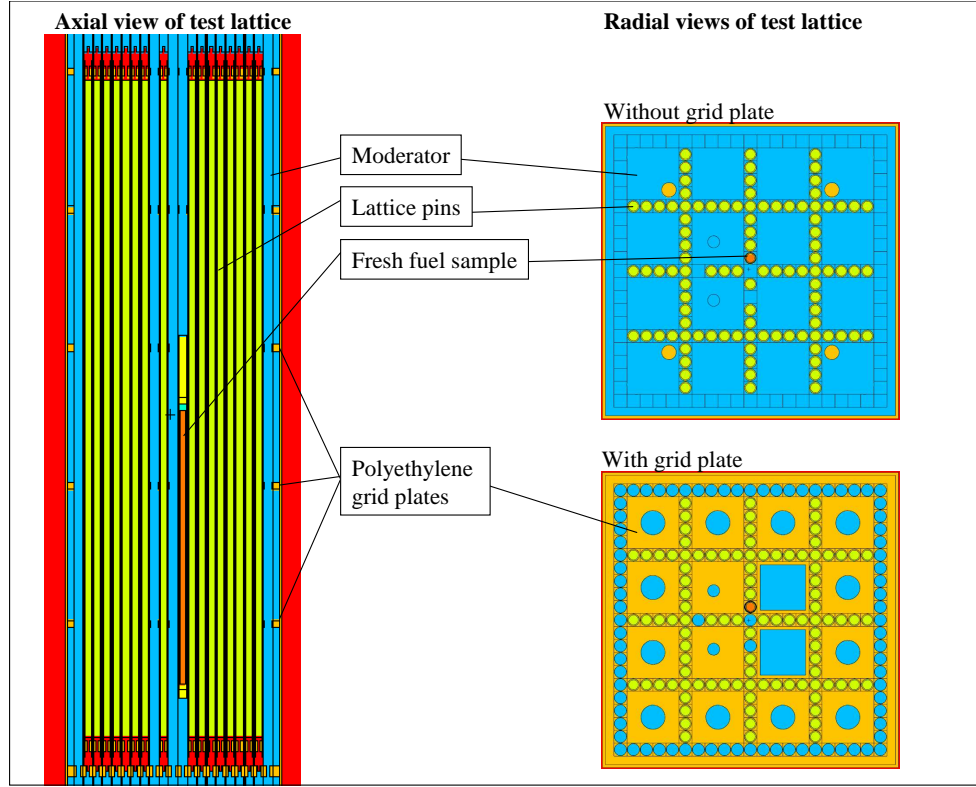


Figure 6.2: Axial and radial views of the test lattice with the fresh fuel sample in position L11.

the total length of their overlappings, as well as the axial positions of the fuel pellets inside their claddings, differed. The two axial positions of the samples in the test lattice are shown in Fig. 6.3.

To derive their axial fission profiles, the burnt and fresh fuel samples were modelled in terms of 20 axial volumes of 2.0 cm and 1.945 cm height, respectively.

6.1.2 Isotopic composition of fuel samples

The fresh fuel sample was modelled according to its average nominal specifications. As mentioned earlier, the isotopic compositions of the burnt fuel samples were modelled according to the results of post-irradiation examination (PIE) measurements on adjacent sections of the fuel pins from which the samples had been cut [Günther-Leopold 07]. In the framework of the LWR-PROTEUS Phase II programme, the number densities of the 53 most important actinides and fission products had been measured by PIE at the PSI Hot Laboratory. In the context of the current work, these were corrected to account for the decay between the PIE measurements and the irradiations of the samples in PROTEUS.

In addition to the measured compositions, isotopic compositions of the spent fuel samples were calculated with the CASMO-4E and HELIOS depletion codes. The CASMO-4E depletion calculations had also been conducted at PSI in the framework of the LWR-PROTEUS Phase II programme and are documented in [Grimm 07]. They were carried out using a reflected-assembly model and cross-sections based on the ENDF/B-VI nuclear data file [McLane 96]. The HELIOS depletion calculations, which are documented in [Kröhnert 06], used a reflected pincell model and a data library also based on ENDF/B-VI.

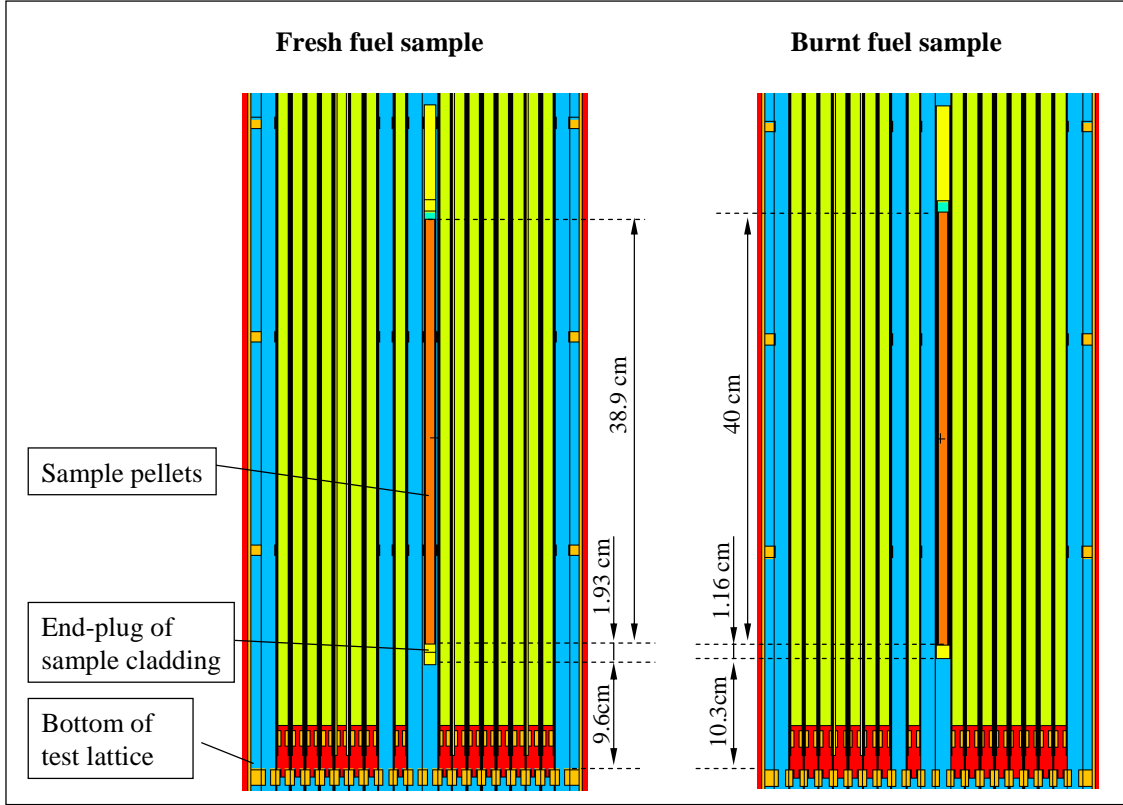


Figure 6.3: Axial positions and axial dimensions of fresh and burnt fuel samples.

The detailed description of the two calculational models and a complete comparison of calculated and measured isotopic densities can be found in [Grimm 10] and [Kröhnert 06]. Table 6.1 indicates the deviations of the calculated isotopic densities from the measured results for ^{235}U , ^{238}U , ^{239}Pu and ^{241}Pu .

Table 6.1: Ratios of measured (Hotlab) and calculated (CASMO, HELIOS) isotopic densities of the main fissioning isotopes.

Sample	Ratio	^{235}U	^{238}U	^{239}Pu	^{241}Pu
36 GWd/t	CASMO/Hotlab	0.967	1.000	1.038	1.098
	HELIOS/Hotlab	0.978	0.999	1.138	1.147
46 GWd/t	CASMO/Hotlab	0.874	0.998	0.922	0.958
	HELIOS/Hotlab	0.980	1.000	0.975	0.955

The CASMO-4E results are seen to show a better agreement with the measurements for the 36 GWd/t sample than for the 46 GWd/t sample. For the HELIOS results, the agreement with the measurements is better for the 46 GWd/t sample. The differences between the CASMO-4E and the HELIOS calculations can be explained by the differences in the used models (assembly and pincell) and by the slightly different irradiation histories used (see Sections 2.3 and 2.5.2).

In the MCNPX model, the fuel compositions of the samples were considered to be homogeneous. For the burnt fuel samples, this is clearly an approximation, as in a real burnt fuel pin the isotopes are radially and also axially distributed. The impact of this assumption on the results has been investigated with the help of sensitivity studies which are presented in Subsection 6.2.2.

6.2 Calculated fission rate ratios

The fresh and the 36 GWd/t samples were modelled in the irradiation positions K7, M8 and L11. The 46 GWd/t sample was modelled in the irradiation position I8. The simulations were run in the KCODE mode calculating 30 inactive cycles of 500,000 neutrons to obtain the fission source distribution in the core, followed by 1000 active cycles of 500,000 neutrons. The achieved 1σ uncertainty on the average fission rates in the fuel samples was about 0.2%. The calculated contributions a_i from ^{235}U , ^{238}U , ^{239}Pu and ^{241}Pu fissions to the total number of fissions had 1σ uncertainties of about 0.2%. The fission rates in the 20 axial segments were calculated with 1σ uncertainties of about 0.6%.

As a reference, the calculated fission rates in the spent fuel samples were estimated using the measured isotopic compositions. For the sake of comparison, some fission rates were also predicted using the fuel compositions as obtained with the CASMO-4E assembly calculations and the HELIOS pincell calculations.

6.2.1 Results

The calculated inter-position and inter-sample fission rate ratios in the fresh, 36 GWd/t and 46 GWd/t samples are given in Table 6.2.

As regards the inter-position comparison, for both fresh and 36 GWd/t samples, the fission rates are seen to be about 30% higher in position M8 as compared to position L11, and about 17-18% lower in position K7 as compared to position L11. The inter-sample comparisons show, independently from the irradiation position, that the fission rates in the fresh fuel sample are about 1.4 and 2.1 times higher than in the 36 GWd/t and 46 GWd/t samples, respectively.

Concerning the impact of the fuel composition, the fission rates in the 36 GWd/t sample obtained using the CASMO-4E isotopic composition did not deviate much from the results based on the measured composition (less than 0.8%), whereas the results obtained with the HELIOS composition were 3.2% lower than those based on the measured composition. The discrepancy between the HELIOS and the measured fuel compositions did not impact the inter-position fission rate ratios. It has, however, a non-negligible impact on the inter-sample fission rate ratio (deviations of about 3%).

Regarding the 46 GWd/t sample, the fission rates using the measured and the CASMO-4E isotopic compositions differed significantly (7%), whereas the results based on HELIOS agreed within 1.2% with those based on the measured composition.

Table 6.2: Calculated estimates for inter-position and inter-sample fission rate ratios.

Inter-position fission rate ratios

Fresh sample

	$\frac{M8}{L11}$	$\frac{K7}{L11}$
M	1.308 ± 0.003 (0.2%)	0.821 ± 0.002 (0.2%)

36 GWd/t sample

	$\frac{M8}{L11}$	$\frac{K7}{L11}$
M	1.292 ± 0.003 (0.3%)	0.832 ± 0.002 (0.3%)
C	1.284 ± 0.003 (0.2%)	
H	1.285 ± 0.003 (0.3%)	

Inter-sample fission rate ratios

Fresh-to-36 GWd/t

	K7	M8	L11
M	1.392 ± 0.004 (0.3%)	1.427 ± 0.003 (0.2%)	1.409 ± 0.003 (0.2%)
C		1.437 ± 0.003 (0.2%)	1.412 ± 0.003 (0.2%)
H		1.392 ± 0.003 (0.2%)	1.367 ± 0.003 (0.2%)

Fresh-to-46 GWd/t

	M8 (I8)
M	2.088 ± 0.005 (0.2%)
C	2.245 ± 0.004 (0.2%)
H	2.113 ± 0.005 (0.2%)

M: Burnt fuel sample modelled using measured isotopic compositions.

C: Burnt fuel samples modelled using isotopic compositions obtained with CASMO-4 assembly calculations.

H: Burnt fuel samples modelled using isotopic compositions obtained with HELIOS pincell calculations.

6.2.2 Sensitivity studies

- **Set of isotopes considered in the spent fuel composition**

The measured isotopic compositions of the burnt fuel samples included 53 actinides and fission products. In comparison, the isotopic compositions obtained with the CASMO-4E and HELIOS depletion calculations contained 136 and 101 isotopes, respectively. Examples of elements not included in the measured results are O, B, Xe, Te, Pd and Kr. To check that the measured 53 isotopes were sufficient to adequately calculate fission rates, the calculated CASMO-4E composition of the 36 GWd/t burnt sample was reduced to the same 53 isotopes and the fission rates in the position L11 was re-calculated. The fission rates obtained with both the reduced and the full set of isotopes were found to be almost identical (within 0.05%). Consequently, one can conclude that the set of 53 measured isotopes was adequate to calculate fission rates in the burnt fuel.

- **Axial elevation of fuel samples in the PROTEUS test zone**

The axial position of the fuel samples inside their cladding, as also the dimensions of the cladding, overladding and end plugs of the samples, were modelled as accurately as possible. However, it could not be excluded that the fuel samples were slightly shifted ($\sim 1\text{--}5\text{ mm}$) axially within their overladding.

The sensitivity of the calculated fission rates to an axial displacement was investigated by calculating the fission rates in the fresh and 36 GWd/t samples in the irradiation position L11 after shifting the samples up by 5 mm. It was found that, in general, the calculated fission rates changed by less than 1% for the change of 5 mm in sample elevation; the sensitivity was slightly higher for the fresh sample (0.96%/5 mm) than for the 36 GWd/t sample (0.51%/5 mm). It should also be mentioned that the contributions a_i from ^{235}U , ^{238}U , ^{239}Pu and ^{241}Pu , which were used for the derivation of measured fission rate ratios, did not vary significantly (less 0.5%) with the change in sample elevation.

- **Axial burn-up profile in the 36 GWd/t burnt sample**

An axial scan of the intrinsic gamma-ray activity (total counts from 400 to 2000 keV) of the spent fuel pin, from which the 36 GWd/t burnt sample had been cut, had revealed that the sample should have a significant axial burn-up gradient, the burn-up changing by about $\sim 10\%$ from its lower to upper end. The measured isotopic composition of the sample currently used referred to the end with the lower burn-up value. Quantifying the exact axial burn-up profile, modifying the measured isotopic compositions accordingly and implementing the changes in the MCNPX models would have been very difficult and too time consuming for this work. Instead, the MCNPX model used axially homogeneous sample compositions and the impact of the burn-up profile on the fission rates was assessed separately using calculated isotopic compositions corresponding to different burn-ups.

The HELIOS pincell model was modified to estimate the change in the isotopic composition of the 36 GWd/t sample assuming a 5% and a 10% higher sample burn-up. This was done by keeping the same irradiation history and increasing the power levels in the depletion calculation. As

example, the changes in the isotopic densities of ^{235}U , ^{238}U , ^{239}Pu and ^{241}Pu , due to increases of 5% and 10% in the sample burn-up, are given in Table 6.3. The two isotopic compositions for the increased burn-up levels were implemented in the MCNPX model, still assuming a homogeneous axial distribution, and the fission rates in the irradiation position L11 were re-calculated. The changes in the contributions of ^{235}U , ^{238}U , ^{239}Pu and ^{241}Pu fissions to the total number of fissions and the changes in the calculated fission rates are also given in Table 6.3.

Table 6.3: Sensitivities of isotopic densities, of contributions to total fissions and of calculated fission rates in the 36 GWd/t sample to assumed burn-up increases.

	Isotopic densities				
	^{235}U	^{238}U	^{239}Pu	^{241}Pu	
5% burn-up increase	-6.6%	-0.2%	+0.6%	+4.6%	
10% burn-up increase	-12.8%	-0.3%	+1.1%	+9.6%	
	Contributions to total fissions				Total fission rate
	a_{U5}	a_{U8}	a_{P9}	a_{P1}	
5% burn-up increase	-6.4%	-0.1%	+0.5%	+4.7%	-2.9%
10% burn-up increase	-12.5%	-2.1%	+1.3%	+10%	-5.2%

The calculated fission rates in the sample with a 5% and a 10 % increased burn-up are seen to be 2.9% and 5.2% lower than those obtained using the nominal burn-up. Consequently, to a first approximation, the burn-up profile could lead to a 3% reduction of the fission rate in the 36 GWd/t sample in the irradiation position L11. Results for the other positions M8 and K7 could be expected to be very similar. One may thus conclude that the inter-position fission rate ratios remain quite insensitive to the axial profile of the 36 GWd/t fuel sample, whereas the inter-sample fission rate ratios between the fresh and 36 GWd/t samples are affected significantly.

It should be noted that, to a lower extent, the measured estimates for the fission rates in the 36 GWd/t sample are also affected by an increase of the sample burn-up. Indeed, to derive measured fission rates, one requires the calculated isotopic fission contributions a_i , which are dependent on the isotopic composition of the sample. Especially the estimates based on the ^{89}Rb (2570 keV) peak were found to be very sensitive to the parameter set a_i (see Subsection 5.3.4). The measured fission rate rate for the 36 GWd/t sample in the position L11, based on the ^{89}Rb (2570 keV) peak, increased by 1.9% using the sample composition with a 5% higher burn-up compared to the results obtained using the original HELIOS composition. In comparison, the impact on the results based on the ^{142}La (2542 keV), ^{138}Cs (2640 keV) and ^{95}Y (3576 keV) peaks was less than 0.7%.

• Radial profile of isotopic compositions

The isotopic composition in the fuel samples was modelled homogeneously also in the radial direction. For the burnt samples, in which the isotopes would normally be radially distributed, the impact of this simplification has been investigated as follows. HELIOS depletion calculations of the 36 GWd/t and 46 GWd/t samples were used to obtain, for each isotope, the normalised radial profile in 6 radial zones of equal areas (radii of 0.186, 0.264, 0.323, 0.373, 0.417, 0.4565 cm). These normalised radial profiles were implemented into the MCNPX model (without changing the average number densities of the considered isotopes in the two samples), and the calculated

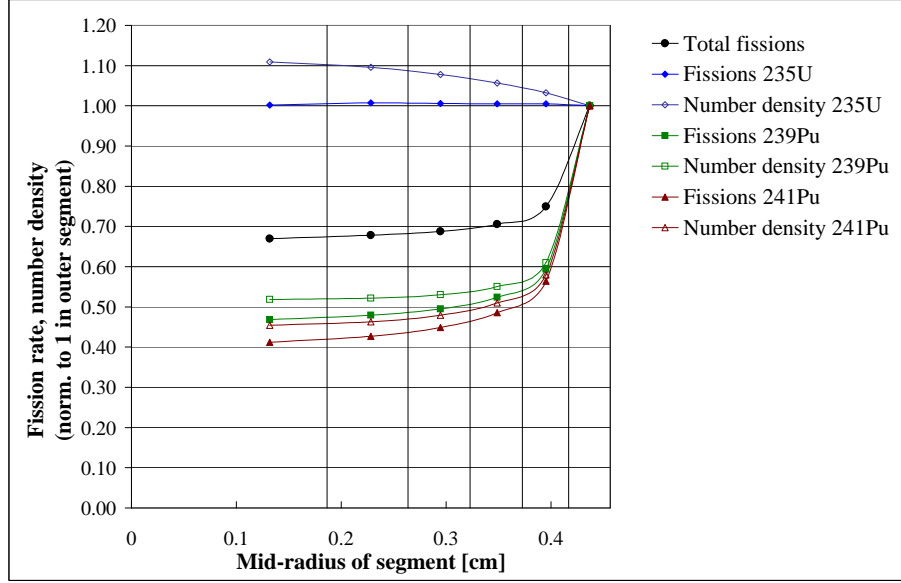


Figure 6.4: Within-sample isotopic densities and fission rates for the 36 GWd/t sample.

fission rates were compared to the original results using the average HELIOS compositions homogeneously distributed.

As an example, the radial distributions of the main fissioning isotopes ^{235}U , ^{239}Pu and ^{241}Pu within the 36 GWd/t sample are shown in Fig. 6.4, along with the resulting radial profiles of their fissions and that of the total number of fissions (example for the irradiation position L11). Although the radial distribution of fissions in the plutonium isotopes are strongly peaked at the rim of the pin, the calculated total number of fissions in the 36 GWd/t sample changed only marginally (0.4%) by introducing the radially distributed isotopic composition. The same was valid for the contributions a_i to the total number of fissions (less than 0.4% deviations). Very similar results were obtained for the 46 GWd/t sample. Consequently, the simplification of a radially homogeneously distributed sample material in the MCNPX model is quite justified.

6.3 Comparison of calculated and experimental fission rate ratios

The MCNPX calculated inter-position and inter-sample fission rate ratios as presented in Table 6.2 are compared in this section to the measured results. For the latter, the values used correspond to the weighted mean of the individual estimates based on the different gamma-ray lines. These mean values are given in Tables 5.16 and 5.17 of the previous chapter.

For each calculation-to-experiment (C/E) ratio, the relative combined total uncertainty $\sigma_{C/E,rel}$ has been obtained with the error propagation law, combining the relative uncertainties $\sigma_{C,rel}$ and $\sigma_{E,rel}$ on the calculated and on the measured fission rate ratios:

$$\sigma_{C/E,rel} = \sqrt{(\sigma_{C,rel})^2 + (\sigma_{E,rel})^2} \quad (6.1)$$

The $\sigma_{C,rel}$ values consider only the Monte Carlo statistical uncertainty, i.e. they depend on the number of simulated neutron histories in the whole-reactor model. The $\sigma_{E,rel}$ values comprise contributions from the uncertainties on the net-count areas, from the nuclear data uncertainties needed in the saturation and decay corrections, and from the statistical uncertainties on the solid angle and attenuation correction factors obtained with MCNPX (see Section 5.5).

6.3.1 Inter-position fission rate ratios

The comparison between calculated and experimental estimates of the inter-position fission rate ratios are given in Table 6.4 for the fresh and 36 GWd/t samples irradiated in the positions K7, M8 and L11, taking the position L11 as reference.

Table 6.4: Comparison of calculated (C) and experimental (E) inter-position fission rate ratios, C/E values.

Sample	$\frac{M8}{L11}$	$\frac{K7}{L11}$
Fresh	1.020 ± 0.006 (0.6%)	0.996 ± 0.006 (0.6%)
36 GWd/t	1.021 ± 0.023 (2.2%)	1.012 ± 0.025 (2.4%)

In general, there is an agreement within 2% between calculated and measured results. The C/E values for the fresh fuel sample have very low 1σ uncertainties (about 0.6%). The results comparing the irradiation positions K7 and L11 agree within this uncertainty, whereas those comparing the irradiation positions M8 and L11 only agree within 3-4 standard deviations. Also for the spent fuel sample, the discrepancy between calculation and experiment appears higher for the M8/L11 ratio than for the K7/L11 ratio. Both these discrepancies, however, are still within the corresponding 1σ uncertainties of about 2.3%.

In contrast to the inter-sample fission rate ratios which are presented in the following subsection, the inter-position ratios are not afflicted with high sensitivities. This is because several of the investigated sensitivities of both measured and calculated fission rates (e.g. to the fuel composition and to the sample position) compensate when taking the ratios.

6.3.2 Inter-sample fission rate ratios

The C/E values for the inter-sample fission rate ratios between the fresh and 36 GWd/t samples (irradiation positions K7, L11, M8), and between the fresh and 46 GWd/t samples (irradiation position M8(I8)), are given in Table 6.5.

For all three irradiation positions, the agreement between the measured and calculated fresh-to-36 GWd/t fission rate ratios is within 1-3 standard deviations, which are 1.7 to 2%. Nonetheless, the results predicted by MCNPX appear on average about 3% higher than the measured values.

Including the considerations made earlier with respect to the axial burn-up profile in the 36 GWd/t sample (see Subsection 6.2.2), the calculated fission rates in this sample should be about 3% lower than those used in Table 6.5. This would increase the observed bias between measurement and

Table 6.5: Comparison of calculated (C) and experimental (E) inter-sample fission rate ratios, C/E values.

Samples	K7	M8	L11
Fresh-to-36 GWd/t	1.020 ± 0.018 (1.8%)	1.045 ± 0.021 (2.0%)	1.031 ± 0.018 (1.7%)
Fresh-to-46 GWd/t	1.012 ± 0.034 (3.4%)		

calculation to about 6%. It is not easy, however, to identify the cause for such a bias. One possible reason could be a slight axial displacement of the 36 GWd/t sample inside the overcladding. As described earlier (see Subsection 5.4.3), the exact position of the fuel in the overcladding was needed to derive the solid angle and attenuation correction factors with the MCNPX model of the sample changer. The sensitivity of the measured fission rate ratios to the modelled elevation of the spent fuel samples was found to be quite high (about 1.5%/1 mm and about 8%/5 mm). Consequently, a displacement of about 3-4 mm of the 36 GWd/t fuel sample could, in principle, account for a 6% discrepancy between calculated and measured results.

To avoid these difficulties in future experiments, care should be taken to ensure a relatively flat burn-up profile in the irradiated fuels (at least in the measured part of the fuel samples). In addition, the sensitivity of the measured results towards the sample elevation can be significantly reduced by using, for all samples, a similar measurement position in front of the detector.

The measured and calculated fresh-to-46 GWd/t fission rate ratios, which were derived for the equivalent irradiation positions M8 and I8, agreed within the 1σ uncertainty of 3.4%, which demonstrates the possibility to extend the currently developed measurement technique to higher burn-ups.

As an example, the individual contributions to the combined uncertainty of the C/E value for the fresh-to-36 GWd/t fission rate ratio are given in Table 6.6, along with the most significant sensitivities of the C, E and C/E values. The presented sensitivities correspond to a 5 mm change in the elevation of the burnt sample inside the overclad, to a 5% burn-up change in the 36 GWd/t sample, and to a 1 second increase in the cooling time of the 36 GWd/t sample between irradiation and measurement. The uncertainties and sensitivities are also given for the estimates based on the separate use, in the measurements, of each of the four gamma-ray lines ^{142}La (2542 keV), ^{89}Rb (2570 keV), ^{138}Cs (2640 keV) and ^{95}Y (3576 keV), where the C value remains unchanged in all cases.

The assumed burn-up of the 36 GWd/t sample and the assumed axial elevation of the sample in the overclad affect both the measured and calculated fission rate ratios. The burn-up change has a much stronger affect on the calculated results, whereas the change in sample elevation mainly impacts the measured results. The increase in cooling time has an impact only on the experimental results. Note that the impacts on the individual estimates based on the different gamma-ray lines can vary quite significantly. As these four estimates were combined by taking the weighted mean, the impact on the final C/E value is the corresponding combination of the results for the particular gamma-ray lines.

It should be noted that, although Table 6.6 refers to the irradiation position L11, very similar results can be expected for the other irradiation positions M8 and K7.

Table 6.6: Uncertainties and sensitivities of the C/E values for fresh-to-36 GWd/t fission rate ratios (irradiation position L11).

	¹⁴² La (2542 keV)	⁸⁹ Rb (2570 keV)	¹³⁸ Cs (2640 keV)	⁹⁵ Y (3576 keV)	weighted mean
Total uncert. C/E	2.8%	5.0%	5.3%	2.6%	1.7%
Statistical uncert., E	2.6%	5.0%	5.2%	2.5%	
Nuclear data uncert., E	0.7%	0.5%	1.0%	0.8%	
Monte Carlo MCNPX uncert., E	0.3%	0.3%	0.3%	0.3%	
Monte Carlo MCNPX uncert., C	0.2%	0.2%	0.2%	0.2%	
Sensitivities to shifting up the 36 GWd/t sample by 5 mm within the overclad:					
C	-0.5%	-0.5%	-0.5%	-0.5%	-0.5%
E	+7.9%	+8.3%	+8.3%	+7.3%	+7.7%
Sensitivities to a 5% increased burn-up of the 36 GWd/t sample:					
C	+3.0%	+3.0%	+3.0%	+3.0%	+3.0%
E	-0.4%	-1.8%	-0.3%	-0.6%	-0.6%
C/E	+3.4%	+5.0%	+3.4%	+3.7%	+3.7%
Sensitivities to a 1 sec longer cooling time for the 36 GWd/t sample measurement:					
E	-0.2%	-1.6%	-0.1%	-0.5%	-0.5%
C/E	+0.2%	+1.7%	+0.1%	+0.5%	+0.5%

6.4 Chapter summary

Simulating the WOLF-B experiments presented in Chapter 4, calculated estimates of inter-position and inter-sample fission rate ratios have been obtained with an MCNPX whole-reactor model, achieving 1σ uncertainties of about 0.3%. The comparison with the measured estimates has shown a satisfactory agreement (within about 2%) for the inter-position fission rate ratios of the fresh fuel sample and of the 36 GWd/t fuel sample. For the inter-sample fission rate ratios, between the fresh and 36 GWd/t samples and between the fresh and 46 GWd/t samples, the agreement is within 4.5%.

The uncertainties of the calculation-to-experiment (C/E) values have mainly consisted of the uncertainties on the measured results. The 1σ uncertainties on the inter-position fission rate ratios for the fresh and 36 GWd/t samples were thus about 0.6% and 2.3%, respectively. The inter-sample C/E values had 1σ uncertainties of 1.7 to 2% for the fission rate ratios between the fresh and 36 GWd/t samples, and 3.4% for the fission rate ratio between the fresh and 46 GWd/t samples. The main contributor to these uncertainties was the uncertainty on the measured net-count areas for the different gamma-ray lines.

The compositions of the spent fuel samples were modelled according to results of post-irradiation examination (PIE). Additional predictions using calculated fuel compositions obtained with the codes CASMO-4E and HELIOS have shown that the calculated fission rates can significantly depend on the estimation of the isotopic composition of the spent fuel (deviations of up to 3.2% for the 36 GWd/t sample and 7% for the 46 GWd/t sample).

Furthermore, the axial burn-up profile of the 36 GWd/t sample complicated the interpretation of the calculated results since the burn-up influences the fuel composition. This burn-up profile (corresponding to an axial variation of about 10%) could not be easily implemented into the MCNPX model, and the fuel composition was therefore modelled homogeneously in the axial direction. Sensitivity studies showed, however, that this simplification could cause a bias in the calculated fission rates of about 3%. This bias would cancel out for the inter-position fission rate ratios of the 36 GWd/t sample, but not for fresh-to-36 GWd/t inter-sample fission rate ratios. In comparison, modelling the fuel homogeneously in the radial direction only caused a minor change in the results (less than 0.4%).

The calculation-to-experiment comparisons have been found to be mainly sensitive to the knowledge of the fuel composition and the exact positioning of the burnt fuel samples during the measurements. The fuel composition was found to be of major importance to accurately derive calculated fission rate ratios (about 3% deviation for a burn-up change of 5% in the 36 GWd/t sample). The assumed elevation of the burnt samples within the overclad had the highest impact on the measured fission rate ratios (deviations of about 8% for a shift of 5 mm). The burnt fuel composition assumed in the MCNPX model also affected the measured fission rate ratios as it determined the contributions a_i of ^{235}U , ^{238}U , ^{239}Pu and ^{241}Pu fissions to the total number of fissions. On the whole, however, the experimental results were not very sensitive to the burnt fuel sample composition. An exception here is the case of results based on the ^{89}Rb gamma-ray line (1.9% variation for a burn-up change of 5% in the 36 GWd/t sample). The ^{89}Rb -based results were also found to be very sensitive to the assumed cooling time between the end of irradiation and the beginning of measurement (1.6% variation for a shift of 1 second).

With respect to future experiments, the sensitivity of the calculated fission rate ratios to the assumed fuel composition will remain problematic, especially because PIE will not be conducted on all burnt fuel pins used in the LIFE@PROTEUS experiments. On the contrary, the very high sensitivity of the currently measured results to axial displacements of the burnt samples can be reduced relatively easily by using similar measurement positions in front of the detector for all samples. An accurate recording of the measurement times will be essential because of the high sensitivity of the results obtained for ^{89}Rb to the exact cooling time between end of irradiation and beginning of measurement. However, as these results also showed a high sensitivity towards the assumed burnt sample composition, it might be advisable not to include the ^{89}Rb (2570 keV) peak in the future analyses. Finally, to reduce the uncertainties on the measured fission rate ratios, one of the major challenges for future measurements is to increase the counting statistics while minimising the system dead time. In this context, a first design of a measurement station for the LIFE@PROTEUS programme is proposed and evaluated in the following chapter. Recommendations concerning the corresponding measurement and irradiation strategies that should be adopted are also given.

Bibliography

- [Günther-Leopold 07] I. Günther-Leopold. *LWR-PROTEUS programme, Phase II, Final Report*. Internal Report TM-43-06-05, PSI, 2007.
- [Grimm 07] P. Grimm. *CASMO-4E Calculations of the Isotopic Inventories of the LWR-PROTEUS Phase II Irradiated Fuel Samples from KKG*. Internal Report TM-41-07-07, PSI, 2007.
- [Grimm 10] P. Grimm. *Comparison of Calculated and Measured Isotopic inventories for the LWR-PROTEUS Phase II Irradiated Fuel Samples*. Internal Report TM-41-09-03, PSI, 2010.
- [Joneja 01] O.P. Joneja, F. Jatuff, P. Grimm, R. Seiler, R. Brogli, G. Meier, H-D. Berger & R. Chawla. *Validation of an MCNP4B whole-reactor model for LWR-PROTEUS using ENDF/B-V, ENDF/B-VI and JEF-2.2 cross-section libraries*. Annals of Nuclear Energy, vol. 28, page 701-713, 2001.
- [Koning 06] A. Koning. *The JEFF-3.1 Nuclear Data Library*, 2006.
- [Kröhnert 06] H. Kröhnert. *Analysis of the nuclide composition of highly-burnt PWR fuel examined in connection with the LWR PROTEUS Phase II project with the spectral code HELIOS*. Institut für Wärme- und Brennstofftechnik, Technische Universität Braunschweig, Diploma thesis, 2006.
- [McLane 96] V. McLane. *ENDF-201 - ENDF/B-VI summary documentation supplement 1 ENDF/HE-VI summary documentation - BNL-NCS-17541*, 1996.
- [Pelowitz 05] D.B. Pelowitz. *MCNPX User's Manual Version 2.5.0*, 2005.
- [Perret 07] G. Perret. *Reactivity worth of burnt samples in LWR-PROTEUS Phase II core configuration 4*. Internal Report, Memorandum, PSI, 2007.

Chapter 7

Analysis and recommendations for the LIFE@PROTEUS measurement station

In Chapters 4 and 5, it was demonstrated how relative fission rates between fresh and spent fuel samples can be measured using gamma-ray lines above 2200 keV emitted by freshly induced short-lived fission products. Final uncertainties were about 2% for fresh-to-36 GWd/t fission rate ratios and 3.4% for fresh-to-46 GWd/t fission rate ratios; the main contribution to these uncertainties were statistical. The low statistics and the fast neutron damage in the detector crystal during reactor operation were found to be two principal aspects which need to be improved in future experiments.

Furthermore, the measured results were found to be highly sensitive (8%/5 mm) to the exact axial measurement position of the spent fuel samples. High sensitivities ($>1.5\%$) were also found towards the assumed composition of the burnt fuel samples when using gamma-ray lines emitted by ^{89}Rb , the fission yields of which strongly depend on the fissioning actinides. In addition, the short half-lives of ^{89}Rb and its precursor caused a high sensitivity ($>1.5\%/1\text{ s}$) towards the exact measurement of the cooling time between the end of irradiation and the beginning of measurement.

The aim of this chapter is to transpose the findings of the presently conducted WOLF-B experiments to the envisaged LIFE@PROTEUS programme and to demonstrate that the limitations of WOLF-B can be largely eliminated in future experiments. It is in this context that a preliminary design of the measurement station for LIFE@PROTEUS is presented and evaluated.

MCNPX models of a representative LIFE@PROTEUS test lattice and of the preliminary design of the measurement station are used to estimate the fast neutron background from the core, the intrinsic gamma-ray background from the burnt fuel pins and the expected high-energy gamma-ray signals from short-lived fission products. For all these aspects, the results of the WOLF-B analysis have served as reference.

The two MCNPX models, i.e. of the test lattice and the measurement station, are presented in Section 7.1. Possible limitations of the measurement station with respect to neutron background, axial detection resolution and expected system dead times are evaluated in Section 7.2. The performance of the measurement station, in terms of expected number of net counts for the high-energy gamma-ray lines from short-lived fission products, is presented in Section 7.3. Uncertainties, as well as sensitivities of measured and calculated fission rate ratios, are discussed in Section 7.4. Section 7.5 deals with possible future optimisation of the presented measurement station, and the chapter is summarised in Section 7.6.

7.1 Reference test lattice and measurement station

Two relevant MCNPX models had already been developed in the framework of conceptual studies for the LIFE@PROTEUS programme at PSI and were thus available for the present investigation. The first model featured the full, as-to-be-refurbished PROTEUS reactor, including a representative test lattice as planned for the LIFE@PROTEUS campaign [Murphy 10]. The second model featured the measurement station and comprised only a simplified modelling of the reactor [Perret 10a].

7.1.1 Reference test lattice model

In the frame of the LIFE@PROTEUS campaign, it is currently planned to mainly investigate three different test lattices. The first will contain only fresh fuel pins, the second fresh and 40 GWd/t spent fuel pins, and the third fresh and 60 GWd/t spent fuel pins [Murphy 10]. The test zone will, in each case, consist of nine 10x10 assemblies. For the two mixed lattices, the fresh and spent interfaces, which are to be studied in LIFE@PROTEUS, will be located in the central assembly.

The lattice configuration containing the 60 GWd/t spent fuel pins has been selected as reference lattice for the current investigation and is shown in Fig. 7.1. The lattice consists of 5% enriched fresh UO_2 pins and a bundle of 35 spent UO_2 fuel pins with a burn-up of 60 GWd/t in the central assembly. The spent fuel has an initial enrichment of 4.3% and a cooling time of 10 years. In each assembly, the 4 corner pins are replaced by structural steel pins. In addition, 8 pins are replaced by B_4C absorber rods in each of the outer 8 assemblies to control the reactivity of the test zone. In total, the lattice contains 768 fuel pins, 733 of which are fresh and 35 spent.

The typical isotopic composition of 60 GWd/t spent fuel pins had been calculated with the CASMO-4E depletion code [Grimm 09]. In the MCNPX model, the isotopic composition of the spent fuel pins was modelled as homogeneous in both radial and axial directions.

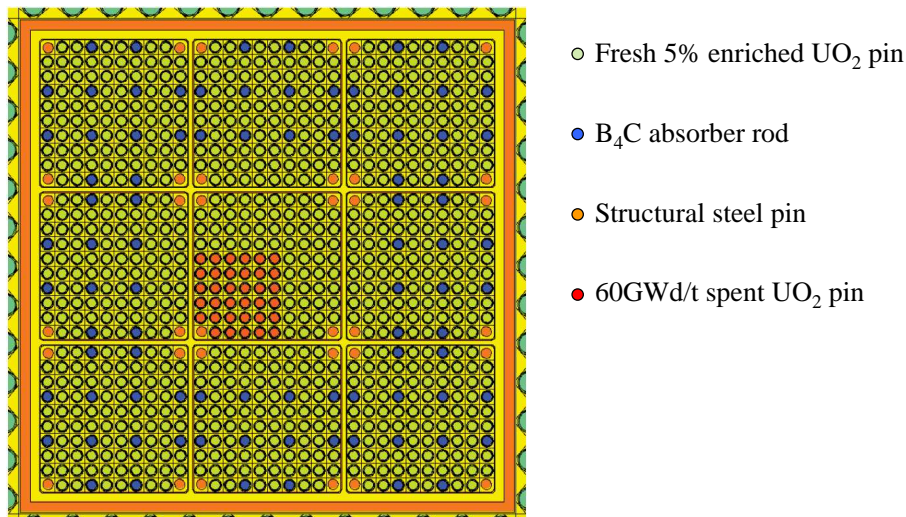


Figure 7.1: Reference test lattice considered for the LIFE@PROTEUS campaign.

7.1.2 Measurement station model

As described in Section 2.4, the measurements during the LIFE@PROTEUS campaign will take place in a measurement station above the test zone. The measurement station will consist of two vertical tubes. The larger tube will contain the detector, and an adjacent smaller one will hold the irradiated pin in the measurement position. The refurbished PROTEUS reactor will feature a much larger water tank, housing the buffer and D₂O-driver zones as well as the test zone. The tubes containing the detector and the measured pin will be both located in the large water tank. While the larger, detector-containing tube will be water tight, the smaller one will be open and hence contain water. Apart from this general concept, however, the exact detection geometry and the shielding of the detector still have to be determined.

As mentioned earlier, an MCNPX model of a first generic measurement station for the LIFE@PROTEUS campaign had already been developed [Perret 10a]. This model has been used as a starting point to develop the preliminary design of the measurement station, which is shown in Fig 7.2. The figure shows an axial and a radial cut of the measurement station, with the two tubes for the detector and the fuel pin. The surroundings of the measurement station, i.e. the concrete shielding of the reactor and the reactor core, are modelled in a simplified way employing simple geometries and homogenised materials based on [Jordan 09].

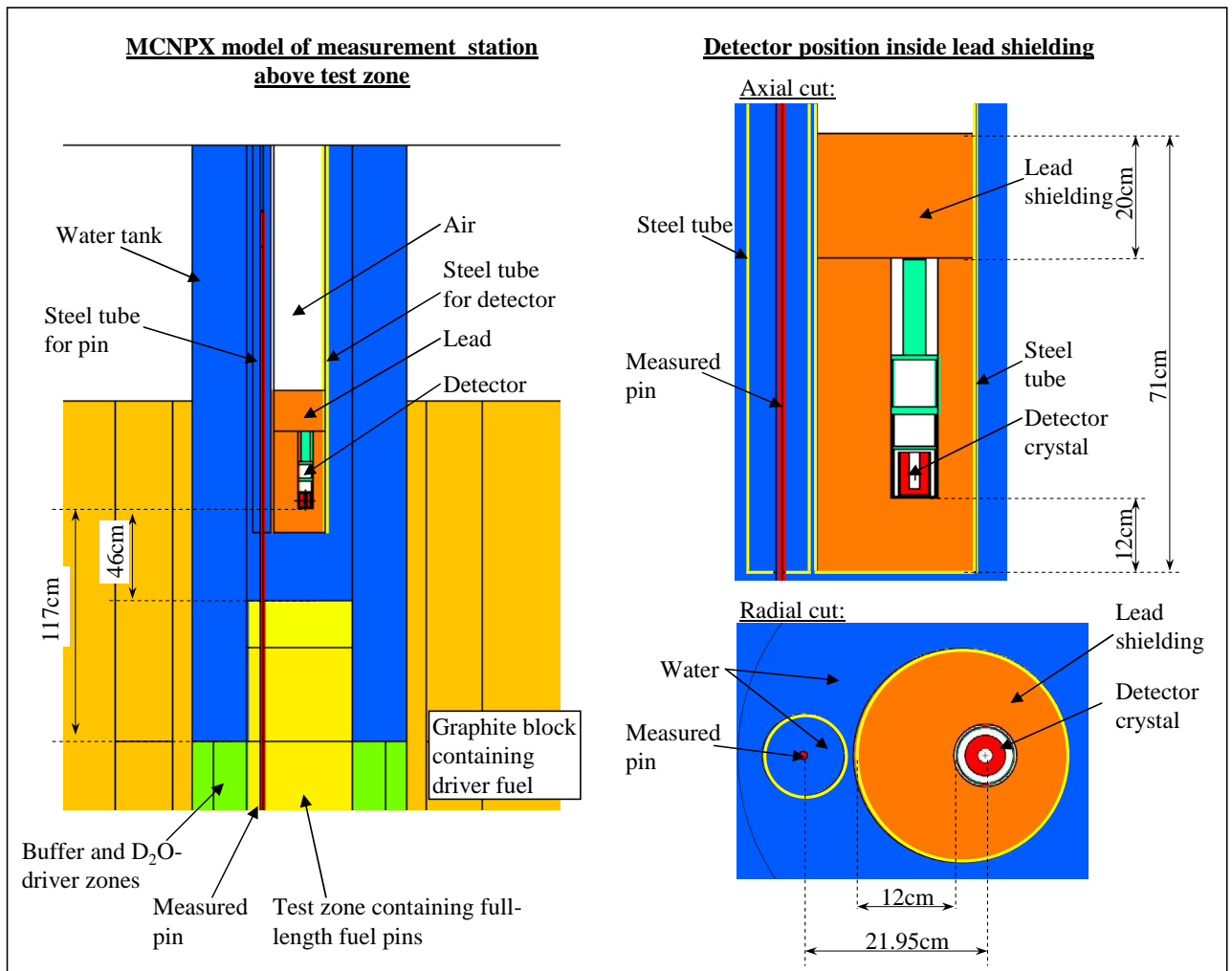


Figure 7.2: Preliminary design of the LIFE@PROTEUS measurement station.

The measurement station, as a whole, will be movable radially (in x- and y-directions) to allow measuring any given lattice pin using the same measurement position in front of the detector. The detector is located about 50 cm above the upper end of the full-length fuel pins of the test lattice and about 1.2 m above the active zone of the test tank. The axial detector position has to be kept relatively low for safety reasons. To limit contamination risks in case of clad failure, one should indeed guarantee that the spent fuel pins remain under water in the water tank, even during measurements. The axial position of the measurement station has been chosen to fulfill this requirement, while measuring a spent fuel pin in a position where its axial burn-up profile is relatively flat (i.e. not towards the end of the pins, but rather close to its axial centre).

The gamma-ray detector is embedded into a 71 cm high cylinder of lead with a diameter of 25.8 cm (total mass ~ 300 kg). The lead shielding below the detector has a height of 12 cm. Above, the detector is shielded against the upper part of the measured fuel pin with 20 cm of lead. Clearly, in the final measurement set-up, this upper lead shielding will have to feature a channel for signal and high voltage cables and for the cooling system of the detector.

The geometry of the HPGe detector and its position inside the lead shielding were chosen on the basis of the WOLF-B campaign. The detector itself was modelled exactly as for the WOLF-B measurements (see Subsection 5.4.1), which simplified the comparison between the WOLF-B and LIFE@PROTEUS set-ups. The detector position inside the lead shielding is shifted 2.95 cm from the centre of the lead cylinder to increase the amount of lead filter between pin and detector. The distance between pin and detector centres is thus 21.95 cm, including 5.5 cm of water and about 12 cm of lead. This detector position has been chosen to yield similar detector responses for uncollided 3576 keV gamma-rays in the LIFE@PROTEUS and WOLF-B set-ups.

In the following section, potential limitations of the measurement station are characterised. These are the neutron background from the reactor core, the spatial resolution of the measurements, and the dead time generated by the intrinsic gamma-ray background from the spent fuel pin. The performance of the measurement station, in terms of the expected number of counts for the high-energy gamma-ray lines, is estimated in Section 7.3.

7.2 Potential limitations of the measurement set-up

This section contains the evaluation of the preliminary set-up proposed for the LIFE@PROTEUS measurement station with respect to the neutron background emitted by the reactor core, the axial detection resolution of the measurement set-up and the intrinsic gamma-ray background emitted by the spent fuel pins in the measurement position.

7.2.1 Neutron background from core during irradiation

A sufficient shielding against neutrons from the reactor core during reactor operation is a fundamental prerequisite for gamma-ray measurements using an HPGe detector in LIFE@PROTEUS.

During the WOLF-B campaign, the number of irradiations, the irradiation duration and the reactor power were strongly limited by the continuous crystal damage caused by fast neutrons during each irradiation. The analysis of the acquired gamma-ray spectra was considerably impaired by the neutron damage which degraded the detector resolution.

After optimising the neutron shielding of the WOLF-B measurement station (see Subsection 4.3.2), the fast neutron flux (0.1 keV-12 MeV) reaching the detector crystal, during an irradiation at 800 W, was estimated to be about $8.5 \cdot 10^5 \text{ cm}^{-2} \text{ s}^{-1}$. The total neutron flux in the detector crystal was about $1.4 \cdot 10^6 \text{ cm}^{-2} \text{ s}^{-1}$. These measurement conditions clearly need to be avoided in LIFE@PROTEUS to prevent the severe crystal damage experienced during WOLF-B.

Using the MCNPX model of the reference set-up of the LIFE@PROTEUS measurement station, the neutron flux reaching the detector during reactor operation could only be estimated with rather high uncertainty (about 15%) because of the poor statistics. Here, the total neutron flux reaching the detector crystal during irradiation at 800 W was estimated to be about $35 \text{ cm}^{-2} \text{ s}^{-1}$, many orders of magnitudes lower ($2.5 \cdot 10^{-5}$) than that during the WOLF-B campaign. The main reason for this low value is the large volume of shielding water between the reactor core and the measurement station, which was not present during WOLF-B.

The presented LIFE@PROTEUS measurement station thus offers enough neutron shielding against the reactor core to rule out strong neutron damage of the detector as was observed during the WOLF-B campaign. This allows, theoretically, an unlimited repetition of irradiations and simplifies the analysis of the measured gamma-ray spectra.

7.2.2 Axial resolution of detection system

In comparison to the WOLF-B experiments, where only 40 cm long samples were measured and no specific importance was given to axial resolution, full-length fuel pins ($\sim 4\text{-}5 \text{ m}$) will be used in the LIFE@PROTEUS experiments. In the power plants (which will provide the spent fuel pins), and also in the PROTEUS reactor, the fuel pins are held in position with the help of spacers, which cause axial heterogeneities regarding the composition of the fuel and the fission rates in the core. The axial distance between the spacers is about 50 cm. To avoid affecting LIFE@PROTEUS measurements by these spacer-induced heterogeneities, the measurement station must offer an axial detection resolution which is better than, or at least in the range of 50 cm.

The axial resolution of the detection system was determined using the MCNPX model of the measurement station with a pin in the measurement position. The pin was subdivided axially into 10 cm segments to identify the origin of the gamma-rays participating to the detector response. An axially and radially homogeneous gamma-ray source was applied to each fuel segment. Using a point detector located in the centre of the detector, the average uncollided fluxes of gamma-rays emitted from the different segments were tallied. The calculations were performed with three different source energies: 1260 keV, 2540 keV and 3576 keV. To predict the system dead time during measurements, the procedure was repeated tallying also the total gamma-ray fluxes (uncollided plus collided). Examples of the detector response to uncollided gamma-rays emitted from the different axial segments of the pin are shown in Fig. 7.3 for the different gamma-ray energies. The detector responses due the individual axial segments are normalised to unity for each energy.

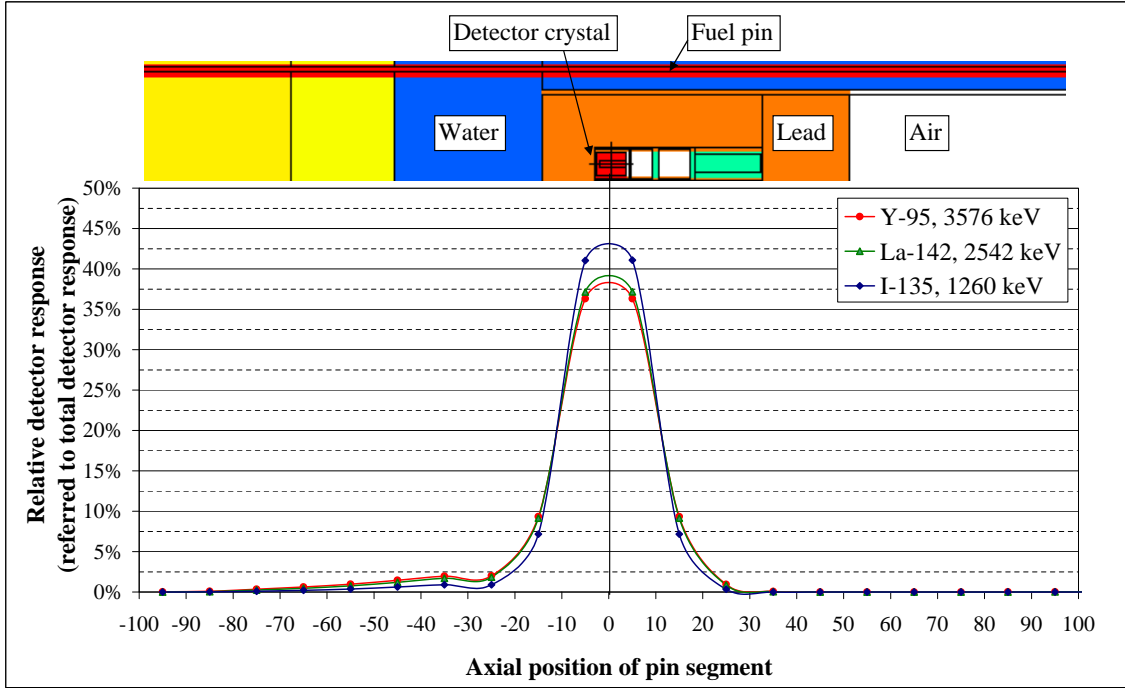


Figure 7.3: Axial detection resolution of LIFE@PROTEUS measurement station for different gamma-ray sources (results for uncollided fluxes).

It is seen that more than 70% of the detected uncollided 3576 keV gamma-rays are emitted from the 20 cm pin section directly in front of the detector. Due to the higher attenuation in the lead at lower energies, this effect is more pronounced for lower gamma-ray energies. For the 1260 keV gamma-rays, more than 80% of the detected uncollided gamma-rays originate from this 20 cm pin section.

The fractions of the total detector responses due to gamma-rays emitted in the 20 cm, 40 cm and 60 cm sections of fuel next to the detector are given in Table 7.1. About 98% of the 1260 keV gamma-rays reaching the detector are seen to be emitted from the 60 cm fuel section facing the detector. For the higher-energy gamma-rays, 94 to 95 % of the uncollided gamma-rays reaching the detector are emitted in this section.

Table 7.1: Fractions of total detector responses for gamma-rays emitted in different sections of the measured fuel pin (uncollided fluxes).

Section of fuel pin	1260 keV (^{135}I)	2540 keV (^{142}La)	3576 keV (^{95}Y)
–10 cm to 10 cm	82.1%	74.3%	72.6%
–20 cm to 20 cm	96.5%	92.6%	91.3%
–30 cm to 30 cm	97.7%	95.3%	94.2%

The results for the total (i.e. uncollided and collided) gamma-ray fluxes show a very similar distribution to those of the uncollided fluxes plotted in Fig. 7.3. This means that the low-energy background counts recorded during measurements originate mainly from the 60 cm fuel section facing the detector. In fact, the lead shielding above the detector was design to limit the system

dead time due to intrinsic gamma-ray lines emitted in the top part of the measured pin. The magnitude of the system dead time for the preliminary measurement station is estimated in the next subsection.

With respect to the required axial detection resolution of ~ 50 cm, the reference measurement station offers an acceptable resolution. In the future, however, it will be important to re-evaluate the spatial resolution. Some further improvements would be beneficial, e.g. by using additional shielding above and below the detector, to avoid any biases in the measurements due to spacer-related heterogeneities.

7.2.3 Intrinsic gamma-ray background from measured burnt fuel pin

The intensity of the intrinsic gamma-rays emitted by the spent fuel reaching the gamma-ray detector is of importance, as this will be the main contribution to the system dead time during the measurements of the LIFE@PROTEUS campaign. The zero-dead-time counting of the ORTEC DSPEC Plus accurately corrects measurements with very high dead times. Nonetheless, the final measurement set-up should aim to keep the dead time as low as possible because the higher the dead time, the higher will be the statistical uncertainties on the net-count areas of the detected gamma-ray lines (see Subsection 5.2.3).

During the WOLF-B measurements, the system dead times due to the intrinsic gamma-ray background from the burnt fuel (before re-irradiation) were about 35% and 62% for the 36 GWd/t and 46 GWd/t samples, respectively. Compared to these values, the additional dead time caused by the freshly induced gamma-ray activity after irradiation was small. Thus, for example, the total dead times caused by these two samples in measurement positions five minutes after an irradiation of 15 min at 800 W were about 45% and 68%, respectively; and a part of this additional dead time was also caused by gamma-rays emitted by activated surrounding materials.

To account for the the zero-dead-time corrections in the WOLF-B analysis, the statistical uncertainties (1σ) had to be multiplied by a factor of 1.3 for the 36 GWd/t sample and a factor of 1.8 for the 46 GWd/t sample. As described in Subsection 5.2.3, the used approximation for the correction factor was $\sqrt{\langle n \rangle}$, $\langle n \rangle$ being the average real-to-live time ratio. Consequently, unless the relative statistical uncertainty can be reduced drastically for the LIFE@PROTEUS measurements, high dead times should be avoided to prevent any significant increase of the statistical uncertainties.

The gamma-ray backgrounds due to the intrinsic activity of the measured pin or sample were determined using the MCNPX models of the LIFE@PROTEUS and WOLF-B measurement stations. The same gamma-ray source, which models the intrinsic activity of burnt fuel, was used in both cases to ease the comparison. To increase the efficiency of the MCNPX calculation of the LIFE@PROTEUS set-up, the source was only assigned to the 60 cm section of the fuel pin facing the detector. In each case, the source was distributed homogeneously in the fuel. The considered energies and their contributions to the modelled source are summarised in Table 7.2.

Table 7.2: Modelled gamma-ray source for the intrinsic activity of the burnt fuel [Jordan 09].

Energy	605 keV	662 keV	706 keV	802 keV	873 keV	996 keV	
Isotope	^{134}Cs	^{137}Cs	^{134}Cs	^{134}Cs	^{154}Eu	^{154}Eu	
Contribution	7.12%	81.18%	6.24%	0.64%	0.73%	0.63%	
Energy	1004 keV	1039 keV	1129 keV	1140 keV	1274 keV	1365 keV	2186 keV
Isotope	^{154}Eu	^{134}Cs	^{154}Eu	^{154}Eu	^{154}Eu	^{134}Cs	^{144}Ce
Contribution	1.07%	0.07%	0.02%	0.01%	2.07%	0.22%	0.001%

The total gamma-ray fluxes (i.e. uncollided and collided) reaching the detector for the LIFE@PROTEUS and the WOLF-B measurement stations are calculated to be $1.1 \cdot 10^{-9} \text{ cm}^{-2} \text{ sg}^{-1}$ and $4.3 \cdot 10^{-9} \text{ cm}^{-2} \text{ sg}^{-1}$, respectively, “sg” denoting source gamma-rays. As the gamma-ray flux tallied by MCNPX is normalised per source gamma-ray, the tallied fluxes had to be corrected for the different source volumes. The resulting ratio, corrected for the different source volumes, is about 0.39. Consequently, the intrinsic gamma-ray background reaching the detector while measuring a full length pin in the LIFE@PROTEUS set-up would be about 40% of the value one had when measuring a 40 cm burnt sample of the same isotopic composition in WOLF-B.

The isotopic composition of the 60 GWd/t burnt fuel pin (4.3% initial enrichment) is comparable to that of the 46 GWd/t burnt fuel sample (3.5% initial enrichment) used in WOLF-B¹. Therefore, the dead time for the 60 GWd/t pin in LIFE@PROTEUS can be estimated using the dead time for the 46 GWd/t sample measured during WOLF-B. For the estimation, dead times were plotted as a function of the total input count rates recorded during the WOLF-B campaign. The system dead time due to the intrinsic activity of the 46 GWd/t sample in the measurement position was 62%; the corresponding total input count rate was 150,000 cps. It was assumed that the system dead time caused by a 60 GWd/t fuel pin in LIFE@PROTEUS corresponded to an input count rate which was 40% of the total input count rate related to the measurement of the 46 GWd/t sample. i.e. 60,000 cps. Thus, using linear interpolation, the system dead time caused by a 60 GWd/t fuel pin in LIFE@PROTEUS was estimated to be about 30%.

A system dead time of $\sim 30\%$ results in multiplying the statistical uncertainty by a correction factor of about 1.2, which is more than acceptable. In other words, a lead filter of 12 cm between pin and detector offers sufficient protection with respect to the intrinsic activity of 60 GWd/t spent fuel pin.

7.3 Estimated counts from short-lived fission products

In this section, the achievable number of counts in the high-energy gamma-ray lines from short-lived fission products are estimated for the proposed LIFE@PROTEUS measurement station. The general methodology to estimate the net counts is described in Subsection 7.3.1. The performance of the measurement station, based on the gamma-ray lines that had been used in the WOLF-B analysis, is presented in Subsection 7.3.2. The same irradiation and measurement

¹Note that the given burn-up value of the 46 GWd/t sample is a nominal value; the true burn-up of the sample is estimated to be 52 to 54 GWd/t [Grimm 07].

times as used in WOLF-B have been assumed. Improvements of the measurement technique to maximise the statistics are investigated in Subsections 7.3.3 and 7.3.4. These improvements consist of using longer irradiation times, on the one hand, and of considering additional gamma-ray lines, which had not been considered in WOLF-B, on the other hand.

7.3.1 Methodology

In general, the number of net counts $N_{net}(E_\gamma)$ obtained in a gamma-ray peak at the energy E_γ , emitted by a fission product FP after an irradiation with the fission rate F , can be written as:

$$N_{net}(E_\gamma) = F \cdot \varepsilon(E_\gamma) \cdot att(E_\gamma) \cdot (b_{\gamma,FP}C_{FP})_{eff} \quad (7.1)$$

where $\varepsilon(E_\gamma)$ is the energy-dependent detection efficiency of the gamma-ray detector, $att(E_\gamma)$ is a correction factor for the solid angle and attenuation between measured pin and detector, and $(b_{\gamma,FP}C_{FP})_{eff}$ is the effective correction factor taking into account the saturation and decay of the considered fission product (see Section 5.1).

The net counts $N_{net,LIFE}$ of a given gamma-ray peak measured with the described LIFE@PROTEUS measurement station can be related to the net counts $N_{net,WOLF}$ of the same gamma-ray peak measured during the WOLF-B campaign, using Eq. 7.2. As the gamma-ray detector is assumed to be the same in both measurement set-ups, the detection efficiency $\varepsilon(E_\gamma)$ cancels out.

$$\frac{N_{net,f,LIFE}(E_\gamma)}{N_{net,f,WOLF}(E_\gamma)} = \frac{F_{f,LIFE}}{F_{f,WOLF}} \cdot \frac{att_{f,LIFE}(E_\gamma)}{att_{f,WOLF}(E_\gamma)} \cdot \frac{(b_{\gamma,FP}C_{FP})_{eff,f,LIFE}}{(b_{\gamma,FP}C_{FP})_{eff,f,WOLF}} \quad (7.2)$$

As indicated in Eq. 7.2, the net-count areas obtained for the fresh fuel sample (index $f,WOLF$) have been used to derive the expected net-count areas for a fresh fuel pin in LIFE@PROTEUS (index $f,LIFE$). In a similar manner, the net counts obtained for the 36 GWd/t burnt sample are used to derive the expected net-count areas for the 60 GWd/t burnt pin in LIFE@PROTEUS². The needed parameters are detailed, one by one, in the following paragraphs.

WOLF-B net-count areas $N_{net,WOLF}$

The net-count areas of the gamma-ray lines ^{142}La (2542 keV), ^{89}Rb (2570 keV), ^{138}Cs (2640 keV) and ^{95}Y (3576 keV) were obtained for both fresh and 36 GWd/t samples, irradiated in the position L11, with the analysis software HyperLab (see Section 5.2). During the WOLF-B campaign, the 36 GWd/t sample had been irradiated twice in each lattice position, and the sum of counts from both irradiations had been used for the final analysis. Here, however, the net counts obtained from a single irradiation of the sample have been used.

Ratios of fission rates F_{LIFE}/F_{WOLF}

The ratios of fission rates in the LIFE@PROTEUS and WOLF-B test lattices were determined using the results from MCNPX whole-reactor models.

²The obtained net counts of the 36 GWd/t sample (and not those of the 46 GWd/t sample) were used as reference because of the much better statistics compared to those obtained for the 46 GWd/t sample.

The calculated fission rates in the fresh and the 36 GWd/t samples irradiated in the lattice position L11 during the WOLF-B campaign (see Section 6.2) have been used as reference. Regarding the LIFE@PROTEUS test lattice, the total fission rates were calculated using the MCNPX whole-reactor model of the refurbished facility [Murphy 10], as briefly described in Section 7.1.

Results for representative fission densities (i.e. with reference to volume and source neutrons) of fresh and 60 GWd/t fuel pins located in the central assembly of the LIFE@PROTEUS test lattice are given in Table 7.3. They are compared to fission densities in the fresh and the 36 GWd/t spent fuel samples irradiated during the WOLF-B campaign. The fission densities for the LIFE@PROTEUS test lattice pins have been obtained as an average over a 30 cm segment located in the middle of the PROTEUS core and correspond to a zone without spacers.

Table 7.3: Calculated fission densities and resulting fission rate ratios in LIFE@PROTEUS and WOLF-B.

		Fission density [$\text{cm}^{-3}\text{sn}^{-1}$]*
LIFE	fresh	$1.65 \cdot 10^{-6}$ (0.4%)
	60 GWd/t	$7.30 \cdot 10^{-7}$ (0.4%)
WOLF-B**	fresh	$1.31 \cdot 10^{-5}$ (0.02%)
	36 GWd/t	$9.26 \cdot 10^{-6}$ (0.02%)
LIFE/WOLF-B ratio of fission rates [-]		
fresh / fresh		0.08
60 GWd/t / 36 GWd/t		0.13

*sn: source neutron

**irradiation position L11

Regarding the fresh fuel, the fission rate in the LIFE@PROTEUS test lattice (assuming the same reactor power) is seen to be about 13% of that in the WOLF-B test lattice. This is due to the higher number of fuel pins in the LIFE@PROTEUS test lattice and the similar distribution of the total power between the different zones of the PROTEUS reactor in the two programmes. During the WOLF-B campaign, the test lattice consisted of 101 fresh lattice fuel pins plus one fuel sample (see Fig 4.3), whereas the LIFE@PROTEUS reference test lattice (see Fig 7.1) contains in total 768 fuel pins (733 fresh and 35 spent).

Comparing the 60 GWd/t pin and the 36 GWd/t sample, the fission rate estimated for the LIFE@PROTEUS lattice is about 8% of that in the WOLF-B test lattice.

All LIFE@PROTEUS irradiations are assumed to be carried out at a reactor power of 800 W. During the WOLF-B campaign, the fresh fuel sample was irradiated at a reactor power of only 100 W (to limit the detector damage due to fast neutrons). Therefore, the LIFE/WOLF-B fresh-fuel ratio of fission rates given in Table 7.3 needs to be scaled up by a factor of 8 for the derivation of net counts in LIFE@PROTEUS. For the spent fuel, no modification is needed, because the 36 GWd/t sample had been irradiated at 800 W.

Ratios of solid angle and attenuation correction factors att_{LIFE}/att_{WOLF}

Solid angle and attenuation correction factors for the WOLF-B measurement set-up were calculated with MCNPX in Section 5.4. They were estimated by tallying the uncollided gamma-ray

fluxes in the germanium crystal of the detector due to mono-energetic gamma-ray sources emitted from the fuel samples. The gamma-ray sources were modelled homogeneously in the radial direction; in the axial direction, they were modelled following the calculated fission profile in the samples during irradiation. As the fresh and the 36 GWd/t spent fuel samples had not been measured in the same position, two different correction factors were calculated for each considered gamma-ray energy, one for each sample.

For the LIFE@PROTEUS measurement set-up, analogous calculations have been carried out, applying a gamma-ray source to the 60 cm section of the fuel pin next to the detector. Here, however, the source was homogeneously distributed in both radial and axial directions. This was a simplification since, in LIFE@PROTEUS, fissions in the fuel pins will be axially distributed according to the axial buckling of the PROTEUS core and will account for the presence of spacers. Furthermore, modelling only 60 cm high gamma-ray sources can lead to a bias of 5-6% for the tallied high-energy fluxes because, in reality, 5-6% of the uncollided gamma-rays reaching the detector crystal originate from outside of the modelled 60 cm section (see Subsection 7.2.2). This means that the currently estimated count rates in the high-energy peaks are 5-6% too low. For the present evaluation of the measurement station, however, this bias is quite acceptable, considering in particular that it is in the conservative direction.

The measurement positions of the fresh and spent fuel pins are the same in LIFE@PROTEUS. Moreover, the self-attenuations in fresh and spent fuel are very similar. The calculations have accordingly only been carried out for the fresh fuel pin, the corresponding factors for the 60 GWd/t pin being assumed to be the same.

The ratios of solid angle and attenuation correction factors were calculated for all considered gamma-ray energies. As an example, the uncollided 2542 keV and 3576 keV fluxes tallied in the germanium crystal, when measuring the fresh and spent fuel segments in LIFE@PROTEUS and in WOLF-B, are given in Table 7.4. The fluxes are normalised to the number of source gamma-rays. The flux ratios, once corrected for the different source volumes, are equal to the corresponding ratios of solid angle and attenuation correction factors. The results are also given in Table 7.4.

Table 7.4: Tallied uncollided fluxes for the LIFE@PROTEUS and WOLF-B measurement set-ups, and corresponding ratios of solid angle and attenuation correction factors.

		Uncollided flux [$\text{cm}^{-2}\text{sg}^{-1}$]*	
		2542 keV	3576 keV
LIFE	fresh and 60 GWd/t	$5.86 \cdot 10^{-8}$ (2.3%)	$7.67 \cdot 10^{-8}$ (2.4%)
WOLF-B**	fresh (38.9 cm)	$1.02 \cdot 10^{-6}$ (0.1%)	$1.74 \cdot 10^{-6}$ (0.1%)
	36 GWd/t (40 cm)	$4.20 \cdot 10^{-8}$ (0.3%)	$8.92 \cdot 10^{-8}$ (0.3%)
LIFE/WOLF-B ratio of solid angle and attenuation correction factors [-]			
fresh / fresh		0.089	0.068
60 GWd/t / 36 GWd/t		2.09	1.29

*sg: source gamma-ray

**irradiation position L11

The solid angle and attenuation corrections for spent fuel measured during WOLF-B and LIFE@PROTEUS are seen to be quite comparable. Their ratios are between 1.3 and 2.1, depending on the gamma-ray energy. In fact, the detector position inside the lead filter of the LIFE@PROTEUS measurement station was chosen with this aim.

As regards the fresh fuel measurements, however, the uncollided gamma-rays reaching the detector in the LIFE@PROTEUS set-up are at least 10 times less than in the WOLF-B set-up. This is due to the specially optimised measurement position of the fresh fuel sample during the WOLF-B campaign, where the sample was measured very close to the detector to increase the counting statistics.

Ratio of saturation and decay correction factors $(b_{\gamma,FP}C_{FP})_{eff,LIFE}/(b_{\gamma,FP}C_{FP})_{eff,WOLF}$

As described in Section 5.3, the saturation and decay correction factors $(b_{\gamma,FP}C_{FP})$ are fission product dependent. They relate the number of gamma-rays of a particular energy E_γ emitted by the fission product FP to the number of fissions occurring in the fuel during irradiation. Effective correction factors $(b_{\gamma,FP}C_{FP})_{eff}$ are calculated according to Eq 5.2 and account for the possibility of several fission products contributing to the same gamma-ray energy.

A Matlab routine was written in order to calculate the saturation and decay corrections for the WOLF-B measurements. The same routine has been used to calculate the saturation and decay factors for the foreseen LIFE@PROTEUS measurements.

In a first study, the same irradiation, cooling and measurement times as for WOLF-B were assumed for the LIFE@PROTEUS measurements. The irradiation time of the spent fuel pin was set to 15 min, whereas the irradiation time of the fresh fuel pin was set to 30 min. The cooling time for both fuel pins was 5 min.

The only difference between the LIFE@PROTEUS and WOLF-B correction factors were the different sets of contributions a_i to the total number of fissions from the four main fissioning isotopes ^{235}U , ^{238}U , ^{239}Pu and ^{241}Pu . The contributions a_i were needed to derive effective fission yields used in the calculation of the saturation and decay of the different fission products.

For the fresh fuel and the 36 GWd/t fuel samples irradiated in position L11 during WOLF-B, the contributions a_i had been calculated using the whole-reactor MCNPX model. For the fresh and the 60 GWd/t pins irradiated in the LIFE@PROTEUS reference lattice, they had been calculated in the framework of preliminary investigations [Murphy 10] and were available for this work. The contributions a_i to the total number of fissions for both LIFE@PROTEUS and WOLF-B are listed in Table 7.5.

The ratios of saturation and decay correction factors for the four gamma-ray lines are given in Table 7.6. Due to the similar contributions a_5 and a_8 in the fresh fuel for both LIFE@PROTEUS and WOLF-B irradiations, the correction factors are almost the same and their ratio is equal to unity. For the 36 GWd/t sample and the 60 GWd/t fuel pin, the contributions to the total number of fissions are very different due to the different isotopic compositions of the fuels. Consequently, the saturation and decay correction factors differ significantly for fission products whose fission yields strongly depend on the fissioning isotopes. For example, in the case for ^{89}Rb , the ratio of correction factors is 0.78.

Table 7.5: Contributions to total number of fissions during the LIFE@PROTEUS and WOLF-B irradiations.

		Estimated contributions to total fissions			
		a_{U5}	a_{U8}	a_{P9}	a_{P1}
LIFE*	Fresh	95%	5%		
	60 GWd/t	27%	7%	53%	13%
WOLF-B**	fresh	97%	3%		
	36 GWd/t	51%	4%	39%	6%

*Given values refer to central 60 cm section of fuel pins.

**irradiation position L11

Table 7.6: Ratios of saturation and decay correction factors between LIFE@PROTEUS and WOLF-B.

Gamma-ray line	$\frac{\text{fresh}}{\text{fresh}}$	$\frac{60\text{GWd/t}}{36\text{GWd/t}}$
	$\frac{(b_{\gamma,FP}C_{FP})_{eff,f,LIFE}}{(b_{\gamma,FP}C_{FP})_{eff,s,LIFE}}$	$\frac{(b_{\gamma,FP}C_{FP})_{eff,f,WOLF}}{(b_{\gamma,FP}C_{FP})_{eff,s,WOLF}}$
^{142}La (2542 keV)	1.00	0.95
^{89}Rb (2570 keV)	0.99	0.78
^{138}Cs (2640 keV)	1.00	0.97
^{95}Y (3576 keV)	1.00	0.92

7.3.2 Estimated net counts for the gamma-ray lines used in WOLF-B

In a first step, the net-count areas which are achievable for the fresh and the 60 GWd/t pins measured in the LIFE@PROTEUS measurement station have been estimated for the four gamma-ray lines which were used for WOLF-B. These are ^{142}La (2542 keV), ^{89}Rb (2570 keV), ^{138}Cs (2640 keV) and ^{95}Y (3576 keV). The main characteristics of these peaks, such as half-lives, gamma-ray intensities and cumulative fission yields for ^{235}U and ^{239}Pu fissions, are given in Table 7.7.

Table 7.7: Characteristics of gamma-ray lines used in WOLF-B analysis.*

Gamma-ray line	Half-life	Gamma-ray intensity	Cumulative fission yields [%]	
			$Y_{th,U5}$	$Y_{th,P9}$
^{142}La (2542 keV)	1.52 h	10.0%	5.86 (1.7%)	4.97 (1.1%)
^{89}Rb (2570 keV)	15.4 min	10.2%	4.69 (1.2%)	1.68 (1.9%)
^{138}Cs (2640 keV)	33.4 min	7.6%	6.69 (1.7%)	5.94 (2.7%)
^{95}Y (3576 keV)	10.3 min	6.4%	6.47 (1.1%)	4.82 (2.0%)

*All nuclear data are extracted from JEFF3.1.

The net-count areas obtained after irradiating the fresh and 36 GWd/t samples in the lattice position L11 have been used as reference. The irradiation times (30 min for fresh fuel, 15 min for burnt fuel), the cooling times (5 min) and the measurement times (1 to 8 hours, depending

on the gamma-ray line) were assumed to be the same for LIFE@PROTEUS and WOLF-B. The reactor power was set to 800 W for all irradiations in LIFE@PROTEUS. The reactor power during WOLF-B was 800 W for the 36 GWd/t sample and only 100 W for the fresh sample. The derived net-count areas are given in Table 7.8.

Table 7.8: Estimated net counts in LIFE@PROTEUS (same irradiation time as for WOLF-B).

Gamma-ray line	Fresh pin $t_{irr} = 30$ min, 800 W		60 GWd/t burnt pin $t_{irr} = 15$ min, 800 W	
	Ratio of counts LIFE/WOLF-B*	Expected counts LIFE	Ratio of counts LIFE/WOLF-B**	Expected counts, LIFE
^{142}La (2542 keV)	9%	4890	16%	1020
^{89}Rb (2570 keV)	9%	2100	12%	370
^{138}Cs (2640 keV)	9%	3650	15%	1270
^{95}Y (3576 keV)	7%	1280	9%	380

*Reference: WOLF-B, position L11, $t_{irr}=30$ min, 100 W, irradiation 9 in Table 4.5.

**Reference: WOLF-B, position L11, $t_{irr}=15$ min, 800 W, irradiation 5 in Table 4.5.

Comparing the 60 GWd/t spent fuel pin (LIFE@PROTEUS) to the 36 GWd/t spent fuel sample (WOLF-B), the estimated net-count areas for LIFE@PROTEUS are only 9 to 16% of the values obtained for the same irradiation time and reactor power in the WOLF-B campaign. Both WOLF-B and LIFE@PROTEUS measurements have similar solid angle and attenuation correction factors, and similar saturation and decay correction factors. The decrease in count rates is mainly due to the different fission rates. The fission rates induced in the spent fuel in the LIFE@PROTEUS test lattice are about 10 times lower than in the WOLF-B lattice.

Comparing the fresh pin to the fresh sample, the estimated net-count areas for LIFE@PROTEUS are about 10% of those for WOLF-B. Here, several aspects have to be considered in the comparison. The reactor power during LIFE@PROTEUS is to be 800 W instead of only 100 W during WOLF-B, which increases the count rates by a factor of 8. However, at the same time, the number of induced fissions in the LIFE@PROTEUS lattice is only about 13% of that in WOLF-B and the uncollided gamma-ray flux reaching the detector is more than ten times lower.

Comparing the fresh and 60 GWd/t fuel pins in LIFE@PROTEUS, the estimated net counts obtained after the same irradiation are about 3 to 6 times higher for the fresh fuel pin than for the 60 GWd/t pin. This is mainly due to the higher fission rates for the fresh fuel pin as compared to the spent fuel. In addition, the effective fission yields tend to be higher than for the spent fuel, as the proportion of ^{235}U fissions is more important. This is particularly true for ^{89}Rb , the fission yields of which for ^{235}U and ^{239}Pu fissions are most different (4.7% and 1.7%, respectively).

Clearly, net-count areas about 10 to 16% of those obtained in WOLF-B are not sufficient. One has to point out that these values refer to rather short irradiation times of 15 and 30 min, for which the longer-lived ^{142}La and ^{138}Cs are not yet saturated. In WOLF-B, these short irradiation times were necessary to limit the neutron damage of the detector. Since in LIFE@PROTEUS the detector will be much better shielded from the reactor core, there is not any such constraint on the irradiation times. In the following subsections, longer irradiation times and additional gamma-ray lines are considered for LIFE@PROTEUS in order to increase the statistics.

7.3.3 Longer irradiation times

The estimated net counts discussed in the previous subsection for the ^{142}La (2542 keV), ^{89}Rb (2570 keV), ^{138}Cs (2640 keV) and ^{95}Y (3576 keV) gamma-ray lines were derived for relatively short irradiation times of 15 to 30 min. Fig 7.4 illustrates the saturation process for the four fission products during irradiation (unlimited irradiation time). It is clearly seen that the activities of ^{138}Cs ($T_{1/2} = 33$ min) and ^{142}La (1.5 h) could be increased significantly using longer irradiation times.

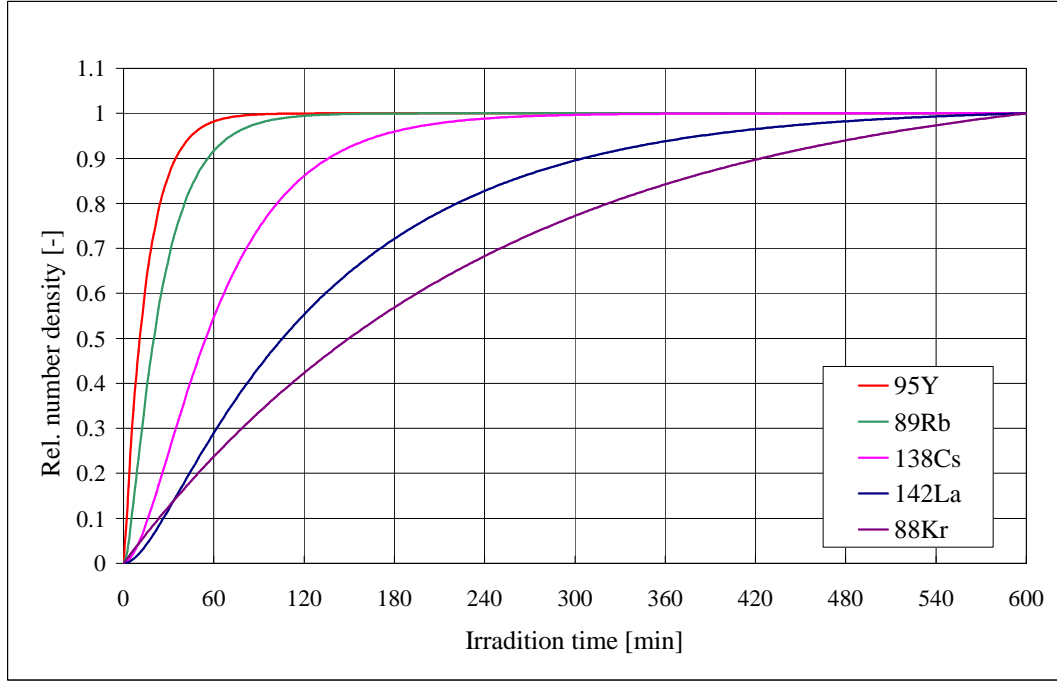


Figure 7.4: Saturation process during irradiation for the fission products ^{142}La , ^{89}Rb , ^{138}Cs and ^{95}Y .

The only negative impact of longer irradiation times might be a higher system dead time during measurement, as the activity of the irradiated fuel pin increases. During WOLF-B, however, it was found that the additional dead time due to the freshly induced fission products is small compared to the dead time caused by the intrinsic gamma-ray activity of the spent fuel samples. Therefore, it is not likely that the overall uncertainty due to system dead-time corrections will increase significantly with longer irradiations.

Net counts for the four gamma-ray lines, assuming longer irradiations for LIFE@PROTEUS, were estimated using the methodology described in Subsection 7.3.1. Only the saturation and decay correction factors for the different fission products had to be adjusted to account for the longer irradiation time t_{irr} . The irradiation times were increased to 1, 2 and 3 h. Longer irradiation times were not considered in view of possible safety limitations, e.g. the maximum integrated reactor power per week³.

The results are summarised in Table 7.9. Due to their short half-lives of 15 min and 10 min, ^{89}Rb and ^{95}Y reach their saturation very quickly. Consequently, the net counts of their gamma-ray

³For example, today, the maximum energy produced by the reactor per week is limited to 2000 Wh in order to guarantee a dose rate lower than $40 \mu\text{Sv/week}$ in the control room [Fassbind 09]. This, and other similar limitations, may have to be re-considered during the refurbishment of the reactor for LIFE@PROTEUS.

peaks do not increase significantly with longer irradiations. The maximum net-count areas of the ^{89}Rb (2570 keV) and ^{95}Y (3576 keV) peaks are less than 800 counts for the 60 GWd/t spent fuel pin. In comparison, the net-count areas for the ^{142}La (2542 keV) and ^{138}Cs (2640 keV) peaks can be increased to more than 4700 and 7000 counts, respectively, by irradiating the spent fuel fuel pin for 3 h.

Table 7.9: Estimated net counts in LIFE@PROTEUS using longer irradiation times.

Gamma-ray line	Fresh pin 800 W			60 GWd/t burnt pin 800 W		
	$t_{irr} = 1 \text{ h}$	$t_{irr} = 2 \text{ h}$	$t_{irr} = 3 \text{ h}$	$t_{irr} = 1 \text{ h}$	$t_{irr} = 2 \text{ h}$	$t_{irr} = 3 \text{ h}$
^{142}La (2542 keV)	8710	14100	17510	3640	5670	7050
^{89}Rb (2570 keV)	2900	3100	3100	720	770	770
^{138}Cs (2640 keV)	8460	11030	11780	3410	4460	4760
^{95}Y (3576 keV)	1490	1520	1520	590	600	600

7.3.4 Additional gamma-ray lines

During WOLF-B, several gamma-ray peaks, which could be potentially used as fission rate indicators, could not be included in the analysis because of their interference with background peaks or because of insufficient statistics. These peaks are ^{138}Cs (2218 keV), ^{88}Kr (2392 keV), ^{142}La (2398 keV), ^{142}La (2971 keV) and ^{84}Br (3928 keV). Their gamma-ray intensities and the most important fission yields are summarised in Table 7.10. Interfering background peaks during the WOLF-B experiments are also given in Table 7.10. Relevant nuclear data and their uncertainties, in relation to the additional gamma-ray lines, are included in Appendix A.

Table 7.10: Characteristics of additional high-energy gamma-ray lines.*

Gamma-ray line	Half-life	Gamma-ray intensity	Cumulative fission yields [%]		Interfering WOLF-B background peak
			$Y_{th,U5}$	$Y_{th,P9}$	
^{138}Cs (2218 keV)	33.4 min	15.2%	6.69 (1.7%)	5.94 (2.7%)	^1H (2223 keV)
^{88}Kr (2392 keV)	2.8 h	34.6%	3.54 (1.8%)	1.25 (2.8%)	^{116m}In (2391 keV)
^{142}La (2398 keV)	1.52 h	13.3%	5.86 (1.7%)	4.97 (1.1%)	^{116m}In (2391 keV)
^{142}La (2971 keV)	1.52 h	3.1%	5.86 (1.7%)	4.97 (1.1%)	
^{84}Br (3928 keV)	31.8 min	7.6%	1.01 (1.9%)	0.45 (4.3%)	

*All nuclear data are extracted from JEFF3.1.

The ^{142}La (2971 keV) and ^{84}Br (3928 keV) peaks were not considered in WOLF-B because of their insufficient counting statistics. Towards the end of the measurement campaign, when the detector resolution was already degraded, the ^{142}La (2971 keV) peak additionally suffered from the interference with the ^{56}Mn background peak at 2960 keV (from the activation of the steel of the sample changer). In the case of the ^{88}Kr (2392 keV) and ^{142}La (2398 keV) peaks, interference was caused by the 2391 keV peak of ^{116m}In , produced by activation of the detector mount. The

interference of the ^{138}Cs (2218 keV) peak was caused by the prompt gamma-rays from the $^1\text{H}(\text{n},\gamma)$ reaction in the polyethylene shielding used for the detector.

In this section, the possibility to use these additional peaks in LIFE@PROTEUS is evaluated by estimating their potential interference in the new detector environment and by quantifying their achievable net-count areas.

Expected background peaks for LIFE@PROTEUS

As mentioned above, the interfering gamma-ray peaks observed in the energy region above 2200 keV during WOLF-B resulted mainly from the activation of materials surrounding the detector. This was due to the large neutron background from the reactor during irradiation. The two most prominent activation products were ^{56}Mn ($T_{1/2} = 2.6$ h) and $^{116\text{m}}\text{In}$ ($T_{1/2} = 54$ min). In the case of LIFE@PROTEUS, it has been seen that the neutron background from the core will be negligibly small (see Subsection 7.2.1). Consequently, the two activation products ^{56}Mn and $^{116\text{m}}\text{In}$ are not expected to be present in the gamma-ray spectra. The ^{88}Kr (2392 keV), ^{142}La (2398 keV) and ^{142}La (2971 keV) peaks will thus be usable, provided sufficiently high net-count areas can be achieved.

As mentioned earlier, the ^1H (2223 keV) background peak originated from prompt (n,γ) reactions in the polyethylene shielding surrounding the detector. This peak was very small compared to the other background peaks and was mainly present in the measurements of the spent fuel samples due to their intrinsic neutron emission. In the LIFE@PROTEUS reference measurement station, there is no polyethylene shielding. Due to the high amount of water surrounding the measurement station, however, the ^1H (2223 keV) peak could be a problem while measuring spent fuel pins. Nonetheless, the ^{138}Cs (2218 keV) peak has been included in the analysis presented in this section. One has to be aware, however, that it might not be easily usable for LIFE@PROTEUS.

To estimate the LIFE@PROTEUS net-count areas of the additional gamma-ray lines, one first needs to evaluate the net-count areas of these peaks during WOLF-B. Some of them could not be determined directly from the measured gamma-ray spectra and were therefore estimated as detailed below.

Determination of net-count areas for WOLF-B

The ^{138}Cs (2218 keV) net counts $N_{\text{net},f,WOLF}(2218\text{keV})$ for the fresh fuel sample could be obtained directly from the measured gamma-ray spectrum using the analysis software HyperLab. For the spent fuel sample, however, this peak interfered with the ^1H (2223 keV) background peak, as mentioned above. Therefore, the net counts $N_{\text{net},s,WOLF}(2218\text{keV})$ for the 36 GWd/t spent sample could not be obtained directly from the gamma-ray spectrum. Instead, the net counts have been estimated in a manner analogous to Eq. 7.2, using the fresh fuel result as reference:

$$\frac{N_{\text{net},s,WOLF}(2218\text{keV})}{N_{\text{net},f,WOLF}(2218\text{keV})} = \frac{F_{s,WOLF} \cdot \text{att}_{s,WOLF}(2218\text{keV})}{F_{f,WOLF} \cdot \text{att}_{f,WOLF}(2218\text{keV})} \cdot \frac{(b_{^{138}\text{Cs}}(2218\text{keV})C_{^{138}\text{Cs}})_{\text{eff},s,WOLF}}{(b_{^{138}\text{Cs}}(2218\text{keV})C_{^{138}\text{Cs}})_{\text{eff},f,WOLF}} \quad (7.3)$$

For the 36 GWd/t sample, the net-count area of the ^{142}La (2971 keV) peak could be obtained directly with HyperLab, although the number of counts was very small. For the fresh sample, due to the advanced degradation of the detector resolution when the sample was measured, the

^{142}La (2971 keV) peak interfered too much with the ^{56}Mn (2960 keV) peak. The net-count area $N_{net,f,WOLF}(2971\text{keV})$ has been therefore obtained based on the spent fuel result:

$$\frac{N_{net,f,WOLF}(2971\text{keV})}{N_{net,s,WOLF}(2971\text{keV})} = \frac{F_{f,WOLF}}{F_{s,WOLF}} \cdot \frac{att_{f,WOLF}(2971\text{keV})}{att_{s,WOLF}(2971\text{keV})} \cdot \frac{(b_{^{142}\text{La}(2971\text{keV})}C_{^{142}\text{La}})_{eff,f,WOLF}}{(b_{^{142}\text{La}(2971\text{keV})}C_{^{142}\text{La}})_{eff,s,WOLF}} \quad (7.4)$$

The net counts in the ^{142}La (2398 keV) peak were obtained for both fresh and spent fuel samples directly with HyperLab. The neighbouring ^{88}Kr (2392 keV) peak coincided with the ^{116m}In peak at 2391 keV and could not be measured directly. Instead, its net-count area was estimated from the net-count area of the ^{142}La (2398 keV) peak, using Eq. 7.5, which is a simplified version of Eq. 7.2. The fission rates F cancel out in this case, as the sample, the irradiation time and the location are all the same. The solid angle and attenuation correction factors att are assumed to be the same for the two energies 2392 keV and 2398 keV, and thus also cancel out. Eq. 7.5 is derived for the fresh fuel sample; the same basic relationship was used for the spent fuel sample.

$$\frac{N_{net,f,WOLF}(2392\text{keV})}{N_{net,f,WOLF}(2398\text{keV})} = \frac{(b_{^{88}\text{Kr}(2392\text{keV})}C_{^{88}\text{Kr}})_{eff,f,WOLF}}{(b_{^{142}\text{La}(2398\text{keV})}C_{^{142}\text{La}})_{eff,f,WOLF}} \quad (7.5)$$

Finally, the ^{84}Br (3928 keV) peak could be determined directly in the measured spectra for both fresh and 36 GWd/t samples, albeit with relatively high uncertainties.

Estimated LIFE@PROTEUS net-count areas

Having derived the net-count areas of the new gamma-ray candidates for the case of WOLF-B, the achievable net-count areas for LIFE@PROTEUS have been obtained as described in Subsection 7.3.1. The reactor power was set to 800 W. Irradiation times of 1, 2 and 3 h were assumed. In each case, the measurement was assumed to start 5 min after irradiation and to last about 8 hours in order to detect at least 90% of the gamma-rays from the longest-lived candidate ^{88}Kr .

The estimated net-count areas are summarised in Table 7.11.

Table 7.11: Estimated net counts for additional gamma-ray lines in LIFE@PROTEUS.

Gamma-ray line	Fresh pin 800 W			60 GWd/t burnt pin 800 W		
	$t_{irr} = 1 \text{ h}$	$t_{irr} = 2 \text{ h}$	$t_{irr} = 3 \text{ h}$	$t_{irr} = 1 \text{ h}$	$t_{irr} = 2 \text{ h}$	$t_{irr} = 3 \text{ h}$
^{138}Cs (2218 keV)	13780	18550	19960	5590	7520	8090
^{88}Kr (2392 keV)	11170	19920	26770	4140	7380	9920
^{142}La (2398 keV)	7750	12790	15980	4640	7660	9570
^{142}La (2971 keV)	2750	4530	5670	1080	1780	2220
^{84}Br (3928 keV)	810	1030	1090	250	320	340

7.3.5 Conclusions with respect to achievable count rates

As compared to WOLF-B, the counting statistics obtained during LIFE@PROTEUS will be impaired because of the much lower (factor of ~ 0.1) fission rates expected in the individual fuel pins. For the longer-lived fission products ^{88}Kr , ^{142}La and ^{138}Cs (minimum half-life 30 min), this effect can be compensated by longer irradiation times. For shorter-lived fission products like ^{89}Rb and ^{95}Y (maximum half-life ~ 15 min), however, this is not possible.

Regarding the gamma-ray lines which were already included in WOLF-B analyses, the two peaks ^{142}La (2542 keV) and ^{138}Cs (2640 keV) appear very suitable for LIFE@PROTEUS. Among the additional gamma-ray lines, which had not been included in the analysis of the WOLF-B measurements, the three peaks ^{88}Kr (2392 keV), ^{142}La (2398 keV), ^{142}La (2971 keV) appear very promising. To maximise the number of achievable counts per irradiation, long irradiation times at high power levels should be chosen for LIFE@PROTEUS. As shown in Tables 7.9 and 7.11, the expected net-count areas for these different gamma-ray lines, recorded after an irradiation of 3 h at a reactor power of 800 W, vary between 2200 and 10000 counts for the spent fuel pin, and between 5700 and 27000 counts for the fresh fuel pin.

Theoretically, the count rates of the peaks from ^{142}La ($T_{1/2} = 1.5\text{h}$) and ^{88}Kr ($T_{1/2} = 2.8\text{h}$) could be further increased with even longer irradiation times. However, as mentioned above, longer irradiation times might not be possible because of safety limitations with respect to the maximum integrated reactor power per week. Therefore, 3 h are assumed to be the maximum irradiation duration.

The ^{89}Rb (2570 keV), ^{95}Y (3576 keV) and ^{84}Br (3928 keV) peaks appear unsuitable for the LIFE@PROTEUS measurements because of their insufficient statistics. The ^{138}Cs (2218 keV) peak, in spite of showing high count rates, will probably not be easily usable during LIFE@PROTEUS because of its interference with the expected ^1H (2223 keV) background peak⁴.

Finally, the five gamma-ray lines ^{88}Kr (2392 keV), ^{142}La (2398 keV), ^{142}La (2542 keV), ^{138}Cs (2640 keV) and ^{142}La (2971 keV) are recommended for the measurement of fresh-to-spent fission rate ratios in LIFE@PROTEUS.

Higher statistics can be reached by repeating the irradiations of one pin and summing the obtained gamma-ray spectra before analysis. Since the damage of the detector due to the fast neutrons emitted from the reactor core will not be a problem anymore for the LIFE@PROTEUS measurement set-up, the number of irradiations is not limited theoretically. This number is limited, however, for practical reasons, and 3 irradiations per pin are currently considered feasible.

In brief, a good example of an appropriate measurement strategy for LIFE@PROTEUS would be to irradiate each pin for 3 h at a reactor power of 800 W, to measure the pins for 8 h and to repeat the whole procedure 3 times.

⁴The ^1H (2223 keV) peak due to the intrinsic neutron emission of the burnt fuel could possibly be quantified with the help of suitable background measurements before irradiation, and the net counts of the ^{138}Cs (2218 keV) peak acquired after irradiation could then be appropriately corrected for.

7.4 Expected uncertainties and sensitivities of fission rate ratios

In this section, the expected uncertainties and sensitivities of measured fission rate ratios between fresh and 60 GWd/t spent fuel pins in LIFE@PROTEUS are estimated, based on the five gamma-ray lines ^{88}Kr (2392 keV), ^{142}La (2398 keV), ^{142}La (2542 keV), ^{138}Cs (2640 keV), and ^{142}La (2971 keV). All the presented results are based on the measurement strategy derived in the previous section, i.e. three irradiations per pin for 3 h at a reactor power of 800 W and gamma-ray measurements for 8 h starting 5 min after the end of each irradiation.

7.4.1 Uncertainties on measured fission rate ratios

Individual estimates for fresh-to-spent fuel fission rate ratios based on single gamma-ray lines are derived in the same way as for the WOLF-B campaign. A final unique fission rate ratio result is then obtained, in terms of the weighted mean of the individual gamma-ray line estimates.

The derivation of measured fission rate ratios and their uncertainties has been explained in detail in Chapter 5 for the WOLF-B campaign. Since in LIFE@PROTEUS the measurement position will be the same for all fuel pins, the solid angle and attenuation corrections are assumed to be the same for the fresh and spent fuel pins. Strictly speaking, the solid angle and attenuation corrections might differ slightly due to different axial fission profiles in the fuel, but this effect is neglected in this study. Therefore, Eq. 5.4 for the individual estimates of measured fission rate ratio $FRR(E_\gamma)$, between a fresh (f) and a spent (s) fuel pin for a given gamma-ray line of the energy E_γ , simplifies to:

$$FRR_{f-s}(E_\gamma) = \frac{N_{net,f}}{N_{net,s}} \cdot \frac{(b_{\gamma,FP}C_{FP})_{eff,s}}{(b_{\gamma,FP}C_{FP})_{eff,f}} \quad (7.6)$$

where N_{net} is the net-count area of the given gamma-ray line, and $(b_{\gamma,FP}C_{FP})_{eff}$ is the correction factor taking into account the saturation and decay of the fission product during and after irradiation.

The combined uncertainty on a measured fission rate ratio $\sigma_{FRR(E_\gamma)}$ is derived from the statistical uncertainties on the two net-count areas $N_{net,f}$ and $N_{net,s}$ and on the ratio of saturation and decay correction factors $(b_{\gamma,FP}C_{FP})_{eff,s}/(b_{\gamma,FP}C_{FP})_{eff,f}$ using the error propagation law:

$$\sigma_{FRR(E_\gamma)} = \sqrt{\sigma_{N_{net,f}}^2 + \sigma_{N_{net,s}}^2 + \sigma_{\frac{(b_{\gamma,FP}C_{FP})_{eff,s}}{(b_{\gamma,FP}C_{FP})_{eff,f}}}^2} \quad (7.7)$$

The individual estimates $FRR(E_\gamma)$ of the fresh-to-60 GWd/t fission rate ratios are combined to yield the weighted mean FRR . In contrast to WOLF-B, however, the individual estimates based on the different gamma-ray lines are not independent of each other. Three of them originate from the same fission product ^{142}La . As a first approximation, however, the weighted mean may be used, neglecting the correlation between the three ^{142}La estimates:

$$FRR = \frac{\sum \frac{1}{\sigma_{FRR_i(E_\gamma)}^2} \cdot FRR_i(E_\gamma)}{\sum \frac{1}{\sigma_{FRR_i(E_\gamma)}^2}}, \quad \sigma_{FRR}^2 = \frac{1}{\sum \frac{1}{\sigma_{FRR_i(E_\gamma)}^2}} \quad (7.8)$$

The uncertainties on the individual estimates $FRR(E_\gamma)$ related to the saturation and decay corrections are calculated as described in Section 5.3 via the Matlab routine used for the WOLF-B analysis. The ratios of the correction factors between the 60 GWd/t spent and fresh fuel pins, along with their uncertainties, are summarised in Table 7.12.

Table 7.12: Ratios of saturation and decay correction factors and their uncertainties as calculated for LIFE@PROTEUS.

Gamma-ray line	$\frac{60\text{GWd/t}}{\text{fresh}}$ $\frac{(b_{\gamma,FP}C_{FP})_{eff,s}}{(b_{\gamma,FP}C_{FP})_{eff,f}}$
^{88}Kr (2392 keV)	0.55 (1.4%)
^{142}La (2398 keV)	0.89 (1.2%)
^{142}La (2542 keV)	0.89 (1.1%)
^{138}Cs (2640 keV)	0.91 (1.3%)
^{142}La (2971 keV)	0.89 (1.2%)

In contrast to the case of the saturation and decay correction factors, the uncertainty on the net-count areas can only be broadly estimated. As a first approximation, the uncertainty $\sigma_{Net,LIFE}$ on the net-count area of a given gamma-ray line may be estimated on the basis of the corresponding uncertainty $\sigma_{Net,WOLF}$ derived during WOLF-B with HyperLab. To this aim, $\sigma_{Net,WOLF}$ values, as obtained in Subsection 5.2.3, have been modified using Eq. 7.9 to account for the different count rates $N_{net,LIFE}$ and $N_{net,WOLF}$, and for the different dead times $\langle n \rangle_{LIFE}$ and $\langle n \rangle_{WOLF}$:

$$\sigma_{Net,LIFE} = \sigma_{Net,WOLF} \cdot \sqrt{\frac{N_{net,LIFE} \cdot \langle n \rangle_{LIFE}}{N_{net,WOLF} \cdot \langle n \rangle_{WOLF}}} \quad (7.9)$$

The derived $\sigma_{Net,LIFE}$ values are somewhat overestimated as the uncertainty $\sigma_{Net,WOLF}$, which was obtained by fitting the distorted gamma-ray peaks within HyperLab, also accounts for the degradation of the detector resolution during WOLF-B. No degradation of the detector resolution is expected in LIFE@PROTEUS and, consequently, the uncertainty should be lower. This is specially true for the fresh fuel pins, as measurements of the fresh fuel sample were conducted with a much degraded detector resolution during the WOLF-B campaign. In particular, the degraded detector resolution led to difficulties in deconvolving the ^{142}La (2398 keV) peak from the ^{88}Kr (2392 keV) and the ^{116m}In (2391 keV) peaks, resulting in artificially high uncertainties.

Considering the half-lives of the fission products, most of the counts in the gamma-ray peaks will be acquired when the system dead time has reached its background level and is only due to the intrinsic activity of the measured pin. As shown in Subsection 7.2.3, the estimated typical dead time due to the intrinsic activity of a 60 GWd/t pin is about 30%. The dead time for a fresh fuel pin (before irradiation) is negligible. Consequently, a conservative average dead-time correction of 35% for the 60 GWd/t pin and 5% for the fresh fuel pin is assumed. This leads to correction factors $\langle n \rangle_{LIFE}$ of 1.24 and 1.03, respectively, for the two pin types. The various estimated net-count areas and their related uncertainties, for the sum of counts from 3 irradiations of 3 h at a reactor power of 800 W, are summarised in Table 7.13.

Table 7.13: Estimated net counts and uncertainties for LIFE@PROTEUS.

Gamma-ray line	Fresh pin Counts	60 GWd/t burnt pin Counts
^{88}Kr (2392 keV)	80320 (2.4%)	29760 (1.9%)
^{142}La (2398 keV)	47940 (2.6%)	28700 (2.0%)
^{142}La (2542 keV)	52540 (1.0%)	21140 (1.8%)
^{138}Cs (2640 keV)	35340 (2.6%)	14290 (4.4%)
^{142}La (2971 keV)	17000 (2.0%)	6660 (3.8%)

7.4.2 Sensitivities of measured and calculated fission rate ratios

During the analysis of the WOLF-B experiments, the measured fission rate ratios have been found to be very sensitive to the assumed axial elevation of the spent fuel samples in their measurement positions. In addition, the results based on ^{89}Rb were very sensitive to the assumed spent fuel composition and to the measured cooling time between the end of irradiation and the beginning of the gamma-ray counting.

In the following, the corresponding sensitivities of the LIFE@PROTEUS results, in relation to measurements of the five gamma-ray lines ^{88}Kr (2392 keV), ^{142}La (2398 keV), ^{142}La (2542 keV), ^{138}Cs (2640 keV) and ^{142}La (2971 keV), are discussed.

- **Sensitivity to axial position of fuel pins**

The position of the samples is needed to calculate the solid angle and attenuation correction factors used for the derivation of measured fission rates. The high sensitivity to the spent fuel measurement position during WOLF-B was caused by the fact that the samples were not measured directly in front of the detector but in an axial position below the detector. In this position, a slight change in sample elevation had a large impact on the amount of attenuating material between sample and detector, as well as on the solid angle between them.

One main difference to the WOLF-B campaign is that during LIFE@PROTEUS, the spent and the fresh fuel pins will be measured at the same position in front of the detector. Shifting the pins axially will therefore not change significantly the distance and the solid angle between detector and pin. Thus, the sensitivities towards the axial elevation are comparable to those related to the fresh fuel measurement position during WOLF-B, which were in the order of less than 0.8% for a relatively large displacement of 5 mm.

- **Sensitivity to assumed spent fuel composition**

Saturation and decay corrections used for the derivation of measured fission rates require one to calculate effective fission yields, i.e. average fission yields weighted by the contributions a_i of the major fissioning actinides (^{235}U , ^{238}U , ^{239}Pu and ^{241}Pu) to the total number of fissions. The contributions a_i are obtained with MCNPX calculations and depend on the modelled composition

of the fuel. Consequently, the saturation and decay correction factors, for fission products which have very different fission yields for fissions in ^{235}U , ^{238}U , ^{239}Pu and ^{241}Pu , are highly dependent on the assumed fuel composition. For example, in WOLF-B, the measured fission rate ratio obtained using the ^{89}Rb peak changed by 1.6% when using the calculated CASMO-4E composition of the 36 GWd/t sample instead of the measured one (see Subsection 5.3.4). In comparison, the results based on ^{138}Cs and ^{142}La were affected by less than 0.2%, because their fission yields are nearly independent of the fissioning isotope.

Among the three fission products ^{138}Cs , ^{88}Kr and ^{142}La which are recommended for the LIFE@PROTEUS experiments, only ^{88}Kr has very different fission yields, varying from 3.45% for ^{235}U to 1.25% for ^{239}Pu and 1.01% for ^{241}Pu (see Table 7.10). This is comparable to the differences in the fission yields of ^{89}Rb , so that a sensitivity similar to that of ^{89}Rb can be expected for ^{88}Kr .

• Sensitivity to cooling time

The cooling time between the end of irradiation and the beginning of measurement is needed for the calculation of the saturation and decay correction factors used in the derivation of measured fission rates.

The cooling time during WOLF-B was 5 min. A sensitivity study showed that a discrepancy of as small as 1 second between the measured and the real cooling time would result in a bias of the fission rates derived from ^{89}Rb of about 1.6% (see Subsection 5.3.5). This high sensitivity is mainly caused by the decay of the parent isotope ^{89}Kr , which has a very short half-life of 189 seconds. In comparison, the fission products ^{138}Cs and ^{142}La and their parent isotopes have relatively long half-lives (at least 10 min), so that an error in the cooling time of 1 second had only a marginal impact (less than 0.2%) on the measured fission rate ratios.

The cooling time for LIFE@PROTEUS is also assumed to be 5 min. Fission rates will be derived from ^{138}Cs , ^{142}La and ^{88}Kr activities. ^{88}Kr has a half-life of 2.8 h and no parent isotope which has to be considered in the analysis. Consequently, the sensitivity to uncertainties in the measured cooling times is expected to be negligible.

7.4.3 Results for uncertainties and sensitivities

The combined uncertainties on the individual gamma-ray line estimates of measured fresh-to-60 GWd/t fission rate ratios in LIFE@PROTEUS, as well as on their weighted mean, are given in Table 7.14. The uncertainties are also split into contributions from the net-count areas and from the nuclear data. Compared to WOLF-B, there is not any contribution from the MCNPX calculation of the solid angle and attenuation correction factors, because the ratio of these correction factors in LIFE@PROTEUS is equal to unity and cancels out in the fission rate ratio (see Eq. 7.6).

The combined 1σ uncertainties on the measured fission rate ratios are between 2 and 3.5% for the gamma-ray peaks ^{88}Kr (2392 keV), ^{142}La (2398 keV) and ^{142}La (2542 keV), and between 4.5 and 5.5% for ^{138}Cs (2640 keV) and ^{142}La (2971 keV). The 1σ uncertainty on the weighted mean is 1.6%.

The uncertainties on the net-count areas are the main contributions (3 to 5%) to the combined uncertainties of the individual gamma-ray line estimates. The uncertainties due to the nuclear

Table 7.14: Estimated uncertainties and sensitivities for experimental fresh-to-60 GWd/t fission rate ratios in LIFE@PROTEUS.

	^{88}Kr (2392 keV)	^{142}La (2398 keV)	^{142}La (2542 keV)	^{138}Cs (2640 keV)	^{142}La (2971 keV)	weighted mean
Total uncert.	3.3%	3.5%	2.3%	5.3%	4.4%	1.6%
Statistical uncert.	3.0%	3.3%	2.0%	5.1%	4.2%	
Nuclear data uncert.	1.4%	1.2%	1.1%	1.3%	1.2%	
Sensitivities to an axial displacement of 5 mm of spent fuel pin during measurements:						
	<0.8%	<0.8%	<0.8%	<0.8%	<0.8%	
Sensitivities to assumed burnt fuel composition:						
	high	low	low	low	low	
Sensitivities to an increase of cooling time by 1 sec:						
	<0.2%	<0.2%	<0.2%	<0.2%	<0.2%	

data are 1.1% to 1.4%, and are mainly due to differences in the effective fission yields for fresh and spent fuel.

It should be pointed out that the quoted statistical uncertainties could only be broadly estimated and are most likely overestimated, whereas the contributions from the nuclear data uncertainties are accurately calculated. Moreover, the statistics of the measurements can be improved, if needed, in a relatively easy way by conducting more irradiations per measured fuel pin. The uncertainties on the measured fission rates due to the nuclear data uncertainties, however, will stay the same as they are related to differences in the fuel compositions.

For comparison with WOLF-B, Table 7.14 also contains the sensitivities of the measured fission rate ratios to the axial position of the measured fuel pins, to the burnt fuel composition, and to the assumed cooling time between the end of irradiation and the beginning of data acquisition. These sensitivities are largely reduced in the LIFE@PROTEUS measurements as compared to WOLF-B.

The only significant sensitivity is expected for the fission rate ratios derived from the ^{88}Kr (2392 keV) line; this is with respect to the assumed spent fuel composition. As mentioned earlier, the fission yields of ^{88}Kr for ^{235}U , ^{238}U , ^{239}Pu and ^{241}Pu are very different one from another (see Table 7.10). Thus, the effective fission yield in this case will strongly depend on the assumed sample compositions, and so will the derived fission rate ratio.

7.5 Further optimisation possibilities

Several measures for improving the counting statistics in the context of the preliminary design of the LIFE@PROTEUS measurement station are discussed in this section. The first two measures represent optimisations of the current set-up without changing the general concept of the measurement station. These are a different detector position within the lead shielding and the use of a HPGe detector with a larger germanium crystal. Compared to these, the last two measures

are less easy to implement as they would require large modifications of the measurement station set-up. These are an alternative measurement geometry for the fresh fuel pins as compared to the burnt ones and the use of several detectors.

Typically, measures to increase counting statistics also involve an undesired increase of system dead time during measurement. Using a detector with a pre-amplifier designed for very high count rates could help to mitigate the problem of excessive dead times. Nonetheless, the final measurement station will always be a compromise between counting statistics and system dead time.

- **Moving the detector closer to the pin within the lead shielding**

In the preliminary design, the distance between the detector and the pin is about 22 cm, containing a filter of about 12 cm lead and 5.5 cm water.

Higher count rates in the measured gamma-ray lines could be obtained by moving the detector closer to the fuel pin within the lead. This would increase the solid angle between pin and detector, as well as decrease the attenuating material between them. The drawback is that the system dead time due to the intrinsic activity of the spent fuel pin also increases during the measurement.

As an example, a measurement set-up was modelled where the distance between pin and detector was only about 21 cm, reducing the lead filter by 0.95 cm to 11.05 cm. With this set-up, the net-count areas of the high-energy peaks obtained for an irradiation of 3 h at 800 W could be increased by about 75%. On the other hand, the total gamma-ray flux due to the intrinsic activity of a spent fuel pin would double. For a 60 GWd/t pin, this would correspond to a system dead time of about 50% (compared to about 30% for the preliminary set-up).

In general, a smaller amount of lead filter increases the total (i.e. uncollided and collided) gamma-ray flux in the detector (which determines the system dead time) more than it increases the count rates of the high-energy peaks. Effectively, the achievement of higher count rates in the high-energy peaks is always paid for with an even higher increase of undesired low energy counts. Nonetheless, further optimisation of the lead filter between pin and detector should be carried out for the final measurement station.

- **Bigger detector crystal**

The detector used in the preliminary design of the LIFE@PROTEUS measurement station is the ORTEC HPGe detector model GEM-15180-P (3600 V), which was employed in the WOLF-B final measurements (see Table 4.1). The crystal of the detector has a length of 57.2 mm and a radius of 50.0 mm; the relative detection efficiency of the model is 18%⁵.

The detection efficiency of an HPGe detector is mainly determined by its crystal size. ORTEC offers HPGe detectors having the same outer dimensions but different crystal sizes. The maximum relative detection efficiency, for a detector with the same outer dimensions which could be fitted into the preliminary design of the measurement station, is 35% [ORT 03b].

⁵The detection efficiency of germanium detectors is generally expressed relative to that of a standard 3 inch x 3 inch (7.62 cm x 7.62 cm) cylindrical NaI(Tl) scintillation crystal [Knoll 00].

Generally speaking, bigger detector crystals lead to higher detection efficiencies than smaller ones. This is specially true for high-energy gamma-rays. In other words, implementing a bigger detector would increase the net-count areas more in the high-energy gamma-ray lines than in the lower energy range corresponding to the intrinsic activity of the spent fuel pins. In addition, the probability to fully deposit the gamma-ray energy in the crystal is enhanced leading to an improved peak-to-Compton ratio which would ease the peak fitting process.

A detector with a bigger germanium crystal clearly represents an attractive measure to optimise the measurement station.

- **Different measurement geometry for fresh fuel pins**

For LIFE@PROTEUS, it is foreseen to measure both fresh and spent fuel pins in the same position in front of the detector. This has the advantage to minimise the sensitivity of the fission rate ratios to errors in the solid angle and attenuation correction factors, as well as to errors in the positioning of the measured sample. In addition, it simplifies the design of the measurement set-up.

However, a filter of 12 cm of lead is only required for spent fuel measurements, where the system dead times due to the intrinsic gamma-ray activity need to be kept reasonably low. For measurement of fresh fuel pins, this filter is clearly oversized.

Higher count rates could be obtained by measuring the fresh fuel pin in a different position with a less strongly attenuating filter, as was done during the WOLF-B experiments. The measurement geometry for the fresh fuel should only be optimised to prevent any large dead time due to the induced gamma-ray activity in the fuel. As the freshly induced activity, however, is low and decreases fast, it is much less problematic than the intrinsic activity of burnt fuel.

- **Several detectors**

In PROTEUS, a gamma-ray scanner with two back-to-back HPGe detectors was routinely used to derive fission rate ratios in fresh fuel pins during the LWR-PROTEUS programme. Using two detectors back-to-back, with the pin in their middle, has the advantage to average any angular dependencies of the fission rate, smooth out any error in the pin position and also increase the counting statistics without increasing the measurement time [Murphy 99].

In principle, the use of several detectors is very attractive because, as opposed to the previous three measures, it would increase the counting statistics without affecting the system dead time. It should be possible, for example, to fit two gamma-ray detectors of the same kind next to each other inside the lead shielding of the LIFE@PROTEUS measurement station, in a way that the solid angle and attenuation between detector(s) and pin are comparable to that in the preliminary design. In this way, the number of conducted irradiations could be decreased drastically. Two independent estimates could be obtained for each measured fission rate ratio and later be combined to decrease the uncertainty.

However, each detector would need its own cooling device, its own high voltage supply and its own multi-channel analyser. Given the limited space in the measurement station for LIFE@PROTEUS, the use of two detectors may be difficult to implement.

7.6 Chapter summary

A preliminary design of the measurement station for the LIFE@PROTEUS programme has been presented and analysed. The measurement station features a distance between measured pin and detector of about 22 cm, of which 12 cm are lead and 5.5 cm water. The detector is positioned about 1.2 m above the active test zone of the reactor and is shielded against the reactor fuel by more than 100 cm of water and 12 cm of lead.

As a first prerequisite, it has been demonstrated that the detector position offers sufficient neutron shielding against the fast neutron background from the reactor core during irradiation. This means that no constraints due to fast neutron damage in the detector crystal are expected during LIFE@PROTEUS. As a second prerequisite, the axial resolution of the detection system has been demonstrated to be in the required range (~ 50 cm), such that axial heterogeneities in the fission rate due to spacers can be minimised. As a third prerequisite, it has been shown that the lead filter between pin and detector adequately limits the dead time of the detection system (30%). Low dead times are desirable for the future experiments, since the dead-time correction increases the uncertainties on the measured net-count areas.

Having demonstrated that neither neutron nor gamma-ray background would constrain the conducted experiments, the achievable accuracy of measured fission rate ratios between fresh and 60 GWd/t spent fuel pins has been estimated. In terms of achievable number of net counts, five gamma-ray lines are found particularly suitable for LIFE@PROTEUS: ^{88}Kr (2392 keV), ^{142}La (2398 keV), ^{142}La (2542 keV), ^{138}Cs (2640 keV) and ^{142}La (2971 keV). Compared to WOLF-B, the fission rates in the fuel pins of the LIFE@PROTEUS test lattice are about 10 times lower and result in lower count rates in the gamma-ray lines of the observed fission products. The gamma-ray line count rates could be increased by longer irradiation times of up to 3 h, except for the short-lived ^{89}Rb and ^{95}Y . Therefore, the two peaks ^{89}Rb (2570 keV) and ^{95}Y (3576 keV), which had been used in WOLF-B, will not be suitable anymore in LIFE@PROTEUS.

For LIFE@PROTEUS, a recommended measurement strategy is to irradiate and measure each pin three times. Each irradiation should last 3 h at a reactor power of 800 W and the results should be analysed on the sum of the three measured spectra. Following this measurement strategy, the obtained net-count areas are estimated to be between 17000 and 80000 counts for the fresh fuel pin, and between 7000 and 30000 counts for the 60 GWd/t fuel pin. Fresh-to-60 GWd/t fission rate ratios based on these results are estimated to have final uncertainties of about 1.6%.

The fission rate ratios measured in WOLF-B showed considerable sensitivities towards the axial position of the spent fuel sample during the measurement. In addition, the results based on the ^{89}Rb (2570 keV) peak were very sensitive with respect to the assumed spent fuel composition and the cooling time between the end of irradiation and the beginning of measurement. These sensitivities are almost entirely ruled out in the proposed LIFE@PROTEUS measurements.

As all fuel pins will be measured in front of the detector in the same position, the geometrical correction factors will be almost identical for all pins, and small shifts in the axial position will not have significant impact on the measurements. Furthermore, because all selected fission products have half-lives longer than 30 min, a shift in the cooling time of some seconds will not change the derived fission rate ratios. Finally, only the fission rate ratios derived from ^{88}Kr are sensitive to the spent fuel composition. This is because of the strongly differing fission yields of

^{88}Kr for the major fissioning actinides. The use of the ^{88}Kr (2392 keV) peak is therefore only recommended in cases where the burnt fuel composition is well known. In comparison, the, ^{142}La (2398 keV), ^{142}La (2542 keV), ^{138}Cs (2640 keV) and ^{142}La (2971 keV) peaks do not have this limitation.

The presented measurement station being a preliminary design proposal, several possibilities have been discussed for further improving the counting statistics of the measured gamma-ray lines. These are the amount of filter between pin and detector, the detector crystal size, an optimised measurement geometry for fresh fuel pins and the use of several detectors.

In conclusion, it can be stated that it will be possible to measure fission rate ratios between fresh and 60 GWd/t spent fuel pins during LIFE@PROTEUS with a satisfactory accuracy of 1 to 2%. The main part of the uncertainties is statistical. However, nuclear data related uncertainties are significant (1-1.4%) and represent an important constraint.

The presented design for the measurement station should be optimised further to improve the measured count rates per irradiation. In particular, employing a detector with a bigger germanium crystal should be considered. Nonetheless, it is pointed out that the main limitation remains the relatively low fission rates in the LIFE@PROTEUS test lattice. Consequently, long irradiation times and repetitions of irradiations appear to be the most adequate measures to increase the statistical accuracy.

Bibliography

- [Fassbind 09] M. Fassbind, O. Köberl & M. Murphy. *Betriebsvorschriften PROTEUS, Phase III der LWR-Experimente*. Internal Report AW-41-06-01, Rev. 3, PSI, 2009.
- [Grimm 07] P. Grimm. *CASMO-4E Calculations of the Isotopic Inventories of the LWR-PROTEUS Phase II Irradiated Fuel Samples from KKG*. Internal Report TM-41-07-07, PSI, 2007.
- [Grimm 09] P. Grimm. *Zusammensetzung von abgebranntem Brennstoff für die Auslegung der LIFE-Experimente*. Internal Report TM-41-09-09, PSI, 2009.
- [Jordan 09] K.A. Jordan. *Dosimetry Calculations of the PROTEUS Reactor Upgrade*. Internal Report TM-41-10-06, PSI, 2009.
- [Knoll 00] G.F. Knoll. *Radiation Detection and Measurements*. Third edition, page 450, ISBN 0-471-07338-5, 2000.
- [Murphy 99] M.F. Murphy. *The LWR-PROTEUS Fuel Pin γ -Scanning Machine*. Proceedings of the Annual Meeting on Nuclear Technology'99, Karlsruhe, Germany, page 425-428, 1999.
- [Murphy 10] M.F. Murphy, G. Perret, O. Köberl, K.A. Jordan, P. Grimm, H. Kröhnert & M. Zimmermann. *Large-scale Irradiated Fuel Experiments at PROTEUS Research Program*. PHYSOR Conference 2010, Pittsburgh, Pennsylvania, USA, CD-ROM, ISBN 978-89448-079-9, 2010.
- [ORT 03b] ORTEC. *GEM Series Coaxial HPGE Detector*, Product Configuration Guide, 2003.
- [Perret 10a] G. Perret. *personal communication*. PSI, 2010.

Chapter 8

Summary and conclusions

The present doctoral research has involved the development of a novel measurement technique to determine fission rates in fresh and burnt nuclear fuel. The new technique has been developed in view of the future experimental programme LIFE@PROTEUS, where interfaces between lattices of fresh and burnt fuel pins are planned to be studied in the zero-power reactor PROTEUS. To discriminate against the high intrinsic activity of the burnt fuel, the investigated approach uses gamma-ray lines above 2200 keV, emitted by short-lived fission products, instead of the commonly used lower-energy lines.

This chapter concludes the presented work. A summary of the thesis is given in Section 8.1. The main achievements and findings are reviewed in Section 8.2. Recommendations for future work are given in Section 8.3, while Section 8.4 provides the concluding remarks.

8.1 Summary

Chapter 1 is the introduction to the thesis and presents the motivation behind the current research. The chapter starts with a general overview of present-day nuclear power generation and describes recent and anticipated developments in modern light water reactors, as also the associated challenges. The main goals of the envisaged LIFE@PROTEUS programme are then presented, and followed by a description of the scope and outline of the thesis.

Chapter 2 provides more specific background information. It gives the current status of measurement techniques using gamma-rays emitted from fission products, as well as a description of the PROTEUS reactor and its recent experimental programmes. Furthermore, the planned LIFE@PROTEUS programme is described in detail, focusing on the required refurbishment of the reactor and on the planned test zone configurations. At the end of the chapter, the two computer codes mainly used in this work, MCNPX and HELIOS, are briefly introduced.

Chapter 3 to Chapter 7 deal with the actual work carried out in the framework of the present research. **Chapter 3** is devoted to three preliminary measurement campaigns which were carried out to establish an extensive database of gamma-ray spectra from short-lived fission products. In the first campaign, fresh UO_2 pellets were irradiated at the Belgian BR1 reactor. Using the fast rabbit system of the reactor, the measurements focused on extremely short half-lives in the range of seconds and minutes. The second preliminary measurement campaign took place at the

PROTEUS reactor. Following irradiation, the measurement of a fresh fuel sample was carried out on top of the reactor shielding, the aim being to investigate longer-lived fission products with half-lives of up to several hours.

The third preliminary campaign, the so-called WOLF-A campaign, was the first which also included burnt fuel samples with burn-ups up to 80 GWd/t. For this measurement campaign, the samples were loaded into a special sample changer made of steel, which was placed on top of the reactor inside the reactor shielding and was used to introduce the samples into the test lattice of the reactor. The gamma-ray detector was placed below the sample changer, and the fuel samples were measured in front of it.

Chapter 4 describes the main measurement campaign carried out during the present research. This was the WOLF-B campaign, during which freshly induced gamma-ray activity was measured in both fresh and burnt fuel samples. For the WOLF-B campaign, the sample changer had been modified to allow the fuel samples to be introduced into different positions of the test lattice and to allow the gamma-ray detector to be placed inside the steel body of the sample changer. A fresh and three burnt 40 cm long fuel samples (nominal burn-ups of 36, 46 and 64 GWd/t) were employed in the campaign. One by one, they were irradiated and their gamma-ray activities after irradiation were measured inside the sample changer. The fresh fuel sample was measured in front of the detector with about 12 cm of steel as filter. Given their intrinsic background activity, the burnt fuel samples were measured further away, to avoid too high system dead times.

The main focus of the campaign was on the investigation of the fresh and the 36 GWd/t burnt fuel samples, irradiated in different positions of the PROTEUS test lattice. Due to the fast neutron flux which reached the detector during reactor operation and damaged the detector crystal, irradiation times were kept relatively short in order to protect the detector as much as possible; they were 15 min for the spent fuel sample and 30 min for the fresh fuel sample. After the main measurements, using the fresh and the 36 GWd/t samples in three different lattice positions, additional irradiations were carried out using the 46 and the 64 GWd/t samples.

Chapter 5 describes the analysis of the WOLF-B campaign, i.e. the derivation of experimental fission rate ratios based on the measured short-lived fission product gamma-rays. Inter-position and inter-sample fission rate ratios have been derived. Inter-position fission rate ratios compare the same sample in different irradiation positions, and have been obtained for the fresh and for the 36 GWd/t samples. Inter-sample fission rate ratios compare different samples in the same irradiation position and have been obtained between the fresh and the 36 GWd/t samples, as well as between the fresh and the 46 GWd/t samples. Individual estimates of the fission rate ratios were derived separately for each of the gamma-ray lines of interest, and then combined into a single weighted mean to yield the final result.

The different steps of the analysis, which are described in detail, are the deconvolution of the gamma-ray spectra to obtain the net-count areas of the gamma-ray peaks, the correction for the saturation and decay of the fission products during and after irradiation, and the correction for the solid angle and attenuation between the samples and the detector. A detailed uncertainty analysis and sensitivity studies have been described as well.

Chapter 6 presents calculated results of the fission rate ratios as obtained using an MCNPX whole-reactor model of PROTEUS. The Monte Carlo analysis carried out includes an assessment of the sensitivities of the results towards different parameters such as the burnt fuel composition

and its modelling, and the axial position of the fuel samples. The chapter also gives the comparison of the calculated fission rate ratios with the experimental values presented in the previous chapter.

In **Chapter 7**, as the final part of the current research, a preliminary set-up for a measurement station for the LIFE@PROTEUS programme is presented and evaluated. The achievable accuracy for the envisaged fission rate measurements in fresh and burnt fuel has been estimated, and recommendations are made for an appropriate measurement strategy.

8.2 Main achievements and findings

This section reviews the main achievements of the present research work, together with the most relevant findings.

- **Measurement of freshly induced fission products in burnt fuel**

During the WOLF-B campaign, it has been possible, for the first time in a zero-power research reactor, to measure the freshly induced fission products in burnt fuel after short re-irradiation at low power. As illustration, Fig. 8.1 shows two spectra of the 36 GWd/t burnt fuel sample, one before and the other after irradiation in the PROTEUS reactor.

The measurement of freshly produced fission products in burnt fuel samples in itself represents a considerable challenge, because of the intrinsic gamma-ray and neutron activity of the burnt fuel. The large intrinsic activity requires the operator and experimentalist to be shielded from the measurement station. Furthermore, an appropriate filter between sample and detector has to be employed to limit the dead time of the detection system due to the intrinsic gamma-ray background of the measured burnt fuel.

To address the first issue, at PROTEUS, the measurements had to be carried out inside the reactor shielding. There, however, the detector had to be shielded against neutron and gamma-ray background from the reactor core. This was done by placing the detector within the steel flask of the sample changer, which also served to introduce the fresh and burnt fuel samples into the reactor core for irradiation. Inside the sample changer, the detector was sufficiently shielded from both gamma-ray and neutron backgrounds from the core during the data acquisition period following the irradiation. However, the relatively high fast neutron flux (about $8.5 \cdot 10^5 \text{s}^{-1} \text{cm}^{-2}$ at 800 W) reaching the detector during the irradiation itself damaged the detector crystal and remained problematic. In fact, this was the main limitation in the measurements, preventing long irradiation times and limiting the number of possible irradiations.

As regards the filter between the measured fuel and the detector inside the sample changer, two different positions were used for the measurements of the fresh and burnt fuel samples. The fresh fuel could be measured directly next to the detector with about 12 cm of steel as filter, whereas the burnt fuel samples had to be moved further down, i.e. away from the detector. The distance between the top of the measured burnt fuel sample and the detector was about 26 cm.

Given the short half-lives of the investigated freshly induced fission products, the dead time of the detection system varied significantly during the measurements. Therefore, for a sufficiently

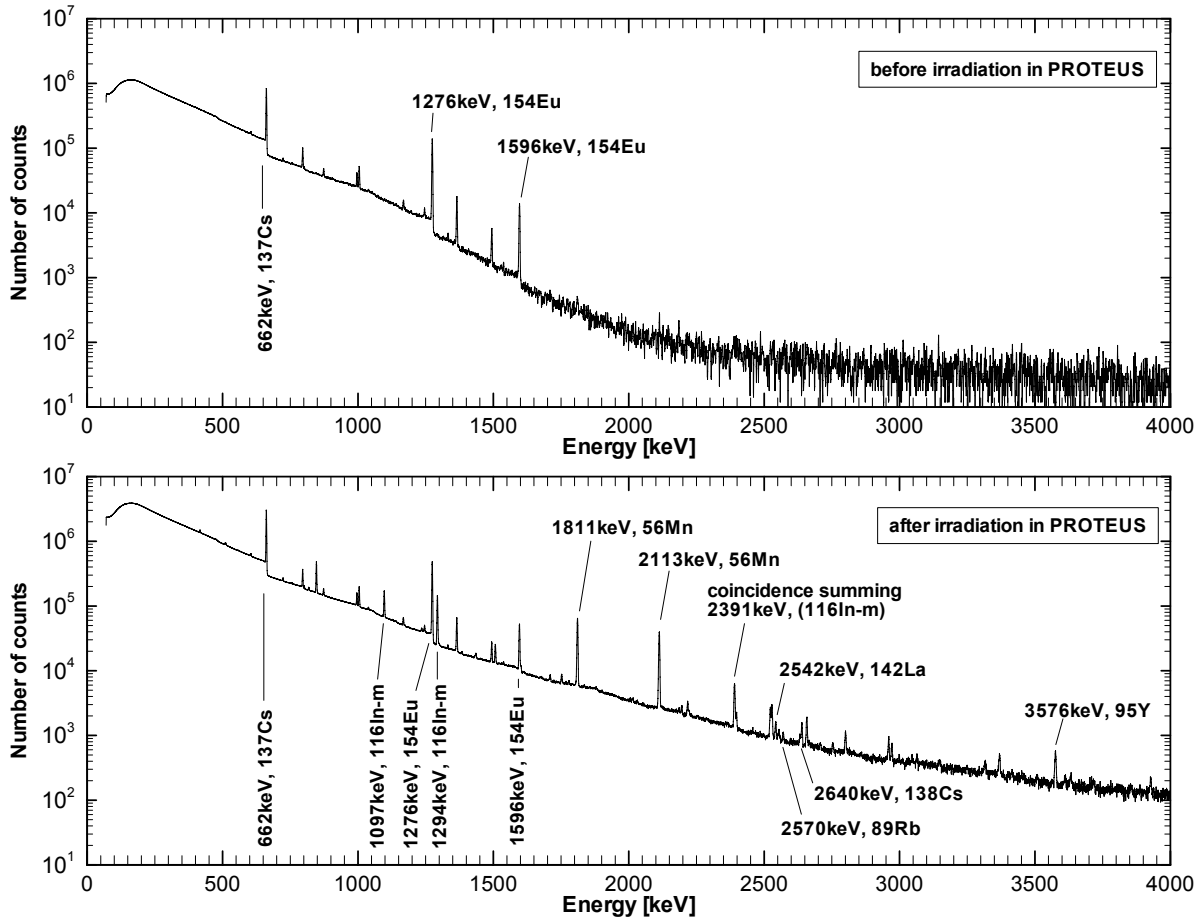


Figure 8.1: Gamma-ray spectra of the 36 GWd/t burnt sample before and after irradiation in PROTEUS.

accurate quantitative analysis of the acquired spectra, the detection system was required to properly correct for the changing dead times. In this work, the deployed EG&G ORTEC DSPEC Plus digital multi-channel analyser fulfilled this requirement.

• Identification of suitable gamma-ray lines

With the help of the preliminary measurements on fresh fuel, a list of gamma-ray lines with potential for being used for the derivation of experimental fission rates in fresh and burnt fuel was established and is shown in Table 8.1. The selection of the gamma-ray lines was made based on several criteria. The main requirement was an energy above 2200 keV, in order to be able to extract the gamma-ray line from the intrinsic background of the burnt fuel. A second requirement was the potential for good counting statistics resulting from a high cumulative fission yield for the corresponding fission product and a high gamma-ray intensity. Furthermore, the counting statistics is favoured for energies relatively close to 2200 keV, because of the higher detection efficiency of HPGe detectors at lower energies. To ease the analysis of the spectra, a third requirement for the gamma-ray line has been a minimal interference with other peaks. Finally, considering the derivation of measured fission rate ratios, a last requirement for the fission product has been to have similar fission yields for the different fissioning isotopes (mainly ^{235}U , ^{238}U , ^{239}Pu and ^{241}Pu). This is desirable to avoid high sensitivities of the derived experimental results to the fuel composition.

Table 8.1: Potential gamma-ray lines for the derivation of fission rates in fresh and burnt fuel.

Fission product	Half-life	Cumulative fission yields [%]		Gamma-ray lines (intensity)
		$Y_{th,U5}$	$Y_{th,P9}$	
^{88}Kr	2.84 h	3.54 (1.8%)	1.25 (2.8%)	2392 keV (35%)
^{142}La	1.52 h	5.86 (1.7%)	4.97 (1.1%)	2398 keV (13.3%), 2542 keV (10%), 2971 keV (3.2%)
^{138}Cs	33.4 min	6.69 (1.7%)	5.94 (2.7%)	2218 keV (15.2%), 2640 keV (7.6%)
^{89}Rb	15.4 min	4.69 (1.2%)	1.68 (1.9%)	2570 keV (10.2%)
^{95}Y	10.3 min	6.47 (1.1%)	4.82 (2.0%)	2632 keV (4.8%), 3576 keV (6.4%)
^{84}Br	31.8 min	1.01 (1.9%)	0.45 (4.3%)	3928 keV (6.8%)
^{90m}Rb	4.3 min	1.36 (14.1%)	0.71 (14.0%)	2753 keV (11.5%), 3317 keV (14.3%)
^{90}Rb	2.6 min	4.37 (3.0%)	1.27 (5.4%)	3383 keV (6.7%) , 4135 keV (6.7%), 4365 keV (8%)

As can be seen in Table 8.1, not all of the listed gamma-ray lines fulfill these requirements equally well. The two fission products ^{142}La and ^{138}Cs (bold in Table 8.1) emerge as the most universally applicable candidates, having several gamma-ray lines in the energy range between 2200 to 3000 keV and having similarly high fission yields for the different fissioning isotopes. However, the finally chosen subset of the gamma-ray lines listed in Table 8.1, which should be used for the derivation of fission rate ratios in a given situation, will always depend on the particular measurement conditions.

For the WOLF-B campaign, only five of the listed gamma-ray lines have been included in the quantitative analysis, namely ^{142}La (2542 keV), ^{89}Rb (2570 keV), ^{95}Y (2632 keV), ^{138}Cs (2640 keV) and ^{95}Y (3576 keV). The other gamma-ray lines either did not have sufficiently high count rates or suffered from interference with background peaks.

Because of their rapid saturation, ^{89}Rb and ^{95}Y have been found to be advantageous in situations in which only short irradiations are possible, as was the case in WOLF-B. The fission products ^{90}Rb and ^{90m}Rb , however, are extremely short-lived and were therefore not suitable for the WOLF-B campaign, where the time needed to bring the fuel sample into its measurement position after irradiation was 2 to 5 min.

As regards the observed background peaks, these mainly originated from activated materials surrounding the detector crystal. The main activation products were ^{56}Mn in the steel of the sample changer and ^{116m}In in the detector mount. In particular, the two gamma-ray lines ^{88}Kr (2392 keV) and ^{142}La (2398 keV) suffered from interference with the ^{116m}In (2391 keV) coincidence sum peak of its gamma-rays at 1097 keV and 1293 keV. With increased degradation of detector resolution due to the fast neutron damage, the ^{142}La (2971 keV) line suffered interference with the ^{56}Mn (2960 keV) peak. Furthermore, the ^{138}Cs (2218 keV) line interfered with the prompt ^1H (2223 keV) gamma-rays emitted from (n, γ) reactions in the polyethylene filter around the detector, caused by the intrinsic neutron activity of the burnt fuel.

- **Derivation of experimental fission rate ratios in fresh and burnt fuel samples**

Based on the gamma-ray measurements carried out during the WOLF-B campaign, first-of-their-kind experimental results have been obtained for inter-position and inter-sample fission rate ratios for fresh and burnt fuel samples.

Regarding the deconvolution of the gamma-ray spectra to determine the net-count areas of the peaks, one challenge has been the lack of calibration sources to cover the energy range up to 3600 keV. Another challenge, particular to the WOLF-B campaign, has been the non-Gaussian peak shapes caused by the neutron damage in the detector crystal. The analysis software Hyperlab has been found to be specially suitable in this context, since it does not required any a priori energy and resolution calibrations and is able to fit even highly distorted peaks.

The saturation and decay corrections for ^{89}Rb have been found to be particularly sensitive to the fuel sample composition because the fission yield strongly depends on the fissioning isotope. Fission rate ratios based on gamma-rays emitted by ^{142}La , ^{138}Cs and ^{95}Y are less dependent on the fuel composition of the measured sample, since the fission yields of these are quite similar for the different fissioning isotopes. This is of course particularly important for burnt fuel, the composition of which is often estimated via depletion calculations rather than being measured.

The solid angle and attenuation correction factors in WOLF-B have been found to be particularly sensitive to the axial positioning of the fuel sample (1.5%/1 mm). This resulted from the burnt fuel samples having to be positioned below the detector, rather than in front of it.

The 1σ uncertainties on the obtained inter-position fission rate ratios were almost purely due to the counting statistics. They were about 0.6% for the fresh sample and about 2.3% for the 36 GWd/t burnt sample.

The 1σ uncertainties on the inter-sample fission rate ratios between the fresh and the 36 GWd/t samples, and between the fresh and the 46 GWd/t samples, were about 1.7-2.0% and 3.4%, respectively. Again, these were mainly due to the counting statistics. However, in this case, the contribution of nuclear data uncertainties in estimating the effective fission yields in the burnt fuel sample amounted to 1.0-1.4%. It has been pointed out that, in contrast to the statistical uncertainties, these nuclear-data related uncertainties will not to be easy to reduce in the future, unless new, more accurate fission yield measurements are carried out.

- **First C/E values for fission rate ratios in fresh and burnt fuel samples**

As discussed previously, the main goal of the LIFE@PROTEUS programme is to experimentally validate neutronics codes for the calculation of power, i.e. fission rate, distributions across interfaces between fresh and highly burnt fuel regions. The calculation-to-experiment (C/E) comparisons, which have currently been presented for fission rate ratios in fresh and burnt fuel, are clearly first-of-their-kind in this context. The calculational results were obtained via whole-reactor modelling of PROTEUS using MCNPX.

In general, the agreement between calculations and measurements has been good with a maximum deviation of about 4.5%. The uncertainties on the C/E values mainly consisted of those on the measured results. As mentioned above, the 1σ uncertainties on the measured inter-position

fission rate ratios for the fresh and the 36 GWd/t samples were about 0.6% and 2.3%, respectively. Those for the inter-sample fission rate ratios were about 2% for the fresh-to-36 GWd/t comparison and 3.4% for the fresh-to-46 GWd/t comparison. Thus, the calculations have been found to agree with the experiments within 1-3 standard deviations.

- **Design of improved measurement station for LIFE@PROTEUS**

As a final part of this thesis, a measurement station for the LIFE@PROTEUS programme has been presented and evaluated. An optimised measurement strategy for fission rate ratios between fresh and burnt fuel pins irradiated during LIFE@PROTEUS has been elaborated and the expected accuracy of the measurements has been estimated. The principal findings in this context are included in the following section.

8.3 Recommendations for future work

This section summarises the recommendations for future work. These are related mainly to future measurement set-ups and strategies, in particular those to be employed in the envisaged LIFE@PROTEUS experiments. Additional recommendations address the analysis of the measurements, as well as the calculation of fission rate ratios using MCNPX. Finally, additional potential applications of the new measurement technique are briefly presented.

- **Measurement set-up and strategy**

Two main requirements for future measurement set-ups are an adequate neutron shielding against the neutrons emitted by the reactor core to prevent any neutron damage of the detector crystal, and an appropriate filter between the measured fuel and the detector to limit the detection system dead time. An additional requirement for the LIFE@PROTEUS measurements is an axial detection resolution better than 50 cm while measuring full-length fuel pins. The latter requirement is mainly aimed at avoiding the need to account for axial inhomogeneities in the fuel composition and in the fission rate profile, introduced by spacers during irradiation in the power plant and in PROTEUS.

In the proposed preliminary LIFE@PROTEUS measurement set-up (see Fig 7.2), a sufficient neutron shielding from the reactor core is guaranteed by a large amount of water (more than 1 m) between the measurement station and the core. A filter of about 12 cm of lead is suggested to keep the system dead time due to the intrinsic gamma-ray background of a 60 GWd/t burnt fuel pin at about 30%. Additional lead shielding on top of the detector is necessary to ensure a reasonable axial detection resolution.

Although the presented preliminary measurement station has been demonstrated to fulfill the main requirements, it is recommended to investigate further optimisations to increase the counting statistics. These could be an optimised filter between pin and detector, an optimised detector crystal size (i.e detection efficiency), the use of two different measurement positions for fresh and burnt fuel, and the use of multiple detectors. The use of a detector with a bigger crystal is the preferred option, since this could be easily implemented and also because this preferentially favours high-energy gamma-ray lines.

Once the measurement station is designed, the net-count rates of the high-energy gamma-ray lines depend on the reactor power, the irradiation time and the number of repeated irradiations. The fission rates in the LIFE@PROTEUS test lattice will be relatively low compared to those in the WOLF-B campaign. Consequently, the measurements will have to emphasise longer-lived fission products (^{142}La , ^{88}Kr and ^{138}Cs), the count rates of which can be increased by long irradiation times. The suggested measurement strategy consists in irradiating each pin at 800 W for 3 h, repeating each measurement 3 times and then carrying out the analysis on the sum of the 3 acquired spectra.

Regarding the data acquisition, as the system dead time is expected to be about 30% for burnt fuel measurements and to change during the measurements, it is highly recommended to use an acquisition system allowing for zero-dead-time corrections, e.g. the DSPEC Plus from ORTEC. Using the DSPEC Plus, both the spectrum corrected for the system dead time (ZDT spectrum) and its variance spectrum (ERR spectrum) should be recorded in parallel. Thus, the true variance of the net-count areas of the gamma-ray lines can be known directly and does not have to be estimated separately as done in this work. In addition, to limit the system dead time, the use of a faster preamplifier than the one used in WOLF-B should be investigated.

• Gamma-ray spectrum analysis and fission rate ratio derivation

Currently, the software HyperLab was used for the gamma-ray line deconvolution and for the determination of net-count areas. HyperLab was particularly suitable because of its capability to fit non-Gaussian peaks. In the LIFE@PROTEUS measurements, the fast neutron flux reaching the detector is negligibly small. Therefore, neither severe degradation of the detector resolution nor distortion of the Gaussian peaks is expected. Nonetheless, HyperLab may still be a very good option because it does not require any energy or resolution calibration.

If the detector resolution is not sufficient to deconvolve neighbouring peaks with reasonable uncertainties, it is advisable to sum such peaks and to derive a unique single fission rate ratio. This was done in the present research work for the two peaks ^{95}Y (2632keV) and ^{138}Cs (2640 keV). The same approach should be considered for the two adjacent peaks ^{88}Kr (2393keV) and ^{142}La (2398keV).

If hydrogen is present in large amounts close to the measurement station, as currently planned for LIFE@PROTEUS, the ^{138}Cs (2218keV) peak is likely to suffer interference from the prompt capture gamma-ray peak of ^1H at 2223 keV. The latter would be caused by the intrinsic neutron background emitted by the burnt fuel during the measurement, or by delayed neutrons emitted from the reactor core and the measured fuel pin shortly after irradiation. Since the measurements will start about 5 min after irradiation, the contribution to the ^1H peak due to delayed neutrons is expected to be negligible during the LIFE@PROTEUS measurements. As regards the contribution due to the intrinsic neutron activity of the burnt fuel, this could possibly be quantified to a sufficient degree of accuracy by measuring the burnt fuel pin before irradiation in PROTEUS. The observed counts in the ^{138}Cs (2218keV) peak could then be appropriately corrected for.

To minimise the uncertainty on the measured fission rate ratios between fresh and burnt fuel pins due to nuclear data, it is recommended to conduct all experiments with the same irradiation, cooling and measurement times. However, even with identical timing, the contributions from the uncertainties on the fission yields will never compensate entirely for two fuel pins which have

very different isotopic compositions. If there are significant doubts about the exact composition of the burnt fuel samples, the use of fission products for which the fission yields strongly depend on the fissioning isotopes (e.g. ^{89}Rb and ^{88}Kr) is not recommended.

- **Calculation of MCNPX fission rate ratios**

As stated earlier, the measured fission rate ratios in the present experiments have been compared to calculational results obtained with an MCNPX whole-reactor model of PROTEUS. The quoted uncertainties on the fission rates calculated with MCNPX only accounted for the statistical Monte Carlo uncertainties. Sensitivity studies have been conducted with respect to the axial elevation of the fuel and the modelled composition of the burnt fuel, but there has not been any systematic quantification made of the corresponding uncertainties.

In future work, the uncertainty analysis for calculated values of the measured fission rate ratios should be carried out more systematically, considering the uncertainties on the burnt fuel composition, on the geometry of the measurement set-up, as also on the position of the fuel during irradiation.

- **Synergy with the delayed neutron technique**

As mentioned earlier, in addition to the presented measurement technique based on gamma-rays from short-lived fission products, a second independent technique is being developed at PSI. This is based on the measurement of delayed neutrons emitted from the fuel after irradiation. The delayed-neutron technique has been successfully applied to derive fission rate ratios between fresh and burnt fuel samples with burn-ups of 36 and 46 GWd/t. The achieved uncertainties on inter-position and inter-sample fission rate ratios are about 1% and 3-5%, respectively [Jordan 10a]. The large uncertainties on the inter-sample fission rate ratios mainly come from the rather large quoted uncertainties on delayed neutron yields and the relative abundances of the delayed neutron groups. First comparisons between experimental and calculated results suggest, however, that these uncertainties are overestimated.

In the future, efforts should be undertaken to combine the gamma-ray and the delayed neutron techniques in an appropriate manner, considering that the systematic errors in the two different experimental approaches are quite independent of each other. Clearly, a significant reduction of net uncertainties on measured fission rate ratios can be expected to results from such synergy.

- **Additional possible applications of the new measurement technique**

It should be noted that the achieved measurements of freshly induced gamma-ray activity in burnt fuel samples, being the first of their kind, could be of high interest to other research activities. For example, as mentioned in the Section 2.1, the use of short-lived fission products has been suggested in connection with safeguards applications but has not been pursued further because of experimental difficulties. The main interest in such work is the derivation of the plutonium content of unknown burnt fuel on the basis of measuring short-lived fission product activity. In this context, the currently obtained gamma-ray spectra could serve as a first database.

In the future, additional types of measurements could be considered. For example, the burnt fuel could be irradiated under different moderator conditions (i.e. using different neutron spectra),

and the ratio between the fissioning isotopes could be determined based on the measured count rates in certain gamma-ray lines using an iterative approach. Here, short-lived fission products with very different fission yields for the different fissioning isotopes, e.g. ^{89}Rb and ^{88}Kr , would be clearly of advantage.

8.4 Concluding remarks

The present research work has successfully demonstrated the feasibility of measuring fission rate ratios between fresh and burnt fuels irradiated in a zero-power facility such as PROTEUS. The presented technique is based on the measurement of high-energy gamma-ray lines from freshly induced, short-lived fission products. To the author's knowledge, such measurements in burnt fuel samples have been performed for the very first time.

The derived first-of-their-kind fresh-to-burnt fuel fission rate ratios have a 1σ accuracy of 1.7 to 3.4%, the main contribution to the uncertainties being statistical. The improvement of the statistics and a better shielding against the fast neutron background from the reactor have been noted as the major challenges for future experiments.

The recommendations for future work have been elaborated focusing on a proposed measurement station for the envisaged LIFE@PROTEUS experiments. It has been demonstrated that, during these experiments, it will be possible to measure fission rate ratios between fresh and highly burnt fuel pins with a satisfactory accuracy of 1 to 2%, using a measurement set-up which is adequately shielded from the reactor core. It has been pointed out that the contribution of nuclear-data related uncertainties (~ 1.1 to 1.4%) could prove to be the main constraint to the achievable accuracy in future experiments. Combining the presented gamma-ray technique with the delayed neutron technique, which is being developed in parallel at PSI, would be an important measure towards further reduction of net experimental uncertainties.

In conclusion, the presented research has led to the development of a key experimental tool for measuring fission rates in mixed lattices of fresh and highly burnt fuel in zero-power research reactors. The work has also pointed out further optimisations which are needed to fully exploit the technique's potential in the future. Using the developed gamma-ray technique in combination with the delayed neutron technique, the LIFE@PROTEUS programme will be able to provide important experimental data which are needed for the validation of neutronics code predictions, if the trends to higher discharge burn-ups and higher initial fuel enrichments in modern LWRs are to be continued.

Bibliography

- [Jordan 10a] K.A. Jordan & G. Perret. *A Delayed Neutron Technique for Measuring Induced Fission Rates in Fresh and Burnt LWR fuel*. submitted to Nuclear Instruments and Methods in Physics Research Section A, 2010.

Appendix A

Nuclear Data

This appendix summarises the nuclear data related to all gamma-ray lines used in the present research work. All nuclear data shown are extracted from JEFF3.1.

Table A.1: Nuclear data of short-lived fission products investigated in the present thesis.

Fission product	Half-life	Gamma-ray energy	Gamma-ray intensity [%]	Cumulative fission yields [%]			Precursor	Isomeric state
				$Y_{th,U5}$	$Y_{f,U8}$	$Y_{th,P9}$	$Y_{th,P1}$	
^{88}Kr	$2.84\text{ h} \pm 108\text{ s}$	2392 keV	34.6 (4.6%)	3.54 (1.8%)	2.32 (4.0%)	1.25 (2.8%)	1.01 (6.3%)	none
^{142}La	$1.52\text{ h} \pm 30\text{ s}$	2398 keV	13.3 (2.4%)	5.86 (1.7%)	4.90 (5.4%)	4.97 (1.1%)	4.74 (2.9%)	^{142}Ba
		2542 keV	10.0 (2.6%)					
		2971 keV	3.1 (4.7%)					
^{138}Cs	$33.4\text{ min} \pm 10.8\text{ s}$	2218 keV	15.2 (2.0%)	6.69 (1.7%)	6.02 (3.7%)	5.94 (2.7%)	6.4 (3.6%)	^{138m}Cs
		2640 keV	7.6 (3.0%)					
		1435 keV	76.3 (2.0%)					
^{84}Br	$31.8\text{ min} \pm 4.8\text{ s}$	3928 keV	6.8 (12.8%)	1.01 (1.9%)	0.61 (15.9%)	0.45 (4.3%)	0.37 (5.5%)	^{84}Se
^{89}Rb	$15.4\text{ min} \pm 12\text{ s}$	2570 keV	10.2 (6.3%)	4.69 (1.2%)	3.03 (2.6%)	1.68 (1.9%)	1.22 (11.0%)	^{89}Kr
^{95}Y	$10.3\text{ min} \pm 6\text{ s}$	2632 keV	4.8 (8.6%)	6.47 (1.1%)	5.19 (1.7%)	4.82 (2.0%)	3.89 (3.8%)	^{95}Sr
		3576 keV	6.4 (8.4%)					
Lower-energy gamma-ray lines, included in the present research for cross-comparison of fresh fuel measurements								
^{135}I	$6.57\text{ h} \pm 72\text{ s}$	1260 keV	28.7 (3.2%)	6.39 (3.4%)	6.42 (4.2%)	6.33 (3.7%)	6.84 (3.4%)	^{135}Te
^{92}Sr	$2.71\text{ h} \pm 36\text{ s}$	1383 keV	93.0 (0.7%)	6.03 (1.1%)	4.37 (3.8%)	3.00 (2.2%)	2.29 (5.2%)	none
Fission products with minor contributions to one of the above listed high-energy gamma-ray lines								
^{101}Mo	$14.6\text{ min} \pm 1.8\text{ s}$	1382 keV	1.1 (3.4%)	5.17 (1.7%)	6.43 (4.5%)	6.17 (4.8%)	5.98 (5.8%)	^{101}Nb
^{93}Sr	$7.4\text{ min} \pm 1.44\text{ s}$	1434 keV	0.9 (7.5%)	6.36 (1.4%)	5.38 (4.9%)	3.71 (3.4%)	2.91 (5.2%)	none
		2544 keV	3.0 (7.0%)					
^{133}Te	$12.5\text{ min} \pm 18\text{ s}$	2542 keV	0.5 (12%)	3.71 (5.4%)	4.99 (4.3%)	3.05 (6.7%)	4.13 (5.3%)	^{133m}Te
^{99m}Nb	$2.6\text{ min} \pm 12\text{ s}$	2544 keV	0.8 (14.2%)	2.20 (7.5%)	2.27 (7.3%)	2.12 (7.1%)	2.01 (9.1%)	none

Table A.2: Nuclear data of considered precursors and isomeric states of fission products investigated in the present thesis.

Considered precursors						
Fission product	Precursor	Half-life	$Y_{th,U5}$	$Y_{f,U8}$	Cumulative fission yields [%] $Y_{th,P9}$	Branching ratio i_{12}
^{142}La	^{142}Ba	10.6 min \pm 12 s	5.80 (1.7%)	4.89 (5.4%)	4.68 (1.3%)	4.70 (2.9%) 1.00 \pm 0.0
^{138}Cs	^{138}Xe	14.1 min \pm 4.8 s	6.41 (1.8%)	5.99 (3.7%)	5.02 (3.3%)	6.11 (3.7%) 1.00 \pm 0.0
^{84}Br	^{84}Se	186 s \pm 6 s	1.00 (1.9%)	0.61 (16.0%)	0.42 (4.5%)	0.36 (5.5%) 1.00 \pm 0.0
^{89}Rb	^{89}Kr	3.2 min \pm 2.4 s	4.43 (1.4%)	3.01 (2.6%)	1.42 (2.7%)	1.14 (11.1%) 1.00 \pm 0.0
^{95}Y	^{95}Sr	23.9 s \pm 0.14 s	5.28 (2.2%)	4.96 (1.9%)	3.23 (5.2%)	3.18 (4.4%) 1.00 \pm 0.0
^{135}I	^{135}Te	19 s \pm 0.2 s	3.84 (7.1%)	5.30 (4.8%)	2.14 (17.5%)	4.43 (6.3%) 1.00 \pm 0.0
^{101}Mo	^{101}Nb	7.1 s \pm 0.3 s	5.05 (1.7%)	6.42 (4.5%)	5.64 (4.9%)	5.85 (5.2%) 1.00 \pm 0.0
^{133}Te	^{133}Sb	2.5 min \pm 6 s	2.41 (12.9%)	5.09 (4.4%)	1.30 (23.2%)	3.32 (8.8%) 0.83 \pm 0.0
Considered isomeric states						
Fission product	Isomeric state	Half-life	$Y_{th,U5}$	$Y_{f,U8}$	Cumulative fission yields [%] $Y_{th,P9}$	Branching ratio i_m
^{138}Cs	^{138m}Cs	2.9 min \pm 4.8 s	0.18 (35.3%)	0.02 (35.2%)	0.61 (30.5%)	0.18 (35.2%) 0.81 \pm 0.0
^{133}Te	^{133m}Te	55.4 min \pm 24 s	2.78 (7.4%)	1.17 (20.0%)	3.29 (6.3%)	2.18 (11.7%) 0.175 \pm 0.030

Acknowledgements

This research work has been carried out in the Experimental Reactor Physics group of the Laboratory for Reactor Physics and Systems Behaviour at the Paul Scherrer Institute. Carried out in the frame of the LWR-PROTEUS and the LIFE@PROTEUS programmes, the work has been strongly supported by the Swiss nuclear utilities (*swissnuclear*). Furthermore, *swissnuclear*, in the context of promoting young professionals, kindly financed my participation to the international conferences ANIMMA 2009 and PHYSOR 2010.

This work could not have been realised without the support of many persons. It is impossible to list all of them here, but I would like to express my special gratitude to some:

- Prof. Rakesh Chawla, the director of my thesis, for giving me the opportunity to carry out this doctoral work, and for his friendly and helpful guidance and advice.
- My supervisors at PSI: Michael Plaschy, Mike Murphy and Gregory Perret. I feel very lucky to have had the chance to work with them, both from professional and personal points of view.
- The whole PROTEUS team. I would like to especially thank Markus Fassbind, Manfred Zimmermann and Alex Stephan for their help and their availability during the experiments, and Kelly Jordan and my officemate Dominik Rätz for making the daily life at PROTEUS so pleasant.
- Flavio Giust, my part-time officemate, for the nice time and for his great help with HELIOS.
- Peter Grimm, for having kindly conducted the CASMO calculations of the burnt fuel samples for us.
- The staff at the BR1 reactor for their support during the measurement campaign in Mol. In particular, I thank Pierre D'Hondt and Jan Wagemans for making the measurements possible and also for their constant interest in the results. Jan deserves a special thanks for his friendly help, whenever it was needed, also long after the BR1 campaign.
- Philippe Jacquemoud for his patient support with the computational infrastructure, as also Aurelia Chenu, Davide Bertolotto and Jordi Freixa for helping me in my general struggle with computer programmes.
- All friends and colleagues at PSI for the great four years.
- My family, for being there for me, even though they are quite far away.

Finally, I would like to thank Prof. H.-D. Berger, Dr. P. D'Hondt and Prof. A. Bay for accepting to form the jury for this thesis.

CURRICULUM VITÆ

Hanna Kröhnert

Work contacts

ENSI, Industriestrasse 19, CH-5200 Brugg
Tel.: +41 (0)56 460 8572
E-mail: hanna.kroehnert@ensi.ch

Home contacts

Pestalozzistrasse 18, CH-8032 Zürich
Tel.: +41 (0)76 221 8111
E-mail: hanna.kroehnert@web.de

Personal details

Date of Birth:	20th May 1980
Place of Birth:	Hamburg, Germany
Nationality:	German

Professional experience

Since Oct. 2010	Swiss Federal Nuclear Safety Inspectorate ENSI Brugg, Switzerland Safety Analysis Division, Reactor and Fuel Technology Section Subject matter specialist
Sept. 2006 - Sept. 2010	Paul Scherrer Institute , Villigen, Switzerland Laboratory for Reactor Physics and Systems Behaviour Doctoral student Development of measurement techniques to determine fission rates in fresh and burnt fuel pins in zero-power research reactors.
Feb. 2006 - Sept. 2006	Paul Scherrer Institute , Villigen, Switzerland Laboratory for Reactor Physics and Systems Behaviour Master student Analysis of the isotopic composition of highly burnt fuels using the spectral code HELIOS.

- Sept. 2005 - Feb. 2006 **Framatome ANP** (now: AREVA), Erlangen, Germany
Pressurised water reactor core design
Trainee
Familiarisation with the core design of pressurised water reactors, in particular using the code system CASCADE-3-D.

Education

- Since Dec. 2006 **Ecole Polytechnique Fédérale de Lausanne (EPFL)**, Lausanne, Switzerland
Doctoral School in Energy
Doctoral study
Research carried out at the Paul Scherrer Institute (see “Professional experience”)
- Oct. 2000 - Aug. 2006 **Technische Universität Braunschweig**, Germany
Master programme in Mechanical Engineering
(Diplomstudiengang Maschinenbau)
Master thesis carried out at the Paul Scherrer Institute (see “Professional experience”)

Publications

- H. Kröhnert, G. Perret, M.F. Murphy, R. Chawla. *Gamma-spectrometric measurement of fission rate ratios between fresh and spent fuel following irradiation in a zero-power reactor.* To be submitted to Nuclear Instruments and Methods in Physics Research Section A.
- H. Kröhnert, G. Perret, M.F. Murphy, R. Chawla. *Freshly induced short-lived gamma-ray activity as a measure of fission rates in lightly re-irradiated spent fuel.* Nuclear Instruments and Methods in Physics Research Section A, 624, page 101-108, 2010.
- H. Kröhnert, G. Perret, M.F. Murphy, R. Chawla. *Fission rate measurements in spent fuel via gamma-ray spectrometry of short-lived fission products induced in a zero-power reactor.* PHYSOR Conference 2010, Pittsburgh, Pennsylvania, USA, CD-ROM, ISBN 978-89448-079-9.
- H. Kröhnert, M.F. Murphy, G. Perret, R. Chawla. *Utilization of freshly induced high-energy gamma-ray activity as a measure of fission rates in re-irradiated burnt UO₂ fuel.* ANIMMA Conference 2009, Marseille, France.
- H. Kröhnert, M.F. Murphy, G. Perret, M. Plaschy, J. Wagemans, R. Chawla. *Measurement of fission rate ratios in fresh UO₂ fuel utilising short-lived high-energy gamma activity.* PHYSOR Conference 2008, Interlaken, Switzerland, CD-ROM, ISBN 978-3-9521409-5-6.
- F. Attale, H. Kröhnert, H.-D. Berger. *On the use of water density correction factors in pin cell calculations for the evaluation of isotope densities of irradiated samples.* Annual Meeting on Nuclear Technology (Jahrestagung Kerntechnik), Karlsruhe, Germany, 2007.